TECHNICAL DIGEST
1996

LASER APPLICATIONS TO CHEMICAL AND ENVIRONMENTAL ANALYSIS

MARCH 20–22, 1996
ORLANDO, FLORIDA

1996 TECHNICAL DIGEST SERIES
VOLUME 3

SPONSORED AND MANAGED BY
OPTICAL SOCIETY OF AMERICA

SF 298 MASTER COPY KEEP THIS COPY FOR REPRODUCTION PURPOSES

REPORT DOCUMENTATION PAGE

Form Approved
OMB NO. 0704-0188

1. AGENCY USE ONLY *(Leave blank)*	2. REPORT DATE	3. REPORT TYPE AND DATES COVERED
	September 13, 1996	Final 02/20/96 - 02/19/97

4. TITLE AND SUBTITLE

Organization of the 1996 Laser Applications to Chemical and Environmental Analysis Topical Meeting

5. FUNDING NUMBERS

DAAH04-96-1-0024

6. AUTHOR(S)

David W. Hennage

7. PERFORMING ORGANIZATION NAMES(S) AND ADDRESS(ES)

Optical Society of America
2010 Massachusetts Ave. NW
Washington, DC 20036

8. PERFORMING ORGANIZATION REPORT NUMBER

9. SPONSORING / MONITORING AGENCY NAME(S) AND ADDRESS(ES)

U.S. Army Research Office
P.O. Box 12211
Research Triangle Park, NC 27709-2211

10. SPONSORING / MONITORING AGENCY REPORT NUMBER

ARO 35178.1-PH-CF

11. SUPPLEMENTARY NOTES

The views, opinions and/or findings contained in this report are those of the author(s) and should not be construed as an official Department of the Army position, policy or decision, unless so designated by other documentation.

12a. DISTRIBUTION / AVAILABILITY STATEMENT

Approved for public release; distribution unlimited.

12 b. DISTRIBUTION CODE

13. ABSTRACT *(Maximum 200 words)*

The Fifth Topical Meeting on Laser Applications to Chemical and Environmental Analysis provided an informal atmosphere to foster communication between researchers in the broad range of fields using optical diagnostics.

Applications of chemical and environmental analysis using laser light are increasing at an incredible pace. New developments in optical sources, instrumentation, and spectroscopic techniques are increasing the capabilities for laser applications. These developments provide opportunities for new applications in a quite diverse range of endeavors.

This meeting not only provided a forum to discuss these optical diagnostics, but also provided an opportunity for commercial laser-based instrumentation companies to expand the potential applications of their products.

14. SUBJECT TERMS

15. NUMBER IF PAGES

16. PRICE CODE

17. SECURITY CLASSIFICATION OR REPORT	18. SECURITY CLASSIFICATION OF THIS PAGE	19. SECURITY CLASSIFICATION OF ABSTRACT	20. LIMITATION OF ABSTRACT
UNCLASSIFIED	UNCLASSIFIED	UNCLASSIFIED	UL

CONFERENCE EDITION

Summaries of the papers
presented at the topical meeting

LASER APPLICATIONS TO CHEMICAL AND ENVIRONMENTAL ANALYSIS

MARCH 20–22, 1996
ORLANDO, FLORIDA

1996 TECHNICAL DIGEST SERIES
VOLUME 3

SPONSORED BY
Optical Society of America

Optical Society of America
2010 Massachusetts Avenue NWS
Washington DC 20011-1023

Articles in this publication may be cited in other publications. To facilitate access to the original publication source, the following form for the citation is suggested:

Name of Author(s), "Title of Paper," in *Laser Applications to Chemical and Environmental Analysis*, Vol. 3, 1996 OSA Technical Digest Series (Optical Society of America, Washington DC, 1996), pp. xx-xx.

Optical Society of America

ISBN

Conference Edition	1-55752-428-9
Postconference Edition (Note: Postconference Edition includes postdeadline papers.)	1-55752-429-7
1995 Technical Digest Series	1-55752-417-3

Library of Congress Catalog Card Number

Conference Edition	95-72748
Postconference Edition	95-72749

Printed in the U.S.A.

Contents

LASER APPLICATIONS TO CHEMICAL AND ENVIRONMENTAL ANALYSIS TECHNICAL PROGRAM COMMITTEE

J. Michael Ramsey, *Oak Ridge National Laboratory, General Chair*

Jay Jeffries, *SRI International, General Chair and OSA Technical Council Representative*

Kay Niemax, *University of Hohenheim, Germany, Program Chair*

Robert P. Lucht, *University of Illinois, Program Chair*

Ernesto Cespedes, *US Waterways Experiment Station*

Alan Fried, *National Center for Atmospheric Research*

Timothy Harris, *AT&T Bell Laboratories*

Ulrich Meier, *DLR EN-CV, Germany*

Andrzej Miziolek, *US Army Research Laboratory*

Reinhard Niessner, *Technical Universitat Munich, Germany*

Nick Omenetto, *European Commission, Joint Research Center, Ispra, Italy*

Jerry Seitzman, *Georgia Institute of Technology*

Volker Sick, *Universitat Heidelberg, Germany*

Michael Winter, *United Technologies Research Center*

WEDNESDAY
MARCH 20, 1996

WINDSOR BALLROOM

7:00am–6:00pm
Registration

WINDSOR BALLROOM

8:25am–8:30am
Opening Remarks

8:30am–10:00am
LWA • Species Selective Detection Techniques
Robert Lucht, *University of Illinois, Presider*

8:30am (Invited)
LWA1 • New trends in analytical atomic laser spectroscopy, James Winefordner, *Univ. Florida.* Laser excited atomic fluorescence and atomic ionization spectrometric approaches for trace elemental analysis are discussed. **(p. 2)**

9:00am
LWA2 • Influence of ambient conditions on the laser air spark, Serife Yalçin, David R. Crosley, Gregory P. Smith, Gregory W. Faris, *SRI International.* We report on the applicability of the laser air spark for in situ quantitative elemental analysis as studied through detailed temperature and electron density measurements under a variety of conditions. **(p. 3)**

9:15am
LWA3 • Diode laser optogalvanic spectroscopy for uranium isotopic analysis: Analytical figures of merit, R. W. Shaw, C. M. Barshick, J. P. Young, J. M. Ramsey, *Oak Ridge National Laboratory.* Semiconductor-diode-laser-excited optogalvanic spectroscopy is coupled with glow discharge sputtering for isotopic analysis. The figures of merit for uranium analysis are described. **(p. 6)**

9:30am
LWA4 • Element selective detection in chromatography by diode laser modulation spectrometry, Kay Niemax, Aleksandr Zybin, *Univ. Hohenheim, Germany;* Christoph Schnürer–Patschan, Henning Groll, *LaserSpec Analytik GmbH, Germany.* Diode laser modulation absorption spectrometry is used for element selective measurements in plasmas and analytical flames coupled to chromatographs. **(p. 9)**

9:45am
LWA5 • Diode laser absorption spectroscopy of combustion gases near 1.57 microns, David M. Sonnenfroh, Mark G. Allen, *Physical Sciences Inc.* An external cavity diode laser is used for high-resolution spectral surveys of CO, CO_2, OH, and H_2O transitions near 1.57 μm in hydrocarbon- and hydrogen-fueled flames. **(p. 12)**

SALONS V–VII

10:00–10:30am
Coffee Break/Exhibits

WINDSOR BALLROOM

10:30am–12:30pm
LWB • Environmental Sensing I and Single Molecule Detection
Kevin McNesby, *Army Research Laboratory, Presider*

10:30am (Invited)
LWB1 • Laser-based sensors for environmental analysis, T. Vo-Dinh, *Oak Ridge National Laboratory.* Abstract not available. **(p. 16)**

11:00am
LWB2 • An in-line photoacoustic sensor for environmental monitoring in water, Scott S. Freeborn, John Hannigan, Hugh A. MacKenzie, *Heriot-Watt Univ., UK;* Frank Greig, *Napier Univ., UK.* A diode laser photoacoustic sensor is constructed for environmental monitoring of hydrocarbons in water from offshore oil production. **(p. 17)**

11:15am
LWB3 • Laser-induced breakdown spectroscopy for real-time detection of Halon alternative agents, Cindy Williamson, Brad E. Forch, Andrzej W. Miziolek, Robert G. Daniel, Kevin L. McNesby, *US Army Research Laboratory.* Laser-induced breakdown spectroscopy is being explored as a real-time, *in situ* sensitive detection technique for use in the Army's Halon replacement program. **(p. 20)**

11:30am
LWB4 • Dynamics of single molecules at room temperature, H. Peter Lu, X. Sunney Xie, *Pacific Northwest National Laboratory.* The room-temperature spectral evolution of single molecules is investigated. Time correlation functions of single-molecule spectral trajectories are obtained, demonstrating that the spectral fluctuation is photoinduced in nature. **(p. 23)**

11:45am
LWB5 • Increasing the rate of detection of single molecules in solution, Lloyd M. Davis, Laurie E. Schneider, Dennis H. Bunfeld, *Univ. Tennessee Space Institute.* An actively quenched avalanche photodiode that permits instantaneous count rates exceeding 10^7 s^{-1} is used for single molecule detection in solution with transit times $<2 \times 10^{-4}$ s^{-1}. **(p. 24)**

12:00m
LWB6 • Photophysics of surfactant molecules in microdroplets, M. D. Barnes, W. B. Whitten, J. M. Ramsey, *Oak Ridge National Laboratory;* S. Arnold, *Polytechnic Univ.* Fluorescence decay rate modification is observed for surfactant molecules in liquid microspheres offering potential sensitivity advantages for single molecule fluorescence detection. **(p. 27)**

12:15pm
LWB7 • High-speed single molecule detection in microdroplet streams, N. Lermer, M. D. Barnes, C.-Y. Kung, W. B. Whitten, J. M. Ramsey, *Oak Ridge National Laboratory.* Fluorescence detection of single dye molecules in falling microdroplets by use of a linear quadrupole to control the droplet trajectory and speed are discussed. **(p. 30)**

12:30pm–7:00pm
Free Time

WINDSOR BALLROOM

7:00pm–8:15pm
LWC • New Developments in Laser Systems
Michael Winter, *United Technologies Research Center, Presider*

7:00pm (Invited)
LWC1 • Frequency-converted diode lasers for analytical applications, Doug Bamford, *Deacon Research.* Abstract not available. **(p. 34)**

7:30pm
LWC2 • Passively Q-switched microchip lasers for environmental monitoring, J. J. Zayhowski, Bernadette Johnson, *MIT Lincoln Laboratory.* Fiber-pumped passively *Q*-switched microchip lasers provide short-pulse, high-peak-power, high-repetition-rate infrared, visible, and/or ultraviolet radiation that is ideal for characterizing common environmental contaminants. **(p. 37)**

7:45pm (Invited)
LWC3 • Extending wavelength coverage and spectroscopic applications of diode lasers, R. W. Fox, L. Hollberg, S. Waltman, *NIST;* K. P. Petrov, F. K. Tittel, *Rice Univ.* The increasing power of diode lasers allows nonlinear mixing to be realized more efficiently. Significant power in the blue is possible with intracavity SHG in $KNbO_3$ and difference frequency mixing with diodes can reach into the IR. **(p. 40)**

WINDSOR BALLROOM

8:15pm–10:00pm
LWD • Poster Session I

LWD1 • Novel rare-earth-doped chalcogenide glasses for high-brightness, room-temperature, broadband infrared sources, J. A. Moon, B. B. Harbison, J. S. Sanghera, I. D. Aggarwal, *US Naval Research Laboratory.* A bright, broadband, optically pumped fiber fluorescent source is described. Fluorescence data obtained from fiber and bulk samples of rare-earth-doped chalcogenide glass are presented. **(p. 44)**

LWD2 • Tunable polymer dye lasers: A review and recent achievements, Vladimir S. Nechitailo, *PolyOptics Ltd., Israel.* Diverse polymer lasers pumped by Nd:YAG lasers produce efficient operation between 550–700 nm. Output energy of 270 mJ and power of 6 W are obtained. **(p. 47)**

LWD3 • Doubly tunable femtosecond pulses generated in the visible using optical parametric amplifiers for time-resolved spectroscopy, P. Matousek, A. W. Parker, P. F. Taday, W. T. Toner, M. Towrie, *Rutherford Appleton Laboratory, UK.* Two optical parametric amplifiers (480–730 nm, >40 nJ) are seeded from white-light continuum and pumped by a frequency-doubled regenerative amplifier at 40 kHz. **(p. 49)**

LWD4 • Tunable InP-based semiconductor lasers for gas analysis, Björn Broberg, *Industrial Microelectronics Center, Sweden;* Stefan Nilsson, Pierre-Jean Rigole, Tiina Klinga, Lena Bäckbom, Björn Stålnacke, *Royal Institute of Technology, Sweden.* By exploiting and modifying telecommunications semiconductor laser technology such as strained quantum wells and tunable lasers, semiconductor lasers suitable for gas analysis are developed. **(p. 52)**

LWD5 • Imaging and time-resolved spectroscopy of single molecules, T. D. Harris, J. J. Macklin, J. K. Trautman, L. E. Brus, *AT&T Bell Laboratories.* We describe room-temperature, far-field microscopy and spectroscopy of single carbocyanine molecules dispersed on a thin film, and discuss implications for measuring protein conformation *in vivo.* **(p. 55)**

LWD6 • High sensitivity detection on microchips, J. C. Fister III, L. M. Davis, S. C. Jacobson, J. M. Ramsey, *Oak Ridge National Laboratory.* High sensitivity confocal fluorescence detection in a microchannel fabricated on a fused silica microscope slide is demonstrated. **(p. 58)**

LWD7 • Modeling fluorescence collection from single molecules in liquid microspheres, S. C. Hill, *Army Research Laboratory;* M. D. Barnes, W. B. Whitten, J. M. Ramsey, *Oak Ridge National Laboratory.* Numerical methods for modeling fluorescence from single molecules and molecular detection efficiencies in microdroplets are discussed. **(p. 61)**

LWD8 • Low-level determinations of uranium hexafluoride using multiphoton ionization time-of-flight mass spectroscopy, Donald P. Armstrong, David A. Harkins, *Lockheed Martin Energy Systems Inc.;* Robert N. Compton, *Oak Ridge National Laboratory.* Under the experimental conditions described the unique nature of the interaction of uranium hexafluoride with light leads to the very efficient generation of doubly charged uranium ions, low levels of which can be detected with use of a mass spectrometer. **(p. 63)**

LWD9 • Near-field scanning optical microscope for biological applications, V. B. Baibyrin, U. P. Volkov, *Saratov Politechnical Univ., Russia;* P. I. Anisimov, N. P. Konnov, A. A. Shcherbakov, *Russian Research Anti-Plague Institute Microbe, Russia.* The design of a new near-field scanning optical microscope is presented. A lateral resolution of the microscope is estimated to be within 500 A. A plague and choler are observed in atmospheric conditions without a metal film coating by means of the NSOM. **(p. 66)**

LWD10 • Single-particle backscatter measurements with size parameters near one, Matthew Hart, C. W. Bruce, *Army Research Laboratory/New Mexico State Univ.* By use of millimeter wavelengths radar cross sections of an assortment of particle types can be measured with use of a portable system. Apparatus and experimental results are discussed. **(p. 68)**

LWD11 • Alternative approaches to sampling and data collection for laser-induced breakdown spectroscopy, Andrzej W. Miziolek, Cindy Williamson, Kevin L. McNesby, Nicholas F. Fell, Jr., Stephen V. Medlin, Brad E. Forch, Robert G. Daniel, *US Army Research Laboratory;* Ernesto R. Cespedes, Brian H. Miles, Javier Cortes, *US Army Engineer Waterways Experiment Station.* We evaluate a laser vaporization/pyrolysis sampling method as well as single photon counting and acousto-optic tunable filters for LIBS spectrochemical analysis. **(p. 71)**

LWD12 • Laser-induced plasma spectroscopy for environmental applications, C. Haisch, M. Clara, U. Panne, R. Niessner, *Technical Univ. Munich, Germany.* The application LIPS to process control and environmental matrices is presented. The merits of LIPS analysis of hot glass melts and hydrocolloids are discussed. **(p. 73)**

LWD13 • Rayleigh and Raman diagnostic of laser-generated plasmas, Deborah Nassif Pugsley, Lutz Hüwel, *Wesleyan Univ.* We use Raman and Rayleigh scattering to determine time-resolved density contour maps of transient, laser-generated plasmas in air and other gases. **(p. 76)**

LWD14 • Laser ignition of gaseous ammonia-oxygen mixtures, David H. Plemmons, Christian Parigger, James W. L. Lewis, *Univ. Tennessee Space Institute.* Nonresonant laser-spark ignition of combustible ammonia-oxygen gas mixtures are investigated. We present temporally and spatially resolved experimental results of ignition kernel development. **(p. 79)**

LWD15 • Hydroxyl measurements in air-breakdown microplasmas, Christian Parigger, James W. L. Lewis, David H. Plemmons, Guoming Guan, James O. Hornkohl, *Univ. Tennessee Space Institute.* OH recombination spectra are measured in decaying laser-induced air plasmas. The analysis uses synthetic spectra computed from line strength files and from molecular parameters. **(p. 82)**

LWD16 • Nitric oxide optical breakdown spectra and analysis by the use of the program NEQAIR, Christian Parigger, James W. L. Lewis, David H. Plemmons, James O. Hornkohl, *Univ. Tennessee Space Institute.* NO emission spectra, recorded in a decaying laser-induced plasma, are analyzed to infer temperature and species densities by use of the nonequilibrium air radiation (NEQAIR) code. **(p. 85)**

LWD17 • Optical emission spectrometry of laser produced plasma with microwave re-excitation for micro-analysis of solid samples, A. Ciocan, *Brigham Young Univ./Institute of Atomic Physics, Romania;* J. Uebbing, *Institut für Spektrochemie und angewandte Spektroskopie, Germany;* K. Niemax, *Univ. Hohenheim, Germany.* Laser ablation of solid samples by pulsed lasers is a convenient and fast sampling technique for elemental analysis of solid samples, with a moderate spatial resolution. This paper presents experimental results and instrumentation for matrix-independent simultaneous multi-element analysis by a method which got the acronym LA-MIP-OES (Laser Ablation-Microwave Induced Plasma-Optical Emission Spectrometry). Typical absolute and relative detection limits in the fg and μg/g ranges respectively, were achieved for a number of elements with one laser shot. **(p. 88)**

WINDSOR BALLROOM

7:00am–6:00pm
Registration

WINDSOR BALLROOM

8:00am–9:45am
LThA • Atmospheric Chemistry
Robert Daniel, *Army Research Laboratory, Presider*

8:00am (Invited)
LThA1 • Ground-based and airborne measurements of atmospheric constituents using tunable diode lasers: An overview and recent measurements, Alan Fried, Scott Sewell, Bruce Henry, Bryan Wert, *The National Center for Atmospheric Research;* James R. Drummond, *Univ. Toronto, Canada.* We describe a highly sensitive tunable diode laser absorption spectrometer for ground-based and aircraft measurements of trace atmospheric constituents. **(p. 92)**

8:30am
LThA2 • Sensitive detection of atmospheric trace gases by laser photoacoustic spectroscopy, M. W. Sigrist, M. Moeckli, *ETH Zurich, Switzerland.* The sensitive and selective monitoring of trace gases with a mobile CO_2 laser photoacoustic system are discussed based on recent measurements of ammonia, ethylene, and CO_2 in a freeway tunnel. **(p. 95)**

8:45am
LThA3 • A study of aerosol–cloud interaction using laser microprobe mass spectrometry, R. Gieray, P. H. Wieser, *Univ. Hohenheim, Germany.* Differences in the chemical composition of cloud droplet residues and cloud interstitial particles are identified by use of laser microprobe mass spectrometry of single particles. **(p. 98)**

9:00am
LThA4 • Ultrasensitive* in situ *atmospheric monitoring with a compact setup based on photothermal deflection (mirage effect) spectroscopy, B. L. Zimering, A. C. Boccara, *Laboratoire d'Optique Physique, France.* We demonstrate environmental and industrial applications of ultrasensitive real-time *in situ* ethylene detection with a compact, rugged setup based on photothermal deflection spectroscopy. **(p. 101)**

9:15am (Invited)
LThA5 • UV laser absorption measurements of tropospheric hydroxyl on a 21-km atmospheric long path, George H. Mount, *NOAA.* Determination of the concentration of the hydroxyl radical is of fundamental importance to understanding the chemistry of the lower atmosphere. We describe the instrument and results from the long-path-laser spectroscopic OH experiment at Fritz Peak, CO. **(p. 104)**

SALONS V–VII

9:45am–10:15am
Coffee Break/Exhibits

WINDSOR BALLROOM

10:15am–12:00m
LThB • Environmental Sensing II
Ernesto Cespedes, *US Waterways Experiment Station, Presider*

10:15am (Invited)
LThB1 • Remote spectroscopy over optical fibers for* in situ *measurement of contaminants in soil, Steve Lieberman, David S. Knowles, Greg A. Theriault, Michele Davey, *Naval Command, Control and Ocean Surveillance Center.* Fiber optic-based sensor probes have been developed that can be pushed up to 50 meters into the soil for remote, real-time detection of petroleum hydrocarbons using laser-induced fluorescence (LIF) and metals via laser-induced breakdown spectroscopy (LIBS). **(p. 108)**

10:45am
LThB2 • Raman techniques for detection of explosive materials, Brian D. Gilbert, James Janni, David Moss, R. W. Field, Jeffrey I. Steinfeld, *MIT;* Alvaro Mercado, *Federal Aviation Administration Technical Center.* Raman techniques, particularly surface-enhanced Raman spectroscopy, are capable of detecting explosive molecules at ultratrace levels. We describe SERS detection of TNT and related explosive materials. **(p. 109)**

11:00am
LThB3 • Advanced laser detection techniques for cone penetrometer sensors, J. Wormhoudt, J. H. Shorter, J. B. McManus, P. L. Kebabian, D. D. Nelson, M. S. Zahniser, C. E. Kolb, *Aerodyne Research Inc.* Applications of tunable infrared laser differential absorption spectroscopy and laser-induced fluorescence with use of diode-pumped solid-state lasers to the detection of explosives contamination in soils are presented. **(p. 112)**

11:15am
LThB4 • Real-time laser ablation MS/MS of individual airborne microparticles, P. T. A. Reilly, M. Yang, R. Gieray, W. B. Whitten, J. M. Ramsey, *Oak Ridge National Laboratory.* Individual airborne microparticles are sized and laser ablated in an ion trap in real-time. This technique permits positive identification of constituents and size correlation. **(p. 114)**

11:30am
LThB5 • Raman spectroscopy of phosphonate solutions by real-time,* in situ *fiber probe with metal oxide adsorbent, D. M. Dagenais, *SFA Inc.;* K. J. Ewing, F. Bucholtz, I. D. Aggrawal, *Naval Research Laboratory.* We combine the selectivity of Raman spectroscopy with the sensitivity of pre-concentration at the end of a fiber-optic probe to obtain quantitative *in situ* real-time detection of traces of organophosphorous compounds both in vapor and liquid phase. **(p. 116)**

11:45am
LThB6 • Raman spectroscopy of explosives and propellants during heating, N. F. Fell, K. L. McNesby, *US Army Research Laboratory.* Laser Raman spectroscopy is used to examine bulk and surface properties of explosives and propellants during heating. Changes in Raman line intensities, shapes, and shift frequencies are correlated with decomposition pathways and impact sensitivities. **(p. 119)**

12:00m–1:30pm
Lunch Break

WINDSOR BALLROOM

1:30pm–4:00pm
LThC • Gas Phase Diagnostics
Jerry Seitzman, *Georgia Institute of Technology, Presider*

1:30pm (Invited)
LThC1 • Applications of infrared spectroscopy for combustion diagnostics, David J. Rakestraw, *Sandia National Laboratories.* Recent developments in the use of infrared degenerate four-wave mixing and cavity ringdown spectroscopy for the detection of trace species in combustion systems are presented. **(p. 122)**

2:00pm
LThC2 • Multiplex degenerate four-wave-mixing thermometry of the C_2 radical, G. M. Lloyd, C. F. Kaminski, I. G. Hughes, P. Ewart, *Oxford Univ., UK.* Multiplex DFWM spectroscopy of C_2 in an oxy-acetylene flame is demonstrated by use of a modeless laser providing accurate single-shot and averaged temperature measurements. **(p. 123)**

2:15pm
LThC3 • Degenerate four-wave-mixing spectroscopy using picosecond lasers: Theoretical analysis, Thomas A. Reichardt, Robert P. Lucht, *Univ. Illinois–Urbana-Champaign.* We investigate theoretically the use of lasers with pulse lengths much shorter than characteristic collision times for quantitative gas-phase degenerate four-wave-mixing spectroscopy. **(p. 126)**

2:30pm
LThC4 • Quantitative detection of CH radicals by laser-induced fluorescence in arcjets and flames, Jorge Luque, Wolfgang Juchmann, Jay B. Jeffries, David R. Crosley, *SRI International.* The CH radical is detected in concentrations of parts per million in arcjets for chemical vapor deposition of diamond and low-pressure flames by means of linear laser-induced fluorescence. **(p. 129)**

2:45pm
LThC5 • A new approach to laser-induced fluorescence detection of nitric oxide in high-pressure flames, Christof Schulz, Volker Sick, *Univ. Heidelberg, Germany;* Johannes Heinze, Winfried Stricker, *Institut für Physikalische Chemie der Verbrennung, Germany.* Merits of detecting nitric oxide by way of laser-induced fluorescence under high-pressure combustion conditions with use of a new detection scheme are discussed. **(p. 133)**

3:00pm
LThC6 • In-flight laser-induced fluorescence from microgravity droplet combustion, Michael Winter, *United Technologies Research Center.* An instrument for performing planar laser-induced fluorescence from droplets burning in a microgravity environment is demonstrated. Experiments on sodium and OH are discussed. **(p. 136)**

3:15pm
LThC7 • OH, NO, and soot measurement in diesel spray flames using laser induced fluorescence and laser-induced incandescence, Hiroshi Nakagawa, Hiroyuki Endo, Yoshihiro Deguchi, Matsuhei Noda, *Mitsubishi Heavy Industries, Ltd., Japan;* Hiroshi Oikawa, Taizo Shimada, *Mitsubishi Motors Corp., Japan.* NO, OH, and soot in diesel fuel flames of a motoring compressed injection test system are measured with use of laser-induced fluorescence and laser-induced incandescence. **(p. 139)**

3:30pm
LThC8 • Application of laser-induced fluorescence and spontaneous Raman scattering to technically applied combustion systems: Four cylinder spark ignition engine and oil burning furnace, V. Beushausen, M. Knapp, A. Luczak, S. Eisenberg, *Laser-Laboratorium Göttingen e.V., Germany;* P. Andresen, *Univ. Bielefeld, Germany.* We describe the latest developments in the application of laser diagnostic techniques for the analysis and characterization of turbulent mixture formation and combustion in spark ignition engines and oil burning furnaces. **(p. 142)**

3:45pm
LThC9 • Multiplex polarization spectroscopy of OH for flame thermometry, M. J. New, P. Ewart, *Oxford Univ., UK;* A. Dreizler, T. Dreier, *Univ. Heidelberg, Germany.* Multiplex polarization spectroscopy is demonstrated by use of a broad bandwidth laser to generate spectra of flame OH from which temperatures are derived. **(p. 145)**

WINDSOR BALLROOM

4:00pm–6:00pm
LThD • Poster Session II

LThD1 • Laser-induced gratings in the red system of molecular oxygen, W. Hubschmid, R. Bombach, B. Hemmerling, *Paul Scherrer Institut, Switzerland.* The temporal evolution of laser-induced gratings generated in molecular oxygen is studied. The use of such gratings for spectroscopic purposes is demonstrated. **(p. 150)**

LThD2 • Nitrocompound analysis by 226 nm laser photofragmentation/fragment detection, R. L. Pastel, R. C. Sausa, *US Army Research Laboratory.* Nitrocompounds are analyzed by 226 nm laser photofragmentation with subsequent NO laser-induced fluorescence and resonance-enhanced multiphoton ionization. Limit of detections are presented and discussed. **(p. 153)**

LThD3 • CARS temperature measurements in a driven jet diffusion flame, Robert D. Hancock, Frederick R. Schauer, Robert P. Lucht, *Univ. Illinois;* Vish R. Katta, K. Y. Hsu, *Innovative Scientific Solutions, Inc.* A CARS instrument is validated with a Hencken burner and then used to observe local super-adiabatic flame temperatures in a driven jet diffusion flame. **(p. 155)**

LThD4 • Two-photon resonant detection of N_2 using polarization spectroscopy and laser-induced fluorescence, C. Kaminski, B. Löfstedt, R. Fritzon, M. Aldén, *Lund Institute of Technology, Sweden.* Two-photon resonant polarization spectroscopy and multi-photon resonant laser-induced fluorescence in N_2 are demonstrated, and their potential as diagnostic probes is evaluated. **(p. 158)**

LThD5 • NO laser-induced fluorescence as a flame thermometer, Jorge Luque, Masayuki Tamura, Joel E. Harrington, Gregory P. Smith, David R. Crosley, Jay B. Jeffries, *SRI International.* Temperature determination from laser-induced fluorescence of NO seeded into flames is evaluated for one- and two-line techniques. Removal of NO by flame chemistry and collisional quenching of the LIF are considered in detail. **(p. 161)**

LThD6 • High-resolution laser spectroscopy of molecular ions, Q. Tu, V. I. Harvey, R. W. Marawar, John W. Farley, *Univ. Nevada–Las Vegas.* Sub-Doppler (0.2 ppm resolution) laser spectroscopy performs on the A←X system of a beam of N_2^+ molecular ions. **(p. 165)**

LThD7 • Effects of valence electron shell structure on ion beam sputtered neutrals, Chun He, *SRI International;* Z. Postawa, *Jagellonian Univ., Poland;* S. Rosencrance, R. Chatterjee, D. E. Reiderer, B. J. Garrison, N. Winograd, *Pennsylvania State Univ.* We show, we believe for the first time, that the excitation probabilities of sputtered atoms are dominated by their electronic shell structure rather than by their excitation energies. **(p. 168)**

LThD8 • Factors affecting detection sensitivities of sputtered neutrals using ultra-high intensity laser post-ionization, Michael L. Wise, Stephen W. Downey, *AT&T Bell Laboratories.* The detection sensitivity of dopants relative to bulk species sputtered from semiconductor materials by non-selective post-ionization using laser intensities $>10^{14}$ W/cm^2 is discussed. **(p. 171)**

LThD9 • Resonant laser ablation ion trap mass spectrometry: Recent applications for chemical analysis, Chris G. Gill, A. W. Garrett, P. H. Hemberger, N. S. Nogar, *Los Alamos National Laboratory.* Resonant laser ablation is a useful ionization mechanism for quadrupole ion trap mass spectrometry. Selective ionization for attogram range analytes, metal ion chemistry, and M^+ CI for chemical analysis are presented. **(p. 174)**

LThD10 • Particle sizing from multiwavelength frequency-domain measurements of photon migration, Joseph E. Pierce, Eva M. Sevick–Muraca, *Purdue Univ.* Multiwavelength, frequency-domain measurements of isotropic scattering coefficient for computation of particle size distributions are demonstrated for concentrated particulate suspensions. **(p. 177)**

LThD11 • Particle sizing using time-domain techniques of photon migration, Jeffrey Kao, Eva Sevick–Muraca, *Purdue Univ.* Work is in progress to measure the scattering coefficients of polydisperse media with use of photon migration techniques. From multiwavelength measurements particle size distributions can be extracted. **(p. 180)**

LThD12 • Mean orientation measurements of fibrous aerosols in atmospheric boundary layer turbulence, R. K. Newsom, C. W. Bruce, A. J. Jelinek, M. Thurston, *New Mexico State Univ. and Army Research Laboratory.* Optical measurements on a suspension of fibrous aerosols in the atmospheric boundary layer indicate a preference for horizontal orientation. The degree of orientation is shown to correlate strongly with independent measurements of the mean turbulent energy density. **(p. 183)**

LThD13 • Four-wave-mixing diagnostics of atmospheric regions with an excess of charged aerosol concentration, K. A. Boyarchuk, G. A. Lyakhov, Yu. P. Svirko, *General Physics Institute, Russia.* We show that the phenomenon of microwave-driven four-wave mixing may be used for remote sensing of atmospheric regions with an excess of charged aerosol concentration. **(p. 187)**

LThD14 • Extinction, absorption, and backscatter cross sections for homogeneous and coated fibrous aerosols at millimeter wavelengths, K. P. Gurton, C. W. Bruce, A. V. Jelinek, *US Army Research Laboratory/Battlefield Environment Directorate.* Several experimental techniques are developed to measure various optical properties for homogeneous and coated thin fibers at millimeter wavelengths. Results compared well with established theory. **(p. 190)**

LThD15 • Prognosis for a mid-infrared magnetic rotation spectrometer for the* in situ *detection of atmospheric free radicals, C. Chackerian, Jr., J. R. Podolske, *NASA–Ames Research Center;* T. A. Blake, *Battelle/PNL;* C. R. Mahon, *Space Physics Research Institute.* Magnetic rotation spectroscopy experiments on nitric oxide are modeled quantitatively. Verified theory is used to specify an instrument that can make *in situ* measurements on NO and NO_2 in the earth's atmosphere at a sensitivity level of a few pptv/sec. **(p. 193)**

LThD16 • On the use of line strengths in applied diatomic spectroscopy, James O. Hornkohl, Christian Parigger, James W. L. Lewis, *Univ. Tennessee Space Institute.* The theoretical aspects of the diatomic line strength and its practical realization, a line strength file, are reviewed with emphasis on applications in diatomic spectroscopy. **(p. 196)**

LThD17 • Diagnostics of boundary layer chemistry in an atmospheric pressure plasma, Thomas G. Owano, Edward H. Wahl, Charles H. Kruger, Richard N. Zare, *Stanford Univ.* Degenerate four-wave-mixing measurements of CH and C_2 radicals perform in the thin boundary layer of a diamond-growth substrate in a plasma CVD environment. **(p. 199)**

LThD18 • Spatial maps of analyte and Ar buffer gas atoms and ions by LIF and ICP-MS, B. Duersch, Y. B. Chen, P. B. Farnsworth, *Brigham Young Univ.;* A. C. Ciocan, *Institute of Atomic Physics, Romania.* Laser induced fluorescence as a selective and sensitive diagnostic tool is used for ion beam analysis downstream from the skimmer in an ICP-MS. Using selected spectral lines, analyte atoms and ions and Ar metastable atoms are measured for a range of ICP operating conditions, vacuum pressures and over a wide range of element's masses. The experiments are performed by optical probes which couple the radiation through optical fibers. Inside the vacuum chamber the optical probes are mounted on a computer-controlled xyz stage which allows spatial mapping of atoms and ions. **(p. 202)**

WINDSOR BALLROOM

7:30am–12:30pm
Registration

WINDSOR BALLROOM

8:00am–9:45am
LFA • Diagnostics of CVD Processes
Jay Jeffries, *SRI International, Presider*

8:00am (Invited)
LFA1 • Optical diagnostics of VUV laser CVD of semiconductors, M. Barth, J. Knobloch, P. Hess, *Univ. Heidelberg, Germany.* Laser CVD of amorphous semiconductors (a-Ge:H, a-Si:H) is studied at 193 nm and 157 nm. Nucleation and growth are monitored *in situ* by FTIR spectroscopy and spectroscopy ellipsometry. **(p. 206)**

8:30am
LFA2 • REMPI/TOF-MS diagnostics for monitoring CVD reactive intermediates, R. W. Shaw, *Oak Ridge National Laboratory;* L. L. Jones, C. S. Feigerle, *Univ. Tennessee.* Resonantly enhanced multiphoton ionization coupled with orifice sampling time-of-flight mass spectroscopy is used to monitor the chemical intermediates in a CVD diamond film growth reactor. **(p. 208)**

8:45am
LFA3 • Investigation of stagnation-flow diamond-forming flames using advanced laser diagnostics, Kenneth E. Bertagnolli, Robert P. Lucht, *Univ. Illinois–Urbana-Champaign.* Gas phase temperature and atomic hydrogen profiles are measured near the deposition substrate in an atmospheric pressure, stagnation-flow diamond-forming flame with use of laser diagnostics. **(p. 211)**

9:00am
LFA4 • Laser-induced fluorescence measurements of the distribution of C_3 in the plume of a dc arcjet during diamond deposition, George A. Raiche, Jay B. Jeffries, *SRI International.* The C_3 radical is observed by laser-induced fluorescence to be spatially distributed in a shell at the outer edge of the arcjet plume. In the boundary layer above the substrate the distribution becomes more uniform. **(p. 214)**

9:15am
LFA5 • Trace NO_x analysis by laser resonance-enhanced multiphoton ionization and photoacoustic spectrometry near 454 nm, R. C. Sausa, R. L. Pastel, *US Army Research Laboratory.* NO and NO_2 are analyzed by a laser-based technique with use of miniature electrodes and microphone. The effects of signal on concentration, pressure, and laser intensities are reported. **(p. 218)**

9:30am
LFA6 • Laser-induced chemistry within clusters, M. Z. Martin, S. R. Desai, C. S. Feigerle, J. C. Miller, *Oak Ridge National Laboratory and Univ. Tennessee.* Laser-induced chemistry within clusters is discussed. The clusters are produced in a supersonic expansion, photoionized with 266 nm light, and are detected by mass spectrometry. **(p. 221)**

WINDSOR BALLROOM

9:45am–10:15am
Coffee Break

WINDSOR BALLROOM

10:15am–12:15pm
LFB • Environmental and Surface Analysis
Timothy Harris, *AT&T Bell Laboratories, Presider*

10:15am (Invited)
LFB1 • Applications of acousto-optic tunable filters in environmental sensors, Xiaolu Wang, *Brimrose Corp. of America.* Various acousto-optic tunable filters based spectroscopic systems for applications in chemical analysis and environmental sensing are reviewed. **(p. 226)**

10:45am
LFB2 • Raman applications with all-silica fiber-optic probe, Yuan-Hsiang Lee, Sheng Dai, Jack P. Young, *Oak Ridge National Laboratory.* We describe our recent analytical applications of an all-silica fiber-optic probe and silver-doped sol-gel film for normal Raman and SERS measurements. **(p. 227)**

11:00am
LFB3 • Diode-laser-based detection of BTXE-aromatics in oil-polluted soil samples, W. Schade, T. Blanke, *Univ. Kiel, Germany.* The application of diode lasers and difference frequency generation in $AgGaS_2$ for the detection of BTXE-aromatics by absorption spectroscopy in the mid infrared is discussed. **(p. 229)**

11:15am
LFB4 • Resonant laser ablation: Applications and mechanistic aspects, J. E. Anderson, A. W. Garrett, C. G. Gill, P. H. Hemberger, N. S. Nogar, *Los Alamos National Laboratory;* T. M. Allen, P. B. Kelly, *UC–Davis.* Resonant laser ablation for depth profiling is described, along with absolute removal rates and detection limits. Possible mechanisms for low-power ablation are discussed. **(p. 232)**

11:30am
LFB5 • Quantitative surface analysis using photoionization of sputtered neutrals, Chun He, Christopher H. Becker, *SRI International.* We show that quantitative surface composition analysis at ppm of a monolayer can be achieved at laser power densities of 10^{14}–10^{15} W/cm^2. **(p. 235)**

11:45am
LFB6 • Characterization of semiconductor materials by the photoionization of sputtered neutrals using ultrahigh laser intensities, Michael L. Wise, Stephen W. Downey, *AT&T Bell Laboratories.* The characterization of semiconductor materials by the nonselective photoionization of sputtered species using ultrahigh laser intensities is discussed. **(p. 238)**

12:00m
LFB7 • Ultratrace analysis of calcium with high isotopic selectivity by resonance ionization mass spectrometry, B. A. Bushaw, F. Juston, W. Nörtershäuser, N. Trautmann, P. Voss-de-Haan, K. Wendt, *Univ. Mainz, Germany.* A RIMS method for ultratrace analysis of stable and long-lived calcium isotopes using diode lasers is presented, which reaches high isotopic selectivity and good overall efficiency. **(p. 241)**

12:15pm–12:30pm
Closing Remarks

Wednesday, March 20, 1996

Species Selective Detection Techniques

LWA 8:30 am-10:00 am
Windsor Ballroom

Robert Lucht, *Presider*
University of Illinois

NEW TRENDS IN ANALYTICAL ATOMIC LASER SPECTROSCOPY

James Winefordner, Department of Chemistry, University of Florida, Gainesville, FL 32611.

Recent advances in laser excited atomic fluorescence spectrometry (LEAFS) and laser excited ionization spectrometry (LEIS) will be discussed. In LEAFS, analytical studies using electrothermal atomization (ETA), inductively couple plasma (ICP) and glow discharge (GD) atom (ion) reservoirs will be stressed. The possibility of achieving very low detection limits will be discussed with respect to the noise sources. The theoretical efficiencies of detection and measurement will be given and will be discussed with respect to measurements near the single atom level. Similarly, in LEIS, analytical studies using flames and furnaces with optogalvanic detection will be stressed, although mass spectrometric detection will also be mentioned. The probabilities of very low detection limits will also be stressed and the theoretical efficiencies of detection and measurement will be given.

The figures of merit and the advantages and disadvantages of LEAFS and LEIS methods will be compared with respect to the big 3 conventional analytical methods, namely Electrothermal Atomization-Atomic Absorption Spectrometry (ETA-AAS), Inductively Coupled Plasma-Optical Emission Spectrometry (ICP-OES), and Inductively Coupled Plasma-Mass Spectrometry (ICP-MS). The figures of merit will include detection limits, relative standard deviations, linear range of response to concentration or amount, spectral and matrix interferences, generality of use, amount of sample required for analysis, and practical matters such as cost of equipment, cost of analysis, speed of analysis, etc.

A major emphasis will be placed on the future use, if any, of LEAFS, LEIS, and other laser-based methods for trace analysis of elements in samples. In addition, the speaker will compare the four quantitative approaches, calibration curve method, standardless additions method, standardless method and absolute method. The former two methods involve the use of standards and the 3rd method involves an occasional standard. The 4th method does not require standards. The latter two methods would have considerable use when standards are not available and can not be prepared. The LEAFS and LEIS methods have considerable potential for both the standardless and the absolute approaches.

Influence of Ambient Conditions on the Laser Air Spark

Serife Yalçin, David R. Crosley, Gregory P. Smith, and Gregory W. Faris
Molecular Physics Laboratory
SRI International
333 Ravenswood Avenue
Menlo Park, CA 94025
(415) 859-4131
FAX (415) 859-6196
FARIS@MPLVAX.SRI.COM

When a powerful laser pulse is focused in air, a bright, free-standing plasma is formed. By measuring the intensities of characteristic emission lines, elemental analysis can be performed in a manner similar to other emission-based techniques.[1] Like other optical emission-based analysis techniques, laser spark spectroscopy can provide rapid and simultaneous measurements of many elements at once. However, the laser spark has the additional ability to perform remote, in-situ, measurements. Also, the laser spark vaporizes molecules and small aerosols, allowing measurement of both gaseous and particulate phases. These abilities make the laser air spark an attractive technique for applications such as monitoring toxic metal emissions from incinerator or power plant stacks.

A key consideration for an in-situ technique is the ability to perform quantitative measurements. In-situ measurements are by their nature subject to variations in ambient conditions. To ascertain the usefulness of the laser air spark for quantitative, in-situ analysis, we are studying the effects of ambient conditions on the laser spark.

The primary parameters that may affect the strength of elemental emission lines in a plasma are the elemental concentration, the plasma temperature, the gas composition, and the electron density. In this paper, we examine the variation of the temperature and electron density with ambient conditions.

The plasma temperature and electron density may be measured by analyzing plasma emission. The ratios of emission lines can be used to determine the temperature using either the Boltzmann or Saha equations (for emission from the same or different ionization stages, respectively). We use the Saha equation for temperature measurement because the wider energy separation of the emitting levels provides better sensitivity to the temperatures in the laser air spark. We have developed a graphical analysis for the Saha equation which combines the multiple line advantages of the Boltzmann analysis with the wide energy spacing of a Saha analysis. The Saha equation requires knowledge of the electron density. Electron densities are measured from the Stark broadening of emission lines based on well-established theory.[2]

The experimental apparatus for our measurements is shown in Figure 1. The second harmonic radiation at 532 nm from a Q-switched Nd:YAG laser is focused with a 15 cm lens into a

cell at atmospheric pressure. Aerosols are produced using a nebulizer, and dried using a heater and condenser.[3] Plasma light is collected with either a pair of lenses or three mirrors and imaged onto the entrance slit of an imaging spectrometer. The dispersed light is detected with an intensified ccd camera. Gating of the intensifier allows measurements to be performed as a function of delay after the laser pulse. The camera can acquire images with wavelength in one direction and one spatial direction in the other. By taking spatially-resolved measurements across the transverse direction of the spark, the data are Abel-inverted to correct for the path integration through the spark and obtain radial distributions.

We have measured temperatures using a number of elements including nitrogen, oxygen, and magnesium. These all gave consistent results. Likewise, consistent results were obtained for electron densities derived from three different emission lines in hydrogen and nitrogen. These results give us confidence in the accuracy of our results.

We have examined the effects of various ambient conditions on the laser spark. These include the humidity, different gases, the presence of particles, and laser energy. We have found that the effects of these parameters result in temperature variations that are less than our experimental error for all of these conditions. The effect of laser energy on temperature is shown in Figure 2. A change in laser energy by a factor of over 3 results in no statistically significant change in temperature. We have found that the electron density varies by less than a factor of two for all of our experimental conditions.

The remarkable constancy of the laser spark conditions is a surprising and promising result. With a consistent plasma environment, there are very good prospects for obtaining quantitative, in-situ results from laser spark spectroscopy.

This research was supported by the U. S. Environmental Protection Agency. S. Yalçin was supported in part by the Scientific and Technical Research Council of Turkey (TUBITAK).

References

1. L. J. Radziemski and D. A. Cremers, "Spectochemical Analysis Using Laser Plasma Excitation," in *Laser-Induced Plasmas and Applications*, L. J. Radziemski and D. A. Cremers, Eds.(Marcell Dekker, New York, 1989), pp.295-325.
2. H. R. Griem, *Spectral Line Broadening in Plasmas* (Academic Press, New York, 1974).
3. Serife Yalçin, David R. Crosley, Gregory P. Smith, and Gregory W. Faris "Spectroscopic Characterization of Laser-Produced Plasmas for In-Situ Toxic Metal Monitoring," to appear in Journal of Hazardous Waste and Hazardous Materials, (1995).

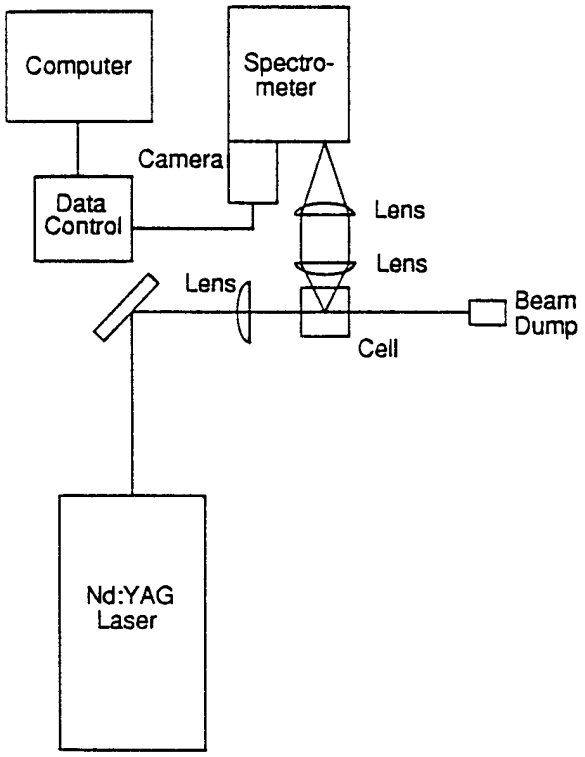

Figure 1. Experimental arrangement for laser spark spectroscopy.

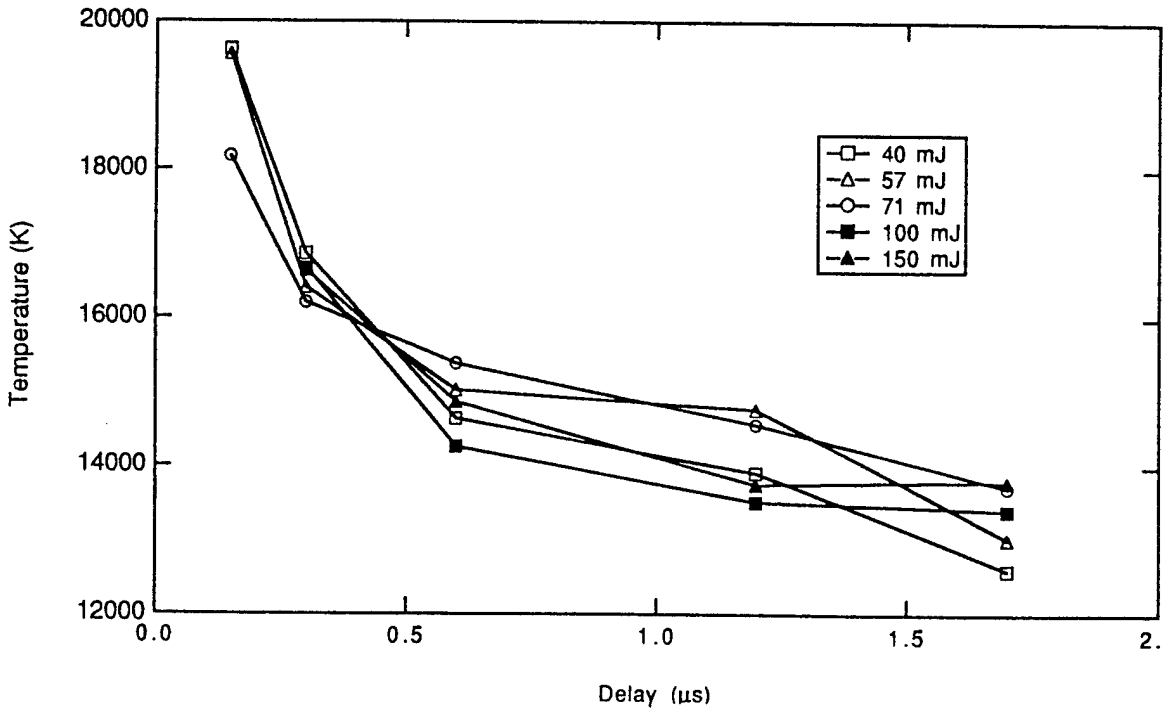

Figure 2. Variation in temperature as a function of laser energy and delay from the laser pulse.

Diode Laser Optogalvanic Spectroscopy for Uranium Isotopic Analysis: Analytical Figures of Merit

R. W Shaw, C. M. Barshick, J. P. Young, and J. M. Ramsey
Chemical and Analytical Sciences Division
Oak Ridge National Laboratory
Oak Ridge, TN 37831-6142

PHN: 423/574-4882
FAX: 423/574-8363

High resolution optogalvanic spectroscopy, excited using near-infrared semiconductor diode lasers, has been utilized for the determination of $^{235}U/^{238}U$ isotopic ratios for uranium and uranium compounds.[1,2] The samples ranged from depleted (0.27%) to enriched (20%) ^{235}U abundance. The goal of this effort has been to develop a technique that is suitable for use in the field for measurements at moderate precision. Glow discharge sampling can be conveniently accomplished in such settings, and diode lasers are sufficiently rugged and simple for incorporation into routine instruments. The concept of using high resolution optogalvanic spectroscopy for isotopic analysis has been also considered by Keller[3], Tong[4], Niemax[5], and Edelson.[6]

Samples were prepared as demountable hollow cathodes by pressing the powder to be analyzed with silver powder, using a press similar to that used for fabrication of KBr pellets for IR spectroscopy. The incorporation of silver powder resulted in conducting sample cathodes even for the case of insulating samples. In some cases, tantalum powder was included in an attempt to getter discharge gas impurities that could lead to formation of small molecules and hence limit the detection sensitivity for atoms. The sample cathodes were mounted in a discharge cell constructed using standard metal gasket vacuum chamber components. A dc discharge was struck in argon fill gas at 8 Torr. The outputs from wavelength-stabilized GaAlAs lasers were mechanically chopped, focused through the sample hollow cathode, and tuned to uranium transitions. The lines were selected for origination from low-lying energy levels, strong oscillator strengths, and large isotope shifts. The ac component of the cathode voltage was processed using a digital lock-in amplifier. Any technique (cell cooling,

feed gas purification, or incorporation of in-cell getters) that removed contaminant gases from the discharge served to improve the signal strength observed.

The 776.19, 778.42, and 831.84 nm uranium lines were examined. In each case, the laser wavelength was scanned over a range encompassing the signatures of the isotopes, and the resulting spectrum was processed by determining the areas under the respective isotope profiles. The Doppler-broadened spectral linewidth observed was < 1 GHz; this was sufficiently narrow for isotopic analysis, in that the isotope shifts for these lines range up to 12.6 GHz. Laser powers ranged from a few to 150 milliwatts. Practical devices for assuring that the operating wavelength was correct (i.e., a laser mode hop or some operational drift had not occurred) have been evaluated.

The method accuracy and precision were measured. Using the 776 nm line and five samples (different isotopic abundances and different chemical compositions), the accuracy was found to range from 2-3% for an enriched sample, to 30% error at depleted abundance. Thermal ionization mass spectrometry was used to benchmark the optogalvanic results. The analytical working curve exhibited excellent linearity with a 0.9998 correlation coefficient.

Analytical Working Curve for the Isotopic Analysis of Four Uranium Samples

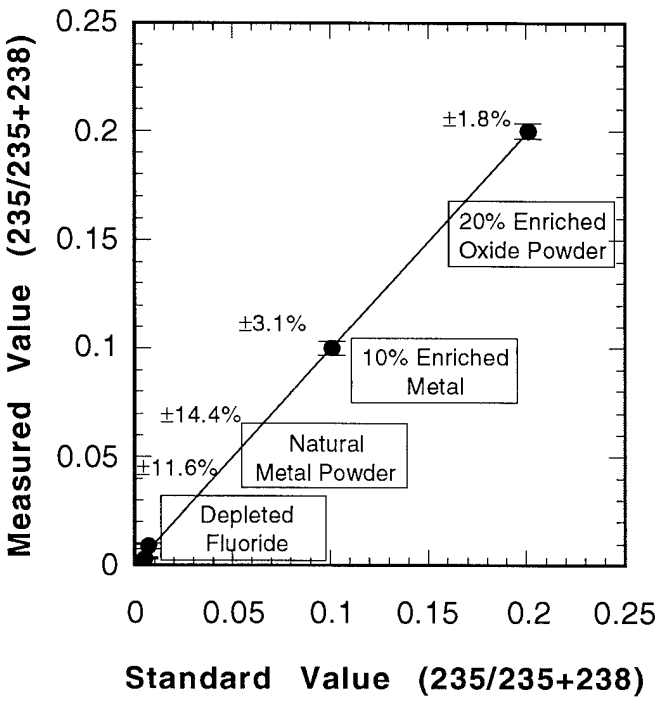

The samples included metal powder, uranium tetrafluoride, and uranium oxide. The latter was originally thought to be problematic in that this tenacious oxide would not dissociate efficiently to yield atoms for measurement; however, the signal strength for oxide samples was only reduced by approximately five-fold, compared to that for metals.

Run-to-run, day-to-day, and sample-to-sample precisions were determined using the 20% enriched oxide sample. The run-to-run precision ranged from ±2 to ±5% RSD, and the day-to-day precision was ±2.6% RSD. The sample-to-sample precision (three different cathodes) was ±3.5 % RSD. Using the 832 nm line where a 150 mW laser was available, the accuracy and precision for a measurement of the depleted metal sample improved to 3.7% and ±8%, respectively.

References:

1. C. M. Barshick, R. W. Shaw, J. P. Young, and J. M. Ramsey; *Anal. Chem.* **1994**, *66*, 4154.

2. C. M. Barshick, R. W. Shaw, J. P. Young, and J. M. Ramsey; *Anal. Chem.* **1995**, *67*, 3814.

3. R. A. Keller, R. Engleman, Jr., E. F. Zalewski; *J. Opt. Soc. Amer.* **1979**, *69*, 738.

4. W. G. Tong and E. S. Yeung; *Talanta* **1984**, *31*, 659.

5. J. Lawrenz, A. Obrebski, and K. Niemax; *Anal.Chem.* **1987**, *59*, 1232.

6. R. J. Lipert, S. C. Lee, M. C. Edelson; *Appl. Spectrosc.* **1992**, *46*, 1307.

Element selective detection in chromatography by diode laser modulation spectrometry

Kay Niemax and Aleksandr Zybin
Institute of Physics, University of Hohenheim, Garbenstr. 30, D-70599 Stuttgart, Germany; phone +49-711-459-2150, fax: +49-711-459-2461, E-mail: niemax@uni-hohenheim.de
Christoph Schnürer-Patschan and Henning Groll
LaserSpec Analytik GmbH, Frankfurter Ring 193a, D-80807 München, Germany; phone +49-89-3246440, fax: +49-89-32464410

Introduction

Diode lasers of the AlGaAs and InGaAsP types are small and easy to operate systems. Their wavelength can be tuned by temperature and by diode current. In particular, the possibility of very rapid tuning by current is important for wavelength modulation spectrometry which allows to suppress the 1/f noise, for example, in absorption measurements. The still limited wavelength range of operation of commercially available laser diodes ($625 < \lambda < 1600$ nm) can be partly overcome by frequency doubling of laser radiation (SHG) in non-linear crystals. The power of diode laser wavelength modulation atomic absorption spectrometry (DL-WMAAS) has been demonstrated recently by AAS measurements in graphite tube atomizers[1], analytical flames[2] and low pressure plasmas[3]. The present contribution reports on the application of this technique for element selective detection in analytical flames and low-pressure plasmas coupled to HPLC and GC, respectively.

Experiment

Laser diodes from Hitachi and Sharp with laser powers up to 50 mW were operated by commercial power supplies (producers: Profile and Melles Griot). The laser diodes were tuned by temperature to the absorption wavelengths of the analytes. Typical stabilities of the optical frequency of about $\pm$25 MHz were obtained at fixed temperature. Additionally to the dc operating current a sinusoidal current (kHz-range) was modulating the wavelength of the lasers. The modulation amplitudes corresponded the widths of the absorption lines. The fundamental radiation of the laser diodes or, after SHG in $LiIO_3$, the frequency doubled radiation passed the absorption volume and was detected either by a photodiode or a photomultiplier. The signals were amplified at 2f of the modulation frequency using commercial lock-in amplifiers.

In the first part of the experiment, Cr(III) and Cr(VI) species were separated in a commercial high-pressure liquid chromatoraph (HPLC) and introduced by hydraulic high-pressure

nebulization (HHPN) into an analytical flame normally used in a commercial AAS spectrometers. The experimental arrangement is shown schematically in the upper part of Fig. 1. The absorption measurements of chromium were performed with frequency doubled radiation (SHG) at 425.44nm.

In the second part, haloginated hydrocarbons were seperated by a gas chromatograph (GC) and introduced to a low-pressure helium microwave induced plasma (MIP). The molecular components were dissociated in the plasma, and the population densities of chlorine and bromine in metastable states were probed by DL-WMAAS at 837.60 and 827.24 nm, respectively. In order to suppress optical interference effects in the optical path, the MIP was also modulated (pulse mode, f_{MIP}=5 kHz). The absorption signal was detected at 2f-f_{MIP}.

Results

Fig. 1 shows chromatograms of deionized water spiked with different amounts of Cr(III) and Cr(VI). Comparable results were obtained with spiked drinking water. The detection limits of about 0.5 ng/ml were found for Cr(VI). Detection limits of the same order of magnitude have been found by other techniques. However, these thechniques are more complex and expensive than the present method. For example, a detection limit of 4 ng/ml was found for both chromium species using ICP-MS detection after separation by HPLC[5].

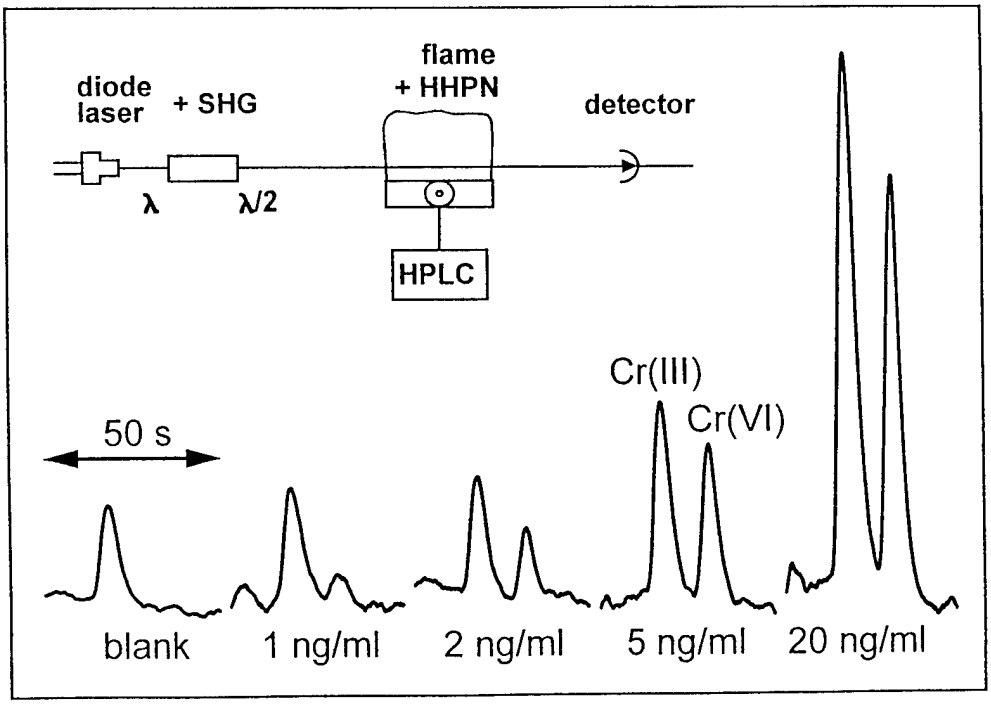

Fig. 1: DL-WMAAS measurements of Cr(III) and Cr(VI) in a air-acetylene flame after separation by HPLC. The experimental arrangement is shown in the upper part.

Fig. 2 displays chromatograms of a haloform solution. The chlorine signal is shown in the upper trace of the figure, while the lower trace was measured on the bromium line. Note, that the measurable absorbance is about 10^{-7}. The detection limits of chlorine were found to be about 0.12 pgs^{-1}, while 4 pgs^{-1} was found for bromine. In particular for chlorine, the present detection limits by DL-WMAAS are about a factor of 20-40 better than the typical detection limits of commercial element selective emission detectors.

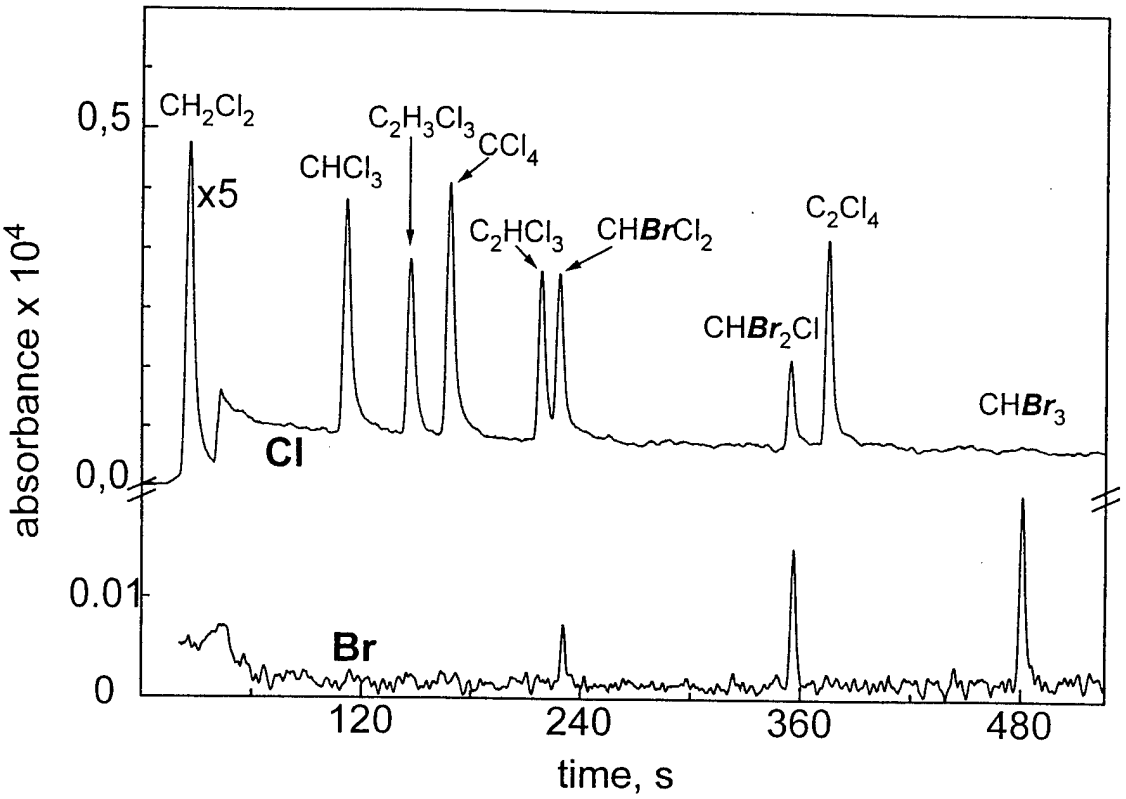

Fig. 2: Chromatograms of diluted haloform mixtures measured by DL-WMAAS of chlorine (upper trace) and bromine (lower trace)

References

1. C. Schnürer-Patschan, A.Zybin, H. Groll and K. Niemax, JAAS **8** (1993) 1103.
2. H. Groll, C. Schnürer-Patschan, Yu. Kuritsyn and K. Niemax, Spectrochim.Acta **49B** (1994) 1463.
3. A. Zybin, C. Schnürer-Patschan and K. Niemax, Spectrochim.Acta **48B** (1993) 1713.
4. N. Jakubowski, I. Feldmann, D. Stüwer and H. Berndt, Spectrochim.Acta **47B** (1992) 119.

Diode Laser Absorption Spectroscopy of Combustion Gases Near 1.57 Microns

David M. Sonnenfroh and Mark G. Allen
Physical Sciences Inc.
20 New England Business Center
Andover, MA 01810
t: 508.689.0003 f: 508.689.3232 e-mail: allen@psicorp.com

Sensors for rapid, *in-situ* measurements of hydrocarbon combustion intermediates and products are required for applications ranging from advanced combustor testing to aeropropulsion engine health monitoring. Recent developments in room temperature diode laser technology and sensitive detection strategies now permit development of a new class of combustion sensors for simultaneous measurements of the speciation of the combustion gases as well as gasdynamic performance parameters of interest, including temperature, velocity, and mass flux.[1,2] This work focusses on absorption measurements of CO, CO_2, H_2O, and OH in combustion gases near 1.57 μm. Experiments are conducted in low-pressure, room-temperature absorption cells and combustion gases of a flat-flame burner with hydrogen and methane fuels. The laser source is a New Focus Model 6262 external cavity diode laser, generating over 1 mW of output power across an 80 nm tuning range centered at 1.55 μm. High sensitivity detection is achieved using a dual-beam, Balanced Ratiometric Detector (BRD)[1] which cancels common-mode laser amplitude noise in the signal channel (passing through the absorbing medium) and reference channel (passing through a non-absorbing gas or fiber).

The solid line in Figure 1 shows an example survey spectrum of 0.067 atm of CO and 0.055 atm of CO_2 in a 50 cm absorption cell. The spectrum was obtained by scanning the laser and detecting the transmission through the cell using a high-pass filter on the output of the BRD. The resulting spectrum shows a derivative-like character and displays portions of the R-branches of the CO (3,0) and the $CO_2(3\nu_1+\nu_3)$ bands. The experimental data are compared to a HITRAN simulation, showing good agreement with the line positions and strengths. This spectral region is particularly interesting due to the coincidence of these CO and CO_2 transitions, as well as neighboring hot-band transitions of H_2O and OH. A single Distributed FeedBack (DFB) laser source may be capable of monitoring all four species.

High temperature measurements are performed in the combustion gases above a flat-flame burner, providing access to a wide range of near-equilibrium gas compositions and temperatures. Shroud flows of N_2 are used to isolate the combustion gases from room air. To increase the absorption strength across the 2.54 cm burner, a multi-pass Herriot cell is used in the signal leg to provide 28 passes over the burner and a total absorption pathlength of 71 cm. For measurements of the concentration of individual species in the gases, the laser is scanned at 100 Hz over the maximum range of a small piezo-electric transducer attached to the cavity end

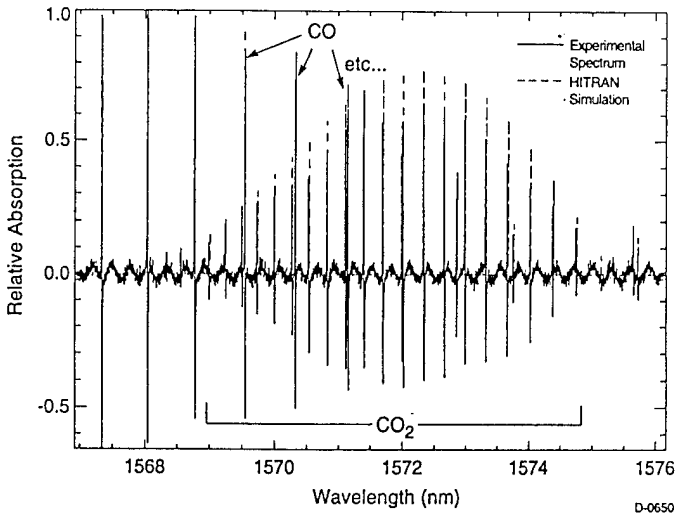

Figure 1. Comparison of experimental and HITRAN simulation of R-branches of the CO (3,0) and the $CO_2(3\nu_1+\nu_3)$ bands. The spectrum was recorded in a single pass through a 50 cm cell filled with 0.067 atm of CO and 0.055 atm of CO_2.

mirror. This results in a scan of 0.69 cm^{-1}, large enough to encompass the entire transition linestrength in the high temperature, atmospheric pressure gases. The lineshape is recorded and integrated to yield a quantity proportional to the product of the number density and linestrength. Temperature corrections to the linestrength are estimated using adiabatic flame temperatures at the metered flame stoichiometry.

Figure 2 is an example of the measured variation of the CO mole-fraction in a methane-air flame as a function of stoichiometry. The data were obtained using the R18 transition at 1.5617 μm and are compared to equilibrium CO mole-fractions calculated at the adiabatic flame temperature and stoichiometry. The experimental data shows the expected increase in measured

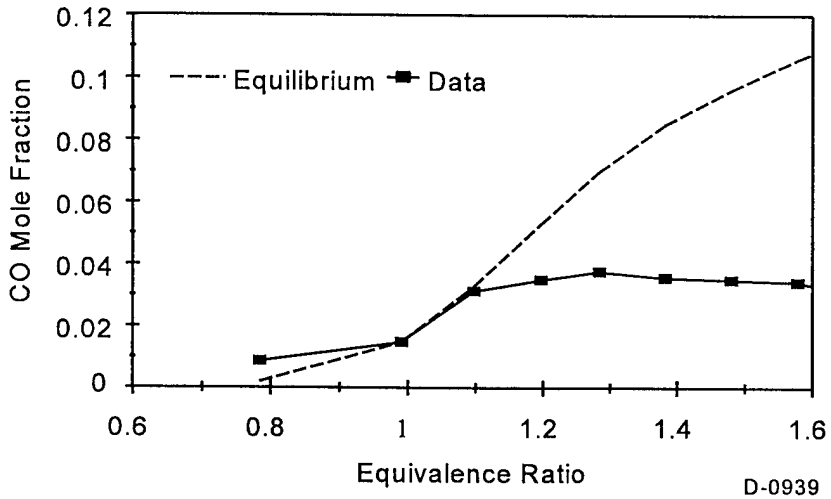

Figure 2. Comparison of measured CO mole-fraction to calculated equilibrium values as a function of methane-air flame stoichiometry.

CO concentration with stoichiometry, although the trend is not in good agreement with equilibrium predictions. Whether this is due to non-equilibrium conditions of systematic experimental errors is uncertain at present. Much of this uncertainty is attributed to interference from dense hot H_2O transitions which complicate the baseline subtraction procedures used to isolate the integrated lineshape. Unfortunately, no published data is available detailing these H_2O transitions and further work is required to characterize the high temperature absorption spectrum in this wavelength regions.

The hydroxyl radical (OH) is of interest in combustion studies and possesses (2,0) band overtone transitions in this spectral region. Figure 3 shows example lineshapes of the P10.5 transition at 1.5562 μm recorded in the methane-air flame at several stoichiometries. As expected, the OH signal peaks on the lean side of stoichiometric combustion and disappears under rich conditions. In addition to direct OH concentration measurements, the ability to detect OH in flame gases using simple diode laser sources is attractive for thermometry applications. We have also detected the first hot-band of this transition in the combustion gases. Due to its large vibrational energy spacing, two-line absorption techniques probing $v'' = 0$ and 1 may yield improved accuracy in flame temperature measurements compared to techniques based on H_2O absorption.[2]

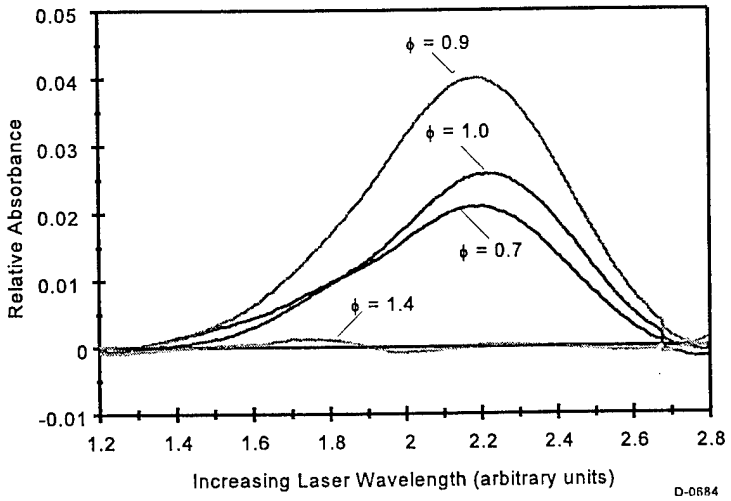

Figure 3. Example OH lineshapes measurements in methane-air combustion gases. The measurements were obtained using the P10.5 transition of the (2,0) band near 1.5562 μm.

1. Allen, M.G., Carleton, K.L., Davis, S.J., Kessler, W.J., Otis, C.E., Palombo, D., and Sonnenfroh, D.M., "Ultra-Sensitive Dual-Beam Absorption and Gain Spectroscopy: Applications for Near-IR and Visible Diode Laser Sensors," *App. Opt.* **34**(18), pp. 3240-3249, 1995.

2. Allen, M.G., Davis, S.J., Kessler, W.J., Palombo, D.A., and Sonnenfroh, D.M., "Diode Laser Instrumentation for Aeropropulsion Applications," Paper No. 95-0427, AIAA 33rd Aerospace Sciences Meeting, 1995.

Wednesday, March 20, 1996

Environmental Sensing I and Single Molecule Detection

LWB 10:30 am-12:30 pm
Windsor Ballroom

Kevin McNesby, *Presider*
US Army Research Laboratory

Laser-Based Sensors for Environmental Analysis

T. Vo-Dinh
Oak Ridge National Laboratory

Summary not available.

An In-Line Photoacoustic Sensor for Environmental Monitoring in Water

S.S. Freeborn, J. Hannigan and H.A. MacKenzie
Department of Physics, Heriot-Watt University,
Riccarton Campus, Currie, Edinburgh, EH14 4AS, Scotland, UK.
Tel.: (+44) 131 451 3053 Fax.: (+44) 131 451 3136

F. Greig
Department of Electrical, Electronic and Computer Engineering, Napier University,
219 Colinton Road, Edinburgh, EH14 1DJ, Scotland, UK.
Tel.: (+44) 131 455 4373 Fax.: (+44) 131 455 4231

Introduction

During the operation of offshore production platforms, sea contamination occurs from leakage, spillage and from the overboard discharge of produced water. Produced water is the terminology applied to water which is obtained during oil production from two main sources. These are naturally from within the oil reservoirs and from sea water used in the oil recovery process. Legislative limits are set in the most of the major oil production regions world wide. These limits vary from region to region but are generally set between 15ppm and 40ppm for dispersed hydrocarbon concentration in water. The volumes of produced water are exceeding that of crude oil production in many offshore oil fields, such as in the North Sea fields to the north-east of the U.K. where in 1994 for a total crude oil production of 114.4 million tonnes, 147 million tonnes of water was produced, the majority of which was discharged back into the sea. The volumes of oil discharged within produced water are the single greatest source of oil contamination from oil production facilities in the North Sea and with similar situations replicated world wide represents a global concern to sensitive marine environments.

The present methods for the detection of oil in produced water are based either on chemical analysis of intermittent samples or bypass pipelines with instrumentation to detect either dissolved or dispersed hydrocarbons by a variety of optical techniques including absorption, scattering and fluorescence. Tests in the U.K. on a range of commercially available instruments have shown that no single one entirely meets either the present needs or satisfies the requirements of the more stringent future legislation which is likely to be introduced in the atmosphere of growing concern for our environment. New instrumentation is required to meet these needs and will require a specification to include both in-line and on-line operation and sensitive measurements on dissolved and dispersed hydrocarbons. The requirement for in-line operation introduces further complexities to the specification due to the optical scattering which can be introduced by sand and other sediments which could not be filtered, and from the high sample flow rates and turbulence which is introduced by the flow rate of $1ms^{-1}$ typically encountered in the discharge pipes.

To meet these needs a new generation of in-line systems for environmental monitoring are being developed based upon the Photoacoustic Spectroscopy technique. The instrumentation is being developed initially for the on-line monitoring of hydrocarbons in produced water but may also find application in the detection of oil and other pollutants in the open sea, rivers, lakes and sewage.

Technical Summary

The theory of pulsed laser Photoacoustic is well understood [1,2]. The technique is based upon the complex transformation from optical to acoustic energy and can offer several advantages over conventional spectroscopic techniques when operating in the near infrared spectral region.

When a pulse of light is absorbed by a liquid, the absorbed optical energy may be dissipated as heat which causes sudden local heating. The subsequent thermal expansion generates a pressure wave which can be detected

with a sensitive acoustic detector. This is a complex interaction in which the amplitude of the acoustic pulse is dependent on physical parameters of the medium including the specific heat, the thermal expansion coefficient, the velocity of sound and the optical absorption, along with the incident optical energy.

The combination of physical parameters does not favour a strong photoacoustic response for water and as a consequence a near infrared photoacoustic spectrum is comparatively weak. This means that analytes which are more responsive to the photoacoustic process can be more readily observed in aqueous systems than by conventional spectroscopy.

It has been demonstrated in the laboratory [3-5] that the photoacoustic technique has the sensitivity to measure both dissolved and dispersed hydrocarbons down to and below the legislative limit. An additional advantage of photoacoustic spectroscopy is a high immunity to optical scattering. Photoacoustics is an energy driven process which is not constrained by the geometrical requirements of conventional absorption spectroscopy. Even if the incoming radiation is scattered, the photoacoustic generation process continues with only minor changes in the magnitude of the acoustic signal. This immunity to scattering is important and means that both dissolved and emulsified components can be detected at comparable sensitivity with our oil in water sensor [6]. The photoacoustic process is also immune to background noise since the acoustic signal is at ultrasonic frequencies.

Instrumentation

Prototype in-line instrumentation has been developed utilising the recent availability of photonic devices and fibre optic components. The instrument consists of three main units viz. the measuring head, the optical and electrical sources and data processing module, and the display. Diode lasers are used as the light sources, miniature lenses are used throughout along with fibre optic components for optical delivery and energy monitoring of the light sources. The instrument has attained simple but rugged design to allow operation in harsh environments with the prospect of low maintenance requirements. In addition, the availability of low cost, compact computational power for fast data acquisition and analysis has resulted in a true "on-line" instrument specification.

Field Testing

The instrument has undergone field testing at the Orkney Water Test Centre (OWTC), Scotland, U.K., where its trend performance to changing hydrocarbon concentrations was successfully investigated. The instrument sensor head was inserted in a 4" pipeline with operating conditions similar to those encountered offshore. Figure 1 shows that the sensitivity was in the low ppm for the measurements on Flotta crude oil concentrations in sea water at ambient temperatures. The results obtained were found to be independent of sample flow rate and resultant turbulence by the introduction of flow rates as high as $1ms^{-1}$ without variation to the instruments response. This was expected due to the 'snap-shot', pulsed nature of the photoacoustic process. The instrument sensor head showed good ruggedness in the field when it returned to original response levels, immediately upon re-insertion into the sample stream after withstanding mechanical forces exerted upon it.

The instrument is now being developed towards a fully calibrated commercially based instrument for future blind testing at OWTC and for testing at an on-shore oil production facility.

Conclusion

The photoacoustic technique has been shown to be suitable for the monitoring of hydrocarbons in produced water. Prototype instrumentation has been developed utilising diode laser sources to meet the environmental needs, legislative requirements and technical challenges. Initial testing into the feasibility of using photoacoustic based instrumentation in field conditions has been successfully undertaken and will be followed by further testing. Although initial development is for the monitoring of hydrocarbons in water, the instrumentation has potential for the monitoring of other environmentally significant pollutants in aqueous systems.

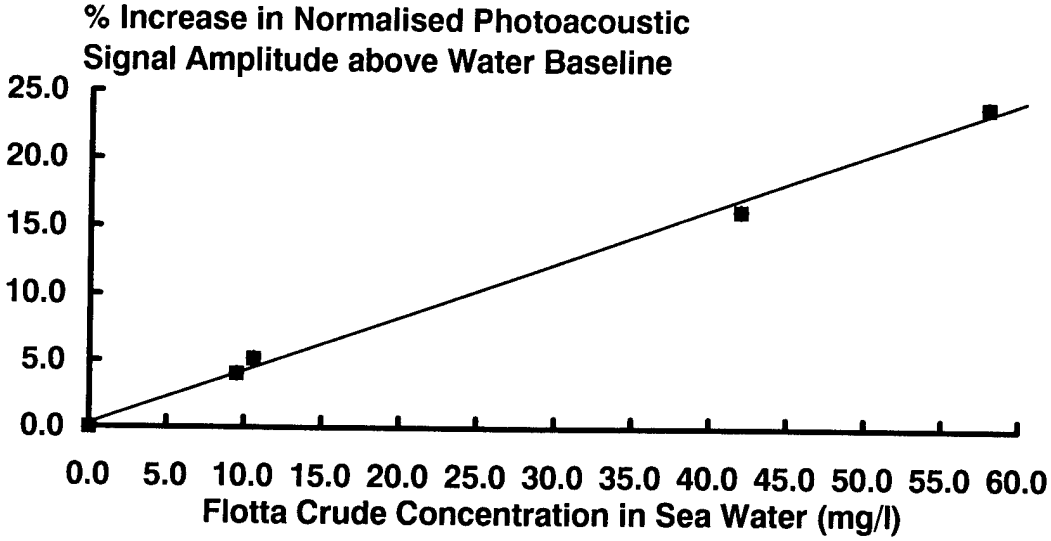

Figure 1 : Increase in sensor response above water baseline in field environment for concentrations of Flotta crude oil in sea water at ambient temperatures for a 904nm diode laser source. Error bars are contained within the symbols.

Acknowledgements

The authors would like to acknowledge the funding and support provided by Shell U.K. Exploration and Production, the Marine Technology Directorate (U.K.) and The Paul Instrument Fund (U.K.).

References

[1] Quan, K.M.; MacKenzie, H.A.; Hodgson, P.; Christison, G.B.; "Photoacoustic generation in liquids with low optical absorption"; Ultrasonics 32, 181, 1993.

[2] Lai, H.M. and Young, K.; "Theory of the pulsed optoacoustic technique"; J. Acoust. Soc. Am.; 72(6), 2000, 1982.

[3] Hodgson, P.; "The Detection of oil in water by near infrared pulsed photoacoustic spectroscopy"; Ph.D. Thesis, Physics Dept., Heriot-Watt University, 1994.

[4] Hodgson, P.; MacKenzie, H.A.; Christison, G.B.; Quan, K.M.; "Laser photoacoustic detection of organic analytes in aqueous media"; in 'Near infrared spectroscopy', Pub. Ellis Horwood, 1992.

[5] Hodgson, P.; Quan, K.M.; MacKenzie, H.A.; Freeborn, S.S.; Johnston, E.M.; Greig, F.; Binnie, T.D.; Hannigan, J.; "Application of Pulsed Laser Photoacoustic Sensors in Monitoring Oil Contamination in Water"; Sensors and Actuators B, 29 (1-3), 339, 1995.

[6] MacKenzie, H.A.; Christison, G.B.; Hodgson, P.; Blanc, D.; "A laser photoacoustic sensor for analyte detection in aqueous systems"; Sensors and Actuators, B, 11, 213, 1993.

Laser Induced Breakdown Spectroscopy (LIBS) for Real-Time Detection of Halon Alternative Agents

Cindy Williamson, Robert G. Daniel, Kevin L. McNesby,
Brad E. Forch, and Andrzej W. Miziolek
U.S. Army Research Laboratory
AMSRL - WT - PC
Aberdeen Proving Ground, Maryland 21005-5066
Ph: 410-278-6149 fax: 410-278-6150 email to rdaniel@arl.mil

INTRODUCTION: Laser induced breakdown spectroscopy (LIBS) is a variation on the method of spark spectroscopy in which the light from a pulsed laser is focused to produce the spark rather than an electric discharge. This technique (LIBS) has been largely developed at Los Alamos National Laboratory and shown to be useful for elemental analysis, concentration determination, or molecular species differentiation depending upon the experimental configuration.[1,2] The capability of determining concentration of analytes at high sensitivity gives LIBS an advantage over some other measurement techniques.

At the Army Research Laboratory, we are involved in the development and evaluation of LIBS as a real-time sensor of candidate Halon alternative agents for the Testing and Evaluation community in the Department of Defense. Presently there are no detectors available to measure in-situ and in real time the concentration distribution of a fire extinguishing agent within military fighting vehicles, aircraft , or vessels. A LIBS based sensor offers the possibility of meeting this important need.

EXPERIMENTAL: The experimental configuration for our laboratory LIBS system is relatively simple, and consists of the following components: a laser source, a sample introduction mechanism, light collection and detection equipment, and data processing chemometrics. Briefly, an optical spark is generated by focusing laser light in a region where the sample has been introduced. The light generated by the plasma is collected, dispersed, and detected, typically with a photomultiplier. Detection of the light with an OMA is available in out laboratory, but not presently in use. The detector output is then processed and stored for analysis.

The plasma for this study was produced by focusing the IR output of a Nd:YAG laser (Quanta

Ray DCR-2A). The pulse energy was typically 80 mJ and had a duration of 9 ns. The radiation was focused with a 100 mm f.l. lens approximately 1 mm above the top of a 0.125 inch (O.D.) tube used to introduce the sample to the plasma (see Figure 1). The sample is a diluted Halon alternative agent in air to represent a typical concentration during use in fire extinguishment. A shroud of argon flows around the sample to help maintain a nonturbulent flow of the sample in the sampling region. The agent and air flows are controlled by mass flow controllers (MKS or Tylan) and mixed just after the flow controllers. The diluted sample then travels through approximately 12 feet of 1/4 inch tubing to insure complete mixing. The total flow rate of the sample was between 1 and 10 L/min, with the majority of the experiments done at 10 L/min for consistency.

The plasma light is collected either with a fiber optic bundle or lenses and introduced to a 0.25 m monochromator (Spex Industries). The output of the monochromator is detected with a photomultiplier tube (9658R or C31034). Signal processing and time resolution of the plasma light is accomplished with a boxcar averager (SRS SR-250) interfaced to a personal computer. The atomic fluorine emission spectrum is collected by scanning the monochromator wavelength through the spectral region of interest, for fluorine this was approximately 615 to 710 nm. This region was chosen as there are no interfering transitions from other atomic species present in the plasma (O, N, C, or Cl). The limit of detection for fluorine has also been determined, as well as a study of the dependence of the signal on the concentration of the analyte.

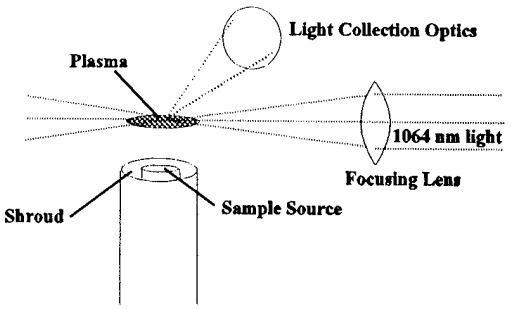

Figure 1. Schematic of plasma light source for the observation of atomic emission.

DISCUSSION: We have observed the atomic emission of fluorine present in an optical plasma generated by focused light from a Nd:YAG laser. A sample spectrum is shown in Figure 2. This information, coupled with the study performed on the signal strength as a function of analyte

concentration, allows LIBS to serve as a sensor for fluorinated compounds at levels of 50 ppm and greater. This sensitivity is much greater than that required by the T&E community (percent range), where the work is directed at how quickly and effectively the Halon alternative agent is dispersed into a region for fire extinguishment. With the appropriate placement of several sensors of this type, one should be able to map the introduction of a fluorinated agent into a complicated space, both spatially and temporally. It is this type of information which is required to judge the efficiency of the agent distribution system, and ultimately the fire protection system..

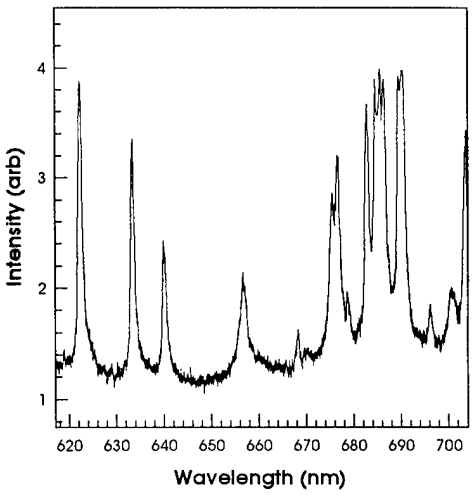

Figure 2. Sample spectrum of atomic fluorine emission collected from an optical plasma generated with focussed 1064 nm light.

At this time, work is continuing to include the detection of chlorine and to expand the number of fluorine containing compounds observed. The inclusion of a fiber optic bundle for the delivery of the radiation to the sampling site is also desirable to aid in the transfer of this technique to the T&E community.

References: Examples of LIBS

1. Cremers, D.A. and L.J. Radziemski, "Detection of Chlorine and Fluorine in Air by Laser-Induced Breakdown Spectrometry," *Anal. Chem.*, vol 55, p 1252, 1983.

2. Locke, R.J., J.B. Morris, B.E. Forch and A.W. Miziolek, "Ultraviolet Laser Microplasma - Gas Chromatography Detector: Detection of Species-Specific Fragment Emission," *Appl. Op.*, vol 29, p 4987, 1990.

DYNAMICS OF SINGLE MOLECULES AT ROOM TEMPERATURE.

H. Peter Lu and X. Sunney Xie,

Pacific Northwest National Laboratory, Environmental Molecular Sciences Laboratory, P.O. Box 999, Richland, WA 99352

Recent advances in fluorescence microscopy have made room temperature single molecule spectroscopy an active area of research. In this work, we investigate the room temperature spectral evolution of single sulforhodamine 101 molecules adsorbed on a silicate glass surface and covered by a PMMA polymer film. Single molecule emission spectra are taken and analyzed with a time resolution of 250 millisecond. Time correlation functions of single molecule spectral trajectories are obtained, with decay time constants inversely proportional to excitation intensities, demonstrating the spectral fluctuation is photo-induced in nature. A stochastic model is developed in order to account for the experimental observations. Understanding the origin of the spectral jumps encountered in the room temperature single molecule experiments is important for conducting further experiments to study chemical dynamics of single molecules in a variety of systems. The latest results of the further experiments will also be presented.

Increasing the Rate of Detection of Single Molecules in Solution

Lloyd M. Davis, Laurie E. Schneider, and Dennis H. Bunfield,
University of Tennessee Space Institute, Center for Laser Applications,
Tullahoma, TN 37388
Ph. (615) 393-7489, FAX (615) 454-2271, email:ldavis@utsi.edu

1. Introduction

Single molecule detection in solution offers the prospect of counting individual molecules within small quantities of sample for ultrasensitive chemical analysis [1] and of enabling new approaches for bio-technology applications, such as rapid DNA sequencing and the detection of rare fluorescently-labeled biomolecules. However, further developments in the techniques are required in order to move from the proof-of-principle experiments reported to date, to the level of capability required for realization of the applications. In particular, an increase in the rate at which single molecules can be efficiently detected is required.

For counting of individual molecules for chemical analysis, the volumetric sample processing rate must be increased if sample volumes of useful size are to be analyzed within a reasonable time. In this case, the cross-sectional area of the probe volume times the flow velocity, which equals the ratio of the probe volume to the mean transit time, should be large. This condition is just the opposite of that required for maximization of the signal-to-noise for single molecule detection, because large probe volumes give rise to greater background, and small transit times give less signal integration time. For the proposed rapid DNA sequencing scheme based on the detection and identification of individual tagged nucleotides that have been sequentially cleaved from a single DNA strand, it will be necessary to detect the single nucleotides before diffusional loss of order occurs. In this case, the time between cleavage and detection must be minimized, which once more dictates a fast flow velocity and hence small transit time. It is apparent that if these and other applications of single molecule detection are to be realized in the future, all practical techniques for increasing the rate of fluorescence photon acquisition and for signal-to-noise recovery should be investigated.

We are currently working on the use of time-gated photon counting at very high instantaneous count rates to decrease the time required for detection of each molecule, while maintaining the advantages of time-gating. Other published reports have demonstrated that single molecule detection can be achieved without time-gating, either by use of a very small sample volume ($\sim$ 0.5 fl) obtained with a high numerical aperture microscope objective and confocal epi-illumination [2], or by use of infrared excitation wavelengths, for which the noise due to Raman scatter from solvent molecules is significantly reduced [3]. Both of these approaches have merits for improving the signal-to-noise, but in each case there are also limitations: If the sample volume is too small, molecular transport through the volume is dominated by diffusion, and it will not be possible to constrict a stream of molecules to pass once (and only once) through the volume. At present there are no suitable infrared dye molecules that are chemically stable in aqueous solution, thereby disabling their use for most biochemical applications. Nevertheless, we are applying some of the advantages of these two approaches in our work, by evaluating the use of smaller sample volumes and longer excitation wavelengths.

2. Experimental Improvements

In our recently reported experiment [1], single molecules of sulforhodamine 101 in aqueous solution are efficiently detected as they pass from a 0.8 μm microcapillary injection tip into a sheath flow, which carries them through an elliptical cylindrical excitation volume of 1.9 pl with a mean transit time of 1.0 ms. Analytical calculations and Monte Carlo simulations [4] of the experiment indicated that the 0.8 μs dead time of the avalanche photodiode used in that work was the most significant factor limiting the time required for the detection of each

molecule. Although photomultiplier tubes exhibit considerably less dead time, use of a high quantum efficiency (> 0.6) avalanche photodiode (EG&G Canada SPCM-200) minimizes the number of molecular excitations required for detection and hence the photodegradation probability.

A new active-quenching circuit has recently been developed and custom modified for subnanosecond time-gated detection [5]. Best timing performance and background afterpulse rate is obtained with a dead time of 55 ns, which enables instantaneous photon count rates of up to 1.9×10^6 s^{-1} with only 10% loss due to pile-up. The previous experimental results were obtained at excitation intensities well below saturation, because of the high rate of promptly scattered photons from solvent molecules ($\sim 3 \times 10^5$ s^{-1}), which were removed by the time-gating circuit but nevertheless gave significant pile-up at the passively-quenched avalanche photodiode. The reduced dead time of the new actively-quenched detector enables higher laser intensities to be used, which in turn enables single molecules to be detected with shorter transit times and faster solution flow rates.

Our Monte Carlo simulation indicates that for faster sheath flow rates less diffusional spreading occurs over the same distance downstream from the microcapillary injector and hence efficient detection can still be accomplished with an excitation volume of smaller cross-section. Dilution of the sample in the sheath flow is reduced and the volumetric rate at which the sample is processed is increased. For our present experiments, we have accordingly reduced the excitation volume to ~ 0.25 pl while increasing the laser excitation intensity by a factor of ~ 5.

To accomplish single molecule detection within faster transit times and higher instantaneous fluorescence photon rates, we have replaced the end components of our data acquisition system. Previously a time-to-amplitude converter (TAC) with 2.5 μs dead time and an analog-to-digital converter with 1 μs conversion time were used to provide software controllable time-gating, while most of the Raman background was removed by a temporal prefilter (a subnanosecond anticoincidence circuit) with a dead time of ~ 10 ns. During the passage of a single molecule, the instantaneous rate of the counts that pass the prefilter was ~ 20 photons/1.0 ms and hence the 2.5 μs TAC dead time gave $< 5\%$ loss. For detection of molecules within shorter transit times, significantly higher instantaneous fluorescence rates occur. Therefore, the output signal from the temporal prefilter is connected directly to a 100 MHz multichannel scalar (Ortec ACE-MCS) and time-gating is accomplished solely by the hardware.

3. Results and Discussion

Fig. 1 shows results obtained in a bulk flow cell, without the capillary injector, under the following conditions: Laser power $P = 23$ mW; circular beam waist $\omega_0 = 3.5$ μm; spatial filter object space diameter = 6.7 μm; full molecular transit time obtained from flow speed and autocorrelation function $2\delta_t = 165$ μs; other parameters the same as in Table 1 of Ref. 1. The dwell time of the multichannel scalar is 50 μs and the data has been processed by a simple sliding sum filter with a bin time of 200 μs. The data represents a factor of 5 decrease in the time required to detect each molecule.

For the experimental parameters used, the peak excitation probability per laser pulse, which occurs when a molecule is in the center of the sample volume, is $P_{\text{excite}} = 0.44$. This indicates a moderate level of saturation of the absorption of the molecule. The mean number of excitations per molecule is ~ 4500, comparable to that in Ref. 1, and hence the burst amplitudes are of comparable size. However, the background noise is considerably reduced despite the higher laser power, because of the smaller sample volume and shorter integration time. To decrease the time required for detection of each molecule much below these results will require an increase in the overall optical throughput.

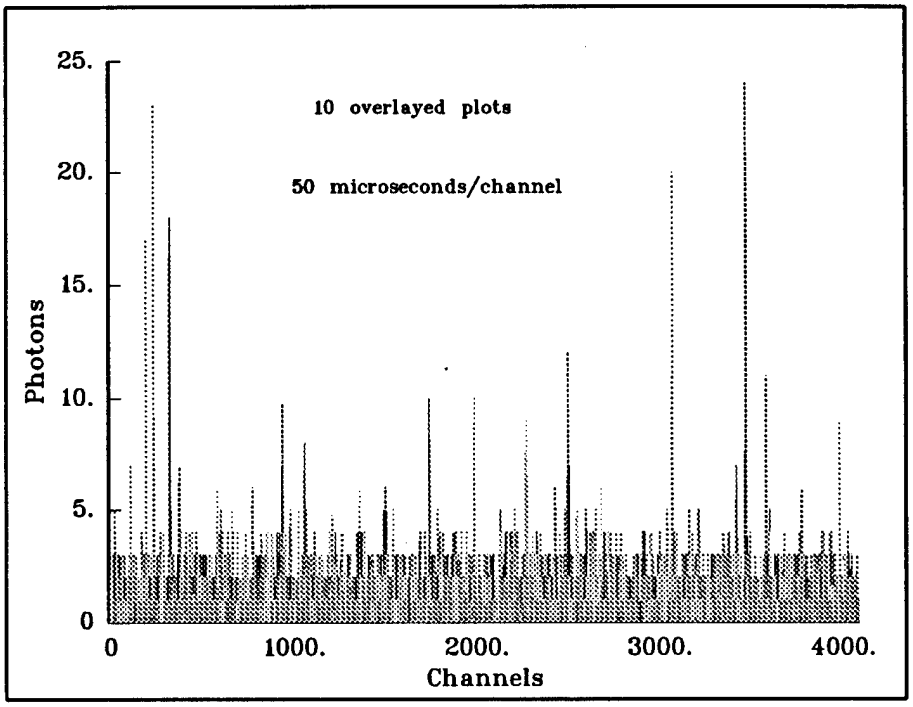

Figure 1: Photon bursts from single molecules of sulforhodamine 101

References

[1] L.Q. Li and L.M. Davis, "Rapid and efficient detection of single chromophore molecules in aqueous solution," Appl. Opt. **34**, 3208 (1995).

[2] M. Eigen and R. Rigler, "Sorting single molecules: Application to diagnostics and evolutionary biotechnology," Proc. Natl. Acad. Sci. USA **91**, 5740 (1994).

[3] Y.H. Lee, R.G. Maus, B.W. Smith, and J.D. Winefordner, "Laser-induced fluorescence detection of a single molecule in a capillary," Anal. Chem. **66**, 4142 (1994).

[4] L.M. Davis and L.Q. Li, "Monte Carlo model of a single molecule counting experiment," in *Laser Applications to Chemical Analysis*, 1994 Technical Digest Series, Vol. 5 (Optical Society of America, Washington, DC, 1994) pp.206-209.

[5] A. Spinelli, L.M. Davis, and H. Dautet, "Actively-quenched single photon avalanche diode for high repetition rate time-gated photon counting," *accepted for publication in* Rev. Sci. Instrum., *submitted* Sept. 20, 1995.

Photophysics of Surfactant Molecules in Microdroplets

M. D. Barnes, W. B. Whitten and J. M. Ramsey
Chemical and Analytical Sciences Division, Oak Ridge National Laboratory
Oak Ridge, Tennessee 37831-6142
Phone: 423/574-4923
Fax: 423/574-8363

S. Arnold
Microparticle Photophysics Laboratory, Polytechnic University
Brooklyn, New York 11021
Phone:708/260-3085

Over the last several years, the study of fluorescence properties in both time and frequency domain of atoms in micron-sized optical cavities has held considerable interest in the physics and quantum optics communities. In addition to fascinating purely scientific aspects of the phenomenon of cavity quantum electrodynamics (QED), the ability to modify molecular fluorescence properties in a microcavity offers potentially significant sensitivity advantages for ultrasensitive - or, single molecule - fluorescence detection. For example, two important quantities which limit sensitivity in single molecule fluorescence detection - the saturated absorption rate and the integrated fluorescence yield - can be significantly increased by enhancing the fluorescence decay rate. We have shown previously that fluorescence decay rates[1] as well as the integrated fluorescence yield[2] of rhodamine 6G can be significantly enhanced in glycerol microdroplets. However, exploitation of these effects in order to gain sensitivity in single molecule fluorescence detection is nontrivial for at least two important reasons. First, the magnitude of decay rate enhancement depends on the position of the molecule within the droplet; molecules near the center of the droplet are not coupled to high Q resonances while molecules near the surface may strongly interact with

cavity resonances associated with droplet. Thus, diffusion limits the amount of time a given molecule may interact with the resonances thereby limiting the fluorescence decay rate. Second, the fluorescence decay rate depends on the orientation of the transition moment with respect to the cavity "axis"; e.g., the surface normal for spherical cavities.

We describe how these problems can be alleviated through use of fluorescent surfactants in microdroplets.[3] As evidenced by fluorescence imaging of trapped microdroplets,[4] surfactant molecules may be naturally localized at the surface of liquid droplets due to the free energy discontinuity at the liquid-air boundary. The molecules are 'locked' to the surface of the droplet and cannot diffuse to the center where the coupling to droplet resonances essentially vanishes. Another important aspect of this scheme is that the transition dipole moments for surfactant molecules on the surface of the sphere are oriented *perpendicular* to the surface normal. We have examined fluorescence properties both in the time and frequency domain for such species in levitated glycerol microdroplets ranging in size from 3.5 to 30 μm in diameter. In sharp contrast with results from previous studies on homogeneously distributed dyes, we find significant deviation from "bulk" behavior at both extremes of the size range. For small droplets (< 6 μm diam.), the fluorescence decay rate is enhanced by a factor roughly proportional to 1/r; for larger sizes (>12 μm diam.), the apparent fluorescence decay rate is *smaller* than the bulk by a factor of about 30%.

The decay rate enhancement observed for the smaller droplets can be understood quantitatively in terms of a semiclassical model which includes spectral broadening effects (Ref 3). However, the anomalous decrease in the decay rate for larger sizes cannot currently be explained in the context of the same model since a bulk component in the fluorescence decay should have been (but was not) observed. This effect has been interpreted as a consequence of intermediate molecule-cavity coupling[5] in which the apparent fluorescence decay rate scales as 1/Q where Q is the quality factor of the resonance. Because the emission occurs preferentially into resonances independently of

size and the molecules cannot diffuse away from the surface, new optical effects related to single molecule quantum optics in spherical microparticles may be observable as well as enhanced sensitivity in single molecule detection.

REFERENCES

[1] M. D. Barnes, W. B. Whitten, S. Arnold, and J. M. Ramsey, J. Chem. Phys. **97**, 7842 (1992).

[2] M. D. Barnes, W. B. Whitten, and J. M. Ramsey, J. Opt. Soc. Am. B **11**, 1297 (1994).

[3] M. D. Barnes, C-Y. Kung, W. B. Whitten, J. M. Ramsey, S. Arnold, and S. Holler, Phys. Rev. Lett. *submitted*.

[4] S. Arnold, S. Holler, J. H. Li, A. Serpenguzel, W. F. Auffermann, and S. C. Hill, Optics Lett. **20**, 773 (1995).

[5] H. M. Lai, P. T. Leung, and K. Young, Phys. Rev. A **37**, 1597 (1988).

High-Speed Single Molecule Detection in Microdroplet Streams

N. Lermer, M. D. Barnes, C-Y. Kung, W. B. Whitten, J. M. Ramsey

Chemical and Analytical Sciences Division, Oak Ridge National Laboratory

Oak Ridge, Tennessee 37831-614

Phone: 423-574-1870

Fax: 423-574-8363

e-mail:Q24@ornl.gov

The detection of individual fluorescent molecules in liquids has been of great interest in recent years. Various fluorescence-based techniques shown to provide single molecule sensitivities include confocal microscopy [1], flow cell techniques [2], and levitated microdroplets [3]. The application of the microdroplet technique to single molecule detection offers many advantages. First, fluoresence decay rates and total fluoresence yield have been shown to be enhanced in glycerol microdroplets [4]. Additionally, the droplet confines the single fluorophore to a small volume thereby removing difficulties arising from diffusion of the fluorophore. Furthermore, the discrete detection unit of the droplet is ideally suited to the application of digital molecular detection for the analysis of ultradilute solutions [5]. Previous liquid microdroplet work has exhibited single molecule detection with signal-to-noise ratios in the range of 10-40 [3]. In our previous work, an electrodynamic trap was employed to trap glycerol microdroplets for a period much longer than the average photochemical lifetime, thus obtaining the maximum possible signal from the analyte. However, the application of digital molecular analysis to real systems requires tens of thousands of droplet measurements [5]; the time required to trap (and to size) the droplet in a levitated system prohibits its application in a high-speed molecular counting technique. In addition, many biological applications of single molecule fluorescence detection require aqueous samples. The present work discusses the development of an instrument designed to permit single molecule detection in water microdroplets at count rates in the range of 10 - 1000 Hz.

There are several aspects of high-speed fluorescence measurements in falling microdroplet streams which make it a considerably more difficult problem than single molecule detection in levitated droplets. First, the laser-analyte interaction time is, by experimental design, typically much shorter than the photochemical lifetime. This precludes observation of 'steps' in the fluorescence signal due to photobleaching as a means of identifying single molecule events. In a high-speed measurement scheme, the signal from each droplet consists of a *number*; single molecule fluorescence bursts must be distinguished from the blanks on the basis of statistical tests. This, of course, requires that photocount statistics for the blanks be well characterized with a minimum (*e.g.*, shot-noise limited) variance. Second, the signal is limited by laser-analyte interaction time; near saturation, the signal will be roughly proportional to $\Delta t/\tau_{fl}$, where Δt is the measurement time and τ_{fl} is the fluorescence lifetime. With typical photon detection efficiencies of the order of $\approx 10^{-3}$, integrated fluorescence signals are limited to ≤ 1000 counts.

Various approaches to achieving high-speed microdroplet fluorometry have been pursued in this laboratory. Initial work focused on the detection of fluorescence from a falling microdroplet passing through the cavity of an argon ion laser. The intracavity excitation source provided a high average power and a larger beam waist to extend the laser-droplet interaction time. However, the experimental design suffered from difficulties in the stability of the droplet and variation in the laser power. In the present work the stable and reproducible production and detection of microdroplets has been achieved by coupling a linear quadrupole trap to the output of a droplet generator. The droplet detection apparatus is shown in figure 1. A trap length of ~7cm prior to the laser interaction region cm allows the droplet to slow from an initial velocity of ~1m/s to a terminal velocity of ~2cm/sec. Preliminary tests have displayed a significant improvement in the positional stability of the droplets over earlier experimental configurations. A photodiode positioned to detect the forward scattered light passing through a focused HeNe laser exhibited a signal uniformity

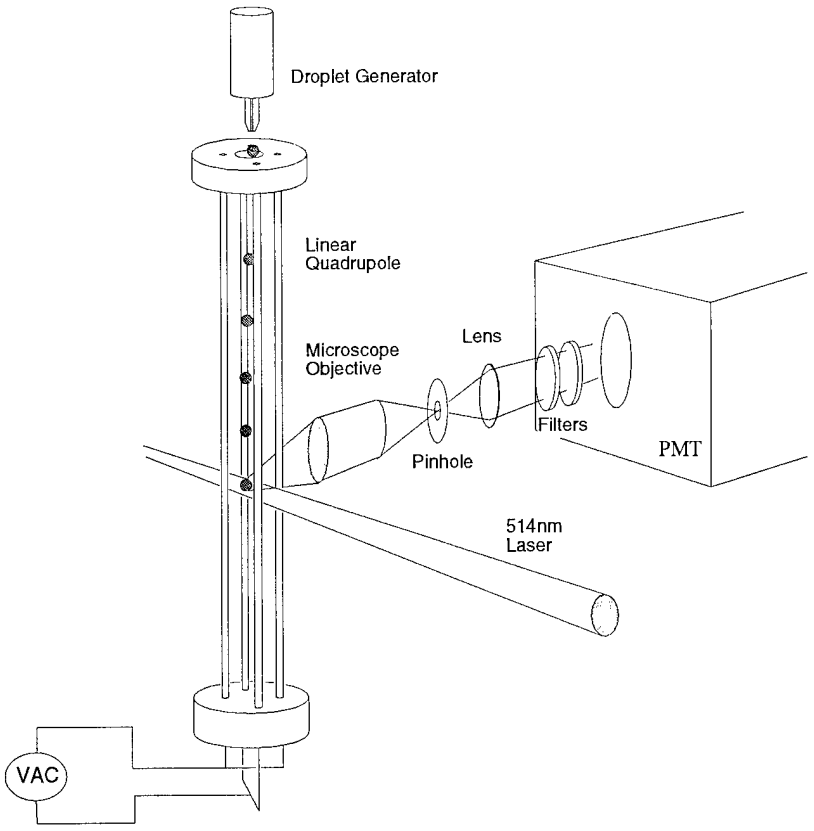

Figure 1. The falling microdroplet linear quadrupole / single molecule detection apparatus.

with less than 2% variation (one standard deviation). This level of stability is essential to discriminate the single molecule fluorescence signal from the background signal (primarily Raman scattering from the solvent). Work towards the goal of rapid single molecule fluorescence detection is in progress.

[1] S. Nie, D. T. Chiu, R. N. Zare, Science, **226** (1994) 1018
[2] See for example, E. B. Shera, N. K. Seitzinger, L. M. Davis, R. A. Keller, S. A. Soper, Chem. Phys. Lett., **174** (1990) 553; S. A. Soper, Q. L. Mattingly, P. Vegunta, Anal. Chem. **65** (1993) 740.
[3] M. D. Barnes, K. C. Ng, W. B. Whitten, J. M. Ramsey, Anal. Chem. **65** (1993) 2360.
[4] M. D. Barnes, W. B. Whitten, S. Arnold, J. M. Ramsey, J. Chem. Phys. **97** (1992) 7842; M. D. Barnes, W. B. Whitten, J. M. Ramsey, J. Opt. Soc. Am. B **11** (1994) 1297.
[5] K. C. Ng, W. B. Whitten, S. Arnold, J. M. Ramsey, Anal. Chem. **64** (1992) 2914.

Wednesday, March 20, 1996

New Developments in Laser Systems

LWC 7:00 pm-8:15 pm
Windsor Ballroom

Michael Winter, *Presider*
United Technologies Research Center

Frequency-Converted Diode Lasers for Analytical Applications

Douglas J. Bamford

Deacon Research

2440 Embarcadero Way

Palo Alto, CA 94303

Phone:(415) 493-6100

Fax:(415) 493-6493

For many analytical applications, a compact, inexpensive laser source is desired. Compactness is needed to move analytical techniques off the laboratory bench and into the real world, while low costs will place laser-based instrumentation within the reach of a larger community of users. Although room temperature diode lasers are small, cheap, and readily available today, they are limited to wavelengths between 0.6 microns and 1.8 microns. Intense efforts to develop new semiconductor lasers at wavelengths outside this range are underway, but these efforts are unlikely to pay off before the end of the century. In the meantime, light at wavelengths needed for analytical applications can be produced using the nonlinear frequency conversion of existing diode lasers.

Nonlinear frequency conversion techniques, such as frequency doubling, difference frequency generation, and optical parametric oscillation, are most commonly used with pulsed pump lasers having peak powers exceeding 1 MW. Since the pump lasers typically cost $100K or more, the nonlinear crystal used for the frequency conversion can cost $1K or more without significantly impacting the system cost. Extending these techniques to pumping by cw diode lasers with peak powers less than 1 W, while keeping the cost of the nonlinear crystal below the cost of the pump laser, requires a new type of nonlinear optical material.

During the past two years, tremendous progress has been made in the development of a new nonlinear optical material capable of efficient nonlinear frequency conversion of diode lasers: periodically poled lithium niobate (PPLN). The conversion efficiency is enhanced (relative to the base $LiNbO_3$ material) by specially patterning crystals of $LiNbO_3$ in a way which allows 90-

degree phasematching to be achieved at any set of wavelengths within the transparency range of the material. This technique, entitled "quasi-phase matching" (QPM) [1] allows nonlinear conversion through the d_{33} nonlinear coefficient, which is significantly larger than the d_{31} coefficient used for birefringent phase matching in the base material. To further increase the conversion efficiency, a waveguide can be formed near the surface of the sample to confine the input beam to a spot size of a few microns over the entire length of the crystal (1 cm or more). Because $LiNbO_3$ plays the same role in the electro-optics industry that silicon plays in the computer industry, procedures for producing waveguides are well-established [2]. High demand for the base material has led to ready availability at very low prices compared with other nonlinear optical materials. A 3" diameter wafer of this material, from which dozens of frequency converter chips can be fabricated, can be purchased for $150.

The key problem to be solved before devices based on PPLN can be made commercially available is the development of a reliable method of patterning the material. The ideal patterned structure is a series of rectangular bars, of equal length, in which the ferroelectric domains of adjacent bars point in opposite directions. The required period of the QPM structure ranges from 4 μ (for frequency doubling) to 30 μ (for difference frequency generation and optical parametric oscillation). During the past two years a technique called "electric field poling" has been shown capable of producing such structures. In our laboratory [3] and elsewhere [4], structures with nearly ideal geometries have been produced. Waveguides have then been fabricated on some of these structures, and nonlinear conversion demonstrations are now being carried out.

During this talk, we will review the current status of frequency-converted diode laser sources based on PPLN. This review will encompass both UV/visible sources based on frequency doubling and IR sources based on difference frequency generation and optical parametric oscillation. The performance to be expected from these light sources will be estimated. Implications of these developments for laser-based chemical analysis will be discussed.

References:

1. M.M. Fejer, G.A. Magel, D.H. Jundt, and R.L. Byer, "Quasi-Phase-Matched Second Harmonic Generation: Tuning and Tolerances", *IEEE Journal of Quantum Electronics*, Vol. 28, No. 11, p. 2631-2654, 1992.

2. H. Nishihara, M. Haruna, and T. Suhara, *Optical Integrated Circuits* (McGraw-Hill, New York, 1989).

3. W.K. Bischel, S.J. Field, D.J. Bamford, M.J. Dyer, and D.A.G. Deacon, "Bulk Poling of Lithium Niobate for Frequency Conversion Applications", *SPIE*, Vol. 2397, p. 363-372, 1995.

4. L.E. Myers, G.D. Miller, R.C. Eckardt, M.M. Fejer, and R.L. Byer, "Quasi-Phasematched 1.064 μm-Pumped Optical Parametric Oscillator in Bulk Periodically Poled $LiNbO_3$", *Optics Letters*, Vol. 20, No. 1, p. 52-54, 1995.

Passively Q-Switched Microchip Lasers for Environmental Monitoring

J. J. Zayhowski and Bernadette Johnson

Lincoln Laboratory, Massachusetts Institute of Technology
244 Wood Street, Lexington, MA 02173-9108

Introduction

The need exists for sensors capable of measuring soil, groundwater, and airborne pollutants without laborious sample collection and analysis. Single-wavelength transmission, differential absorption, laser-induced fluorescence (LIF), stimulated Raman scattering, and laser-induced breakdown spectroscopy (LIBS) are all highly sensitive methods for providing quantitative values of concentrations of chemical species. These optical techniques have been proven to provide high sensitivity and chemical selectivity for a large number of the materials on the EPA's priority pollutant list.

In recent years, remote optical measurements have been performed via optical fibers [1] – [4]. For many applications of interest, the wavelengths that provide the highest sensitivity are those for which the strongest absorption lines exist or that have the largest scattering cross section. In fields as diverse as hydrocarbon and pollutant monitoring of soil and groundwater, and smokestack effluent monitoring of polycyclic aromatic compounds, the optimum wavelengths lie in the ultraviolet (UV) region of the spectrum. Current UV schemes utilize a pulsed UV laser at the source and deliver the interrogating laser pulse to the remote region via an optical fiber. Unfortunately, optical fibers transmit poorly in the UV spectral region and powerful lasers are required to provide sufficient energy at the fiber's distal end to ensure adequate detection sensitivity. In addition, the sensitivity is critically dependent on the fiber length.

An approach that overcomes these limitations, developed at MIT's Lincoln Laboratory, uses a multimode silica fiber to transmit near-infrared diode-laser radiation to a remote passively Q-switched microchip laser and a set of nonlinear optical crystals. The laser and crystals efficiently convert the cw (continuous-wave) pump photons into infrared, visible, and/or ultraviolet laser pulses with wavelengths selected for efficient detection of contaminants. We have already demonstrated the ability of this novel laser-probe technology to detect subsurface petroleum-derived aromatic compound, including the BTEX species (benzene, toluene, ethylbenzene, xylene), using 266-nm radiation derived from the fourth harmonic of the 1064-nm Nd:YAG laser line. We have also demonstrated that the power at the fundamental frequency of this device (1064-nm) is sufficient to perform laser-induced breakdown spectroscopy (LIBS) for the detection and identification of heavy-metal contaminants (e.g. Pb, Hg, Cd, Cr, Zn). Work is underway to develop laser-based Raman probes for the detection of chlorinated compounds (e.g. CCl_4, CH_3CCl_3), and a laser-based subsurface NO_x detector for the detection of energetic contaminants (e.g. TNT, RDX, HMX).

Passively Q-Switched Microchip Lasers

The heart of the fiber-based sensors developed at Lincoln Laboratory is the passively Q-switched microchip laser (U.S. Patent 5,394,413) [5]. This laser is constructed by bonding a thin, flat wafer of gain medium to a thin, flat wafer of solid-state saturable absorber. The composite structure is dielectrically coated and diced into small pieces, creating laser cavities that are typically 1 mm long and 1 mm across. The infrared device is completed by bonding this laser cavity to the end of an optical fiber. A diode laser coupled to the opposite end of the fiber provides the optical power to energize, or "pump" the device.

The principle behind the operation of a passively Q-switched laser is that the presence of a saturable absorber within the laser cavity prevents the onset of lasing until the average inversion density within the cavity reaches a critical value. The onset of lasing, at this point, produces a high intracavity optical field which quickly saturates, or bleaches, the sat-

λ (nm)	1064	532	355	266	213
E_p (μJ)	8	3.5	0.3	0.7	0.01

Table 1: Energy/pulse E_p obtained for the first five harmonics of the 1064-nm Nd:YAG laser line.

urable absorber, increasing the Q of the cavity and resulting in a Q-switched output pulse. The short cavity length of the microchip laser results in short optical pulses, and the infrared passively Q-switched microchip laser, pumped by a 1-W cw diode laser, can produce 218-ps pulses with peak powers up to 25 kW and ideal beam quality (diffraction-limited TEM_{00} transverse mode; transform-limited single longitudinal mode; linearly polarized). The ability of the passively Q-switched laser to produce short pulses without any electrical signal adds to the relative simplicity (and low cost) of a microchip-laser-based sensor; the nearly monolithic, all-solid-state construction results in extremely robust devices.

Harmonic Generation

The high peak power and ideal beam quality of the passively Q-switched infrared microchip laser allows for efficient frequency conversion to the visible and ultraviolet regions of the spectrum using nonlinear optical crystals. Up to 70% conversion efficiency has been obtained for frequency doubling in a 5-mm-long crystal of KTP ($KTiOPO_4$) placed adjacent to the laser [5]. This 532-nm green radiation has been subsequently doubled to produce 266-nm ultraviolet radiation with 20% efficiency in a 5-mm-long crystal of BBO (β-BaB_2O_4) [6]. A slightly lower conversion efficiency is obtained when the 532-nm radiation is combined with the 1064-nm light to produce 355-nm UV light. The 266-nm radiation has also been combined with the fundamental to generate 213-nm light. Table 1 lists the pulse energy obtained at each of the first five harmonics of the 1064-nm Nd:YAG laser line. In all cases, the nonlinear crystals have flat faces and are placed in the output path of the laser with no intervening optics.

A frequency-quadrupled passively Q-switched microchip laser producing 0.5-μJ ultraviolet pulses at a repetition rate of 10 kHz has been packaged in a stainless-steel cylinder 1 cm in diameter by 3 cm in length. A schematic of the device is shown in Fig. 1. This device operates over a large temperature window, with at least 0.1 μJ/pulse of ultraviolet over a range from 0 to 70° C. The infrared and green outputs have an even larger temperature window than the ultraviolet (see Fig. 2).

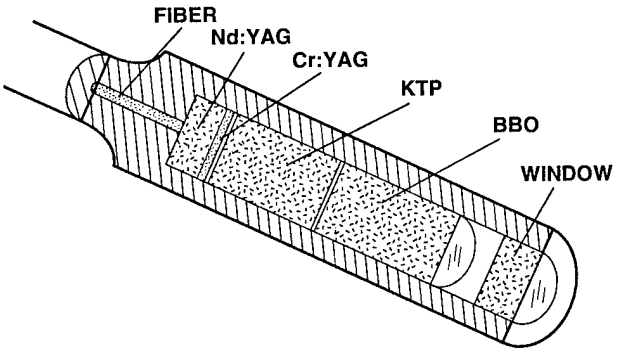

Figure 1: Schematic of a frequency-quadrupled passively Q-switched microchip laser.

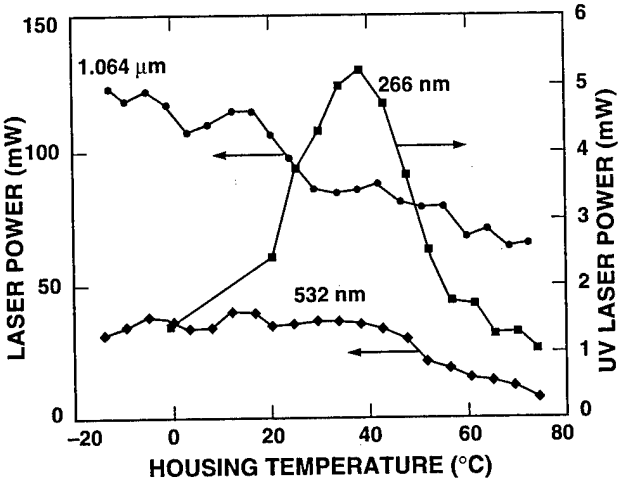

Figure 2: Time-averaged output vs. temperature for a frequency-quadrupled passively Q-switched microchip laser.

Sensor Head

The 266-nm source discussed above has been incorporated into a compact sensor head (patent pending) that is 2.5 cm in diameter by approximately 12 cm long and includes the laser, collection optics, and fast detectors. The laser light is filtered to remove the infrared and visible light before it is focused outside of a sapphire window. Fluorescence generated from material in contact with the window is collected with $f1$ collection optics and focused into a 500-μm-core return fiber for subsequent spectral analysis. Fig. 3 shows the time-averaged spectrum

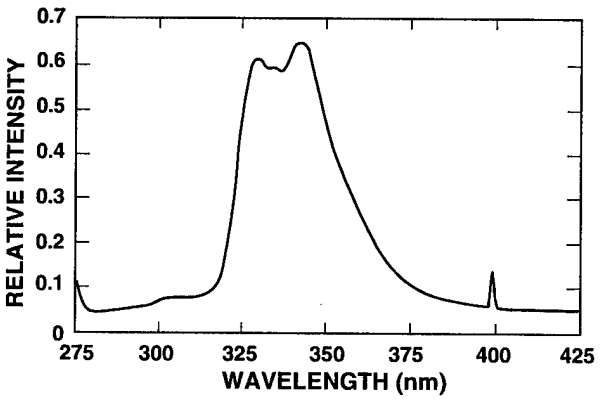

Figure 3: Spectrum of jet fuel obtained with sensor head.

obtained from jet fuel when a 3-m length of return fiber is used. The large peaks around 340 nm are characteristic of naphthalene. At wavelengths below 300 nm there is short-lived fluorescence, primarily due to BTEX compounds, that becomes readily apparent in time-resolved spectra.

A portion of the collected UV radiation is also spectrally filtered and focused on fast photodetectors collocated in the sensor head with the laser. The short duration of the excitation pulse facilitates accurate measurements of the decay times of even the short-lived BTEX compounds. By collocating the detectors with the laser, the attenuation and dispersion of the return fiber does not affect the measurements. Using a high-speed miniature photomultiplier tube we have measured the fluorescence decay times of the BTEX compounds, naphthalene, humics, and various mixtures. These decay times range from about 2 ns to greater than 60 ns. Measurements of the decay times offers greater chemical selectivity than measurements of the spectra alone [2]. In addition, for compound that do not fluoresce appreciably, such as the chlorinated solvents, we have measured Raman spectra and used the time domain to distinguish the Raman lines from fluorescence due to interferents in the same spectral region.

Conclusions

There is ongoing work at Lincoln Laboratory to develop a variety of fiber-based remote monitoring systems based on passively Q-switched microchip lasers. The high performance of these devices and their potential for low-cost production make them an attractive source for fiber-based monitoring systems. Applications include soil and groundwater monitoring of environmental contaminants, in-situ monitoring of biological processes in the marine environment, and smokestack monitoring of effluents for emission-regulation compliance and/or process control.

Acknowledgments

This work was supported by the Department of the Air Force, the Department of the Navy, and the SERDP Program Office.

References

[1] S. H. Lieberman, G. A. Theriault, S. S. Cooper, P. G. Malone, and R. S. Olsen, "Rapid Subsurface, In Situ Field Screening of Petroleum Hydrocarbon Contamination Using Laser-Induced Fluorescence Over Optical Fibers," in *Proc. Second International Symp. on Field Screening Methods for Hazardous Wastes and Toxic Chemicals*, pp. 57-63 (1991).

[2] R. W. St. Germain and G. D. Gillispie, "In-situ Tunable Laser Fluorescence Analysis of Hydrocarbons," in *Envronmental Process and Treatment Technologies*, Proc. SPIE 1637, pp. 159-171 (1992).

[3] E. R. Cespedes, B. H. Miles, and S. H. Lieberman, "Development of Optical Sensors for the Site Characterization and Analysis Penetrometer System (SCAPS)," in *Optical Sensing for Environmental Monitoring*, (Air and Waste Management Association), SP89, pp. 621-632 (1994).

[4] W. C. McGinnis, M. Davey, K. D. Wu, and S. H. Lieberman, "Capabilities and Limitations of a Cone Penetrometer Deployed Fiber Optic Laser Induced Fluorescence (LIF) Petroleum Oil and Lubricant (POL) Sensor," in *Optical Sensing for Environmental and Process Monitoring 1*, Proc. SPIE 2367 (1995).

[5] J. J. Zayhowski and C. Dill III, "Diode-Pumped Passively Q-Switched Picosecond Microchip Lasers," Opt. Lett. 18, pp. 1427-1429 (1994).

[6] J. J. Zayhowski, J. Ochoa, and C. Dill III, "UV Generation with Passively Q-Switched Picosecond Microchip Lasers," in *Conference on Lasers and Electro-Optics Technical Digest*, vol. 15 (Optical Society of America), p. 139 (1995).

Extending Wavelength Coverage and Spectroscopic Applications of Diode Lasers

R. W. Fox, L. Hollberg, S. Waltman, K. P. Petrov[1] and F. K. Tittel[1]

National Institutes of Standards and Technology, 325 Broadway, Boulder, CO 80303

[1]Rice Quantum Institute, Rice University, Houston, TX 77251-1892

Atomic spectroscopy of an electronic transition from the ground state often requires a tunable blue or UV source. Traditionally one approach in the laboratory has been to double or sum-frequency mix pulsed or CW-dye lasers to obtain the necessary wavelength. These lasers and nonlinear crystals such as $LiNbO_3$, and $LiIO_3$, have also been used in difference frequency experiments to reach the molecular vibrational bands in the infrared. However, these laboratory lasers suffer the well known litany of size, cost and complexity when compared to solid-state diode lasers. To reach these wavelength regions starting with less expensive diode lasers would allow for the possibility of decreased size, cost and power.

The main factor that has permitted progress in this area is the increase in power now available from commercial single-mode diode lasers in the near-IR and visible region. Advances in the quality of nonlinear crystals along with the emergence of quasi-phasematching techniques are also contributing to the progress towards higher blue/UV powers and new wavelengths. Together with techniques such as using resonant cavities for doubling, significant amounts of blue light (10~150 mW) are available using 90° phase matching in $KNbO_3$ with high-power AlGaAs diodes. Commercial systems based on this technique have recently appeared on the market. Although the nonlinear coefficients vary from crystal to crystal (and orientation), one may typically expect a single-pass nonlinear efficiency (P_2 / P_1^2) on the order of $E \approx 0.015\ W^{-1}\ cm^{-1}$ for a near Gaussian beam. Since this amounts to 10's of microwatts when starting with a moderately priced (50 mW) laser, very simple single-pass absorption experiments are possible with $KNbO_3$.

Higher tunable power requires that a build-up cavity be used that can be scanned. The tuning range of such a system is often limited by the maximum extension of a piezo (PZT) mounted mirror, and thus a small cavity with a large free-spectral-range (FSR) will result in a wider wavelength scan. To achieve such a system we have modified a monolithic $KNbO_3$ ring resonator by anti-reflection coating one end, and mounting an external PZT controlled mirror close (~1 mm) to the $KNbO_3$ surface. The cavity FSR is 9 GHz in the IR, which gives 18 GHz of scanning in the blue for 0.43 μm of mirror motion. This semi-monolithic cavity (figure 1) produces about 13 mW of blue light near 425 nm with 100 mW incident, and is limited by the reflectivity of the input coupler, which is not optimum.

Unfortunately $KNbO_3$ can not be phasematched for frequency doubling below a fundamental

wavelength of 834 nm. At the present time, in the wavelength region $710 \leq \lambda \leq 834$ nm we have the options of conventional angle-tuned doubling in another crystal or using a quasi-phasematched crystal, and the latter is not yet commercially available. At 810 nm, $LiIO_3$ has a conversion efficiency more than twice that of BBO. When a diode is collimated with a high-quality objective and the beam is circularized with anamorphic prisms, the $LiIO_3$ efficiency will be $\sim 10^{-4}$ (W^{-1} cm^{-1}). Thus several microwatts are possible with a single-pass using a 150 mW single-mode diode available near 810 nm. Higher powers require a ring cavity to enhance the fundamental. In this manner we obtained 150 μW at 405 nm with only 35 mW incident on the cavity. The fundamental build-up in the cavity was about 40 and the spatial mode-match of the input beam (using prisms) allowed us to couple about 75% of the incident diode power into the cavity mode, which is typical in our experience. Also in this manner 1.8 mW of usable power at 397 nm was recently reported using a lower loss cavity with a 100 mW IR diode.[1]

At shorter wavelengths there are narrow spectral bands in which a 90° phasematched crystal coincides with available diode wavelengths for SHG (RDA @ 680 nm and RDP @ 630 nm). However a wider portion of the UV spectrum may be reached by sum-frequency generation in angle-tuned BBO. Depending on the lasers and the phasematching angle, tens to hundreds of nanowatts single-pass of tunable CW light can be produced. Although these power levels are not sufficient for many applications, sensitive absorption measurements are possible.

For instance we are currently working towards generating 283.3 nm for Pb spectroscopy. The system uses sum-frequency mixing in BBO of a 850 nm DFB laser with 425 nm light produced in a $KNbO_3$ build-up cavity. A second 850 nm laser is coupled into the build-up cavity. Although one high-power 850 laser would be sufficient to reach 283 nm, the two-laser approach has the advantage that the $KNbO_3$ cavity does not need to be scanned in wavelength.

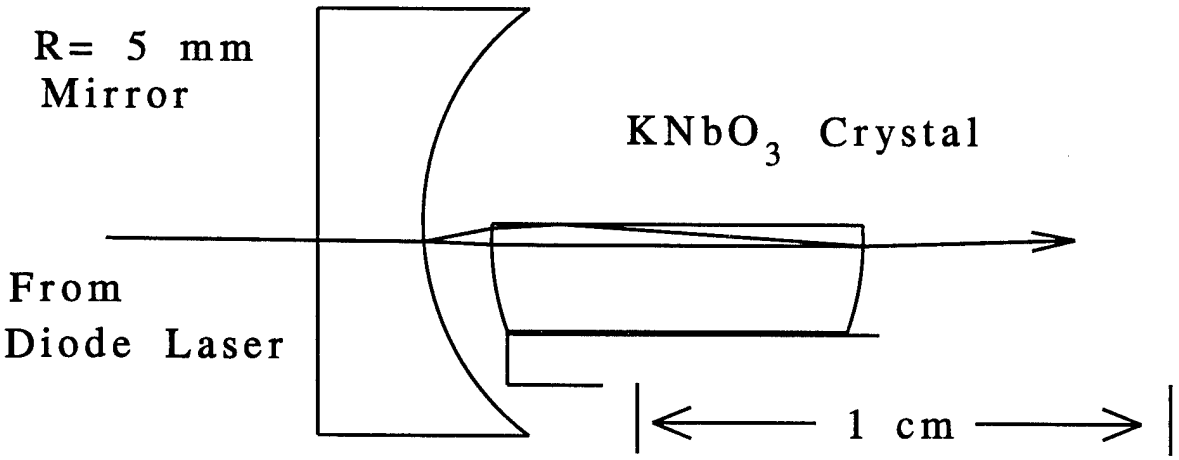

Figure 1. A semi-monolithic doubling cavity that can be tuned. The left surface of the $KNbO_3$ crystal is AR coated; The right surface coating is R>99% in the IR, and T>95% in the blue. The phase-matching length in the $KNbO_3$ is 7 mm, and the cavity mode is stable for a mirror-crystal separation out to about 1.3 mm. One micrometer of mirror motion is equivalent to 42 GHz of blue tuning.

In addition to sum-frequency mixing to reach electronic transitions, difference-frequency mixing between diodes can be used to generate tunable IR radiation in the molecular "fingerprint" region. (Cryogenic lead-salt diode lasers have been used very successfully in this wavelength region (> 3 um) for years, but these lasers remain relatively expensive and problematic). Again, as the power of the commercial visible and near-ir lasers increases, options for tunable diode-based CW sources in these spectral regions are becoming available.

In particular the nonlinear crystal $AgGaS_2$ can be phasematched for difference frequency generation in the 2 to 8 μm region using source lasers in the 600 to 1200 nm region.[2] In a difference-frequency experiment with the lasers, crystal and detectors all at room temperature, we detected methane in air (natural abundance ~1.8 ppm) with a s/n of 150 m^{-1} $s^{-1/2}$. As shown below, a diode-pumped YAG (1064 nm) was mixed in $AgGaS_2$ with an 800 nm diode to generate 3.2 μm. The cavity was locked to the YAG laser and the diode swept in wavelength. Power fluctuations in the IR beam were compensated for by controlling the 800 nm diode power with an acousto-optic modulator. About 6 μW at 3.2 μm was produced with 40 mW of diode power and 230 mW of YAG power incident on the cavity (build-up of approximately 15 at 1064 nm).

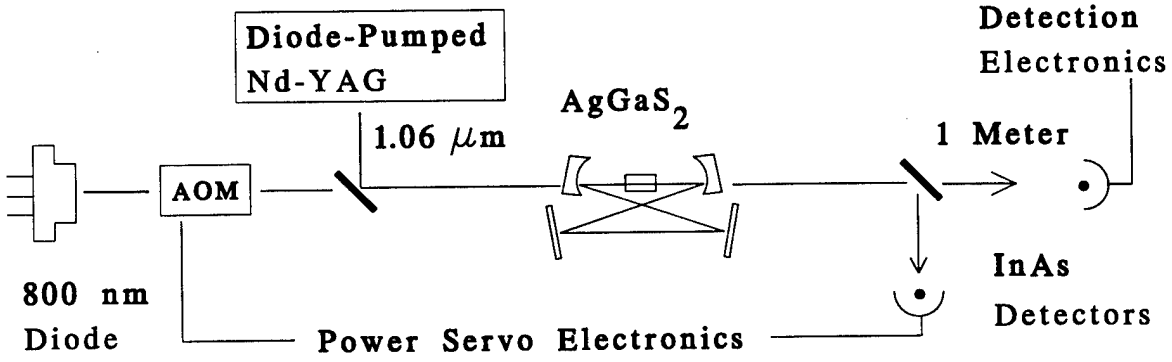

Fig. 2. Diagram of difference-frequency source for tunable IR. Using 230 mW of Nd-YAG and 40 mW of 800 nm diode power, the system generates approximately 6 μW at 3.2 μm.

References
1) K. Hayasaka, M. Watanabe, H. Imajo, R. Ohmukai, and S. Urabe, App. Opt. 33, 2290 (1994), and; Chr. Tamm, Appl. Phys. B 56, 295 (1993).
2) U. Simon, S. Waltman, I. Ioa, F. K. Tittel, and L. Hollberg, J. Opt. Soc. Am. B12, 323 (1995).

Wednesday, March 20, 1996

Poster Session I

LWD 8:15 pm-10:00 pm
Windsor Ballroom

Novel Rare-Earth Doped Chalcogenide Glasses for High-Brightness, Room-Temperature, Broad-Band Infrared Sources

J. A. Moon, B. B. Harbison, J. S. Sanghera, and I. D. Aggarwal

Code 5603, Infrared Materials and Chemical Sensors Section
U.S. Naval Research Laboratory
Washington DC 20375
(202)767-2466; (202)767-5792 (FAX)

For many infrared spectroscopic applications in the 3-5 μm spectral region, a compact, fiber optic and fiber optically pumped source of infrared radiation is needed [1]. In many cases, the ultimate detection limit of an infrared chemical sensor can be improved by increasing the optical "brightness" or radiance (in $\mathrm{Wcm^{-2}Sr^{-1}}\mu$m) of the source, and not necessarily increasing the source's total optical power. The radiance R_{bb} of a black-body "glow-bar" source in the 3-5 μm region is practically limited by the source's temperature to around $R_{bb} \simeq 0.17$ $\mathrm{Wcm^{-2}Sr^{-1}\mu m^{-1}}$ (T=1100K, $\lambda = 4.5\mu$m.) Optically pumped fluorescent sources do not suffer from this limitation, and have several other important advantages over blackbody sources. These other advantages include remote location, compact size, insensitivity to electrical interference, room temperature operation, and non-reactivity with harsh or explosive environments.

A schematic for a fiber optic device based on optically pumped broad- band rare-earth fluorescence is shown in Figure 1. The emitted radiance R_e at the active fiber tip can be calculated as

$$R_e = \frac{\eta P_p}{2\pi A \Delta\lambda_e}\left(\frac{\Delta\Omega_c}{4\pi}\right)\left(\frac{\lambda_p}{\lambda_e}\right) \tag{1}$$

where P_p is the pump power in W, λ_p and λ_e are the pump and emission wavelengths, respectively, A is the cross-sectional area of the fiber, η is the quantum efficiency, $\Delta\lambda_e$ is the emission bandwidth, and $\Delta\Omega_c$ is the captured solid angle of the emission in the fiber core. It is assumed that all the pump radiation is absorbed in the fiber, the radiation is emitted in 2π Sr at the fiber end, and that the backward traveling fluorescence is reflected at the pump end of the active fiber. Assuming that $A = 10^{-4}$ cm^2, $\Delta\lambda_e = 0.5$ μm, $\lambda_p/\lambda_e \sim 0.5$, and the index of refraction is $n = 2.5$ giving $\Delta\Omega_c/4\pi = 0.6$ for a core-only fiber, the radiance per milliwatt of pump power is $R_e/P_p \simeq 1\eta$ $\mathrm{Wcm^{-2}Sr^{-1}\mu m^{-1}mW^{-1}}$. Since near-IR laser diodes are currently easily capable of several hundred milliwatts of output power, even a 1% quantum efficient transition will have a radiance of several $\mathrm{Wcm^{-2}Sr^{-1}\mu m^{-1}}$, an order-of-magnitude greater than a typical black-body.

We report here novel rare-earth doped heavy-metal chalcogenide glass compositions which look promising for development of a such a remotely pumped, high-brightness, broad-band fiber optic source of infrared radiation. The compositions of the glass studied were based on Ba - In - Ga - Ge - S (BIGGS) doped from 100ppm up to 20 wt % of the rare-earths Er and Pr. Chalcogenide glasses are mechanically and chemically durable, are not hygroscopic, are stable glass formers, and have high ($n \sim 2.5$) indices of refraction. In addition, the BIGGS compositions have a very high rare-earth solubility and can be fiberized. To date other chalcogenide glass systems have been studied primarily for their potential for efficient 1.3 μm optical amplifiers [2-6].

The emission spectrum of the Er:BIGGS material was measured through a 0.5m spectrometer using a cooled InSb detector, and using an 808 nm GaAs diode laser to excite the samples. The fluorescence

spectrum of a 1% Er:BIGGS sample is shown in Figure 2. The lifetimes of the transitions labeled in Figure 2 were measured using the same apparatus, except that a pulsed Ti:Sapphire laser tunable between 750-850 nm was used to excite the samples. The time-resolved data for the 1% Er sample are shown in Figure 3. Of particular importance is the lifetime (0.5 ms) of the "B" transition observed at 1.7 μm. The excited states of this fluorescence (the $^4I_{9/2}$ and, via upconversion $^4S_{3/2}$) also produce ~4.5 μm and ~3.5 μm fluorescence. The lifetime of this transition shortens to 0.1 ms in 10% Er:BIGGS. These relatively long lifetimes show the feasibility of using the long- wavelength fluorescence, provided other materials issues (discussed below) are solved.

As proof-of-principal, a 100 ppm praseodymium-doped composition of this material was drawn into a 300 μm diameter core-only fiber and pumped at 1.57 μm with a pulsed optical parametric oscillator. Only about 3 cm of fiber was used for this measurement which gave a very weak pump absorption, so the fluorescence signal was small. The result of a time-resolved measurement of the spectrally integrated signal from 3.5-5 μm is shown in Figure 3. A lifetime of ~63 μs is observed in this sample.

An issue which needs to be resolved before these materials will become practical for mid-IR applications is the removal of hydrogen. An H-S absorption band is present and centered at about 4 μm and leads to a reduction in the fluorescence signal in part of the 3-5μm range (although the hydrogen apparently does not quench the fluorescence.) New techniques and compositions are presently being tested to remove this band. We note that this hydrogen band has been reduced to less than 10dB/m ($\alpha \simeq 0.02$ cm^{-1}) at its peak in arsenic trisulfide fibers. (Arsenic trisulfide, unfortunately, exhibits a very low rare-earth solubility.) This level of hydrogen reduction in a BIGGS composition would be sufficient for making an efficient 3-5μm emitting device.

1. J. S. Sanghera and I. D. Aggarwal, Proc. SPIE **2367**, 99 (1995).

2. K. Wei, D. P. Machewirth, J. Wentzel, E. Snitzer, and G. H. Sigel, J. Non-Cryst. Sol. **182**, 257 (1995).

3. J. Heo, J. Mat. Sci. Lett. **14**, 1014 (1995).

4. A. G. Clare, Key Eng. Mat. **94-95**, 81 (1994).

5. D. R. Simons, A. J. Faber, and H. de Waal, J. Non- Cryst. Sol. **185**, 283 (1995).

6. Y. Ohishi, A. Mori, T. Kanawri, K. Kujiura, and S. Sudo, Appl. Phys. Lett. **65**, 13 (1994).

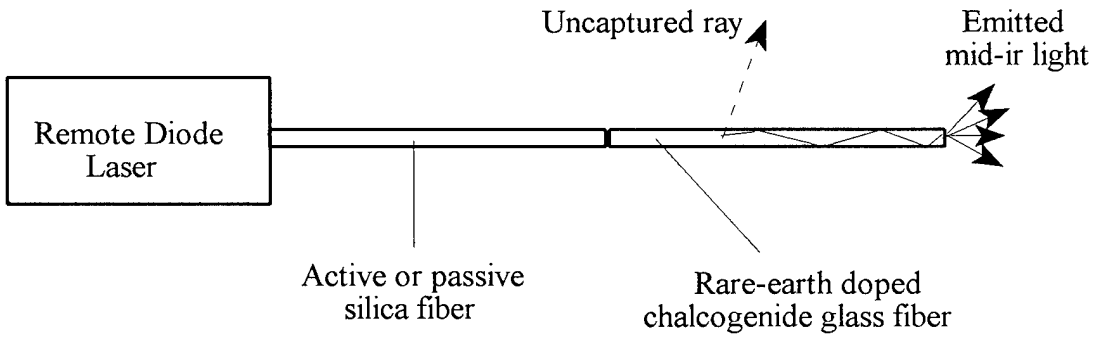

Fig. 1. Proposed fluorescent fiber device geometry.

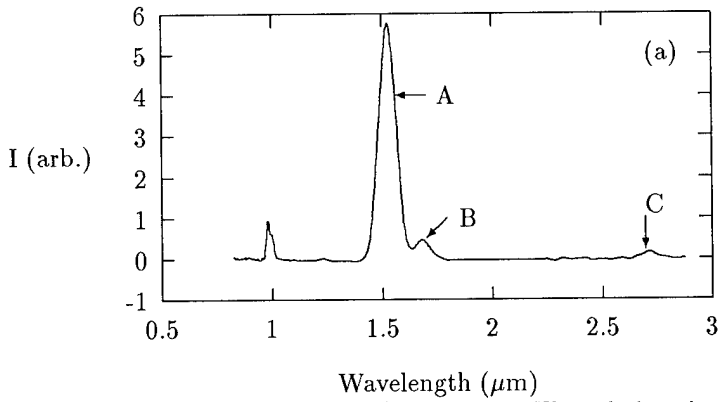

Fig. 2. Emission spectrum of 1% Er:BIGGS. The relative sizes of the peaks are uncorrected for detector/spectrometer response.

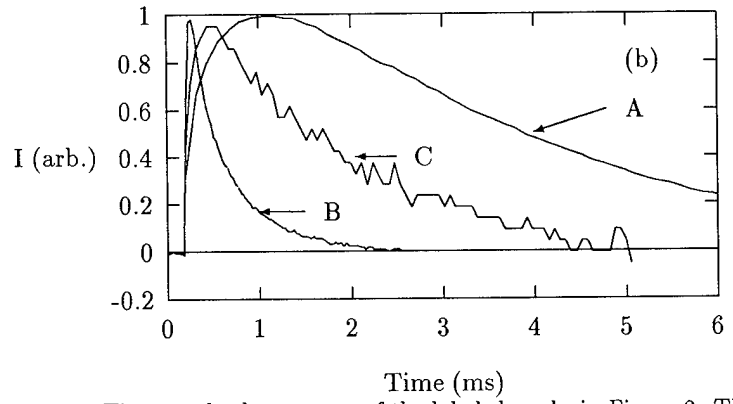

Fig. 3. Time resolved spectrum of the labeled peaks in Figure 2. The lifetimes are A $\sim$ 5 ms, B=0.48 ms, and C=1.5 ms respectively.

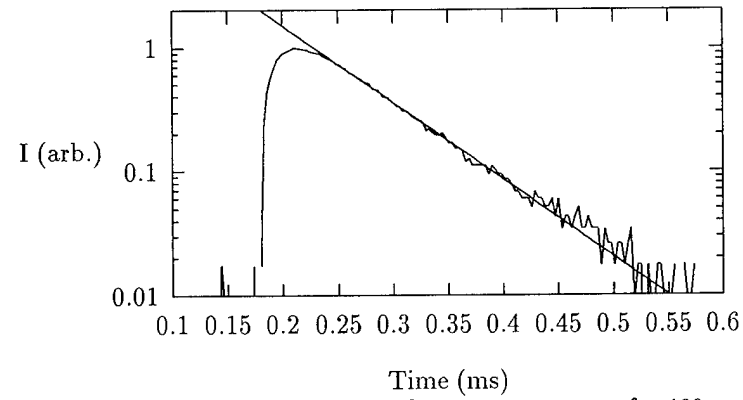

Fig. 4. Time-resolved emission in the 3.5-5 μm range of a 100ppm Pr:BIGGS core-only fiber pumped by a 1.57μm pulse. The observed lifetime is 63 μs.

TUNABLE POLYMER DYE LASERS: A REVIEW AND RECENT ACHIEVEMENTS

By:
VLADIMIR S. NECHITAILO
PolyOptics Ltd., Nahal - Soreq, Yavne 81800, ISRAEL
Tel: 972 - 8 - 434508 Fax: 972 - 8 - 434798

The first plastic-host dye laser was built by Soffer and McFarland in 1967. A lot of efforts have been made to develop tunable solid state lasers in the visible spectrum afterwards.

Transparent polymers doped with laser dyes were extensively investigated and proved to be one of the most promising candidates for these laser systems. However, this class of polymer lasers has not been widely used yet mainly because of the low laser damage threshold of ordinary polymer materials and the low photoresistance of impregnated dyes.

Unique laser resistant modified polymer materials [1,2] and excellent pyrromethene laser dyes doped in modified polymers [3,4] have sparked renewed interest in solid state dye lasers demonstrating high efficiencies exceeding 70% and lifetimes more than 100,000 pulses for a fixed area at high (about 0.5 J/cm^2) fluence levels.

Laser engineers throught the world are currently working on new designs that incorporate solid-dye technology. Designers find this material attractive for several reasons, including the facility of changing wavelengths by swapping dye rods, the simplicity of the operation and maintenance, high reliability. We can expect the development of diverse commercial polymer lasers for scientific, medical and industrial applications, including chemical and environmental analysis.

Experimental results for various type of polymer lasers, pumped by different frequency doubled Nd:YAG lasers with pulse energies from 1mJ to 300 mJ, pulse widths from 5 nsec to 500 nsec and pulse repetition frequencies (PRF) from 1 Hz to 25 kHz are presented.

Limitations for polymer-host dye lasers, arising at high PRF due to low thermal conductivity of polymer materials, were overcome by special design of the solid-state active elements.

An average output power of more than 6 Watt and efficiency in excess of 70% have been achieved in a broad band operation mode. A tunability over 550 - 700 nm wavelength range was demonstrated in a narrow band operation mode (linewidth 0.4 cm^{-1}) with 30% peak conversion efficiency.

A stable output for more than 2.6 million pulses at 570 nm for motionless active element and more than 200 million pulses for movable polymer element has been achieved.

All developed polymer lasers enable tuning of output wavelength in the visible spectrum or adjusting laser output to the most suitable wavelength for different applications.

REFERENCES:

1. K. M. Dyumaev, A. A. Manenkov, A. P. Maslyukov, G. A. Matyushin, V. S. Nechitailo, and A. M. Prokhorov, " Dyes in modified polymers: problems of photostability and conversion efficiency at high intensities," J. Opt. Soc. Am., B 9 (1), 143 - 150 (1992).

2. A.A. Manenkov, A.P. Maslyukov, G.A. Matyushin, and V.S. Nechitailo "Modified polymers - effective host materials for solid-state lasers and laser beam control elements: a review", Visible and UV Lasers, SPIE Publ. 2115 ,136-147 (1994).

3. Z. Azar, A. S. Bank, D. L. Donskoy, and V. S. Nechitailo, "Tunable solid - state laser system for dermatology applications", Medical Applications of Lasers II, SPIE Publ. 2327, 8-15 (1994).

4. A.S. Bank, D.L. Donskoy, and V. S. Nechitailo, "High average power quasi-CW tunable polymer laser", UV and Visible Lasers and Laser Crystal Growth, SPIE Publ. 2380, 292-297 (1995).

Doubly Tunable Femtosecond Pulses Generated in the Visible using Optical Parametric Amplifiers for Time-resolved Spectroscopy

P.Matousek, A.W.Parker, P.F.Taday, W.T.Toner and M.Towrie

Central Laser Facility, Rutherford Appleton Laboratory, Oxfordshire, OX11 0QX, UK
Telephone: +44(0)1235 821900
Fax: +44(0)1235 445888
E-mail: P.Matousek@rl.ac.uk

1. Introduction

Many time-resolved spectroscopy techniques require two broadly and independently tunable, synchronised light pulses. This requirement can be met by optical parametric oscillators (OPOs) [1] and travelling wave optical parametric amplifiers (OPAs) [2, 3, 4, 5]. The latter capable of providing higher pulse energies. Our aim was to develop a multikilohertz repetition rate OPA system capable of providing femtosecond/picosecond, synchronised and independently tunable pump and probe pulses in the visible part of the spectrum for time-resolved absorption and resonance Raman spectroscopies.

The generation of two independent short pulses tunable in the infra-red has recently been demonstrated using a synchronously pumped optical parametric oscillator (OPO) [1]. We believe this work reports for the first time on synchronously pumped travelling wave OPAs. The design described in [5] was adopted for the development of the dual independently tunable OPA system.

2. Description of the System

A block diagram of the system is shown in Fig. 1. An output pulse (100-150 fs, 800 nm) from a femtosecond Ti:Sapphire laser (Tsunami, Spectra Physics) was amplified up to around 17 μJ in a Ti:Sapphire regenerative amplifier (Spitfire, Spectra Physics/Positive Light) at 40 kHz repetition rate. WLC was generated by using a quarter of the regenerative amplifier output in a sapphire crystal. The remaining light at the fundamental was frequency doubled. Using 50 % beamsplitters the 400 nm pulse and WLC were split to provide pump and seed for the two optical parametric amplifiers.

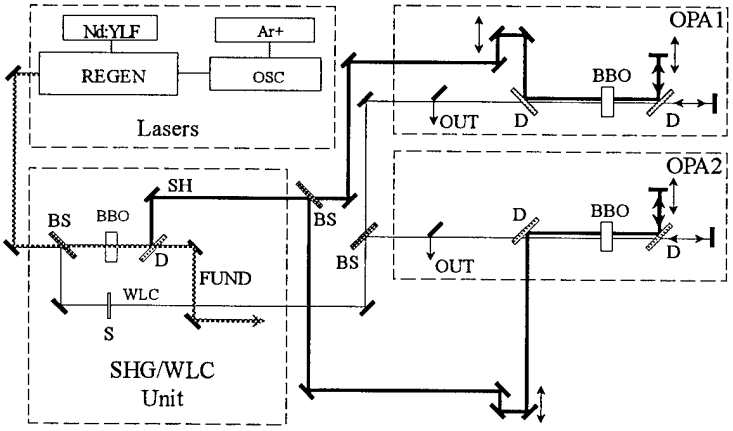

Figure 1: A block diagram of the parametric amplifier system.
Legend: Nd:YLF - Q-switched Nd:YLF laser, Ar^+ - 10W argon ion laser, REGEN - Ti-Sapphire regenerative amplifier, OSC - femtosecond Ti:Sapphire laser, BS - beamsplitter, BBO - BBO crystal, D - dichroic mirror, S - sapphire crystal, FUND -

fundamental output of the regenerative amplifier, SHG - second harmonic generator, SH - second harmonic of the fundamental, OUT - output beam, WLC - white-light continuum, OPA1, OPA2 - optical parametric amplifier units.

Both the seed and pump pulses are focused into the OPA crystal (1 mm-thick (OPA1) or 2 mm-thick (OPA2) type I BBO crystal cut at 29°) using a 80 mm focal length achromatic lens. Both pulses are then delayed and reflected back into the OPA crystal for a secondary amplification.

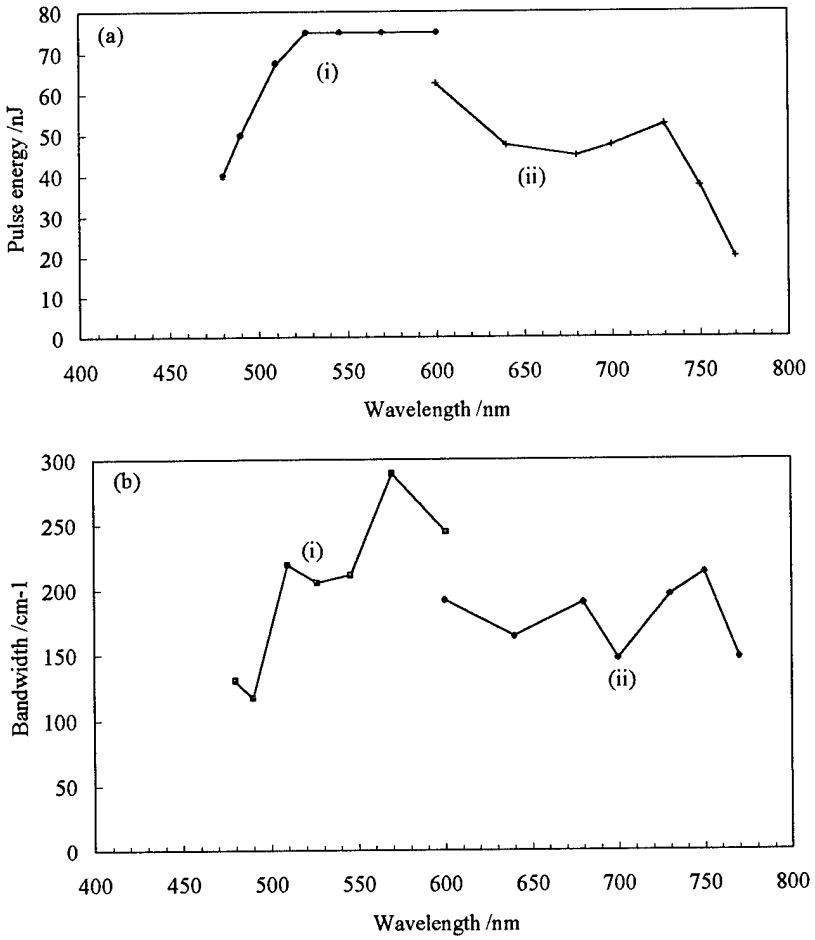

Figure 2: Tuning curves of the OPAs pumped at 400 nm with 1 μJ showing (a) the pulse energy and bandwidth (b) dependencies on signal wavelength. The curves marked (i) were obtained without using an interference filter to control the OPA bandwidth. The (ii) curves were obtained with 10 nm bandpass interference filters inserted after the WLC source.

3. Results

A typical tuning curve for each OPA is shown in Fig 2. The cross correlation widths between the uncompressed OPA outputs were measured to be between 540-610 fs (FWHM). Prism pulse compression of the OPA outputs reduced the cross correlation to 150 ± 10 fs (FWHM) measured for the combination of 595 and 600 nm (see Fig 3).

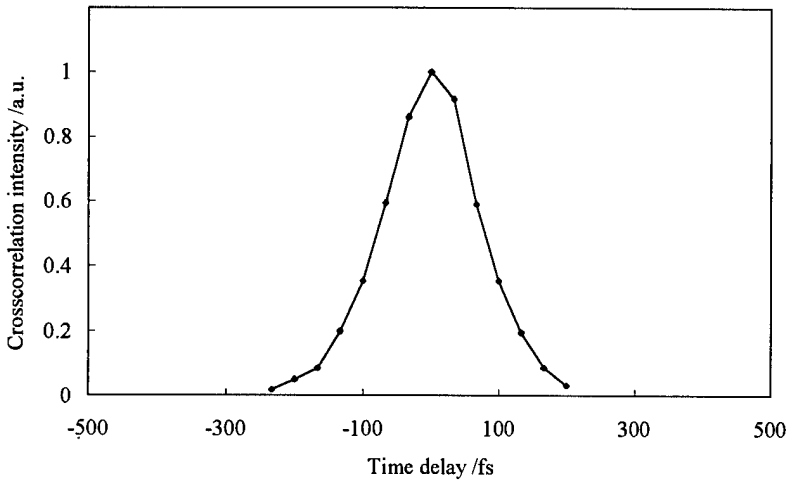

Figure 3: Normalised crosscorrelation functions of the two OPAs compressed pulses at 595 and 600 nm with the width of 150 fs (FWHM).

4. Conclusion

A system, based on optical parametric amplifiers, generating doubly tunable femtosecond synchronised pulses with pulse energies 40 - 75 nJ over a 480-730 nm has been described and its basic characteristics measured.

References

[1] R.Laenen, A.Laubereau, SPIE 2379 (1995) 202.

[2] G.P.Banfi, C.Solcia, P.Di Trapani, R.Danielius, A.Piskarskas, R.Righini, R.Torre, Optics Comm. 118 (1995) 353.

[3] R.Danielius, A.Piskarskas, A.Stabinis, G.P.Banfi, P.Di Trapani, R.Righini, J.Opt.Soc.Am. B 10 (1993) 2222.

[4] U.Emmerichs, H.J.Bakker, H.Kurz, Optics Comm. 111 (1994) 497.

[5] M.K.Reed, M.K.Steiner-Shepard, D.K.Negus, IEEE Journal of Quantum Electronics 31 (1995), 1614.

Tunable InP based semiconductor lasers for gas analysis

Björn Broberg
IMC - Industrial Microelectronics Center, Box 1084, S-164 21 Kista, Sweden
telephone +46-87521045, fax +46-87505430
e-mail: bjorn@imc.kth.se

Stefan Nilsson, Pierre-Jean Rigole, Tiina Klinga, Lena Bäckbom, Björn Stålnacke
Royal Institute of Technology, Electrum 229, S-164 40 Kista, Sweden

Fiber optics communications has been the driving force for research on advanced semiconductor lasers based on InGaAsP-InP. Thus, single frequency and tunable lasers with good modulation properties have been developed. The normal wavelength range achievable in the InGaAsP-InP system is ca 1.2-1.67μm. However, using compressively strained quantum wells the wavelength range can be extended to ca 2μm. We have exploited this possibility, by modifications of telecommunications laser designs and processes, to fabricate very compact, rugged and potentially cheap application specific semiconductor lasers suitable for gas analysis. These lasers find applications in instrumentation for real-time industrial process control, smoke-stack emission and environmental monitoring etc. The technology has advantages such as a high sensitivity for many important gases, an unsurpassed selectivity, short response time, and is inherently explosion-proof.

In a semiconductor laser based gas sensing system the laser is typically tuned to an absorption line of the gas in question, and can be locked to this frequency. When the laser is frequency modulated around this absorption wavelength the gas concentration can be determined in a very sensitive, fast and selective way from the derivatives of the transmitted signal. Multisection DFB lasers can be tuned typically 1-2nm while maintaining a narrow linewidth. The tuning is normally continuous. If properly biased the multisection DFB laser can have a uniform FM response from very low frequencies up to 10-20GHz. The lasers are regrown by semiinsulaitng InP to reduce the parasitic capacitance, which is a key factor to achieve high modulation bandwidths. We have developed three-section DFB lasers (Fig.1) for a variety of wavelenghts for different gases. In some cases they have reached commercial deployment in this application (Ref.1).

Even for laser at longer wavelengths we have used the three-section DFB structure successfully. Example of performance of such a laser in the 1.7-1.8μm region is threshold current of about 20mA, output power of about 40mW CW and side mode suppression ratio exceeding 45 dB. In this case the active material consists of three compressively strained InGaAs quantum wells, surrounded by a GRIN-SCH structure giving a staircase-like bandgap profile for the confinement of carriers and light.

The DBR (Distributed Bragg Reflector) laser, where the feedback is accomplished by a passive tuning section, has the advantage of wider tuning range (typically 5-10nm in a quasi-continuous manner) at the expense of a linewidth broadening during tuning. In gas analysis the wider tuning has an obvious attraction as in some cases it allows simultaneous measurements of more than one absorption line (Ref 2).

A key problem in the manufacture of lasers for gas analysis is the control and reproducibility of the wavelength. In both DFB and DBR lasers the lasing wavelength is determined by the period of the Bragg grating in conjunction with the propagation constant of the grating loaded waveguide. This propagation constant is in turn dependent on material refractive indices of the layers of the waveguides and their surroundings, and on the precise geometry. The layer thicknesses can be controlled quite accurately in the MOVPE growth. For improved control of the mesa width we have substituted wet chemical etching by dry etching. The number of free carriers in the waveguide affects the wavelength as well. In a DFB laser the wavelength determining waveguide is lasing, thus the carrier density (and wavelength) will depend on the gain and loss in the laser. In the DBR case the wavelength determining element is outside the active section of the waveguide and has only doping level of carriers (unless tuned). Consequently it is less difficult to reach a specific wavelength with DBR lasers than with DFB.

If even wider tunability would be availible it would be possible to measure more than one gas using the same laser and the same instrument. The tuning of the DFB and DBR lasers is proportional to, and limited by, the changes in waveguide refractive index. Wider tuning ranges require different filter mechanisms. There is a wide variety of designs proposed and demonstrated. One such a design is the vertical codirectional coupler. This concept gives a great change of coupling wavelength for a certain index variation, but suffers often from a poor selectivity. Other approaches are sampled grating (S-DBR) or super-structure grating (SSG-DBR) lasers. For the latter structure 40nm complete wavelength coverage has been obtained (Ref.3). Combinations of codirectional couplers and S-DBR or SSG-DBR structures, such as the GCSR laser (Fig.2 and Ref.4) have proven to be promising in terms of wide tuning ranges, wavelength range coverage and wavelength selectivity. 114nm tuning has been achieved by the GCSR laser as shown in Fig.3.

A conclusion is that the stage of development and the availability of custom designed compact, rugged and potentially cheap tunable semiconductor lasers now opens up to practical applications in gas analysis.

References

1, H. Ahlberg, S. Lundqvist, R. Tell, and T. Andersson, "Industrialized High Sensitivity Fiber-Optic Near-IR Diode Laser Based Gas Analysis System," Invited paper at the SPIE conference for Optical Sensing for Environmental Monitoring, Atlanta, Georgia, USA, October 1993.

2, L. Sandström, S. Höjer, H. Ahlberg, B. Broberg, "Advanced semiconductor laser structures for gas analysis spectroscopy". paper CMI5, CLEO/Europe'94, Amsterdam, the Netherlands, 28/8-2/9 1994

3, M. Öberg, P.-J. Rigole, S. Nilsson, T. Klinga, L. Bäckbom, K. Streubel, J. Wallin and T. Kjellberg: "Complete single mode wavelength coverage over 40 nm with a super structure grating DBR laser". J. Lightwave Technol., Vol.13, No.9, pp 1892-98, (Sept.'95).

4, P.-J. Rigole, S. Nilsson, L. Bäckbom , T. Klinga, J. Wallin, B.Stålnacke, E.Berglind and B.Stoltz: "114 nm wavelength tuning range of a vertical grating assisted codirectional coupler laser with a super structure grating distributed Bragg reflector". Photonics Technology Letters, Vol. 7, No.7, pp 697-699, (July 95).

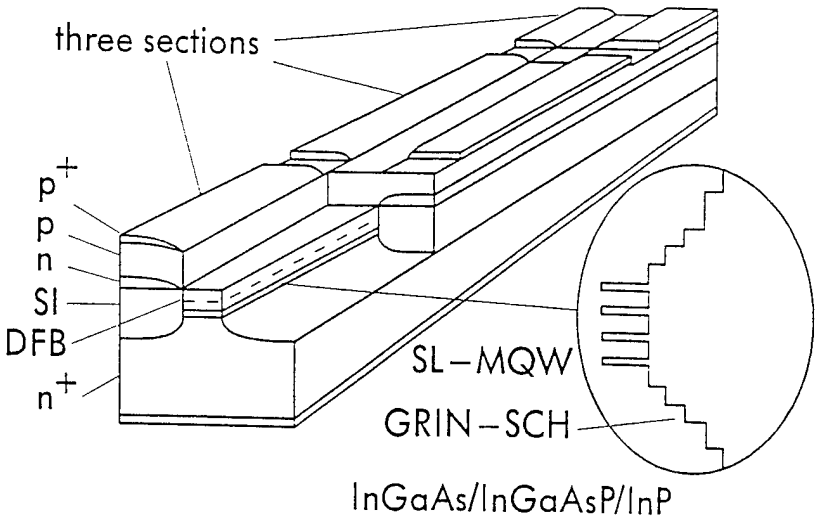

Fig. 1 Schematic view of a three-section DFB laser with MQW active waveguide in a GRINSCH structure and semiinsulating regrowth

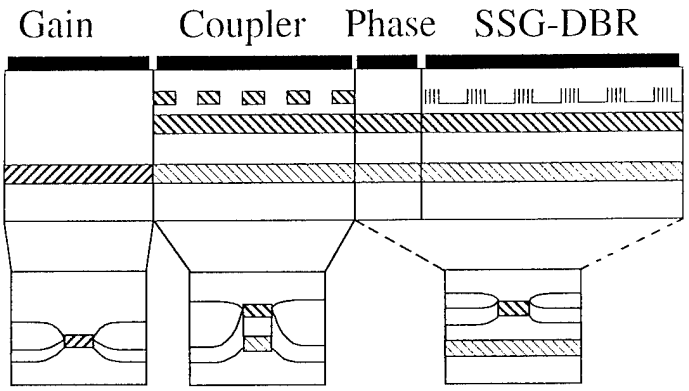

Fig.2 Schematic view of the GCSR laser

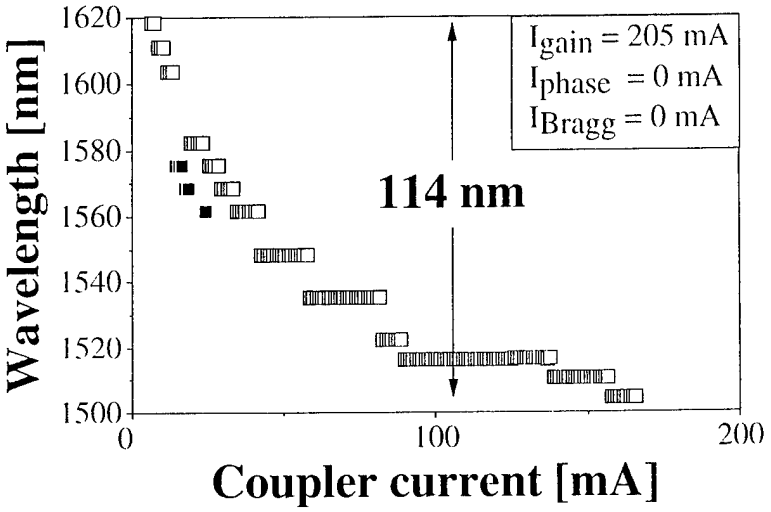

Fig.3 114nm tuning of a GCSR laser

Imaging and Time-Resolved Spectroscopy of Single Molecules

T. D. Harris, J. J. Macklin, J. K. Trautman, and L. E. Brus
AT&T Bell Laboratories
Murray Hill, NJ 07974
(908) 582-3932, -3958 Fax

Recent progress in the fluorescence detection of individual molecules [1-8] suggests that a single dye molecule can be a useful tool to probe chemical identity and activity. Measurement of fluorescence lifetime [5,6] and spectrum [6] can be augmented by knowledge of molecular orientation using polarized light [3], and triplet [2] and photoisomer excitation, as well as diffusion processes, via fluorescence-intensity correlation. Applications of fluorescent probes include the study of the dynamic conformation of membrane-bound proteins, transport of and signaling by messenger molecules, and the optical detection of the sequence of DNA. While molecules can be spatially located using near-field microscopy [5-8], near-field probes can perturb the molecule under study. We show here that molecular properties can be determined easily and in a non-perturbative manner using far-field illumination, and we obtain unperturbed spectral and lifetime data that cannot be extracted from an ensemble measurement.

Fluorescence excitation and detection is obtained using a scanning microscope with epi-illumination optics, as shown and discussed in Fig. 1. The objective is used at its full NA of 1.25 for collecting fluorescence, but used at 0.82 NA for focusing the laser. Individual carbocyanine molecules, $diI_{12}C(3)$ (Molecular Probes, Inc.), spin-coated onto a 20-nm thick polymethylmethacrylate (PMMA) film on a quartz coverslip with typically 1-5 molecules/μm^2 coverage, can be spatially located in a fluorescence image.

Figure 2 shows sequential images of a field of diI molecules, using polarized 532-nm laser light. The relative fluorescence rate versus laser polarization can determine the dipole orientation, since the absorption rate is proportional to $\cos^2\phi$, where ϕ is the angle between the laser field polarization and the absorption-dipole component in the xy plane. Based on the change in fluorescence with laser polarization, we find that molecules (a)-(c) are oriented principally along the x-axis, molecules (d)-(g) oriented along the y-axis, and molecules (h)-(i) are oriented about 45^o from the x-axis. A molecule may have a dipole component perpendicular to the surface, which is not excited by the laser. This is the reason that molecule (f) is 40% weaker than molecule (d), although both are oriented along the y-axis. The brightest molecules, which lie entirely in the xy plane, have maximum emission rates of 280-300 counts/pixel (10 ms = 1 pixel) and a signal to background of 30:1. These count rates are consistent with that calculated for a single molecule lying along the laser field.

Time-resolved spectroscopy can be performed once a molecule is located. Figure 3 shows an image, spectrum, and fluorescence decay for two of 130 molecules probed. As the Figure shows, molecules can differ significantly in both peak fluorescence wavelength and in lifetime. The peak wavelength is used here to characterize a molecular spectrum. For comparison, a single ensemble measurement of spectrum and fluorescence decay averaged over several hundred molecules exhibits a peak wavelength of 565 nm and a fluorescence lifetime of 2.7 ns.

The variation in lifetime with peak wavelength is shown in Fig. 4 for (a) sixty-eight molecules located at a PMMA/air interface, and (b) sixty-two molecules on a PMMA surface that is overcoated with several microns of either immersion oil or PMMA. The dielectric contrast of the interface is thus reduced from 0.48 in (a) to less than 0.02 in (b). While the mean values of lifetime and peak wavelength are consistent with those measured for an ensemble, the dispersion in these spectral properties, and particularly the correlation of lifetime with spectral shift, provide information that cannot be obtained from the ensemble measurement. First, the peak fluorescence wavelength shifts 30

nm for some dil molecules. PMMA is locally polar and polarizable, and dil is expected to have a large excited-state polarizibility, so that the transition energy and hence the fluorescence emission wavelength is sensitive to local perturbations. Second, Fig. 4 shows a trend of longer lifetimes for molecules with red-shifted spectra. If the fluorescence decay is mainly radiative, the lifetime is proportional to the spectrally-averaged inverse cube of the emission frequency. When the dipole matrix elements are independent of the external perturbation that shifts the transition energies, then to a small approximation, the radiative lifetime will increase as the cube of the peak fluorescence wavelength.

Third, for the molecules located at the PMMA/air interface, Fig. 4(a), the fluorescence lifetime varies by up to 50% for the same peak wavelength and spectral shape. We attribute this to the modification of the radiative decay rate by the interface, which can be expressed by:

$$\tau_{rad}(\theta_e) = \tau_{rad}^{\infty} \times \left(L_{\|} \sin^2\theta_e + L_{\perp} \cos^2\theta_e\right)^{-1} , \qquad (1)$$

where τ_{rad}^{∞} is the radiative rate in an infinite PMMA medium, and the quantity in brackets arises from the boundary conditions at the PMMA/air interface on the radiation emitted by the molecule. This effect depends on the tilt angle θ_e of the emission dipole measured from the plane of the surface, and on the ratio of refractive indices. For molecules very close to the interface, algebraic expressions for $L_{\|}$ and $L_{\perp}$ are given in Ref. [9] for a dipole parallel or perpendicular to the surface. For molecules more than an optical wavelength from the interface, $L_{\|}$ and $L_{\perp}$ approach unity, and the lifetime approaches the infinite-medium value. This is nearly the case in Fig. 4(b), where we can approximately fit the wavelength-dependent lifetime to $\tau_{rad}^{\infty} = 2.57 \times (\lambda/565)^3$. The derived value of 2.57 ns at 565 nm, in agreement with the value of 2.63 ns found elsewhere[10], and a cubic dependence on wavelength, provides good agreement to the data. Based on these values, and using Eq. 1 above, we find the long fluorescence lifetimes seen in Fig. 4(a) are consistent with molecules on the PMMA side of the interface, with emission dipoles tilted up to 30° from the surface. We have checked that very long lifetimes (up to 5.5 ns) are observed for weakly fluorescencing molecules, where a small fluorescence rate indicates a molecule oriented nearly perpendicular to the surface, and therefore weakly excited by the laser.

Far-field single-molecule spectroscopy can determine the dispersion in molecular properties easily and in a non-perturbative manner. Our measurements here on dil reveal two components of dipole orientation, a lifetime variation of 8% in the absence of a dielectric interface, and that the lifetime is effected by an interface through the orientation of the emission dipole moment. The large spectral shifts induced by the local environment reveals that the correlation of lifetime to wavelength is consistent with the frequency dependence of spontaneous emission. We will discuss the application of single-molecule imaging and spectroscopy to the fluorescence labeling of proteins, and describe methods to determine all components of the dipole orientation, which can allow a measurement of the change in protein structure. Limitations due to photobleaching, as well as background fluorescence for in vivo measurements, will also be discussed.

1. W. P. Ambrose, Th. Basche, and W. E. Moerner, J. Chem. Phys. **95**, 7150 (1991);
2. J. Bernard, L. Fleury, H. Talon, and M. Orrit, J. Chem. Phys. **98**, 850 (1993).
3. E. Betzig and R. J. Chichester, Science **262**, 1422 (1993).
4. J. K. Trautman, J. J. Macklin, L. E. Brus, and E. Betzig, Nature **369**, 40 (1994).
5. X. Sunney Xie and R. C. Dunn, Science **265**, 361 (1994).
6. W. P. Ambrose, P. M. Goodwin, J. C. Martin, and R. A. Keller, Science **265**, 364 (1994).
7. S. Nie, D. T. Chiu, and R. N. Zare, Science **266**, 1018 (1994).
8. T. Funatsu, Y. Harada, M. Tokunaga, K. Saito, and T. Yanagida, Nature **374**, 555 (1995).
9. W. Lukosz and R. E. Kunz, Opt. Commun. **20**, 195 (1977); J. Opt. Soc. Am. **67**, 1607 (1977).
10. E. Akesson, V. Sundstrom, and T. Gillbro, Chem. Phys. Lett. **121**, 513 (1985).

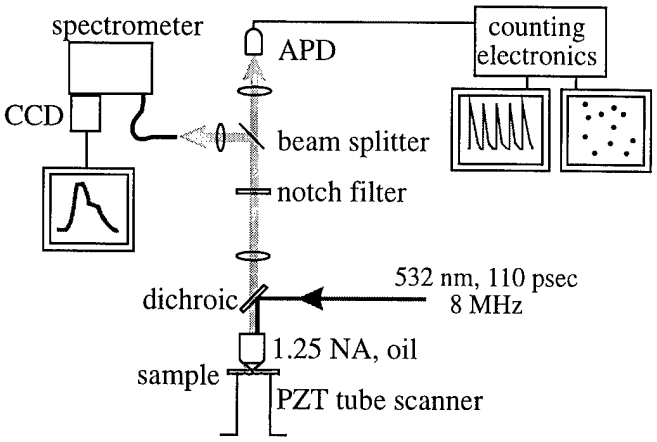

Fig. 1. Arrangement for detecting single molecules using a scanning microscope with epi-illumination optics. Mode-locked 532-nm laser pulses are focused to a 0.38-μm spot on a sample of molecules by a 1.25-NA oil-immersion objective. DiI molecules are spin-coated onto a 20-nm thick PMMA film on a quartz coverslip. This diI-coated sample is mounted upside down on a piezoelectric tube (PZT) and, for imaging, raster-scanned across the focused laser spot, while fluorescence is collected by the objective and focused onto an avalanche photodiode (APD). For spectroscopy, the PZT positions a molecule under the laser spot, and a beamsplitter is inserted. Time-correlated photon counting determines the fluorescence decay, so spectrum and lifetime are obtained simultaneously. The time-averaged laser intensity is about 0.5 KW/cm^2.

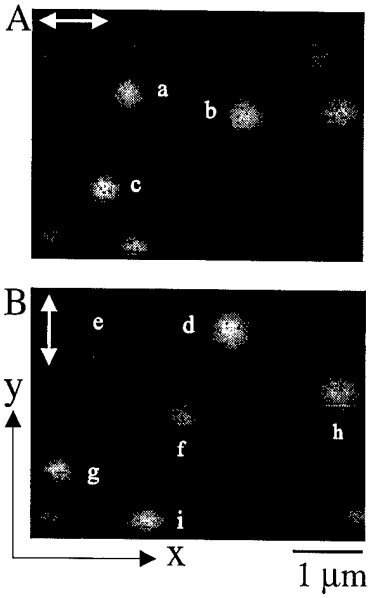

Fig. 2. Sequential fluorescence images of the same field of diI molecules, taken with 532-nm laser light polarized as indicated by the arrows. Absorption dipole orientation in the xy plane is found from the fluorescence rate versus laser polarization. Molecules (a)-(c) are oriented principally along the x-axis, molecules (d)-(g) along the y-axis, and molecules (h)-(i) oriented about 45° from the x- axis.

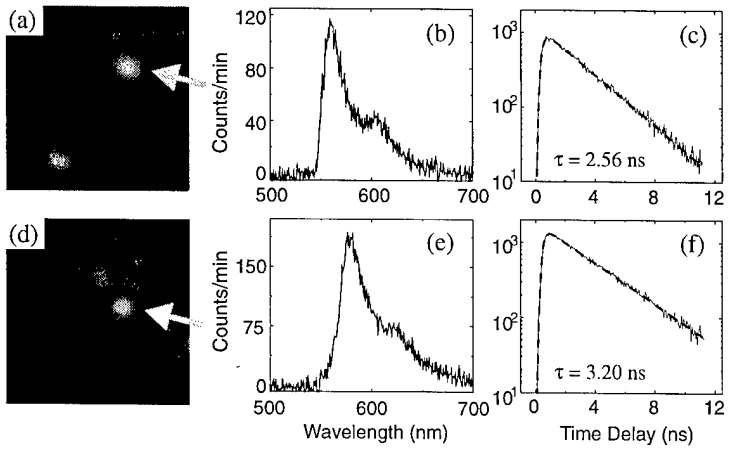

Fig. 3. Fluorescence image (a) and (d), from which a spectrum (b) and (e), and lifetime (c) and (f), are obtained for the molecules indicated. Each lifetime is fit to a single-exponential (dotted curves), with a 1/e time of 2.58 ns (χ^2 = 1.05) in (c), and 3.20 ns (χ^2 = 1.16) in (f). The peak emission wavelength differs by 20-nm for these two molecules.

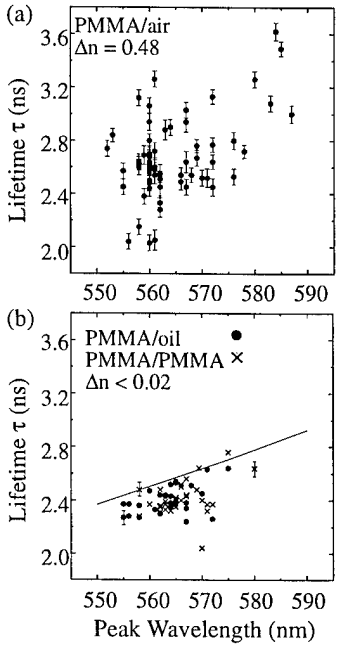

Fig. 4. Lifetime versus peak wavelength for molecules at (a) PMMA/air interface, with a refractive index difference of 0.48, (b) PMMA/oil or PMMA/PMMA interface, where the index difference is < 0.02. In (b), line approximates the maximum observed lifetime, $\tau = 2.57\ (\lambda/565)^3$.

High Sensitivity Detection on Microchips

J. C. Fister III; L. M. Davis; S. C. Jacobson; J. M. Ramsey

Chemical and Analytical Sciences Division, Oak Ridge National Laboratory

Oak Ridge, Tennessee 37831-6142

Phone 423-576-1870

Fax 423-674-8363

e-mail: f1t@stc10.ctd.ornl.gov

High efficiency separations coupled with rapid response times have been demonstrated on capillary electrophoresis devices micromachined on glass substrates. [1-3] Although detection of single organic dyes has been achieved with fluorescence detection in capillaries, [4] such detection limits have not yet been demonstrated in micromachined channels. Efficient, single molecule detection is desirable for many potential applications such as rapid DNA sequencing. The structure of microfabricated separation channels, however, does not readily facilitate a 90° fluorescence excitation/collection geometry which has been used to achieve high sensitivities in capillaries. [4] This optical geometry allows efficient spatial rejection of scattering at the capillary solution interfaces. Confocal detection in which the excitation source is introduced through the collection optics provides a means of achieving both high axial resolution and high collection efficiency .

Zare et al demonstrated the use of confocal optics for real time detection of single molecules in condensed media. [5] They used laser excitation to define a probe volume of ~5 x 10^{-16}. A small detection volume is necessary to limit fluorescence and Rayliegh and Raman scattering from the solvent and interfaces. Photon bursts from single molecules were observed as they diffused through the detection zone. We are developing a similar approach for detecting single molecules in microfabricated channels.

In order to use confocal optics to efficiently detect single molecules in a microchannel having a width of ~ 50 μm and depth of ~ 10 μm, steps must be taken to increase the size of the probe volume relative to the microchannel. Increasing the probe volume in the axial dimension to just less than the channel depth was possible using an appropriately sized pinhole. The radius of the detection zone may be increased by decreasing the waist size of the exciting laser. To facilitate ease of use, a 40x air objective rather than an oil immersion objective was employed despite the ~ two-fold reduction in collection efficiency. The resulting probe volume was ~ 2 x 10^{-14} L which required efficient rejection of both Rayliegh and Raman scattering. We have used a holographic notch filter with an optical density of > 10^{6} at 514 nm to improve rejection of Rayliegh scattering. A bandpass filter (+/- 20 nm) centered at 540 [5] nm rejects a significant fraction of the solvent Raman scattering. A single photon avalanche diode (SPAD) detector having a low dark count and quantum efficiency of > 50% was used. [6]

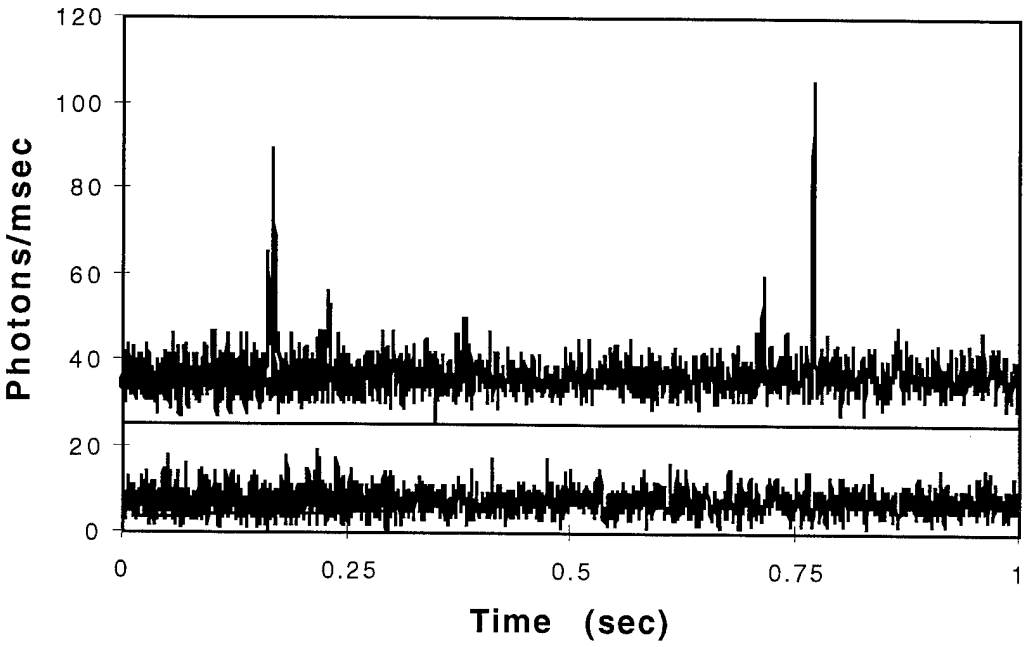

Figure 1. Single molecule detection of R6G. Top: 40 fmolar R6G in water. Bottom: Blank.

To determine the feasibility of single molecule detection with this design, preliminary studies were conducted on a microscope slide having a 1mm deep depression. Real-time detection of single dye molecules diffusing through the probe volume in a 40 fm solution of rhodamine 6G was demonstrated as shown in Figure 1. The probability of having two or more molecules in the probe volume was ~ 1×10^{-4} %.

Current efforts are under way to improve the S/N ratio of single molecule detection in microchannels. Fused silica substrates and coverslips will reduce the fluorescence background relative to soda lime glass and provide some improvement in index matching relative to BK7 glass. The shape of the probe volume can be optimized relative to the channel by using eliptical pinholes or cylindrical excitation optics. [7] Electrokinetic flow will be used to introduce dye molecules into the probe volume as a first step towards high sensitivity detection of separations.

References

1. Manz, A.; Harrison, J.; Verpoorte, E. M. J.; Fettinger, J. C.; Paulus, A.; Ludi, H.; Widmer, H. M. *J. Chromatogr.* **1992**, *593*, 253.

2. Harrison, D. J.; Manz, A.; Fan, Z.; ludi, H.; Widmer, H. M.; *Anal. Chem.* **1992**, *64,* 1926.

3. Jacobson, S. C.; Hergenroder, R.; Koutny, L. B.; Ramsey, J. M. *Anal. Chem.* **1994**, *66*, 1114-1118.

4. Castro, A.; Shera, E. B. *Anal. Chem.,* **1995**, *67*, 3181.

5. Nie, S.; Chiu, D. T.; Zare, R. N *Science*, **1994**, *266*, 1018.

6. Li, Q.; Davis, L. M. *Rev. Sci. Instrum.* **1993**, *64*, 1524.

7. Woolley, A. T.; Mathies, R. A. *Anal. Chem.* **1995**, *67*, 3676.

Modeling Fluorescence Collection from Single Molecules in Liquid Microspheres

S. C. Hill
Army Research Laboratory, White Sands Missile Range
White Sands, New Mexico 88002-5501
Phone: 505 / 678-4078
Fax: 505 / 678 -2845
e-mail: shill@NMSU.edu

M. D. Barnes, W. B. Whitten, and J. M. Ramsey
Chemical and Analytical Sciences Division
Oak Ridge National Laboratory
Oak Ridge, Tennessee 37831-6142
Phone: 423 / 574-4923
Fax: 423 / 574 - 8363
e-mail: nmz@ornl.gov

Optimization of molecular detection efficiencies is of central importance in analytical applications involving single molecule detection.[1] In addition to limitations imposed on the fraction of molecules which can be detected by the average signal-to-noise ratio, experimental factors such as excitation inhomogeneity and molecular diffusion conspire to further limit "molecular detectability." Recent single molecule detection experiments in microdroplets suggest that such experimental limitations can be significantly reduced primarily because the molecule cannot diffuse away from the excitation volume. However, unlike fluorescence detection from bulk streams where the fluorescence intensity is isotropic in space, the large refractive index change at the surface of microdroplets implies that the fluorescence intensity collected by a lens will be strongly dependent on the position of the molecule within the droplet. In addition, the same refractive index discontinuity at the droplet surface produces a complicated excitation intensity distribution within the

droplet as a result of interference between refracted and totally-internally-reflected rays. Thus, issues such as whether molecules near the surface of the sphere can "hide" from the detector as a result of total internal reflection of emission near the droplet surface, or poor excitation efficiency due to the molecule being located in a "shadow" region of the droplet will have a potential effect on molecular detection efficiencies. These questions are nontrivial to address in a quantitative way. Here we discuss development of numerical tools for modeling the fluorescence collected from a single molecule within a microdroplet as a function of position, orientation, and detection geometry based on the semiclassical electrodynamics formalism developed by Chew[2] for light scattering in dielectric microspheres. In addition we also examine effects of excitation inhomogeneity within the sphere, molecular diffusion, and transition rate modification in order to obtain a realistic model of molecular detection efficiencies in microdroplets.

REFERENCES

[1] M.D. Barnes, W. B. Whitten, and J. M. Ramsey, Anal. Chem. **67**, 418A, 1995

[2] H. Chew, Phys. Rev. A **38**, 3410 (1988).

Low Level Determinations of Uranium Hexafluoride Using Multiphoton Ionization Time-Of-Flight Mass Spectroscopy

Donald P. Armstrong
Lockheed Martin Energy Systems, Inc.*
Environmental Management and Enrichment Facilities Technical Support
P.O.Box 2003, Bldg. K1004L, MS-7266
Oak Ridge, TN 37831-7266
Phone: 423-574-9327 FAX: 423-576-2930 E-mail: armstrongdp@ornl.gov

David A. Harkins
Lockheed Martin Energy Systems, Inc.
Environmental Management and Enrichment Facilities Technical Support
P.O.Box 2003, Bldg. K1004L, MS-7266
Oak Ridge, TN 37831-7266
Phone: 423-574-7311 FAX: 423-576-2930 E-mail: harkinsda@ornl.gov

Robert N. Compton
Oak Ridge National Laboratory
P.O.Box 2006, Bldg. 4500S, MS-6125
Oak Ridge, TN 37831-6125
Phone: 423-574-6233 FAX: 423-576-4407 E-mail: comptonrn@ornl.gov

The uranium enrichment enterprise in the United States uses the gaseous diffusion method to achieve the desired level of enrichment of the ^{235}U isotope. The feedstock for this process is gaseous uranium hexafluoride (UF_6). In addition to the current production facilities there are also facilities which have been idled due to programmatic reasons, but may still contain residual, low levels of (UF_6). For the case of certain of these industrial processes or laboratory scale applications, the need to observe low levels of uranium hexafluoride (UF_6), often in the presence of other gases, is an important, but difficult, problem. UF_6 is a highly reactive gas particularly when acting as a fluorinating agent, and is very reactive with even trace levels of moisture. For these reasons, meticulous chemical drying techniques and containment vessels of suitable materials must be used. An accepted manner of analysis for the detection of UF_6 is to use a Fourier-transform infrared (FTIR) spectrometer. These units work reasonably well for observing UF_6 levels on the order of a few dozen ppm, but the reactive nature of the gas greatly limits the choice of infrared windows. The fundamental vibration of interest in UF_6 is the υ_3 band at ~ 625 wavenumbers, but spectral interferences can occur from other gaseous species which may be mixed with the UF_6 thereby complicating the analysis. We describe a laser technique which can provide sub-ppm levels of detection for UF_6 in the presence of other gases using commonly available laser hardware.

We have previously described the interaction of UF_6 with pulsed laser light from a Nd:YAG laser and discussed the unique features of this technique [1]. Using a Nd:YAG laser operating

at λ=266 nm, with a pulse width of ~ 5 ns, in conjunction with a pulsed nozzle for delivery of the gas sample containing the UF_6, copious quantities of U^{2+} can be formed in the focal volume during the multiphoton ionization of UF_6. Very modest energy levels are required, typically <1 mJoule. These ions are subsequently separated from the gas mixture and detected using a time-of-flight mass spectrometer. This method can be effectively used with relatively low backing pressures in the pulsed nozzle; hence, large amounts of sample are not required. This technique has several advantages over standard FTIR spectroscopy. The gases present with the UF_6 , whether present as additives or reaction products, do not undergo photoionization in the same manner as the UF_6; hence, few extraneous ions are formed. Since no infrared windows are utilized, there is no potential for reactions between the sample and the window surfaces; in addition, there are virtually no 'memory' effects in the sample vessel. Using this (briefly) described technique which incorporates a low-repetition rate Nd:YAG laser, a standard TOFMS, a pulsed nozzle, and a microchannel plate detector, sub-ppm level detection of UF_6 is possible. The mass spectra shown in Figure 1 represent successive dilutions of UF_6.

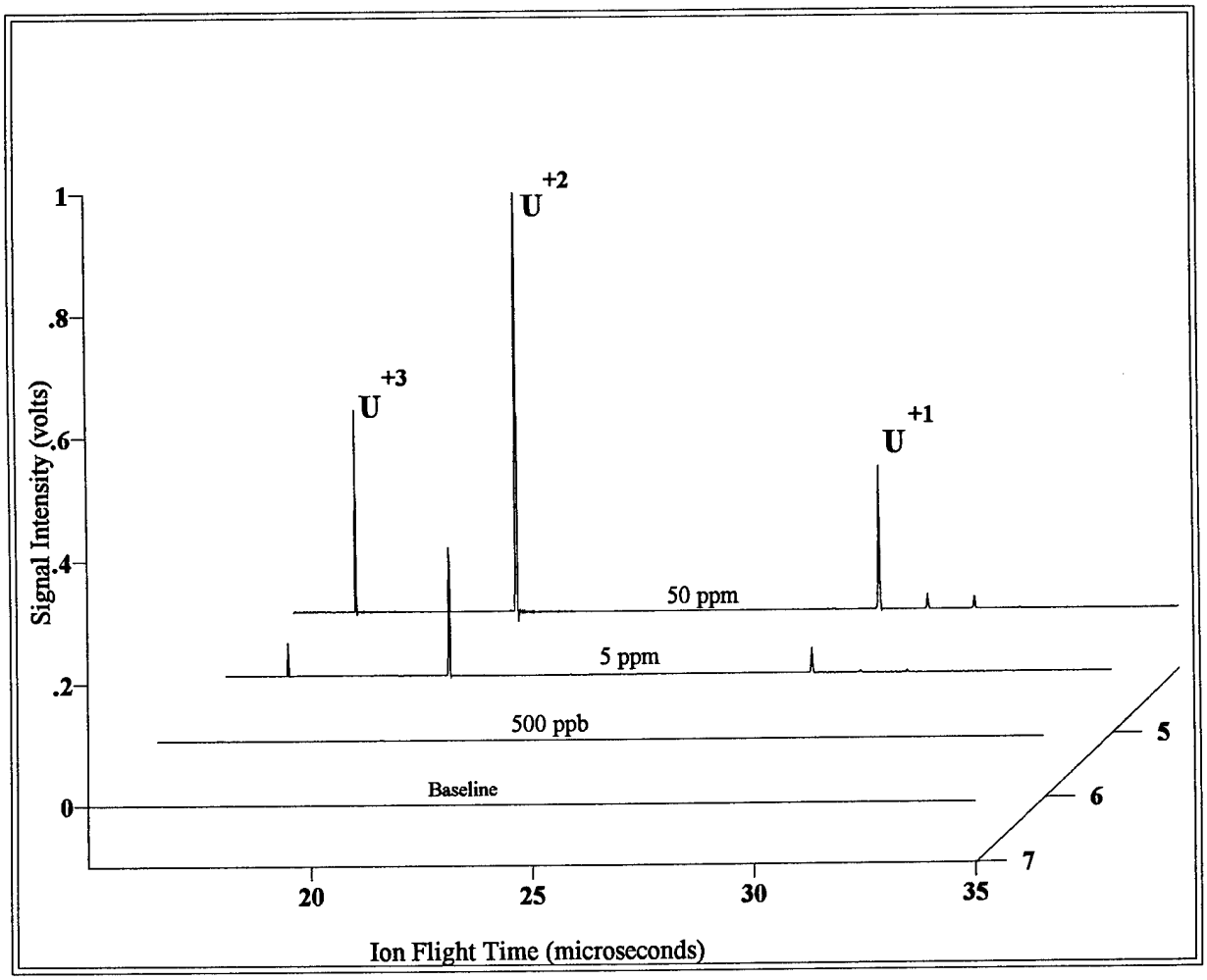

Figure 1

In Figure 2, the final spectrum has been rescaled to show the relative signal-to-noise possible for a mass spectrum obtained using an approximate 500 ppb sample of UF_6.

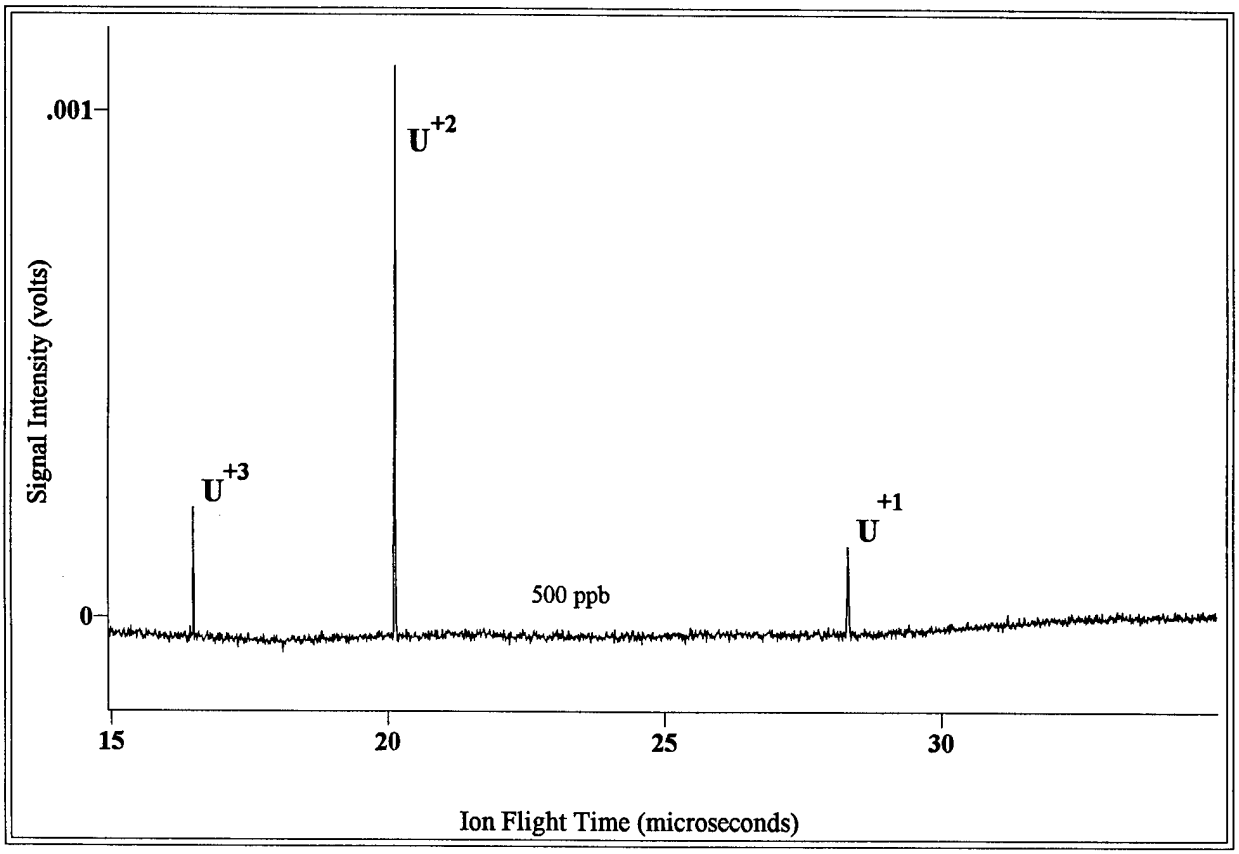

Figure 2

REFERENCES

[1] D.P.Armstrong, D.A.Harkins, R.N.Compton, and D.Ding, J. Chem. Phys., **100**, 28 (1994).

*Managing contractor for the Department of Energy under Contract DE-AC05-84OR21400.

Near field scanning optical microscope for biological applications.

Baibyrin V. B. Prof. of Saratov Politechnical University, Politechnitcheskaja 77 Saratov 410016,Russia,ph(8452-257750),fax.(8452-506740)

Anisimov P.I. Dr. of Russian Research Anti-Plague Institute "Microbe", Saratov 410071, Russia,ph.(8452-248579)

Konnov N. P. Prof. of Russian Research Anti-Plague Institute "Microbe", Saratov 410071, Russia,ph.(8452-248579)

Shcherbakov A.A. Prof. of Russian Research Anti-Plague Institute "Microbe", Saratov 410071, Russia, ph.(8452-248579)

Volkov U. P. Postgraduate of Saratov Politechnical University, Saratov 410056, Rachova 91/101, fl.10,ph.(8452-507049)

In our biophysical laboratory systematic investigations of plague and choler microbes are carried out by different methods (conventional electron microscopy, scanning tunneling microscopy and atomic force microscopy). At present for the investigations we have develop a near field scanning optical microscope (NSOM).

A construction of our apparatus in the main follows that of conventional NSOM [1]. The microscope can be operated in two modes viz. in collection mode and in illumination mode. In illumination mode light emitted from a small aperture at a single mode fiber end transmit through a sample and is received by photomultiplier tube. In collection mode light transmitted through the sample is collected by the aperture at the fiber end. The small aperture is fabricated by selective etching techniques using ammonium fluoride- buffered hydrofluoride acid solution [2] followed by coating the fiber end with Al. A curvature radius

of the optical fiber tip is estimated as 80 nm by measuring the geometrical profile of the SEM images of a number of fiber tips. In our microscope sample is scanned near the fixed optical fiber tip. The maximum scanning range is about 1x1 μm. A rough lateral displacement unit allows to move the sample on distance about 1x1 mm. Coarse approaching of the sample to the tip is performed with an adjustment unit similar that of our STM [3]. The adjustment unit allows to move sample on distance about 1mm, the step size is approximately 0.05 μm. The tip fine movement on distance about 1 μm is performed with piezoelectric tube. Small size and high rigidity of the NSOM allow to operate in ordinary laboratory without any additional vibration isolation. The NSOM control unit includes digital raster generator and digital feedback circuit. In the microscope two different laser light sources are used viz. HeNe λ=0.63μm,P=20mW and N_2 λ=0.35μm,P=2mW. As test objects we used a diffraction grating and thin metal films (Al, Pt, Au). The NSOM lateral resolution is estimated as 500 A.

At present we have only preliminary data of investigations of plague and choler cells by means of the NSOM. Plague (Yersinia pestis) and choler () cells were grown and were fixed according to conventional procedure. Various methods of increasing of cell image contrast were tested such as use ultraviolet light, coloring and coating with metals (Al, Pt, Au). The images are compared with ones obtained by other methods.

References

1.E.Betzig, M.Isaacson, H.Barshatzky, et al.,Ultramicroscopy,v.25(1988),p.155-164

2.S.Jiang,N.Tomita,H.Ohsawa,M.Ohtsu,Jap.J.Applied Physics,v.30(1991),No.9A, p.2107-2111.

3.U.Volkov,V.Tsykanov,SPIE Proceedings ,v.2083 (1993),p.190-194.

Single Particle Back Scatter Measurements with Size Parameters Near One

Matthew Hart, C.W. Bruce
U.S. Army Research Laboratory / New Mexico State University

New Mexico State University
Box 30001 / Dept. 3D
Las Cruces, NM 88003-8001

Tel: (505) 646 - 1610
Fax: (505) 646 - 1934
Email: mhart@nmsu.edu

We have developed a technique to measure the back scatter from particles using millimeter wavelengths. The system consists of two major components, the microwave source/receiving setup and the scattering chamber (lined with microwave absorbing material) [Fig. 1]. Millimeter wavelengths are used and thus size parameters near one are natural targets for the system. A waveguide horn antenna is utilized as both the source and the receiver. Ambient radiation, due to chamber reflections and antenna mismatch, is a major source of error in the system and is minimized by way of a cancellation bridge. The bridge adds to the received radiation a signal of equal amplitude and of opposite phase to the ambient leaving only the desired back scatter component. Although confined to the small (25 cm radius) vessel we have been able to perform far field measurements with good results.

Liquid droplets pass through the chamber center and the back scatter signal is measured as a function of time as they fall past the source/receiver horn. With moderate ease identical successive drops can be produced from a continuously functioning dropper and a boxcar average over many drops produces a good signal to noise ratio. For water droplets the shapes are very close to spheroidal, oscillating from oblate to prolate, and will vary from the spherical by as much as 15% for observations of the back scatter cross sections on droplet form. Other

geometries/materials may be suspended on dielectric fibers in front of the antenna and are typically rotated to achieve back scatter verses incident angle. This technique has been used for fibers and overlapping-sphere targets.

To date types of particles which have been examined with this system include single metallic spheres, spheroidal water drops, overlapping metallic spheres, thin conductive cylinders, and metallic coated thin cylinders. These measurements provide comparison data for several computational models from Mie theory to more contemporary scattering theories.

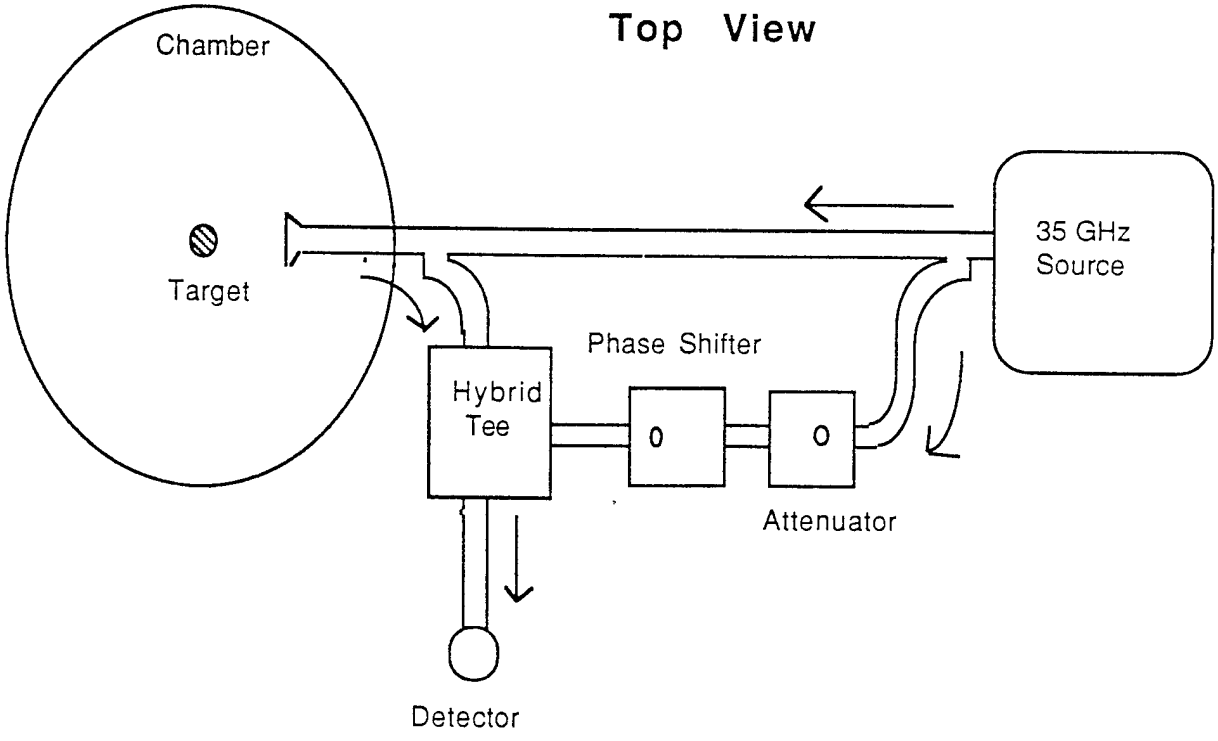

Fig. 1

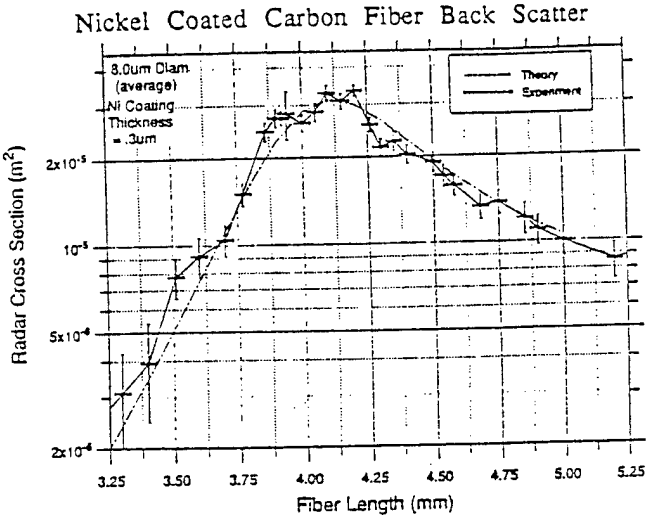

Some Past Results

Fig. 2

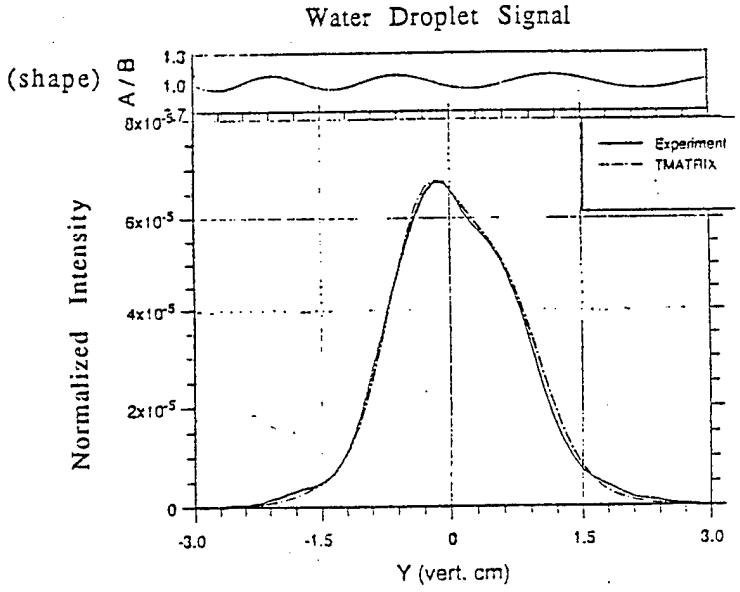

References

Gordon Videen, Dat Ngo, Matthew Hart; *Light Scattering From a Pair of Conducting Osculating Spheres*, Opt. Comm., In Press. (Overlapping Spheres)

P. C. Waterman and J. C. Pederson; to be published.
(Coated Thin Finite Cylinders)

P. C. Waterman and J. C. Pederson, *Electromagnetic Scattering and Absorption by Finite Wires* , J. Appl. Phys. 78, 656-667, July, 1995.
(Finite Cylinders)

P. W. Barber and S. C. Hill, *Light Scattering by Particles: Computational Methods*, World Scientific, 1990. (Spheroidal Particles, Tmatrix)

Alternative Approaches to Sampling and Data Collection for Laser Induced Breakdown Spectroscopy (LIBS)

Andrzej W. Miziolek, Cindy Williamson*, Kevin L. McNesby, Nicholas F. Fell, Jr.*, Stephen V. Medlin*, Brad E. Forch, Robert G. Daniel
U.S. Army Research Laboratory
AMSRL-WT-PC
Aberdeen Proving Ground, MD 21005-5066
410-278-6157 Tel, 410-278-6150 FAX, miziolek@arl.mil
and
Ernesto R. Cespedes, Brian H. Miles, Javier Cortes
U.S. Army Engineer Waterways Experiment Station
CEWES-EE-S
3909 Halls Ferry Road
Vicksburg, MS 39180-6199

LIBS is a very powerful technique for spectrochemical analysis, particularly for the detection of metals in vapors, aerosols, liquids, and solids. Much of the pioneering work in LIBS development has occurred at Los Alamos National Laboratory[1]. Typically, a short-pulse laser beam is focussed into the sample causing optical breakdown and the plasma light is collected unto a spectrograph and detected by an array detector. This relatively straightforward set-up affords high sensitivity and efficiency in terms of data generation and collection. In traditional LIBS analyses a single laser is used to vaporize and ionize the sample.

We are pursuing certain alternative methods and instrumentation for LIBS analyses. These include the use of a second laser for sample volatilization/pyrolysis as well as the use of an acousto optic tunable filter (AOTF) as a replacement for the spectrograph and single photon counting for increased sensitivity. The use of the second laser is motivated by our interest in evaluating LIBS as a means of detecting energetic molecules for analysis of soil contamination. Typically the goal of LIBS is to break most or all chemical bonds and to induce elemental emission in a high temperature environment. This works particularly well for the sensitive detection of various metals, including those of environmental concern such as Pb, Hg, Cr, Cd, etc. LIBS research generally has not concentrated on molecular fragment detection, although such analyses are indeed possible[2]. We believe that LIBS may be useful for the detection of energetic molecules such as TNT and the nitramines but only if the sampling and plasma conditions are different than usual. Specifically, nitro-containing energetic molecules can be considered as semi-volatile as compared with typical soil constituents. The use of a volatilizing laser which drives such molecules from the soil for subsequent LIBS analysis of the vapor phase addresses the problem of interference from inorganic nitro/nitrate compounds. Also, it avoids the spectral

cluttering that would result from plasma excitation of the metal constituents of the soils. One important question that we are in the process of answering is whether the gaseous energetic materials can generate easily detectable unique fragment emissions as were previously observed for hydro- and halo-carbon vapors[2].

Acousto optic tunable filters (AOTFs) offer the advantage of high throughput, ruggedness, and all solid-state operation as wavelength discriminating devices which could be mated to very sensitive photomultiplier tubes or photodiode detectors. Such an alternative detector system to the traditional spectrograph/OMA appears to be quite attractive for its compactness, ruggedness, and energy efficiency. An AOTF/PMT system has a major disadvantage of being able to only process one wavelength segment per LIBS laser shot, and thus would need to be coupled with a high repetition rate LIBS laser.

We have recently purchased a state-of-the-art high resolution (few Angstroms) AOTF device. Unfortunately, in early testing this device exhibited insufficient stray-light rejection for LIBS use. However, the manufacturer has added additional optics to address this problem and we are in the process of reevaluating this device. In principle, the AOTF can spectrally jump to wavelength locations that are of interest for a particular analysis, thus avoiding large spectral regions devoid of useful information, a situation that typically occurs when using OMAs. AOTFs have been used recently at LANL for the time-resolved imaging of the LIBS plasma plume[3].

A number of years ago our laboratory demonstrated that single photon detection of resonant emission subsequent to ionization is possible and can lead to sensitive analyte detection[4]. The source of the single photons is the recombination of initially produced ions and electrons, a process that leads to the emission of resonant radiation as the highly excited recombination product proceeds to thermal equilibrium. The single photons are detected after the initial LIBS plasma has decayed (past 10 microseconds). The results of our evaluation and comparison of the single photon approach to standard LIBS analysis will be presented.

References

1. *Laser-Induced Plasmas and Applications*, L.J. Radziemski and D.A. Cremers, eds., Marcel Dekker: New York, 1989.
2. R.J. Locke, J.B. Morris, B.E. Forch, and A.W. Miziolek, Appl. Opt., vol. 29, p. 4987, 1990.
3. D.A. Cremers, presented at the 1995 Optical Society of America Annual Meeting, Portland, OR.
4. R.C. Sausa, A.J. Alfano, and A.W. Miziolek, Appl. Opt., vol. 26, p. 3588, 1987.

* NAS/NRC Postdoctoral Research Associates

Laser-Induced Plasma Spectroscopy (LIPS) for Environmental Applications

C. Haisch, M. Clara, U. Panne and R. Niessner

Institute of Hydrochemistry,
Technical University of Munich, Marchioninistr. 17, D-81377 Munich, FR Germany

Laser-Induced Plasma Spectroscopy (LIPS) is a powerful instrument for quantitative elemental analysis of solid, liquid and gaseous matrices. For LIPS an intense, pulsed laser beam is focused on the sample of interest, resulting in the dissociation and partial ionisation of the sample in an expanding plasma cloud. Approximately 100 ns after the laser pulse recombination followed by relaxation of the atoms can be observed in the plasma cloud. The spectrally and temporally resolved detection of the atomic emission lines reveals analytical information about the elemental composition of a sample. The lack of sample preparation and the low costs for a single measurement make this technique a useful tool for environment analysis. The presented applications are excellent examples for the versatility of LIPS.

1. *Quantification of Main Elements in Hot Glass Melts.* The objective is the development of an on-line process-control system for the vitrification of glass-like ashes from waste incineration. Using a LIPS-based sensor system the optimum composition is monitored to guarantee the complete immobilisation of hazardous heavy metal compounds in the produced glass pellets. Responsible for the inertisation are mainly the oxides of silicon, aluminium, magnesium, sodium and potassium.

The plasma was generated by a Q-switched Nd:YAG-Laser ($\lambda = 1064$ nm), which is focused by a planoconvex lens on the surface of the liquid glass. Emission of the plasma was collimated by the same lens, reflected by a 45° mirror perpendicular to the laser beam and imaged on the entrance slit of a 0.275-m-spectrograph.

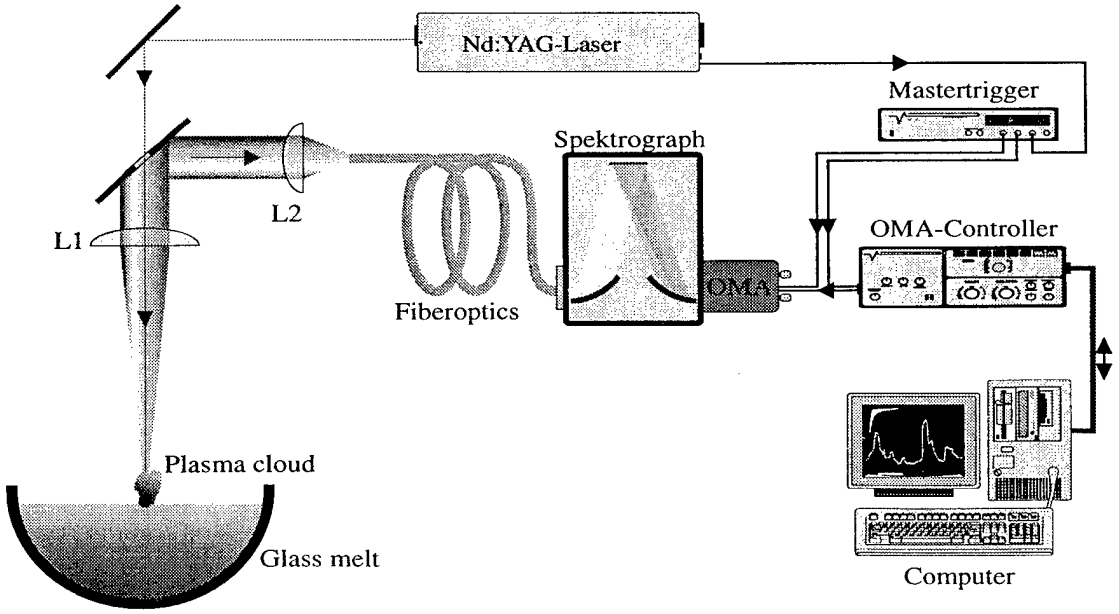

Figure 1 *Experimental set-up for the LIPS-characterisation of hot glass-melts.*

The excitation beam of the laser passes through a 5 mm hole of this mirror (50 mm diameter). The detection was carried out with a gated, intensified Optical Multichannel Analyzer (OMA). Major advantages of this optical arrangement are: (i) A low sensitivity for variations at the surface level and position of the plasma cloud due to the focusing/collimating lens. (ii) Industrial applications require to probe the melt through a very small access hole in the melting chamber in order to minimise the energy loss of the oven; for the described system a hole of a 30 mm diameter is sufficient for both excitation and detection.

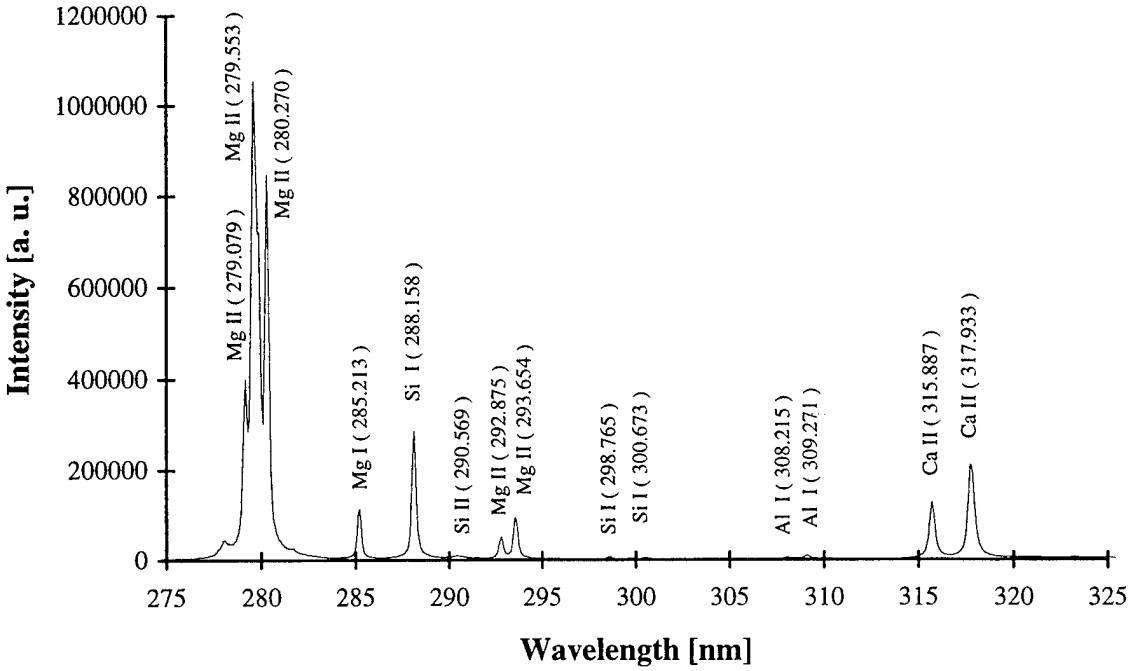

Figure 2 *Typical LIPS-spectrum of a hot glass melt.*

Figure 2 shows a typical LIPS-spectrum of hot glass melt acquired with the described set-up. To correlate the atomic lines intensities with corresponding element concentration, the influence of the fluctuating plasma properties has to be corrected by normalisation. With the electron temperature and density from the relative line intensities of one element, a linear correlation of signal and concentration with a very low RSD (< 3 %) was achieved.

2. *Characterisation of Hydrocolloids.* Hydrocolloids are suspected as carriers of pollutants in water, permitting an accelerated transport in aquatic systems. Especially heavy metals and residues of organic contaminants can be bound to colloidal matter by a variety of functional groups. As the particulate transport depends on size and material of the particles, a characterisation of colloidal systems in terms of number density, size distribution and chemical composition is of increasing interest for migration studies of environmentally relevant substances. Field flow fractionation (FFF) covers a class of generic chromatographic separation methods for separation of particles with high resolution and a dynamic range up to five orders of magnitude. FFF is a one-phase fractionation technique in which a flow field, applied perpendicularly to a particle-containing flow, forces dissimilar particles to partition among flow lines of different velocity. Like all chromatographic techniques, FFF provides no quantitative information and therefore has to be combined with a suitable particle detector. Since normally only light-scattering detectors are employed, the detection is restricted to particle diameters above 200 nm.

The objective here was to utilise LIPS in combination with Flow-FFF for separation and chemical analysis of aquatic colloids. The hyphenation of FFF with LIPS provides not only a way to count particles quantitatively, but also to determine major chemical constituents. With knowledge of the retention time, i.e., the particle size, it is possible to calculate the number density and size distribution. In order to avoid quenching of the plasma by the surrounding water, the colloids were removed from the solution. This was achieved by collecting the colloids from FFF on a filter. Partitioned pumping with steps of 50 µl through filter tape allows to maintain a sufficient time resolution of the FFF. The resulting "colloid spots" are probed by the LIPS with a detection system similar to figure 1.

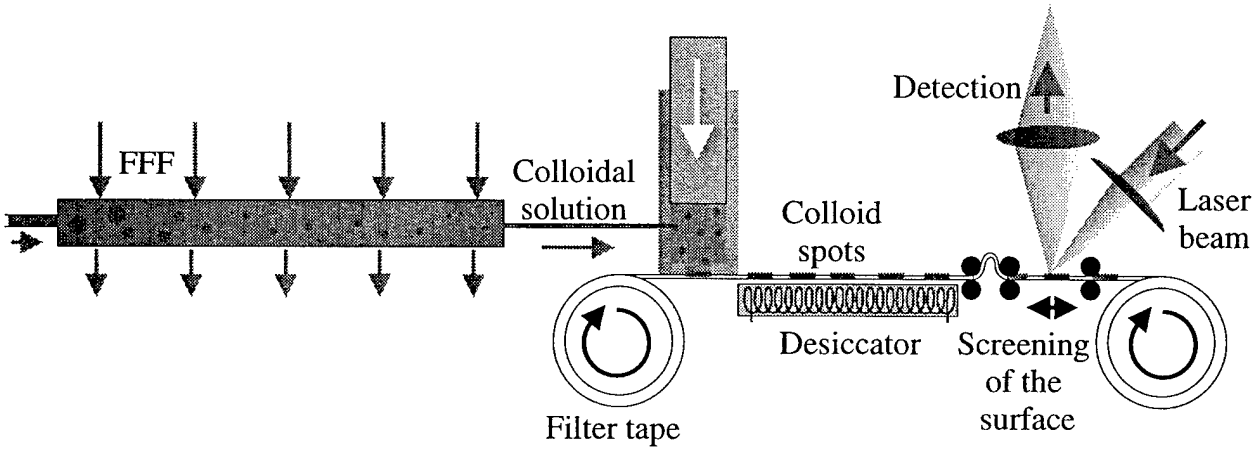

Figure 3 *Experimental set-up for the LIPS-characterisation of colloids.*

With this set-up a LOD (3σ) of 0.6 ppm of SiO_2-colloids (dp = 500 nm) was achieved. The subsequent excitation of atomic fluorescence in the plasma is a promising future approach for improving the sensitivity for a number of elements, which can allow the detection of the colloid-bound heavy metals.

Literature:

1. Radziemski, L.J. and Cremers, D.A., *Laser-Induced Plasmas and Applications.* 1989, New York: Marcel Dekker.
2. Radziemski, L.J., *Review of selected analytical applications of laser plasmas and laser ablation, 1987-1994.* Microchem. J., 1994. **50**(3): p. 218-234.
3. Wisbrun, R., Niessner, R., and Schröder, H., *Laser-Induced breakdown spectrometry as a fast screening sensor for environmental analysis of trace amounts of heavy metals.* Anal. Methods and Instrum., 1993. **1**(1): p. 17-22.
4. Moenke-Blankenburg, L., *Laser Micro Analysis.* 1989, New York: John Wiley & Sons.

RAYLEIGH AND RAMAN DIAGNOSTIC OF LASER GENERATED PLASMAS

Deborah Nassif Pugsley and Lutz Hüwel
Wesleyan University, Physics Department, Middletown CT 06459-0155
phone: (860) 685-2052; FAX: (860) 685-2001

Laser-produced plasmas have long attracted the attention of researchers because of their unusual properties coupled with ease of generation. With laser power densities above approximately 10^{13} W/cm^2 high electron densities and temperatures can be achieved and here x-ray lasers and laser fusion are important applications. At lower intensities, among other applications plasma etching and spectrochemical analysis make use of laser plasmas. We have found[1] that for laser power densities of about 10^{10} W/cm^2 the temperatures in the aftermath of Q-switched laser sparks in air (or other gases) can be several thousand degree Kelvin, even at times as late as 100 μs after ignition. Obviously, the plasma must eventually decay and approach ambient temperature. At least in principle, this opens the possibility to access conditions relevant for combustion and other high temperature chemical processes - even if only on a small spatial scale and during short time intervals. To study the feasibility of such high rep rate generation of temperatures in the range from say 300 to 3000 K we have investigated the spatial and temporal structure of Nd:YAG laser generated sparks in air and other gases during their final stages of decay, i.e. when their temperature and pressure approaches that of the surrounding gas.

Following work that reported on spatially resolved measurements of temperature and density of majority species in flames[2] and in an internal combustion engine[3] obtained from Rayleigh and spontaneous Raman scattering, we have adopted these techniques for the experiments described here. Briefly, the pulse of a Q-switched Nd:YAG laser (1064 nm, 15 ns, 250 mJ, 10 Hz) is focused via a shape optimized 10 cm focal length lens into a chamber containing the gas under investigation. The resulting small plasma globule, brightly emitting for a short time (≈ 100 μs), is the object of a time delayed probe pulse delivered by a second, synchronized Nd:YAG laser (355 nm, 10 ns, 30 mJ). The diagnostic laser is slightly focused by a 50 cm focal length lens and interrogates the plasma along a line perpendicular to the direction of the ignition laser which in turns defines the axial direction of the plasma. With careful alignment of the two lasers we can achieve near perfect overlap of the two lasers and hence radial probing of the plasma. Rayleigh and Raman scattered light is imaged from the probe laser line through the plasma onto the slit of a 0.6 m monochromator with the slit height parallel to the probe laser direction. With this arrangement, the dispersing properties of the monochromator are used to separate elastically and inelastically scattered contributions - thus making use of the species sensitivity of the Raman effect - while maintaining the spatial information along the slit. A gated linear diode array (in the absence of a highly desirable CCD camera) is mounted in the exit plane of the monochromator. Depending on its orientation relative to the slit, the array can record either the spectral composition of the signal integrated along the slit or the spatial information of a selected Raman (or Rayleigh) line. The temporal resolution of the detector is determined by the pulse duration of the image intensifier used in conjunction with the linear diode array and can be as short as 75 ns, although we typically operate the intensifier at "shutter" opening

times of 3 μs. Crucial to the good signal to noise we obtain in our data is a polarization subtraction technique which exploits the fact that Rayleigh and Raman scattered light is highly polarized whereas background and surface scattering is not. Rotation by 90° of the direction of polarization of the probe laser via a λ/2-plate for 355 nm indeed reveals a strong modulation of the signal when the chamber is filled with gas while scattered light in vacuum shows almost no polarization dependence.

Data scans consist of traces of the various scattered intensities measured along the radial direction at various axial positions in the plasma taken at several fixed delay times relative to plasma ignition. Spontaneous light scattering is directly proportional to the density of the scatterer and free of any complications due to quenching. Also, at the temperatures found in the current experiment contrary to temperatures above about 10^4 K, the degree of thermal ionization is extremely small so that Thomson scattering is entirely negligible. Therefore, normalization of the data to scattering intensities for the gas at ambient conditions (taken with the same setup without the plasma creating Nd:YAG laser) immediately yields absolute densities in terms of the ambient gas density n_0 which can easily be determined by pressure and temperature measurement of the gas in the chamber. Figure 1 shows an example of such linear density traces obtained from Rayleigh scattering in air sparks at atmospheric pressure at various delay times from 240 to 1250 μs after the plasma formation. To the extent that at the late delay times the pressure in the plasma afterglow has already reached the value of the surrounding gas, assumption of ideal gas law behavior allows a conversion of the absolute density into temperature curves as shown in figure 2. At first sight, one might interpret the obviously still ongoing radial expansion of the hot gas as the remnant of the initial blast wave and this would certainly preclude the assumption of a constant pressure across the spatial profile. However, a quantitative analysis of the rate of expansion reveals a value of about 5.9 m/s - clearly incompatible with the much higher speed expected for a shock wave. It appears then that the observed expansion is driven by conduction and diffusion and that the assumption of constant pressure may be approximately satisfied. Further investigations of these high temperature gas clouds by laser induced fluorescence and measurements of the Doppler width of absorption lines will be used to corroborate the present results.

References:

[1]R. C. Alam, S. J. Fletcher, K. R. Wasserman, and L. Hüwel, Phys. Rev. **A 42**, 383 (1990)

[2]W. Reckers, L. Hüwel, G. Grünefeld, and P. Andresen, Appl. Opt. **32**, 907 (1993)

[3]G. Grünefeld, V. Beushausen, and P. Andresen, Appl. Phys. **B 58,** 333 (1994)

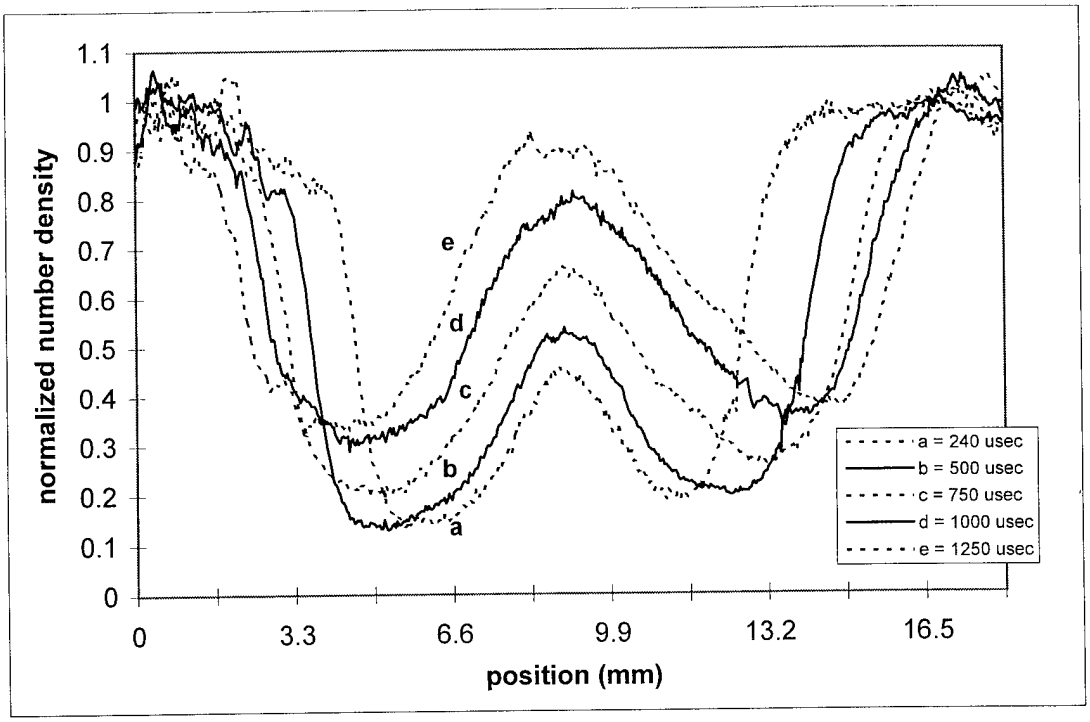

Figure 1

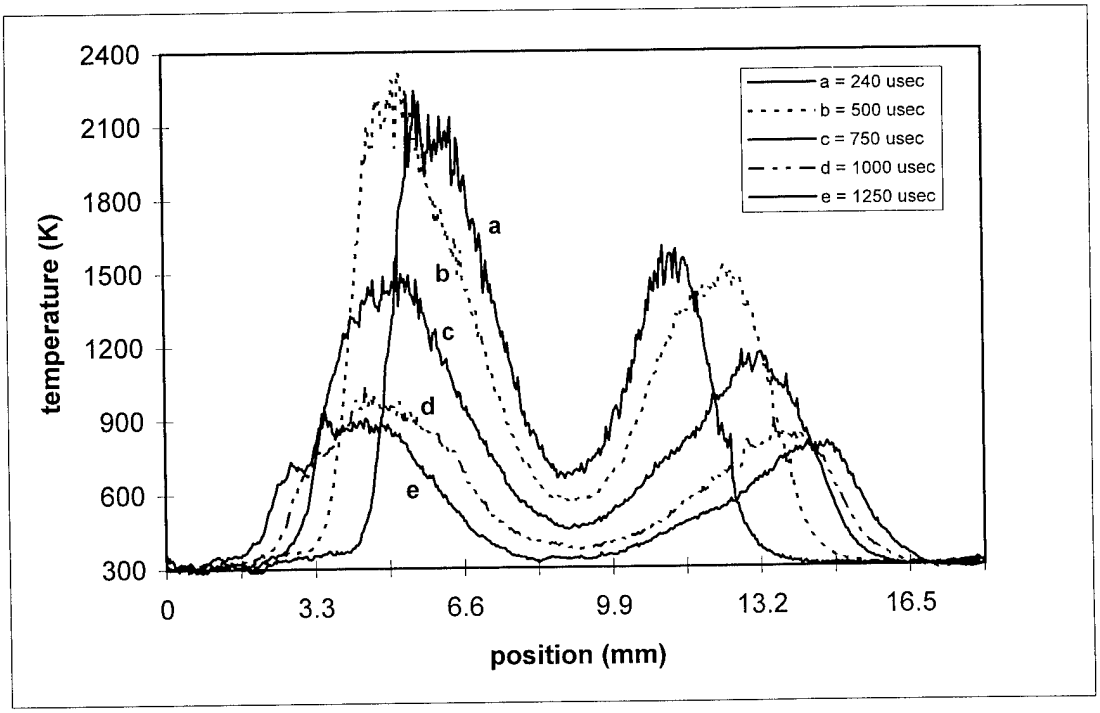

Figure 2

Laser Ignition of Gaseous Ammonia-Oxygen Mixtures

David H. Plemmons, C. Parigger, and J. W. L. Lewis
The University of Tennessee Space Institute
Center for Laser Applications
Tullahoma, Tennessee 37388-8897
Phone: 615-393-7338, Fax: 615-454-2271

1. Introduction

Laser ignition of combustible gas mixtures has been studied by numerous investigators.[1–10] We are interested in laser sparks resulting from nonresonant laser-induced breakdown generated by focusing Nd:YAG 1.064 μm, 4.5 ns full width at half maximum (FWHM) pulses into combustible ammonia-oxygen gaseous mixtures. The temporal and spatial evolution of the optical breakdown plasma into an ignition kernel, and subsequently into a propagating flame, is monitored using planar laser-induced fluorescence (PLIF) and shadowgraph imaging.

The PLIF images are acquired through a resonant excitation of the NH free radical which is a reaction intermediate in ammonia-oxygen combustion. The shadowgraph images measure density variations by illuminating the microplasma/kernel with 308 nm, 10 ns FWHM excimer laser pulses. The PLIF and shadowgraph probe beams are operated synchronously so that the PLIF and shadowgraph images can be correlated. A schematic of the experimental arrangement is shown in Fig. 1.

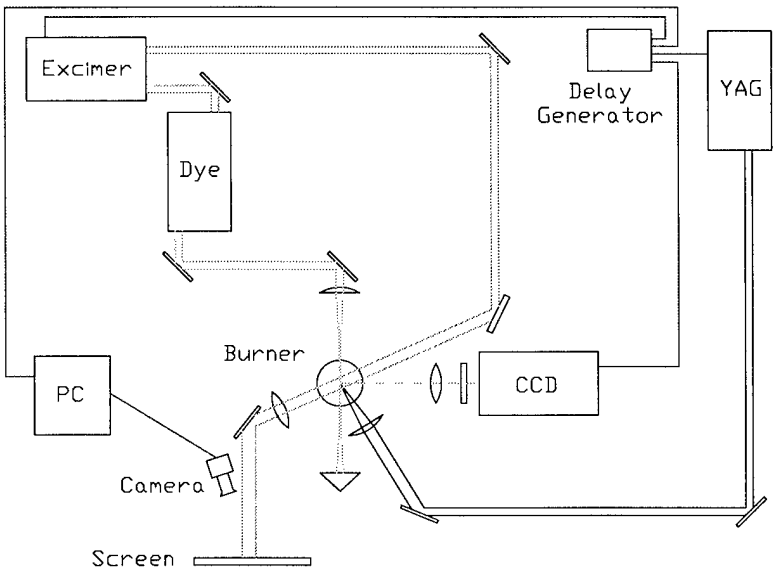

Fig. 1. Schematic representation of the experimental layout.

2. Results and Discussion

Figure 2 shows experimental results at time delays (with respect to the Nd:YAG laser) of 1.4 μs (left) and 20.4 μs (right). The PLIF images are shown at the top of the figure and the shadowgraph images are shown at the bottom.

In the 1.4 μs delay PLIF image the central bright region is dominated by NH spontaneous emission in the microplasma. The outer "ring" of ground state NH becomes visible only with the PLIF excitation and is most likely due to shock heating of the gas by the expanding shockwave (the outer dark ring in the 1.4 μs shadowgraph.) The NH ring is also visible at the 20.4 μs delay where the plasma spontaneous emission is no longer observable. This ring can be interpreted by referring to Fig. 3 which shows theoretical NH mole fractions and mass densities which occur across the flame front of a laminar, freely propagating ammonia-oxygen flame.[11]

We see that in the flame front there exists a well defined region of NH free radicals and that the band of NH lags behind the density gradient, in good agreement with the 20.4 μs PLIF and shadowgraph images. Using time-sequenced PLIF and shadowgraph images, such as those shown in Fig. 2, we probe phenomena such as ignition delays, flame speeds and gas dynamic effects.

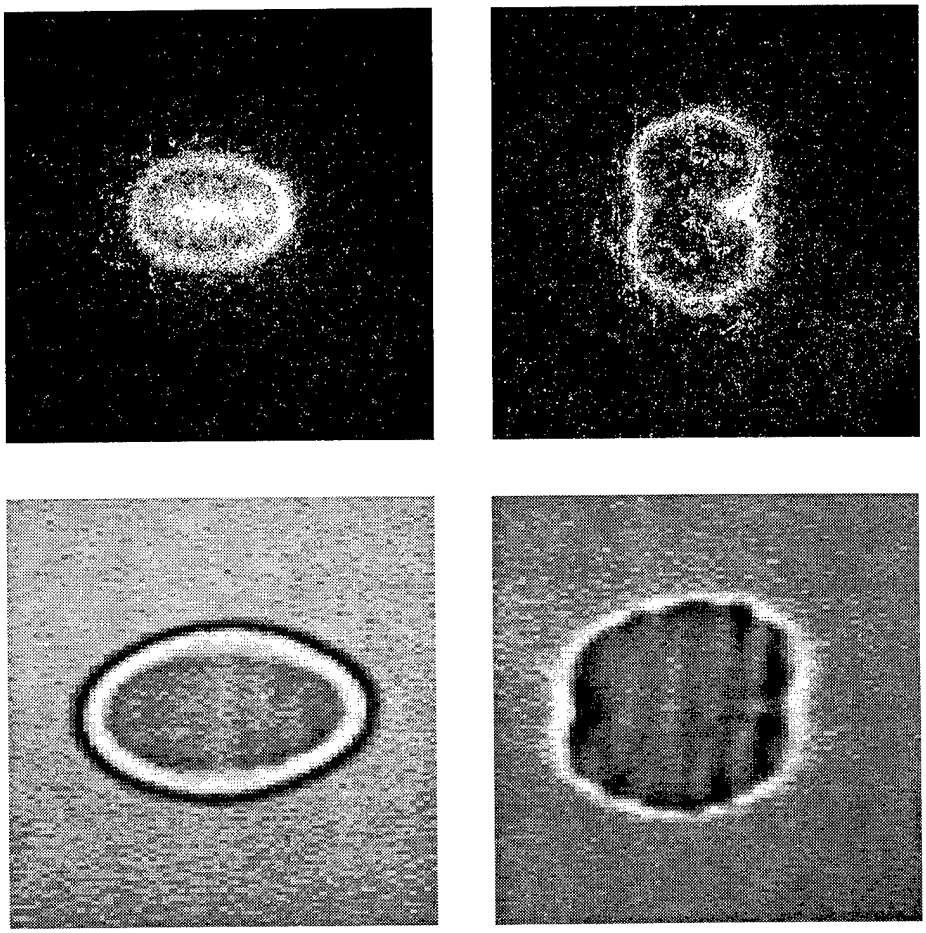

Fig. 2. PLIF (upper) and shadowgraph (lower) images showing the spatial temporal development of a laser ignited ammonia-oxygen flame.

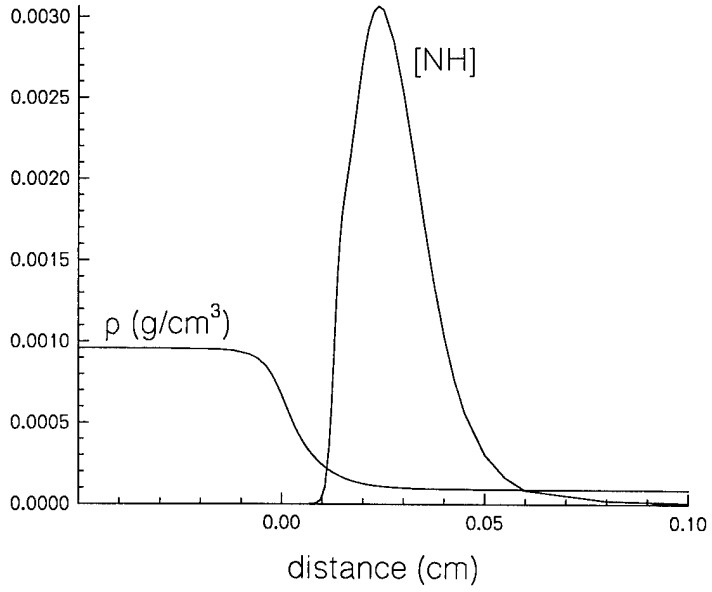

Fig. 1. Theoretical mass density and NH mole fraction for a freely propagating stoichiometric NH_3-O_2 flame.

1. T. A. Spiglanin, A. McIlroy, E. W. Fournier, R. B. Cohen and J. A. Syage, " Time-resolved imaging of flame kernels: laser spark ignition of H_2/O_2/Ar Mixtures," *Combust. Flame* vol. 102, pp. 310-328 (1995).
2. B. E. Forch and A. W. Miziolek, "Laser-based ignition of H_2/O_2 and D_2/O_2 premixed gases through resonant multiphoton excitation of H and D atoms near 243 nm," *Combust. and Flame* vol. 85, p. 254-262 (1991).
3. J. A. Syage, E. W. Fournier, R. Rianda and R. B. Cohen, "Dynamics of flame propagation using laser-induced spark initiation: ignition energy measurements," *J. Appl. Phys.* vol. 64, no. 3, p. 1499-1507 (1988).
4. J. M. Seitzman, P. H. Paul and R.K. Hanson, "Digital imaging of laser-ignited combustion," AIAA Thermophysics, Plasmadynamics and Laser Conference, San ANtonio, TX, Paper # AIAA- 88-2775 (1988).
5. R. A. Hill, "Ignition-delay times in laser initiated combustion," *Appl. Opt.* vol. 20, no. 13, p. 2239-42 (1981).
6. R. W. Schmieder, "Laser spark ignition and extinction of a methane-air diffusion flame," *J. Appl. Phys.* vol. 52, no. 4, p. 3000-3003 (1981).
7. R. Hickling and W. R. Smith, "Combustion bomb tests of laser ignition," *SAE paper 740114*, (1974).
8. J. H. Lee and R. Knystautas, "Laser spark ignition of chemically reactive gases," *AIAA Journal* vol. 7, no. 2, pp. 312-17 (1969).
9. F. J. Weinberg and J. R. Wilson, "A preliminary investigation of the use of focused laser beams for minimum ignition energy studies," *Proc. Roy. Soc. Lond. A* vol. 321, pp. 41-52 (1971).
10. In addition to the references listed above there is a recent review article by P. D. Ronney, "Laser versus conventional ignition of flames," *Optical Engineering* vol. 33, no. 2, pp. 510-521 (1994).
11. R. J. Kee and J. F. Grcar and M. D. Smooke and J. A. Miller, "A FORTRAN program for modeling steady one dimensional flames," Sandia Report SAND85-8240, Sandia National Laboratories (1985).

Hydroxyl Measurements in Air-Breakdown Microplasmas

Christian Parigger, J. W. L. Lewis, D. H. Plemmons, G. Guan, and J. O. Hornkohl
The University of Tennessee Space Institute
Center for Laser Applications
Tullahoma, Tennessee 37388-8897
Phone: 615-393-7338, Fax: 615-454-2271

1. Introduction

The hydroxyl radical has been extensively investigated for the thermal- and chemical characterization of combustion processes.[1–4] High temperature OH spectra are also of interest for the characterization of laser-induced air plasmas and laser-ignited gaseous combustible mixtures. Spectral studies of laser-induced breakdown microplasmas in laboratory air were performed and time-resolved OH recombination emission spectra were measured and compared with theoretical predictions. Particularly in view of laser ignition of, for example, gaseous combustible mixtures, analysis of such recombination spectra is required prior to the use of OH as a combustion indicator in laser-ignited media.

2. Experimental Details

Laser-induced optical breakdown in nominal STP laboratory air was accomplished by the focusing of the Nd:YAG 1064-nm radiation of 3.5-ns pulse width, with intensities of typically 10^{13} W/cm^2. A Coherent Infinity 40-100 Nd:YAG laser was operated at a frequency of 10 or 100 Hz. The spectra were resolved with a 0.275-m Jarrel-Ash or a 0.64-m Jobin-Yvon spectrometer, and detected using an optical multichannel analyzer. Wavelength calibrations were performed with standard light sources, and the sensitivity correction was accomplished with a deuterium lamp. The detector's data were corrected for dark-noise contributions.

3. Results and Discussion

Figure 1 shows a time-resolved OH spectrum that was measured at a time delay of 100 μs after the optical breakdown event in air.

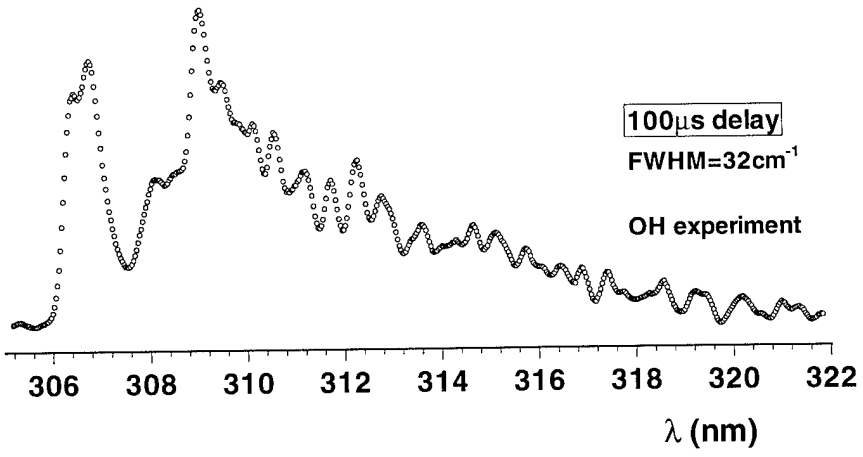

Fig. 1. OH optical breakdown spectrum, 100 μs time delay.

The recorded experimental OH spectra from air breakdown were analyzed: (1) by the use of the nonequilibrium air radiation (NEQAIR) code[5–8] with computed mole fractions of the plasma composition[9] and temperature as input, and (2) by the application of the University of Tennessee Space Institute (UTSI) line strength file for the $A^2\Sigma \leftrightarrow X^2\Pi$ uv-system of OH.[10]

The spectroscopic temperature of T=3900K is obtained by the use of NEQAIR8,[7] but assuming thermodynamic equilibrium. Figure 2 shows a least-square fit to the experimental data. NEQAIR uses semi-empirical term-value equations which introduce significant error in the computed wavelengths of the OH uv-system, as Fig. 2 indicates.

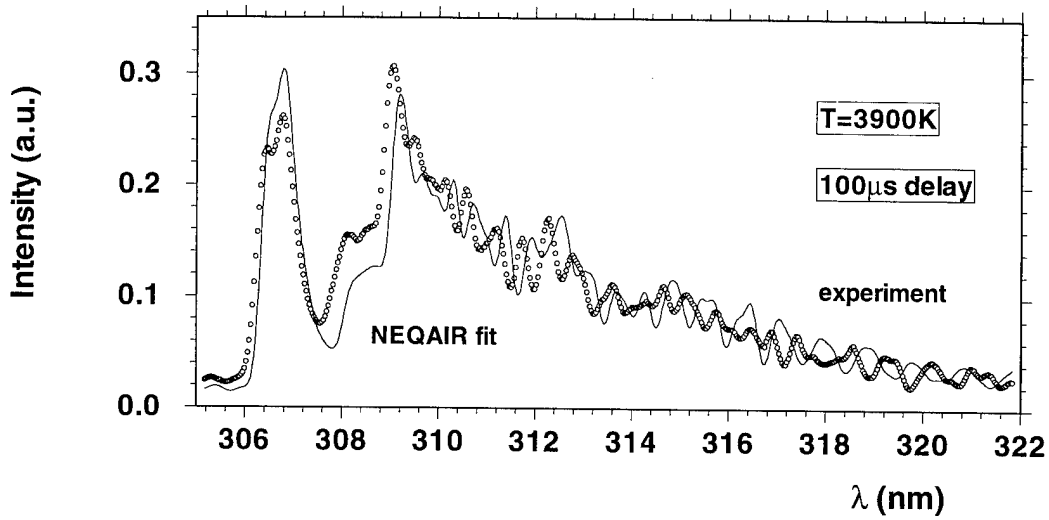

Fig. 2. NEQAIR fit to the OH optical breakdown spectrum, 100 μs time delay.

The computation of the diatomic line-strengths[11] for OH was accomplished using Tellinghuisen's RKR algorithm,[12,13] the Hamiltonian diagonalization method of Zare et al,[14] and OH spectral data bases.[15–18] Figure 3 shows the least-square fit of the UTSI synthetic spectra and NEQAIR background spectra to the experimental data, from which a temperature of T_{OH}=3700K was inferred. The improvement in the results of Fig. 3 over those of Fig. 2 is clear.

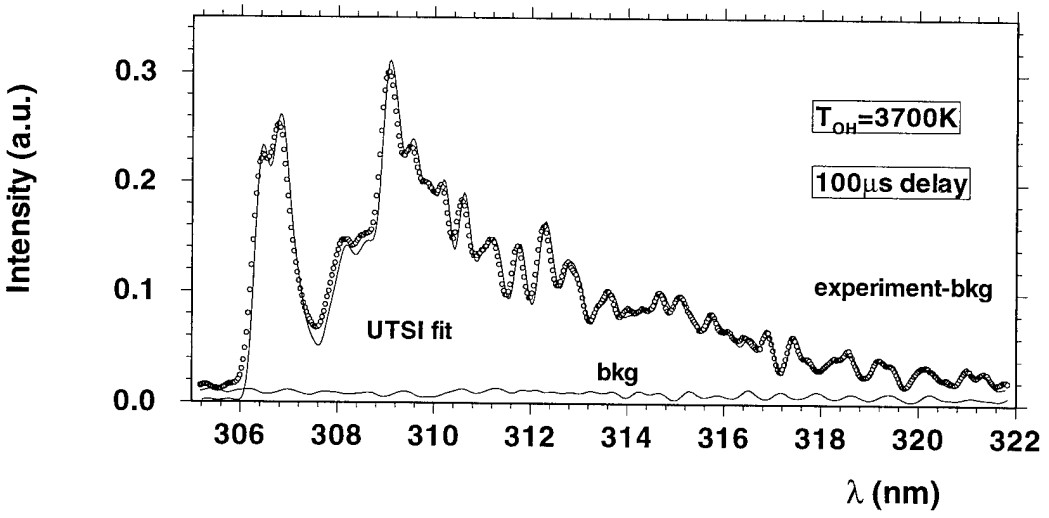

Fig. 3. UTSI fit to the OH optical breakdown spectrum, 100 μs time delay.

Accurate determination of the OH temperature using such overlapped spectra requires both accurate wavelength computations and correction for the background radiation of other molecules, such as the N_2 second positive system, in this OH spectral region. Although NEQAIR inadequately predicts the wavelength positions for the OH transitions, it can be used for the background radiation prediction. Such background computations were combined with UTSI line-strength computations to determine the OH temperature from the measured spectra.

---

1. B. E. Battles and R. K. Hanson, "Laser-induced fluorescence measurements of NO and OH mole fractions in fuel-lean high-pressure (1-10 atm) methane flames: fluorescence modeling and experimental validation," J. Quant. Spectrosc. Radiat. Trans. 54, 521 (1995).
2. J. E. Harrington, A. R. Noble, G. P. Smith, J. B. Jeffries, and D. R. Crosley, "Evidence for a new NO production mechanism in flames," Western States Section of the Combustion Institute, Stanford, CA 94305, Paper # WSS/CI 95F-193 (1995).
3. M. Rumminger, N. H. Heberle, R. W. Dibble, G. P. Smith, J. B. Jeffries, and D. R. Crosley, "Gas temperature above a porous radiant burner: comparison of measurements and model predictions," Western States Section of the Combustion Institute, Stanford, CA 94305, Paper # WSS/CI 95F-212 (1995).
4. The above references are examples of recent hydroxyl-radical research.
5. C. Park, "Nonequilibrium Air Radiation (NEQAIR) Program: User's Manual," NASA TM 86707, Ames Research Center, Moffet Field, CA 94035, 1985.
6. C. O. Laoux, "Optical Diagnostics and Radiative Emission of Air Plasmas," Ph.D. Dissertation, Department of Mechanical Engineering, Stanford University, CA 94305, August 1993.
7. E. E. Whiting, private communication.
8. The documentation of the computer code for nonequilibrium air radiation together with all the improvements during the past 10 years, including recent updates from NEQAIR8, is to appear in a NASA TM, 1995.
9. S. Gordon and B. McBride, "Computer program for calculation of complex equilibrium compositions, rocket performance, incident and reflected shocks, and Chapman-Jouguet detonations," NASA Lewis Research Center, Interim Revision, NASA Report SP-273 (1976).
10. J. O. Hornkohl, private communication.
11. J. O. Hornkohl and C. Parigger, "Angular Momentum States of the Diatomic Molecule," accepted for publication in Am. J. Phys. (1996).
12. J. Tellinghuisen, "Fast, accurate RKR computations," J. Mol. Spectrosc. 44, 194 (1972).
13. J. Tellinghuisen, "A fast quadrature method for computing diatomic RKR potential curves," Computer Phys. Comp. 6, 221 (1974).
14. R. N. Zare, A. L. Schmeltekopf, W. J. Harrop, and D. Albritton, "A direct approach for the reduction of diatomic spectra to molecular constants for the construction of RKR potentials," J. Mol. Spectrosc. 46, 37 (1973).
15. G. H. Dieke and H. M. Crosswhite, "The ultraviolet bands of OH," J. Quant. Spectrosc. Radiat. Trans. 2, 97 (1962).
16. J. A. Coxon, "Optimum molecular constants and term values for the $X^2\Pi$ and $A^2\Sigma^+$ states of OH," Can. J. Phys 58, 933 (1980).
17. J. A. Coxon and S. C. Foster, "Rotational analysis of hydroxyl vibration-rotation emission bands: Molecular constants for OH $X^2\Pi$, $6 \leq v \leq 10$," Can. J. Phys. 60, 41 (1981).
18. J. A. Coxon, A. D. Sappey, and R. A. Copeland, "Molecular constants and term values for the hydroxyl radical, OH: The $X^2\Pi(v=8,12)$, $A^2\Sigma^+(v=4\text{-}9)$, $B^2\Sigma^+(v=0,1)$, and $C^2\Sigma^+(v=0,1)$ states," J. Mol. Spectrosc. 145, 41 (1991).

Nitric Oxide Optical Breakdown Spectra and Analysis by the Use of the Program NEQAIR

Christian Parigger, J. W. L. Lewis, D. H. Plemmons, and J. O. Hornkohl
The University of Tennessee Space Institute
Center for Laser Applications
Tullahoma, Tennessee 37388-8897
Phone: 615-393-7338, Fax: 615-454-2271

1. Introduction

Optical breakdown air plasmas are generated by focused Nd:YAG ir laser radiation of 10^{12} to 10^{14} W/cm^2 intensity, and rich emission spectra result. Time-resolved spectroscopy techniques are applied to characterize the decaying laser-induced plasma. Recombination spectra that are dominated by nitric oxide are measured and analyzed with the objective of obtaining temperature and species density information.

In the near-uv wavelength region of 205-300 nm, the emission spectra are comprised of overlapped electronic transitions of primarily NO and N_2 and to a lesser degree of O_2 and atomic species. The spectral analysis of these superimposed spectra of such multiple species is most challenging, and the computer code for nonequilibrium air radiation (NEQAIR) is applied in the spectral analysis of the transient microplasma.

The program NEQAIR[1,2] is widely used to predict and interpret optical spectra from air plasmas. The majority of NEQAIR applications concern atmospheric radiation, but the program is also applied in simulation facilities and has other applications such as the prediction of laser sustained plasmas. In this paper we apply the non-equilibrium air radiation code, in the form of NEQAIR8,[3,4] to our knowledge for the first time, in the analysis of time-dependent optical breakdown spectra.

2. Results and Discussion

The analysis of the recorded experimental spectra from air breakdown is based on the use of calculated number densities of a dry air plasma composition at a pressure of 100 kPa.[5] With the assumption of local thermodynamic equilibrium, a one-parameter least-square fitting procedure is applied to find the spectroscopic temperature. Figure 1 shows the time-resolved experimental spectrum, recorded at a time delay of 50 μs from the optical breakdown event in air, and it also shows the fitted synthetic spectrum.

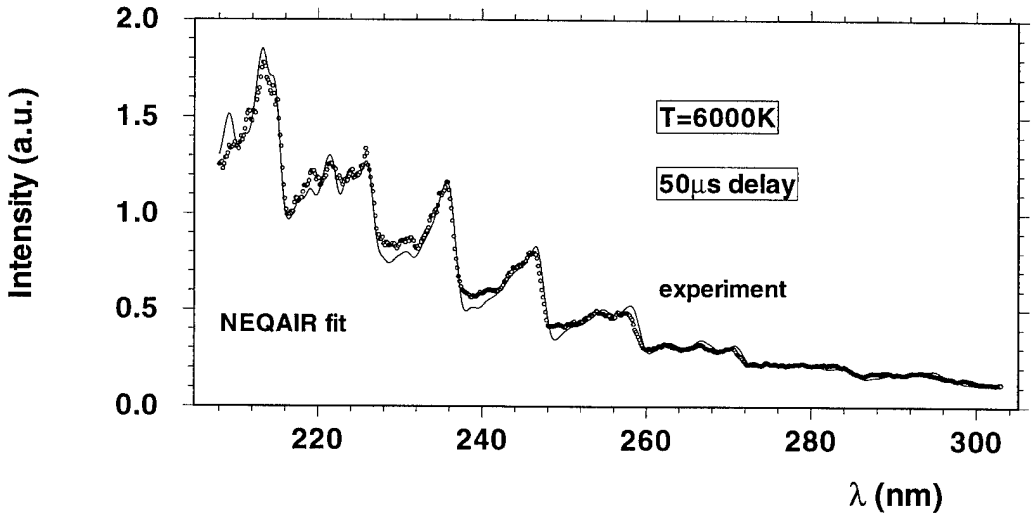

Fig. 1. NO optical breakdown spectrum, 50 μs time delay, and NEQAIR synthetic spectrum.

Figure 2 shows the experimental spectrum, recorded at a time delay of 25 μs from the optical breakdown event in air, and the fitted synthetic low-resolution NO spectrum.

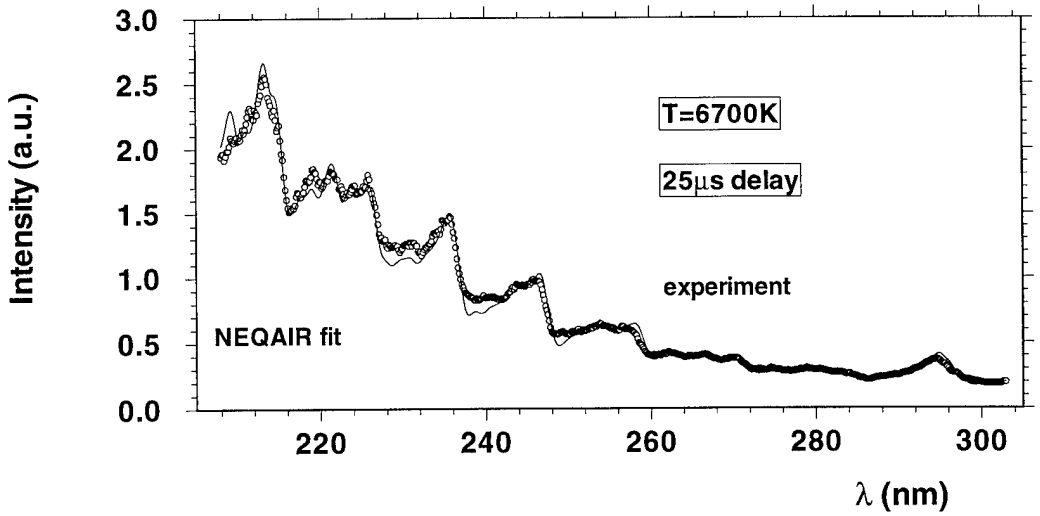

Fig. 2. NO optical breakdown spectrum, 25 μs time delay, and NEQAIR synthetic spectrum.

Air is considered to be a mixture of nitrogen, oxygen and argon at room temperature, with all other species neglected. Starting from one mole of air at room temperature, the number densities of the species N, O, Ar, N^+, O^+, Ar^+, N_2, N_2^+, O_2, O_2^+, NO, NO^+, and the free electrons e, are given as function of temperature. These data are used for computation of synthetic spectra; i.e., a Boltzmann distribution with equal translational, rotational, vibrational and electron temperatures was assumed in our analysis.

Tables 1 and 2 summarize the temperature and number densities that were utilized as input for the computer code NEQAIR8.

Table 1. Neutral species number densities [cc^{-1}] for T=6000K and T=6700K.

T[K]	N	O	Ar	N_2	O_2	NO
6000	2.3×10^{17}	3.9×10^{17}	8.5×10^{15}	6.6×10^{17}	3.3×10^{14}	1.0×10^{16}
6700	4.6×10^{17}	3.1×10^{17}	6.8×10^{15}	3.6×10^{17}	7.8×10^{13}	4.5×10^{15}

Table 2. Ionized species and free electron number densities [cc^{-1}] for T=6000K and T=6700K.

T[K]	N^+	O^+	Ar^+	N_2^+	O_2^+	NO^+	e
6000	0	0	0	0	0	2.7×10^{14}	2.7×10^{14}
6700	4.7×10^{13}	4.8×10^{13}	0	0	0	4.4×10^{14}	5.4×10^{14}

The results indicate significant potential of the program NEQAIR for applications in combustion[6–9] and plasma diagnostics. The "background" contributions appear to be predicted well for selected diatomic transitions, and the synthetic NEQAIR spectra are particularly useful for the analysis of spectral studies with low spectral resolutions. Of course, non-equilibrium computations are of interest, e.g., for different rotational and vibrational temperatures,[10] but here we restricted our analysis to equilibrium distributions. Synthetic NEQAIR spectra are also presented for the diatomic molecules CN, C_2, and N_2^+, that were previously investigated in a decaying laser-induced breakdown plasma.[11–13]

---

1. C. Park, "Nonequilibrium Air Radiation (NEQAIR) Program: User's Manual," NASA TM 86707, Ames Research Center, Moffet Field, CA 94035, 1985.
2. C. O. Laoux, "Optical Diagnostics and Radiative Emission of Air Plasmas," Ph.D. Dissertation, Department of Mechanical Engineering, Stanford University, CA 94305, August 1993.
3. E. E. Whiting, private communication.
4. The documentation of the computer code for nonequilibrium air radiation together with all the improvements during the past 10 years, including recent updates from NEQAIR8, is to appear in a NASA TM, 1995.
5. M. I. Boulous, P. Fauchais, and E. Pfender, *Thermal Plasmas - Fundamentals and Applications,* (Plenum Press, New York, 1994), p. 241.
6. B. E. Battles and R. K. Hanson, "Laser-induced fluorescence measurements of NO and OH mole fractions in fuel-lean high-pressure (1-10 atm) methane flames: fluorescence modeling and experimental validation," J. Quant. Spectrosc. Radiat. Trans. 54, 521 (1995).
7. J. E. Harrington, A. R. Noble, G. P. Smith, J. B. Jeffries, and D. R. Crosley, "Evidence for a new NO production mechanism in flames," Western States Section of the Combustion Institute, Stanford, CA 94305, Paper # WSS/CI 95F-193 (1995).
8. M. Rumminger, N. H. Heberle, R. W. Dibble, G. P. Smith, J. B. Jeffries, and D. R. Crosley, "Gas temperature above a porous radiant burner: comparison of measurements and model predictions," Western States Section of the Combustion Institute, Stanford, CA 94305, Paper # WSS/CI 95F-212 (1995).
9. The above three references are examples of recent nitric-oxide research.
10. L. Labracherie, M. Billiotte, and L. Houas, "Nonequilibrium determination of temperature profiles by emission spectroscopy," J. Quant. Spectrosc. Radiat. Trans. 54, 573 (1995).
11. J. O. Hornkohl, C. Parigger, and J. W. L. Lewis, "Temperature measurements from CN spectra in a laser-induced plasma," J. Quant. Spectrosc. Radiat. Transfer 46, 405 (1991).
12. C. Parigger, D. H. Plemmons, J. O. Hornkohl, and J. W. L. Lewis, "Spectroscopic temperature measurements in a decaying laser-induced plasma using the C_2 Swan system," J. Quant. Spectrosc. Radiat. Trans. 52, 707 (1994).
13. C. Parigger, D. H. Plemmons, J. O. Hornkohl, and J. W. L. Lewis, "Temperature measurements from first-negative N_2^+ spectra produced by laser-induced multiphoton ionization and optical breakdown of nitrogen," Appl. Opt. 34, 3331 (1995).

Optical emission spectrometry of laser produced plasma with microwave re-excitation for micro-analysis of solid samples

A.Ciocan*, J.Uebbing** and K.Niemax***

* -Institute of Atomic Physics, POBox MG-07, Magurele-Bucharest, Romania

** - ISAS., Bunsen-Kirchhoffstr.11, Dortmund 44139, Germany

*** - Universitaet Hohenheim-Institut Physik, Garbenstr. 30,Stuttgart 70593, Germany

Laser ablation of solid samples by pulsed lasers is a convenient and fast sampling technique for element analysis of solid samples. Furthermore, if the laser beam is focused, microbulk analysis with a spatial resolution limited by diffraction is possible. This paper presents experimental results and instrumentation for matrix-independent simultaneous multi-element analysis by a method which got the acronym **LA-MIP-OES** (**L**aser **A**blation - **M**icrowave **I**nduced **P**lasma - **O**ptical **E**mission **S**pectrometry).

The experiments were performed with a pulsed Nd:YAG laser (Spectron SL401, τ=5ns) operating at its fundamental wavelength (λ=1.06μ) for ablation of solid samples. The Ar microwave induced plasma was running continuously in the range of 30-300W at reduced pressure (200hPa). The spectra were recorded by the sensitized, gateable diode array detector head of an optical multichannel analyzer (OSMA by Stanford Instruments). For simultaneous multi-element measurements, optical fibers and imaging lens system were interfaced between a compact high-resolution Echelle spectrograph (Carl Zeiss Jena), and the gateable OSMA detector head [1]. Integrated background corrected spectra were recorded during about 100μs and 8ms interval delay time after the laser shot, when

microwave induced plasma was not any longer perturbed by the ablated material, independent on matrix [2]. Up to ten simultaneous elements were possible to be measured by this set-up.

Typical absolute and relative detection limits in the fg and μg/g ranges respectively, were achieved for a number of elements with one laser shot [3,4]. The emission spectra were measured by time-gated detection, normalized by internal standardization and calibrated with relevant spectra of standard reference samples. The power of LA-MIP-OES technique is demonstrated with the measurements of lithium and sodium in high-purity quartz used for production of glass fibers. Detection limits were found to be about 20ng/g (Li) and 10ng/g(Na), applying ten laser shots and 3σ criterion. Measurements of trace element correlations and inhomogeneities in microbulk have been also performed for different samples (steel, aluminum, high-pu. ity quartz and high-temperature superconducting ceramic: YBa2Cu3O7). The spatial resolution is moderate, depending on the focusing laser beam and its Gaussian shape.

Bibliography:

1. L.Hiddemann, J.Uebbing, A.Ciocan, O.Dessenne and K.Niemax, Anal.Chim.Acta 283(1993), 152.

2. J.Uebbing, A.Ciocan and K.Niemax, Spectrochim.Acta 47B, 5(1992), 601.

3. A. Ciocan, J.Uebbing and K.Niemax, Spectrochim. Acta 47B, 5(1992), 611.

4. A. Ciocan, L.Hiddemann, J.Uebbing and K.Niemax, J.Anal. Atom. Spectrom. 8(1993), 273.

Thursday, March 21, 1996

Atmospheric Chemistry

LThA 8:00 am-9:45 am
Windsor Ballroom

Robert Daniel, *Presider*
US Army Research Laboratory

Ground-Based and Airborne Measurements of Atmospheric Constituents Using Tunable Diode Lasers: An Overview and Recent Measurements

Alan Fried, Scott Sewell, Bruce Henry, and Bryan Wert

The National Center for Atmospheric Research
Atmospheric Chemistry Division
PO Box 3000
Boulder, Colorado 80307
303 497 1475

and

James R. Drummond
The Department of Physics
University of Toronto
Toronto, Ontario, Canada

The application of tunable diode laser absorption spectroscopy (TDLAS) for studying the chemistry of the atmosphere on various platforms is well documented.[1] This technique, for example, has been employed in laboratory kinetics and spectroscopic studies, in ground-based measurements, in measurements on conventional as well as high flying aircraft, and on balloon-borne payloads. The present talk will give a brief overview of these capabilities, detailing some of the atmospheric gases studied, the sensitivities achieved, and the current limitations of the technique. This will be followed by a discussion of a ground-based TDLAS system developed at the National Center for Atmospheric Research (NCAR) for studying various constituents, including the important reactive intermediate formaldehyde (HCHO). This system has recently been modified for aircraft operation and this will also be described

Measurements of trace atmospheric gases oftentimes requires extremely high sensitivity. In the case of HCHO, a trace reactive gas formed by the oxidation of many hydrocarbons, measurement precision below 0.1 parts-per-billion by volume (ppbv) is typically required to further our understanding of atmospheric processes. Aircraft measurements provide extended spatial and vertical coverage of HCHO as well as many other constituents not possible in ground-based studies. However, such measurements demand high sensitivity along with fast response times of several minutes or less. Numerous hardware and software features were incorporated in the ground-based TDLAS system developed at NCAR to achieve these stringent requirements. These features include: a high pathlength small volume astigmatic Herriott cell; rapid background subtraction; digital signal processing lockin demodulation; Fourier filtering; demeaning and wavelength shifting on a scan-by-scan basis; on-line spectral fitting; and full computerized automation using the Lab View Graphical System.

Many of these features will be discussed in the present talk. However, rapid background subtraction and the resulting significant performance improvement (factor of 4 to 5) will be given specific emphasis. In this technique, made possible by the small volume sampling cell, sample and background spectra were acquired in a time period fast (≈ 20 to 30 seconds) compared to changes in background structure. Subtraction of the averaged-background (immediately before and after the sample) very effectively removed performance-degrading optical noise. Based upon replicate measurements of HCHO gas standards employing 5-minute integration periods, routine detection sensitivities of 0.04 ppbv have been achieved over many hours using this technique in an actual field setting. The relationship between replicate and fit precision, a precision estimator obtained with every fit, will be given in this discussion. Employing Fourier filtering and scan-by-scan demeaning, improved the HCHO detection sensitivity even further to 0.02 ppbv in 4-minutes of integration, one of the lowest HCHO detection limits reported by an actual field TDLAS system. This corresponds to a minimum detectable absorbance (S/N = 1) of 6×10^{-7}. The instrument performance of the newly developed aircraft system, which incorporates these same features, will be discussed.

References

1. A. Fried, D.K. Killinger, and H.I. Schiff, editors, Tunable Diode Laser Spectroscopy, LIDAR, and DIAL Techniques for Environmental and Industrial Measurements, Proceedings of the SPIE, volume **2112**, 11 - 14 October, 1993, Atlanta, Georgia.

Sensitive Detection of Atmospheric Trace Gases by Laser Photoacoustic Spectroscopy

M.W. Sigrist and M. Moeckli
ETH Zurich, Institute of Quantum Electronics
CH - 8093 Zurich, Switzerland
phone: +41-1-633´2289, fax: +41-1-633´1077

Introduction

The sensitive and selective detection of trace gases is of great current interest. Various detection schemes have been proposed including spectroscopic techniques [1]. Recently, diode lasers in the 1.53 μm and 1.65 μm wavelength region have been used for monitoring specific species such as ammonia (NH_3) [2,3]. A detection sensitivity of 8 ppb has been reported for laboratory measurements at atmospheric pressure by applying photoacoustic (PA) detection [2] and of 55 ppm-m at a total pressure of 76 Torr by using derivative absorption [3]. However, in order to apply a detection scheme to environmental conditions, a sufficient detection selectivity is often more difficult to achieve than the sensitivity. The stringent requirements are best met by using the fundamental or mid IR region between 3 and 20 μm. Hence, the combination of widely tunable lasers and photoacoustic (PA) detection appears to provide a powerful tool for atmospheric sensing particularly with respect to multicomponent capability, detection sensitivity and selectivity. During the last years we have developed a CO laser-, a mobile CO_2 laser- and a continuously tunable, high-pressure CO_2 laser-PA system [4]. This paper discusses the main characteristics and most recent results obtained with the mobile system as well as current efforts on novel developments of tunable IR lasers with wide tuning range and narrow bandwidth based on nonlinear optical effects.

Mobile CO_2 laser PA system

This system employs a cw sealed-off CO_2 laser. The laser is line-tunable over ~80 laser transitions between 9.2 and 10.8 μm (910 to 1090 cm^{-1}) with the $^{12}C^{16}O_2$ isotope or between 9.6 and 11.2 μm (890 to 1040 cm^{-1}) with the $^{13}C^{16}O_2$ isotope. A special cell design of the resonant PA cell permits measurements on flowing air samples even in noisy environments. The entire system is computer-controlled and installed in a trailer. It permits the detection of numerous gases with a minimum detectable absorption coefficient of ~10^{-8} cm^{-1}. Depending on the molecular absorption cross section this limit corresponds to ppb concentrations. The dynamic range comprises ≥ 5 orders of magnitude which enables measurements near emission

sources as well as in rural areas. The sensitivity could be still further improved but at the cost of dynamic range by using intracavity operation. An example of a recent measurement is depicted in Fig. 1. It shows temporal concentration profiles taken at the exit of a freeway tunnel. The NH_3 (ammonia), C_2H_4 (ethene) and CO_2 concentrations (upper three curves) have been derived with our photoacoustic system by automatically tuning the $^{12}CO_2$ laser to the appropriate wavelengths. The CO and traffic data stem from automatic continuous recordings by the local authorities. All gas concentration profiles are more or less closely related to the temporal traffic flux. As expected rather high C_2H_4 concentrations at the few 100 ppb level occur. In measurements performed in rural air far away from any traffic we recorded C_2H_4 concentrations of 2 to 4 ppb near our detection threshold [1]. The NH_3 concentrations are surprisingly high and stay above 100 ppb even at nighttime. The reason is the high percentage of cars equipped with catalytic converters that reduce the NO, NO_x and VOC emissions but increase the NH_3 emissions. These data allowed us to derive emission factors (grams of gas emitted per mile) that were until now only partly known. In a different measurement we have also recently applied our system to study trace gas emissions of C_2H_4, alcohols and terpenes, from plants and fruits. Some data will be presented that are of interest from both environmental and agricultural aspects.

Conclusion and outlook

These investigations demonstrate the versatility and potential of CO_2 laser PA spectroscopy even in extremely noisy environments. The analysis of data of multicomponent gas mixtures, however, may cause problems owing to interfering spectra of individual molecules on the one hand and the limited (line) tunability on the other hand. More recently we have therefore concentrated on the development of continuously tunable sources. These include a high-pressure CO_2 laser with a continuous tuning range of 76 cm^{-1} between 9.2 and 10.8 µm at a linewidth of only 0.018 cm^{-1} as well as a continuously tunable IR laser source on the basis of a commercial Nd:YAG laser-pumped optical parametric oscillator and subsequent frequency mixing between the idler output and the 1.06 µm Nd:YAG laser radiation in $LiNbO_3$. A continuous tuning range between 2.5 and 4.5 µm at a linewidth of 0.2 cm^{-1} is expected for this source. Preliminary experiments have demonstrated a considerable improvement in detection selectivity with such laser sources. In addition, a novel approach based on difference frequency mixing in silver gallium selenide ($AgGaSe_2$) will be used to develop a compact laser spectrometer for trace gas monitoring beyond 4.5 µm.

References

1. M.W. Sigrist, Ed. *Air Monitoring by Spectroscopic Techniques*, Chem. Anal. Series, Vol. 127 (Wiley, New York, 1994)
2. M. Fehér, Y. Jiang, J. P. Maier and A. Miklós, Appl. Opt. **33**, 1655-1658 (1994)
3. P. Cancio, C. Corsi, F.S.Pavone, R. U. Martinelli, R.J. Menna, Infrared Phys. Technol. **36**, 987-993 (1995)
4. M.W. Sigrist, Opt. Engin. **34**, 1916-1922 (1995)

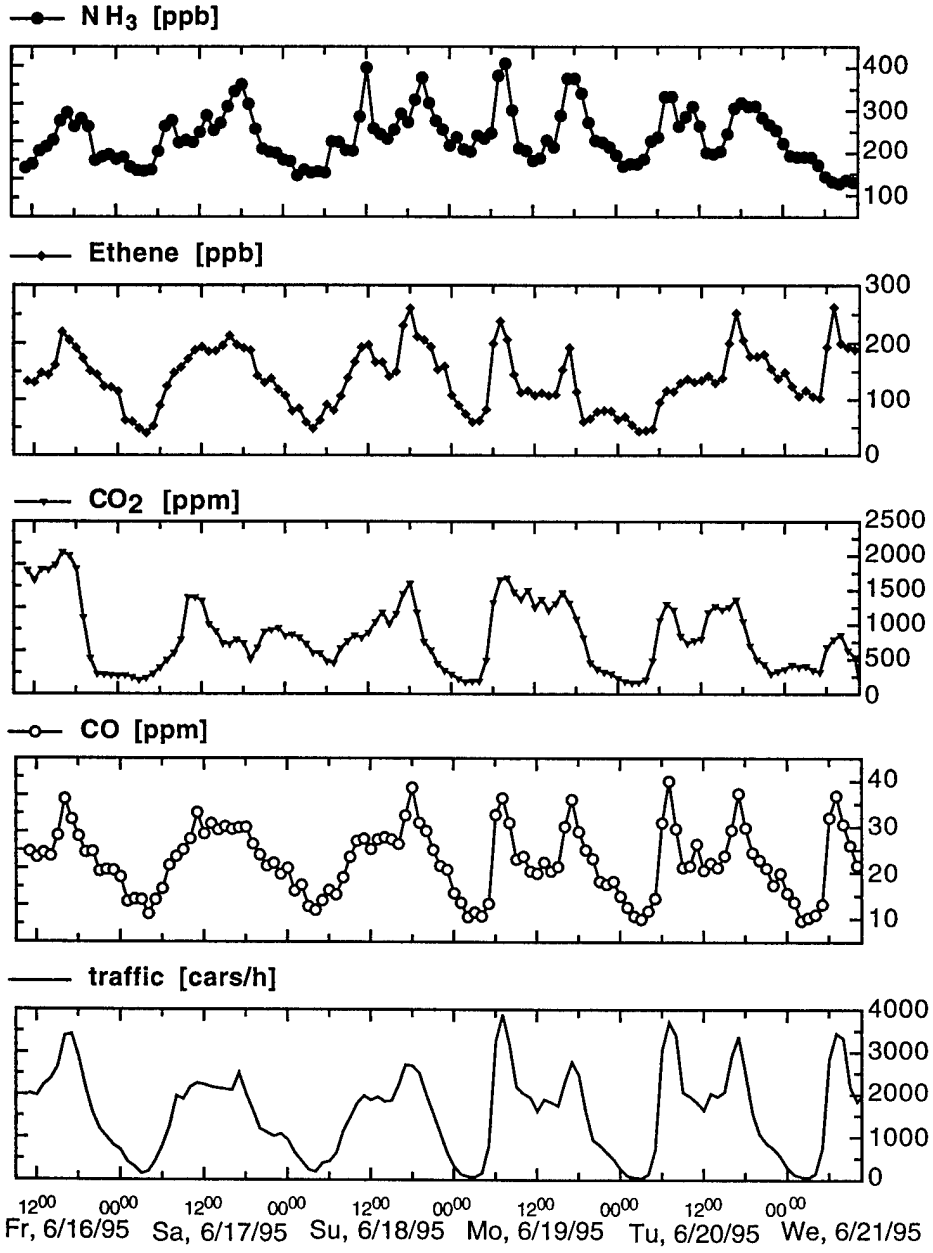

Fig. 1 Temporal concentration profiles of NH_3, C_2H_4, CO_2 and CO measured at the exit of a freeway tunnel. The upper three concentration profiles have been derived from PA data while the CO concentration and the traffic data originate from automatic recordings performed by local authorities.

A Study of Aerosol-Cloud Interaction using Laser Microprobe Mass Analysis

R. Gieray† and P.H. Wieser
Institute of Physics, University of Hohenheim, Garbenstr.30, D-70599 Stuttgart, Germany
++49-711-459-2155
++49-711-459-2146 FAX
Wieser@ruhvm.rz.uni-hohenheim.de

† Present Adress: Chemical and Analytical Sciences Division, Oak Ridge National Laboratory, P.O. Box 2008, M/S 6142, Oak Ridge, Tennessee 37931-6142
423-574-4882
432-574-8363 FAX

Cloud formation, radiative properties and cloud droplet chemistry is strongly affected by the size distribution and chemical composition of the atmospheric aerosol on which the cloud has been formed. Once a particle is incorporated into a droplet, chemical reactions in aqueous solution may occur changing the loading of air pollutants (e.g. oxidation of dissolved SO_2 under the catalytic influence of metal ions). In addition the incorporation of airborne particles into cloud droplets play an important role in determining the atmospheric residence time of air pollutants.

In order to improve our present understanding of aerosol-cloud interactions, the chemical composition of cloud droplet residues and particles of the cloud interstitial aerosol were compared using laser microprobe mass spectrometry (LAMMS). Size fractionated samples were collected during the 3rd joint European field campagne of the EUROTRAC subproject "Ground-based cloud experiments" at the Great Dun Fell, United Kingdom, spring 1993[1,2].

Cloud droplet residues and interstital particles were collected simultaneous using five stage mini cascade impactors[3]. In order to collect droplet residues a counterflow virtual impactor[4] (CVI) was used as the inlet system for the mini cascade impactors. The CVI seperates droplets larger than a given size from the ambient air and transfers them into a dried, heated and particle free carrier gas. The droplets evaporate in airborne state and a fraction of the remaining residues is collected in a mini cascade impactor. In order to collect interstial particles, the mini cascade

impactors were equipped with an inlet system that prevents sampling of cloud droplets. In the mini cascade impactors particles were deposited on pioloform coated nickel grids that are fastened to the impaction plates. After exposure the grids are removed and then stored in a closed box and refrigerated until analysis.

About 30,000 droplet residues and interstial particles from orographic clouds were analyzed with a modified LAMMA®500 (Leybold, Cologne) instrument. Methods of multivariate statistical methods were used to classify the normalized mass spectra and to identify main types of particles present in the investigated air masses.

In the case of strong continental influenced air, the ratio of soluble sulfate and presumably insoluble carbonaceous materials seems to be an important parameter to estimate whether or not submicron sized particles will be incorporated into cloud droplets by water vapour condensation (nucleation scavenging). The fraction of carbonaceous particle constituents is estimated from the backbone fragmentation pattern typically found in the negative ion mode mass spectra of e.g. long chain hydrocarbons (paraffines, fatty acids, alcanols), terpenes and soot. Marker elements like vanadium and nickel found in association with these materials indicate that at least a part of the carbonaceous material derives from combustion processes, with only a minor fraction related to soot. We found that the probability for a particle to to be incorportated into a droplet increases with a decreasing fraction of carbonaceous materials. So, one might presume that particles composed of a large fraction of carbonaceous materials might have a longer residence times in the atmosphere than completely soluble particles of the same size.

However, we found cases where no significant correlation between particle composition and and partitioning were observed. In these cases, the interstitial aerosol included large sea salt and sulphate particles without any experimental hints of a substantial amount of insoluble or unwettable constituents. In our opinion, this observation can be best explained by spatial and temporal fluctuations of water vapour supersaturation due to entrainment of air from above the cloud and turbulent mixing processes[5].

As a further result, it was observed that the external mixture of particles of different chemical composition is at least partly preserved in the droplet phase. As an example, in the case of marine influenced air masses droplets formed on large sea salt particles exist side by side with droplets formed on smaller ammonium sulfate and methanesulfonate containing particles. Obviously chemical inhomogeneities in the droplet phase do exist. This fact has to be regarded when analytical results from bulk samples of cloud water are interpreted[6].

[1] R. Colvile et al., Atmos. Environ. (susbmitted)
[2] R. Gieray et al., Atmos. Environ. (submitted)
[3] P.H. Wieser and R. Wurster, in: Physical and Chemical Characterization of individual Airborne Particles (Ed. K.R. Spurny), Ellis Horwood Ltd. Chichester U.K., 1986, 251-270.
[4] J.A. Ogren, J. Heintzenberg and R.J. Charlson, Geophys. Res. Lett., 12, 1985, 121-124.
[5] B. Arends et al., Atmos. Environ. (submitted)
6 F.M. Perdue and K.C. Beck, J. Geophys. Res 93D, 1988, 691-698.

Ultrasensitive *In Situ* Atmospheric Monitoring with a Compact Setup based on Photothermal Deflection (Mirage Effect) Spectroscopy.

B. L. Zimering and A. C. Boccara
Laboratoire d'Optique Physique, UPR A0005 CNRS, ESPCI,
10 rue Vauquelin, 75005 Paris, France
phone: +33 1 40 79 45 94 (office secretary) fax: +33 1 43 36 23 95

Photothermal spectroscopic methods, notably photoacoustic, thermal lens and mirage detection, may be seen as alternatives to direct absorption spectroscopy for trace gas detection and offer many advantages, most notably high sensitivity and signal reference to a true zero. While direct absorption measures the typically weak signal difference between input and output energy, photothermal methods measure a signal either directly (thermal lens and mirage detection) or indirectly (photoacoustic) proportional to energy absorbed by the sample.

Photoacoustic (PA) techniques have been used for trace gas detection into the ppb and 10 part per trillion (ppt) range by measuring the acoustic expansion of a sample heated by laser absorption[1-4]. One limitation with this technique is that an enclosed cell is usually employed, requiring gas sampling, making real time *in situ* measurements difficult. Temperature and vibration stability are also critical for maximum performance, and as PA spectroscopy is an indirect (bulk volume) technique, local sample probing may not be performed.

Photothermal deflection or mirage effect spectroscopy has been extensively developed for nondestructive testing in the solid phase, but has been rarely used for gas phase detection[5,6]. This technique has roughly the same order of sensitivity as that of PA spectroscopy, with more flexibility. When studying transparent media such as a gas, the sample is excited by absorption of a modulated pump laser source. The gas heats locally through kinetic quenching, inducing a local modulated thermal gradient. The thermal gradient in the sample induces in turn a time dependent refractive index gradient within the heated region, and a second, probe laser beam passing through this region is deflected through an angle directly related to the thermal gradient and frequency of modulation. The periodic beam deflection is measured with a pair of photodiodes to reduce laser intensity noise. The photodiode signal is amplified by a lock in amplifier referenced to the pump laser modulation frequency.

For gas phase samples, the energy absorbed depends on the density corrected absorption coefficient α. The thermal gradient, and corresponding deflection signal is therefore directly dependent on the concentration of the absorbing species and its absorption spectrum. If the modulation frequency is high enough so that the thermal diffusion length is much smaller than the pump beam diameter, the angular deflection is given by the following expression[7]:

$$\phi = -2\left(\frac{x_0}{a^2}\right)\left(\frac{1}{n}\right)\left(\frac{dn}{dT}\right)\frac{P}{\omega\rho c\pi^2 a^2}[1-\exp(-\alpha l)]\exp\left(\frac{-x_0^2}{a^2}\right)$$

The parameters **P**, **a**, and **w** refer to the pump laser power, beam diameter, and modulation frequency respectively, **r**, **c** and **n** refer to the gas density, specific heat and index of refraction respectively, which are constant for a given gas species. Geometric parameters $\mathbf{x_0}$ and **l** refer to the two parallel beams' separation distance and interaction length, respectively. In trace gas detection, αl is small, and the signal exhibits a linear dependence on gas concentration.

Selectivity between different gas species depends on the ability to distinguish absorption spectra. A tunable pump laser is used, and a frequency resonant with a vibrational mode of the species to be detected is chosen. One hopes to avoid resonance with other molecules in the mixture, but as this is rarely possible in practice, measurements are performed on several laser lines, and the results normalized with known absorption spectra. Since there is no signal when there is no absorption, the measurement may be referenced to a true zero, and since the signal generated is proportion to the absorbed energy, sensitivity may approach the shot noise limit.

The experimental setup is shown schematically in Figures 1(a) and in detail in 1(b):

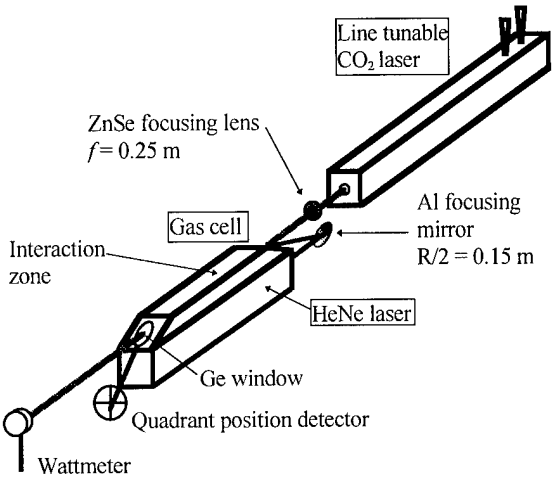

Figure 1(a) Schematic of the Setup

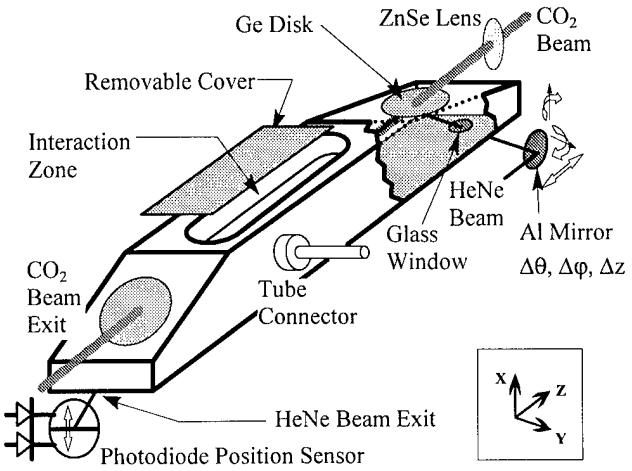

Figure 1(b) Detail of Beam Interaction and Detection

The CO_2 (pump) laser beam passes through the cell, positioned and focused by a ZnSe lens. The Ge windows are transparent in the IR and are set at the Brewster angle for the CO_2 laser. The HeNe (probe) laser located below the cell is focused and oriented by an Al mirror onto the inside of the entry Ge window which is opaque at 632 nm. The probe beam is thus deflected and crosses through the cell, parallel to the CO_2 beam, to be rereflected off of the exit Ge window, and exits the cell to be measured by a quadrant photodiode position detector.

The CO_2 pump laser is capable of operating on lines having resonance with many important pollution species including volatile hydrocarbons (CFCs, exhaust gases, DDT), NO_x, O_3, NH_3, and SO_2. Amongst this plethora of possibilities, we have conducted numerous measurements with ethylene (C_2H_4) to evaluate fundamental performance of the setup. Ethylene is included in many trace gas studies because of its strong absorption of the CO_2 10P14 line at 10.525 μm. This gas is also interesting because of its role in agriculture and bioscience[8].

Calibration of the setup has been conducted with known gas mixtures, and we estimate the practical detection limit of ethylene in air to be 0.25 ppbv (2.5×10^{-10}). This limit is based on the noise incurred by the pump laser cooling which is superior to the air turbulence noise in typical (indoor) conditions, and is an order of magnitude larger than the photon noise in the detection cell, which represents the theoretical limit of the apparatus. The detection limit for other gases may be extrapolated based on known absorption coefficients, shown in **Table 1** below. We have demonstrated *in situ* trace gas detection capabilities by measuring open laboratory air spectra; absorption (due mainly to water vapor) has been measured down to a signal level corresponding to one order of magnitude greater than the practical noise limit.

Table 1. Extrapolated limits for some important gases

Gas	Detection limit, ppb	Gas	Detection limit, ppb
Ethylene	0.25	1,2 Dichloroethylene	55
Benzene	12	Vinyl Chloride	2
Monochloroethylene	7.5	Ammonia	0.5
Trichloroethylene	2.5	Ozone	2.5

Although designed for environmental background monitoring, the setup also lends itself to other domains. We have explored applications to agricultural and biological science by measuring real time emissions of ethylene gas from various plant samples placed directly onto the cell opening. Many plants release this gas in response to chemical or mechanical attack (stress), and we may thus follow processes which occur within the plant body. For instance, we have characterized intracellular communication in cherry tomato seedlings by measuring gas released in one location in response to the application of weak H_2SO_4 acid (simulated acid rain) in another location[9]. Gas production levels as low as 100 nL/(g-hr) have been recorded. Plant response to chemical treatment (e.g. pesticides) may be studied with precision, or the plant may be integrated as a broad spectrum pollution biomonitor.

We have also briefly investigated applications to photochemical process control by measuring gas products of polymer degradation induced by UV light. Samples of Low Density Polyethylene (LDPE) films from different manufacturers were studied, and differences in gas production rate and composition (based on absorption spectra) are explained owing to the relative crosslinking density[9].

In conclusion, we have demonstrated a compact mirage effect based system for real time *in situ* detection of important pollution gases, with an estimated ethylene detection limit of 0.25 ppb in open air. The resistance to air turbulence and the compact size of the setup marks the trade-off between absolute closed cell sensitivity and flexibility in operation. We have performed trace gas measurements of known mixtures for calibration, as well as of gas emissions from solid and semi-solid (biological) samples to explore associated applications of the technique.

References

1. A. Thöny, B. Brand, M. Ferro-Luzzi, and M. W. Sigrist, in *Photoacoustic and Photothermal Phenomena III* (D. Bicanic, ed.), Springer-Verlag, Berlin, 1992
2. H. Sauren, D. Bicanic, and H. Jalink, J. Appl. Phys. **66**, 5085 (1989)
3. R. A. Rooth, A. J. L. Verhage, and L. W. Wouters, Appl. Opt. **29**, 3643 (1990)
4. F. Harren, et. al. in *Photoacoustic and Photothermal Processes in Gases* (P. Hess, ed.), Springer-Verlag, Berlin, 1989
5. D. Fournier, A. C. Boccara, N. M. Amer and R. Gerlach, Appl. Phys. Lett. **37**, 519 (1980)
6. H. DeVries, *Local Trace Gas Measurements by Laser Photothermal Detection; Physics Meets Physiology*, Cip-Gegevens Koninklijke Bibliotheek, Den Haag, 1994
7. A. C. Boccara, D. Fournier, W. Jackson and N. M. Amer, Opt. Lett. **5**, 377 (1980)
8. F. B. Abels, P. W. Morgan, and M. E. Saltveit, Jr, *Ethylene in Plant Biology*, Academic Press, San Diego, California, 1992
9. B. Zimering and A. C. Boccara, Workshop '95 on Photoacoustics and Photothermics, Ebernburg, Germany, October 4-6, 1995 (oral comunication)

UV Laser Absorption Measurements of Tropospheric Hydroxyl on a 21-km Atmospheric Long Path

George H. Mount
Aeronomy Laboratory
National Oceanic and Atmospheric Administration
Boulder, CO 80303

The hydroxyl radical (OH) plays a central role in the chemistry of the Earth's lower and middle atmosphere. The determination of its concentration is essential to an understanding of the chemistry of the lower atmosphere since this molecule controls the lifetimes, and therefore the concentrations, of many chemical species under both clean and polluted conditions. Predicted midlatitude tropospheric concentrations of OH range approximately from 0.1 pptv at the noontime maximum in the winter to several tenths pptv at noontime in the summer. These low values are extremely difficult to measure; sensitivity at least a decade smaller is essential to measure the daily growth and decay inorder to understand the photochemical variation of OH.

OH concentrations have been measured with good success in the stratosphere and lower mesosphere. Rocket instruments have measured the OH concentration of the lower mesosphere and upper/middle stratosphere; balloon experiments have measured OH in the middle and lower stratosphere by in-situ air sampling and by LIDAR techniques. A long term series of measurements has been made of total vertical column OH over Fritz Peak Observatory, Colorado.

Tropospheric OH is formed (mainly) by the reactions,

$$O_3 + h\nu \text{ -----> } O_2(^1\Delta_g) + O(^1D) \quad (< 310 \text{ nm}) \qquad (1)$$

Under normal conditions up to about ten percent of the $O(^1D)$ in the planetary boundary layer reacts with water vapor to give OH,

$$O(^1D) + H_2O \text{ -----> } OH + OH \qquad (2)$$

OH is removed mainly by reaction with carbon monoxide (dominant in the clean troposphere),

$$OH + CO \text{ -----> } HO_2 + CO_2 \qquad (3)$$

and methane,

$$OH + CH_4 \text{ -----> } H_2O + CH_3 \qquad (4)$$

which is followed by

$$CH_3 + O_2 + M \text{ -----> } CH_3O_2 + M \qquad (5)$$

and CH_3O_2 reacting with NO and O_2 to form formaldehyde and again HO_2. The majority of tropospheric OH reactions in the clean troposphere eventually convert OH to HO_2. HO_2 is recycled back to OH via

$$HO_2 + NO \text{ -----> } OH + NO_2 \qquad (6),$$
$$HO_2 + O_3 \text{ -----> } OH + 2O_2 \qquad (7)$$

The cycling reactions happen so fast that OH and HO_2 are essentially in photochemical equilibrium.

We have chosen the method of long path spectral absorption of light to make our measurements to provide a robust and well calibrated measurement.. The experiment utilizes a laser source and very high resolution ultraviolet absorption spectroscopy to measure the concentration of OH in a clean environment at a measured sensitivity limit of approximately 5×10^5 cm^{-3} (0.01 pptv) with an integration time of several minutes. This limit is substantially below predicted noontime OH concentrations and is low enough to provide a rigorous test of photochemical theories of hydroxyl formation. Spectroscopic measurement of the atmospheric line profiles of individual OH molecular rotation lines in the A-X electronic transition absorbed in the near ultraviolet over a long path is a particularly clean method of determining OH concentration. It depends only on well measured spectroscopic parameters determined from laboratory experiments with good accuracy, physical variables (such as light path length) which are easily determined accurately, and the measured fractional spectral absorption. In fact, the long path absorption technique can be considered a primary determination of OH concentration since no elaborate calibration techniques or inferential interpretations are required as in most of the chemical and laser induced fluorescence methods.

The experimental apparatus used consists of six basic components: (1) a spectrally bright and broad (tens of mJ per pulse over several tenths of nanometers) ultraviolet laser light source with optics for directing a low divergence, expanded light beam into ambient air outside of the observatory, (2) a mirror system located 10.3 km distant to collect the light beam and return it to

the observatory for a total absorption path length of 20.6 km, (3) a telescope collector located in the laboratory at the observatory, (4) a very high resolution (resolving power > 500,000) dual-channel spectrograph to allow accurate measurement of atmospheric absorption of individual rotational lines in the ultraviolet electronic OH bands near 308 nm, (5) a two-channel array detector system that allows simultaneous observation of both laser and absorbed laser light in a spectral interval sufficient to include measurement of several OH rotational lines simultaneously, and (6) a data collector/analysis system that allows computer control of the hardware.

In addition to this system for OH abundance determination, a completely independent instrument at the observatory uses a 1000-W white light continuum source and a low resolution double crossed Czerny-Turner spectrograph with a sensitive array detector to measure, simultaneously with the OH determination, the concentration of nitrous acid, ozone, water vapor, nitrogen dioxide, nitrogen trioxide, sulfur dioxide, and formaldehyde which affect the concentration of OH along the same long path. Ultraviolet photometers covering the spectral region between atmospheric cutoff at 295 nm and 330 nm measure the solar flux (both direct and diffuse) transmitted through the atmosphere. Another independent instrument system working in the infrared measures simultaneously CO and CH_4 (the major OH sinks in the clean troposphere) along the absorption path.

In fall 1993, the Tropospheric OH Photochemistry Experiment (TOHPE) was held at Fritz Peak, Colorado. A primary goal of TOHPE was to compare the OH concentrations measured using a variety of different techniques: the NOAA long path spectroscopic instrument, an in situ ion assisted chemical conversion instrument, a laser resonance fluorescence instrument, and a liquid scrubber instrument, all with sensitivities at or below 1 x 10^6 molecules cm^{-3}. In addition to the OH measurements, a nearly complete suite of trace gas species that affect the OH concentration were measured simultaneously, using both in situ and/or long path techniques, to provide the information necessary to understand the OH variation and concentration differences observed. Measurements of OH, NO_2, CH_2O, SO_2, H_2O, and O_3 were made using long path spectroscopic absorption of white light, or laser light, and OH, NO, NO_2, NO_y, O_3, CO, SO_2, CH_2O, $j(O_3)$, $j(NO_2)$, RO_2/HO_2, HO_2, H_2O, SO_2, PAN, PPN, HNO_3, and aerosols (size and composition) and ozone and nitrogen dioxide j-values were measured using in situ instruments. Meteorological parameters at each end of the long path and at the Idaho Hill in situ site were also measured. Over the period of the TOHPE experiment, OH concentrations were typically low with noontime maximum concentrations near 3 x 10^6 /cc.

This paper describes the instrumentation developed to make the measurements.

Thursday, March 21, 1996

Environmental Sensing II

LThB 10:15 am-12:00 m
Windsor Ballroom

Ernesto Cespedes, *Presider*
US Waterways Experiment Station

Remote Spectroscopy over Optical Fibers for *In Situ* Measurement of Contaminants in Soil

Steve Lieberman, David S. Knowles, Greg A. Theriault, Michele Davey
Naval Command, Control and Ocean Surveillance Center

Fiber optic-based sensor probes have been developed that can be pushed up to 50 meters into the soil for remote, real-time detection of petroleum hydrocarbons using laser-induced fluorescence (LIF) and metals via laser-induced breakdown spectroscopy (LIBS).

Raman Techniques for Detection of Explosive Materials

Brian D. Gilbert, James Janni, David Moss, R.W. Field, and Jeffrey I. Steinfeld
Department of Chemistry and G.R. Harrison Spectroscopy Laboratory, Massachusetts Institute of Technology, Cambridge, Mass. 02139

Telephone: (617)253-4525
Fax: (617)253-7030

and

Alvaro Mercado
Aviation Security Research and Development, Federal Aviation Administration Technical Center, Atlantic City,N.J. 08405

Telephone: (609)485-5388
Fax: (609)383-1973

A key requirement for prevailing against terrorist threats to both transportation systems and stationary structures [1,2], as well as for facilitating the massive cleanup efforts required at decommissioned military bases [3,4], is the ability to detect trace quantities of explosive materials in the presence of a wide variety of interfering species. Numerous analytical techniques are being investigated for this problem, among which laser-based spectroscopic methods show enormous potential. Methods under investigation [1,2] include absorption spectroscopy of explosive vapors detected by photothermal or modulation techniques, detection of decomposition fragments by chemiluminescence, frequency-modulation spectroscopy, or modulated magnetic rotation spectroscopy [5], and resonance-enhanced multiphoton ionization spectroscopy.

Within this set of approaches, Raman spectroscopy is emerging as a uniquely powerful tool for explosives detection. Raman spectra of explosive materials have been obtained by Akhavan [6] and Lewis et al. [7]. Recent significant advances in Raman instrumentation, particularly the use of long-wave excitation to suppress fluorescence interference, charge-coupled device (CCD) detectors to enhance sensitivity for near-infrared Raman scattering, and sophisticated digital signal processing algorithms to enhance the information contained in the CCD signal outputs, have opened the possibility of detecting explosives at the ultratrace levels and in the presence of interfering species needed for security and forensic applications, as well as for environmental applications (*i.e.*, site remediation).

One approach utilizes Raman microprobe technology for imaging explosive particles in fingerprints and other forensic samples [8]. This technology is currently being upgraded for performing rapid *in-situ* analysis of explosives potentially found on samples encountered in field screening applications. Our investigation has focused on the use of Surface-Enhanced Raman Spectroscopy (SERS) as a method for obtaining the sensitivity which will ultimately be required for detecting explosive materials at ultratrace levels. Using a Kaiser Raman spectrometer, Princeton Instruments CCD detector, and gold colloid as the SERS substrate, we have observed enhancement factors up to 10^5 for trinotrotoluene (TNT) in methanolic solution, which enabled us to acquire recognizable spectra from ca. 1 picogram of TNT [9]. The selective enhancement of ceratin vibrational bands of the molecule provides information about the adsorption geometry on

the SERS substrate, which in turn may aid in interpreting sticking probabilities and particulate adhesion forces on various surfaces -- an important issue in designing practical explosives detectors.

Another approach for improving the sensitivity of *in-situ* Raman spectroscopy, that is currently being pursued, involves the search for ultraviolet (UV) resonance enhancement for low levels of explosives adhering to non-SERS active substrates. This investigation uses a monochromator and CCD detector coated for the UV as the optical instrument, plastic explosive particles suspended in water as the sample, and second harmonic generation to produce excitation lines at wavelengths below 300 nm. Identifying Raman bands for UV resonance enhancement will aid in the rapid pre-blast analysis of explosives found on a variety of surfaces.

In this paper, we will report further measurements on SERS enhancements and Raman scattering cross sections for the explosive molecules themselves (TNT, PETN, and RDX), typical explosive formulations such as Detasheet, and selected taggant and simulant species. The cross sections, which have been referenced to the well-characterized 1350 cm^{-1} band of nitrobenzene, will aid in the intercomparison of the various Raman methods. We will also describe preparation and characterization of the SERS substrates [10,11] and their incorporation into Raman sensor devices. In addition, we will report our initial findings on resonance enhancement of the Raman cross sections of RDX and PETN in plastic explosives, and the severity of collateral effects such as laser-induced fluorescence, UV photodecomposition of the samples, and UV fracturing of the materials, which might compromise the effectiveness of the resonance Raman approach.

Acknowledgment. This work is supported by a grant to M.I.T. from the Federal Aviation Administration (FAA-93-G-056) and a TSWG RDT&E Project at the FAA Technical Center. We thank the staff of the Laser Biomedical Research Center at the G.R. Harrison Spectroscopy Laboratory (Drs. R. Dasari, Y. Wang, and K. Kniepp) for assistance with the Raman measurements.

References

1. A. Fainberg, "Explosives Detection for Aviation Security", Science **255**, 1531 - 1537 (1992).

2. A.M. Rouhi, "Government, Industry efforts yield array of tools to combat terrorism", Chem. and Eng. News, pp. 10 - 19 (July 24, 1995).

3. M. Renner, "Cleaning up after the Arms Race", in *State of the World: 1994* (L.R. Brown, ed.), Worldwatch Institute / W.W. Norton & Co., New York (1994), pp. 137 - 155.

4. "Environmental Security", DoD Annual Report to the President and Congress (January 1994), pp. 82 - 90.

5. J.M. Smith, J.C. Bloch, R.W. Field, and J.I. Steinfeld, "Trace detection of NO2 by frequency-modulation-enhanced magnetic rotation spectroscopy", J. Opt. Soc. Amer. **B12,** 964 - 969 (1995).

6. J. Akhavan, "Analysis of high-explosive samples by Fourier transform Raman spectroscopy", Spectrochim. Acta **47A,** 1247 - 1250 (1991).

7. I.R. Lewis, N.W. Daniel, Jr., N.C. Chaffin, P.R. Griffiths, and M.W. Tungol, "Raman spectroscopic studies of explosive materials: toward a fieldable explosives detector", Spectrochim. Acta **51A** (1995), in press.

8. C. Cheng, T.E. Kirkbride, D.N. Batchelder, R.J. Lacey, and T.G. Sheldon, J. Forensic Sci. **40**, 31 - 37 (1995).

9. K. Kniepp, Y. Wang, R.R. Dasari, M.S. Feld, B.D. Gilbert, J. Janni, and J.I. Steinfeld, Spectrochim. Acta **51A** (1995), in press.

10. G. Frens, "Controlled nucleation for the regulation of the particle size in monodisperse gold suspensions", Nature **241**, 20 - 22 (1973).

11. K.C. Grabar, R.G. Freeman, M.B. Hommer, and M.J. Natan, "Preparation and characterization of Au colloid monolayers", Anal. Chem. **67**, 735 - 743 (1995).

Advanced Laser Detection Techniques for Cone Penetrometer Sensors

J. Wormhoudt, J. H. Shorter, J. B. McManus, P. L. Kebabian, D. D. Nelson, M. S. Zahniser, and C. E. Kolb
Center for Chemical and Environmental Physics
Aerodyne Research, Inc.
45 Manning Road
Billerica, MA 01821
(508) 663-9500 (Phone) / (508) 663-4918 (Fax)

This paper presents work in two areas of laser detection technique development for application to cone penetrometer measurements of contaminants in soils. In both cases, the initial target contaminants are explosives and energetic materials, and the basic technique involves detection by heating contaminated soils and quantifying the resulting pyrolysis gases. In the first area, tunable infrared laser differential absorption spectroscopy (TILDAS) is being applied in two ways: as a sensitive, specific real-time diagnostic of laboratory experiments designed to improve understanding of basic mechanisms, and as a potential *in situ* detection technique for inclusion in a penetrometer probe. In the second area, a novel class of miniature laser devices will be extended to provided visible and ultraviolet light sources for laser induced fluorescence (LIF) detection of pyrolysis gases.

A currently fielded cone penetrometer probe has demonstrated the detection of TNT, using an electrochemical cell sensitive to NO as a detector, and a pyrolyzer consisting of two loops of platinum wire wrapped around a ceramic sleeve on the outside of the probe. Our laboratory investigations have provided support for the hypothesis that decomposition of TNT to NO does not take place in the soil matrix, as originally believed, but that instead TNT is first evaporated from the soil, and then TNT vapor which passes close to the pyrolyzer wire decomposes to NO in the gas phase.

A key element of a TILDAS device which could be accommodated inside the 2.5 cm inside diameter of a cone penetrometer probe is a multipass absorption cell with a high path length to volume ratio. Over the past few years we have done substantial development of astigmatic off-axis resonator (Herriott) cells for laser spectroscopy.[1] These cells fill the available mirror area with recirculating beams, thus reducing beam overlap and the interference fringes which are often the limiting factor for sensitivity of laser absorption in multipass cells. In this paper we will present

results of new calculations which show that useful TILDAS path lengths can be achieved inside a cone penetrometer probe. For example, a cell designed to fit inside a standard probe might have 2 cm diameter mirrors and a base length of 20 cm. We find that for wavelengths less than 5 microns and a ratio of beam spacing to Gaussian beam width at the mirror of 10, the maximum number of passes is 22 and the path length is 4.4 m. Using this path length and the minimum detectable optical depths in current TILDAS field instruments (in the range 10^{-4} to10^{-5}), we can estimate minumum detectable densities of the TNT decomposition products NO and NO_2, as well as N_2O which is a distinctive product of decomposition of nitramine compounds such as RDX and HMX. These detection limits are gas phase mixing ratios in the 0.1 to 10 ppbv range, which can translate into concentration levels in the soil of the order of 1 ppm by weight.

As attractive as the characteristics of TILDAS are, including positive species identification and quantitative determination without calibration, the technique of laser induced fluorescence is of great interest because of its even greater sensitivity. LIF detection of NO in a cone penetrometer sensor has been recognized as particularly challenging because the short wavelengths (in the 200-230 nm range) mean that light from a laser source on the surface cannot be transmitted to the probe using fiber optics. We will report on a program to apply laser systems developed at MIT Lincoln Laboratory[2] to LIF detection of the explosives pyrolysis gases NO and NO_2. These laser systems consist of a near-infrared diode laser pump, which would remain on the surface and whose output is easily transmitted to the probe via fibers, and a series of crystals which convert the pump light into visible and ultraviolet wavelengths inside the probe. We will report on expected detection sensitivities for NO and NO_2 using these laser sources.

1. J. B. McManus, P. L Kebabian, and M. S. Zahniser, "Astigmatic mirror multiple pass absorption cells for long pathlength spectroscopy," Applied Optics **34**, 3336-3348 (1995).

2. J. J. Zayhowski and C. Dill, III, "Diode-pumped passively Q-switched picosecond microchip lasers,", Opt. Lett. **19**, 1427-1429 (1994).

Real-Time Laser Ablation MS/MS of Individual Airborne Microparticles

P. T. A. Reilly, M. Yang, R. Gieray, W. B. Whitten, and J. M. Ramsey
Chemical and Analytical Sciences Division
Oak Ridge National Laboratory
P.O. Box 2008, M/S 6142
Oak Ridge, Tennessee 37831-6142
423-574-4882
423-574-8363 FAX
ReillyPT@ornl.gov

In the past, chemical analysis of airborne particulates was done in the bulk. In other words, particles were collected on a filter and later extracted and subjected to chemical analysis. This provides only a very time consuming statistical constituent analysis of the ensemble of particles that is generally incomplete. All information about composition and chemistry of the individual particles was lost. Recently, mass spectrometric techniques have been applied to individual particles in real-time.[1,2,3] Analysis of individual particles via time-of-flight has had great success with the lighter inorganic constituents, but is unenlightening when used on organic based particles. Application of ion trap MS/MS techniques to organically derived particulates permits positive identification of any of the constituents.

Individual airborne microparticles are directly introduced into an ion trap mass spectrometer through a differentially pumped inlet. As a microparticle enters the vacuum chamber, it is detected by light scattering from a CW laser. This scattered light pulse is used to trigger the charging of the ablation laser. The ion trap is held in ion collection mode until a particle reaches the center of the trap by halting the CPU in the ion trap electronics. When the microparticle reaches the center of the trap, it is again detected via light scattering from another CW laser. This second light pulse then triggers the firing of the ablation/ionization laser and subsequently reactivates the ion trap electronics. The collected component ions are then mass analyzed using standard ion trap techniques. The combination of laser ablation/ionization with the MS/MS capabilities of the ion trap permits detailed interrogation of the composition of any

type of airborne particulate. This capability is especially useful for studying organic based particulates. Accurate correlation of the individual microparticle flight times between the light scatter detection points with aerodynamic particle size is also possible.[2] This technique permits complete categorization of particle size with chemical composition.

---

[1]J. M. Ramsey, M. Yang, P. T. A. Reilly, and W. B. Whitten, *Proceedings The 43rd ASMS Conference on Mass Spectrometry and Applied Topics*, **1995**, 3.
[2]K. A. Prather, C. Noble, K. Salt, T. Nordmeyer, D. Fergenson, and B. Morrical, *Proceedings The 43rd ASMS Conference on Mass Spectrometry and Applied Topics*, **1995**, 1.
[3]M. V. Johnston, P. G. Carson, B. A Mansoori, and A. S. Wexler, *Proceedings The 43rd ASMS Conference on Mass Spectrometry and Applied Topics*, **1995**, 2

Raman Spectroscopy of Phosphonate Solutions by Real time, In-Situ Fiber Probe With Metal Oxide Adsorbent

D.M. Dagenais
SFA Inc., Landover MD 20785
Tel. (202) 767-9347
FAX (202) 767-5792
and
K.J. Ewing, F. Bucholtz, I.D. Aggrawal
Naval Research Laboratory
Code 5603
Washington, DC 20375

Introduction

Fiber optic Raman spectroscopy is a powerful tool for in-situ detection and selectivity, but it lacks sensitivity. Significant enhancement has been obtained by pre-concentration in a matrix of metal oxide, leading to selective in-situ detection of traces of DMMP, DIMP and MPA both in water and in gas phase, for a potentially portable device for detection of traces of chemical break-down products.

Experimental Set-Up

Light from an Argon-ion laser is injected into a multi-mode fiber (fig.1) and guided to a probe containing a bed of aluminum oxide powder with high active surface area (155 m^2/g). The bed is maintained in a tube by porous polymer plugs. Organo-phosphorus vapors or aqueous solutions of organo-phosphorus compounds can be pumped through the tube while the fiber probe monitors the scattered signal with collection fibers surrounding the excitation fiber. The fiber bundle signal is filtered with an edge holographic filter and focused into the slit of a conventional Spex 270M spectrometer equipped with a CCD detector array [1].

It has been shown that alumina chemisorbs phosphorus compounds [2]. The spectral data, obtained with a 20 second averaging time, shows the increase of the Raman intensity for the CH vibration lines for incremental levels of solution passed through the bed. All data is processed by subtracting a synthetic background, obtained by curve fitting, from the Raman signal. Detection limits Y_{min}, are calculated from linear extrapolation as $Y_{min} = 3Y_{std}/m$, where Y_{std} is the standard deviation of the Y intercept and m the slope of the calibration curve. When performing replicate measurements near the detection limit, detection limits are computed as $Y_{min} = sY_{std}/n$, where s is the t value for 95% confidence interval, Y_{std} is the standard deviation of the spectral intensity and n the number of degrees of freedom (or n+1 the number of replicate measurements).

Results and Discussion

In the case of gas phase detection, a known amount of DMMP obtained from a bubbler [3] was passed through the tube containing basic alumina, for 1 hour. The resulting tube exhibited 35% adsorption of the total DMMP passed through. Replicate Raman spectra were then collected with the fiber probe and yielded a 6ppm detection limit (fig. 2). This detection level is expected to improve for longer exposure times, until saturation is reached in the alumina bed.

Raman spectra of the various neat compounds are shown in figure 3, showing the excellent selectivity. These spectra were also easily separated from potential interferences, for example insecticides such as diazinon. Selectivity was also studied by acquiring spectra of a mix of DMMP and DIMP vapors. Fitting was obtained by a weighted addition of the pure DMMP and

DIMP vapor phase spectra obtained when the vapors were chemisorbed onto alumina. Fig. 4 shows the result of a vapor mix obtained from a 40% DMMP, 60% DIMP mix in the liquid phase. Fits obtained for mixtures of DMMP/DIMP varying from a 9 to 1 ratio to a 1 to 9 ratio in solution phase show the reproducible trend of a linear summation of the two spectra of the neat vapors.

Raman spectral measurements were also acquired for MPA in the liquid phase, as chemisorbed onto neutral alumina. Measurements were taken for a series of concentrations of MPA and ten replicate measurements for each flow level produced the standard deviation error for each condition (fig.5). The acquired data lead to the determination of the slope of the analytical curve as a function of concentration, the intensity of the Raman peak at saturation as a function of concentration as well as the extraction of a minimum detectable level of 2ppm for MPA in water solution.

Conclusion

We have demonstrated that fiber Raman sensing combined with pre-concentration on aluminum oxide exhibits quantitative, selective detection of organo-phosphorus compounds with detectable levels in the 5 ppm range, in gaseous and liquid phase.

References

1- T. Vo-Dinh, D.I. Stokes, Y.S. Li, G.H. Miller, "Fiberoptic sensor probe for in situ surface-enhanced Raman monitoring",Chemical, Biochemical and Environmental Fiber Sensors II, SPIE Vol. 1368, 203 (1990).

2- M.K. Templeton, W.H. Weinberg, " Adsorption and Decomposition of Dimethyl Methylphosphonate on an Aluminum Oxide Surface", J. Am. Chem. Soc., **107**, 97 (1985).

3- D.S. Ballantine, Jr., S.L. Rose, J.W. Grate, H. Wohltjen, "Correlation of Surface Acoustic Wave Device Coating Responses with Solubility Properties and Chemical Structure Using Pattern Recognition", Anal. Chem., **58**, 3058 (1986).

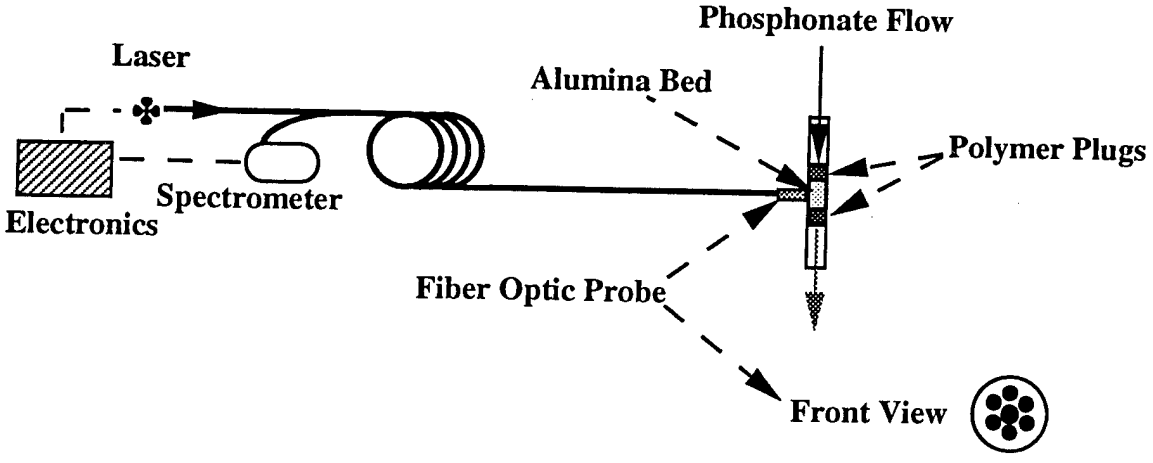

Fig.1-Experimental Set-Up of Raman Fiber-Optic Sensing.

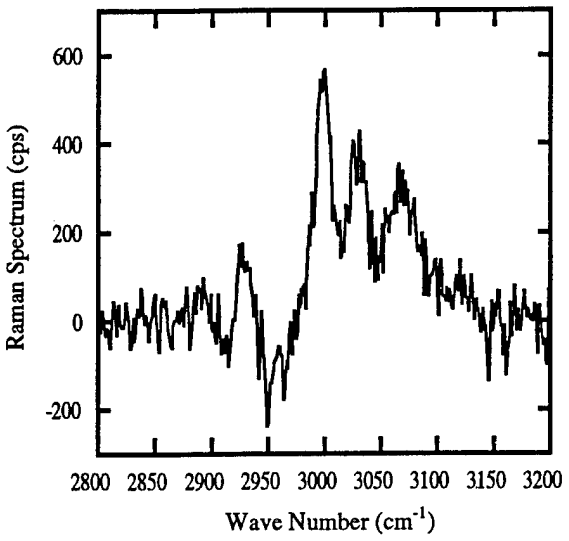

Fig 2- Raman spectrum of DMMP vapor phase adsorbed onto alumina.

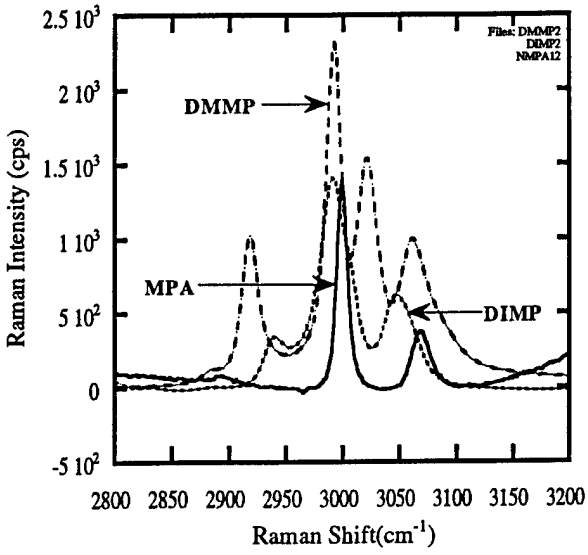

Fig 3- Raman spectra of pure compounds DMMP, DIMP and MPA .

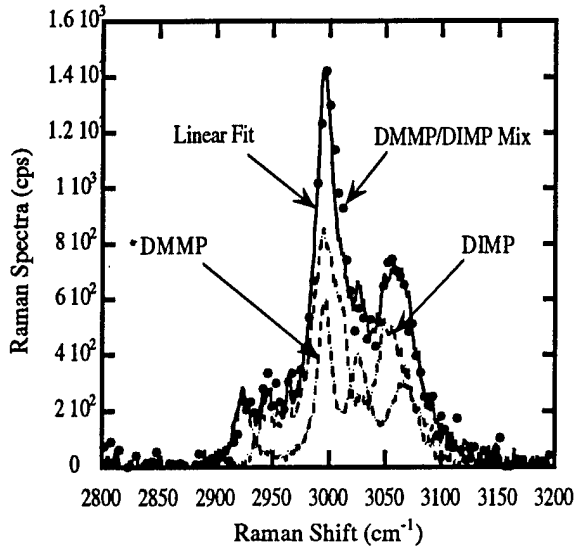

Fig 4- Raman spectrum of a mix of DMMP and DIMP vapors, adsorbed onto Alumina. Curve fitting is obtained from the summation of the spectra of the pure vapors adsorbed onto alumina.

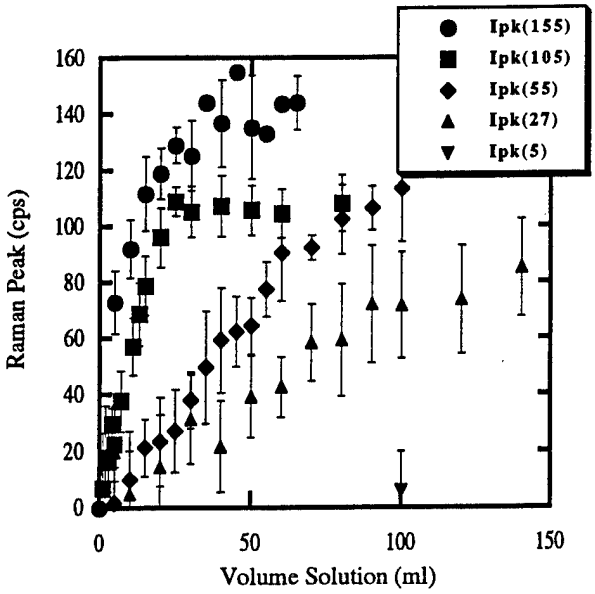

Fig 5- Analytical curves of MPA solutions adsorbed onto alumina. Each curve corresponds to a specific concentration of MPA solution (in ppm). Each point = mean value of ten replicate measurements. The error bar = ± one standard deviation.

Raman Spectroscopy of Explosives and Propellants During Heating

N.F. Fell and K.L. McNesby
U.S. Army Research Laboratory
AMSRL-WT-PC
Aberdeen Proving Ground, MD 21005-5066
TEL: (410) 278-6163
FAX: (410) 278-6150
email mcnesby@arl.mil

In this paper we report Raman spectra of nitramine and nitrocellulose based explosives and propellants measured during heating of the sample. Raman spectra are measured using a Fourier transform spectrometer employing 1064 nm laser radiation as the scattering source, and using a dispersive system employing 514.5 nm laser radiation as the scattering source. For most explosives and propellants, the longer wavelength radiation (1064 nm) measures scatter from the bulk sample during heating, while the shorter wavelength, visible radiation (514.5 nm) is used to measure changes in the surface of the sample during heating.

Raman spectra of energetic materials (especially nitramines and nitramine-based propellants) have been shown to be superior[1] to spectra measured using absorption-based vibrational spectroscopies. Figure 1 shows a portion of the Raman spectrum of the nitramine-based (RDX) explosive C-4 during heating from room temperature to 140° C. Even over this small temperature range, there are numerous changes in peak contours and relative intensities. These changes may be correlated to decomposition pathways in the explosive, and may be used to compare the effect of binders and plasticizers on decomposition mechanisms in differing propellant formulations.

Because Raman spectroscopy allows measurement of low energy lattice vibrations in crystalline materials (phonons), it is possible to measure the vibrational modes believed to be responsible for introduction of thermal energy into the higher energy internal vibrational modes of the molecule. The distribution of these low energy "doorway" modes can provide insight into the impact sensitivity of energetic materials, and may provide a means of predicting impact sensitivities of newly synthesized materials. The development of a methodology to spectrally detemine impact sensitivities of nitramine-based energetic materials is currently underway in our laboratory.

1. K.L. McNesby, J.E. Wolfe, J.B. Morris, and R.A. Pesce-Rodriguez, J.Raman Spec., **25**, 75 (1994).

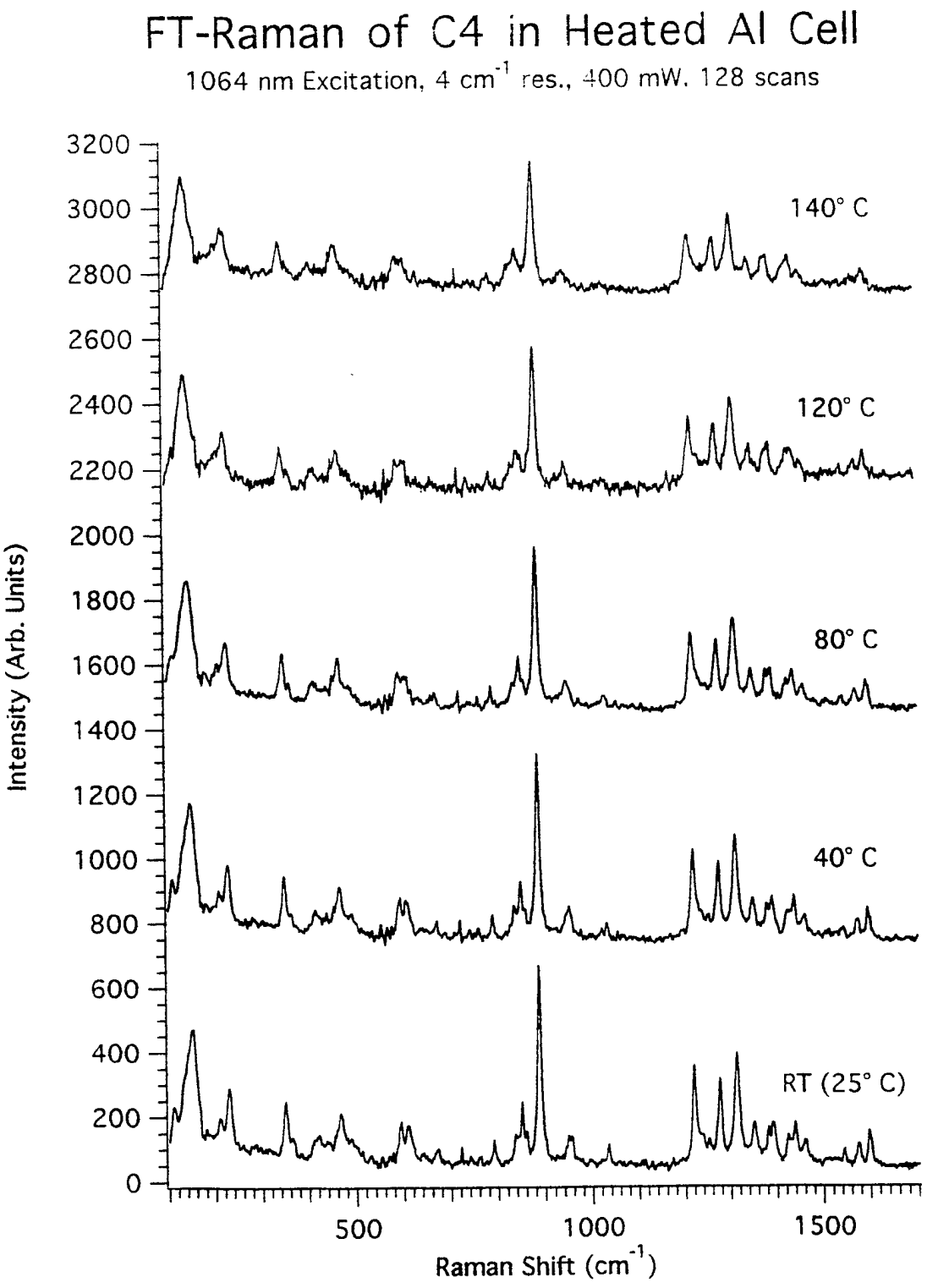

Figure 1: The FT-Raman spectrum of the explosive C-4 measured while the sample was heated from room temperature to 140° C.

Thursday, March 21, 1996

Gas Phase Diagnostics

LThC 1:30 pm-4:00 pm
Windsor Ballroom

Jerry Seitzman, *Presider*
Georgia Institute of Technology

Applications of Infrared Spectroscopy for Combustion Diagnostics

David J. Rakestraw
Combustion Research Facility
Sandia National Laboratories
Livermore, CA 94551

The application of infrared spectroscopies for combustion diagnostics offers an exciting new opportunity to measure a wide range of polyatomic molecular species. The ability to measure low concentrations of many species important in combustion chemistry has been limited to a great extent to molecules that that can be probed using laser-induced fluorescence in the visible and ultraviolet spectral regions. Over the past several years our group has been investigating the use of infrared spectroscopies in an effort to greatly expand the polyatomic molecules that can be probed using laser diagnostics. This effort has benefited from advances in laser technology as well as the development of new spectroscopic approaches. The work discussed in this paper makes use of a tunable single-mode optical parametric oscillator system to provide high resolution rovibrational spectra. Degenerate four-wave mixing (DFWM) and cavity ringdown laser absorption spectroscopy (CRLAS) are the two spectroscopic techniques investigated.

The spectroscopic investigations have been conducted using infrared radiation in the region of 2500 - 3300 cm^{-1}. This spectral region allows numerous molecular species to be probed via the fundamental stretching frequencies of C-H, O-H and N-H bonds. Degenerate four-wave mixing provides an excellent method to probe infrared transitions while maintaining high temporal and spatial resolutions. CRLAS can often provide increased sensitivity at the expense of obtaining path integrated measurements and losing some temporal resolution. In addition, CRLAS has the advantage of providing absolute number densities. This paper will examine the merits of using both DFWM and CRLAS and present experimental results obtained from low pressure flames (10-100 Torr).

Multiplex Degenerate Four Wave Mixing Thermometry of the C_2 Radical.

G.M. Lloyd, C.F. Kaminski, I.G.Hughes, P. Ewart

Clarendon Laboratory, Oxford University,
Parks Road, Oxford, OX1 3PU. UK

Fax: + 44 1865 272400; Phone + 44 1865 272220
E-mail to: P.Ewart@physics.oxford.ac.uk

In recent years an increasing use has been made of laser based techniques for non-intrusive temperature measurements and analysis of combustion and other hostile environments. Degenerate four-wave mixing (DFWM) is a single photon resonant process producing a collimated signal which enables spatial discrimination of background and scattered light. Scanning DFWM has been used for detection of several radical species including OH [1] and C_2[2] and for thermometry [3]. Of particular use for diagnostics, however, are single-shot temperature measurements, especially for studying rapidly varying environments. The feasibility of single-shot multiplex DFWM thermometry of the hydroxyl radical has been demonstrated[4,5].

We report here multiplex DFWM of the C_2 radical created in an atmospheric pressure oxy-acetylene flame. A broad bandwidth laser was used with sufficient bandwidth to excite signal simultaneously from over 100 rotational lines. The spectra obtained showed a high level of consistency and stability and gave a mean temperature consistent with that expected for the flame.

A theoretical treatment of the DFWM signal has been conducted in the limit of monochromatic pump and probe beams[6], and also when the spectral bandwidth of the beams considerably exceeds the width of the transition involved[7]. While the latter is more relevant to the situation under investigation, both limits lead to the same variation of signal intensity with the parameters most relevant to thermometry. In the conventional geometry a DFWM signal is produced when strong counterpropagating forward and backward pump beams are intersected by a weak probe beam at some small angle to the pump beams. When the frequency of the beams is resonant with a transition of a molecule present within the intersecting volume, a DFWM signal is produced counterpropagating to the signal beam. For laser intensities much less than the saturation intensity for the transition, I_{sat}, the signal is proportional to the product of the intensities of the three incoming beams. When all three beams derive from the same laser source, this leads to a cubic dependence on the laser intensity. As the laser intensity increases to much above I_{sat}, the magnitude of the signal at line centre varies as I^x, with x reducing to 0, in the monochromatic case, for $I>>I_{sat}$. The dependence on dipole moment for the transition also varies with intensity, from a μ^8 dependence for $I<<I_{sat}$ to a μ^2 variation for $I>>I_{sat}$ in the monochromatic case. With negligible excited state concentration, the signal is proportional to the square of the number density of the molecules occupying the relevant ground state for the transition. Comparing the signal intensity from several rotational lines can therefore yield a rotational temperature for the molecule by assuming a Boltzmann distribution amongst the rotational levels of the ground state.

Multiplex spectra involving transitions in the $d^3\Pi_g \leftarrow a^3\Pi_u$ (0,0) Swan band system of C_2 were excited around 516 nm. Broad bandwidth radiation was provided by a modeless laser (ML) [8] operating with Coumarin 500 dye. The ML contains no optical resonator ensuring that its output contains no longitudinal mode structure thus minimising mode noise. The frequency and bandwidth of the emitted radiation are controlled by the incorporation of a diffraction grating in the laser. The ML was pumped with up to 45 mJ of 355 nm laser radiation from a Q-switched Nd:YAG laser, (10 Hz, ~ 7 ns duration), to give up to 6 mJ of tunable light in a bandwidth variable from 1 to 5 nm. The resultant beam was spatially filtered and passed through a polariser-waveplate assembly to give a uniform beam profile and continuously variable intensity. This also enabled measurements of the saturation level of the DFWM signal to be made. Typically 10 to 100 μJ of the emitted pulse was used for the thermometry measurements, with a 1 mm beam diameter. The usual phase conjugate geometry was used and the signal beam was directed into a 1m monochromator, fitted with an unintensified CCD to record the full spectrum of the emitted signal. The flame probed was a standard oxy-acetylene welding torch mounted on a translation stage using a slightly fuel rich mixture. Flame emission was attenuated by use of a chopper wheel to a fairly constant low background level which could be subtracted from the recorded spectra.

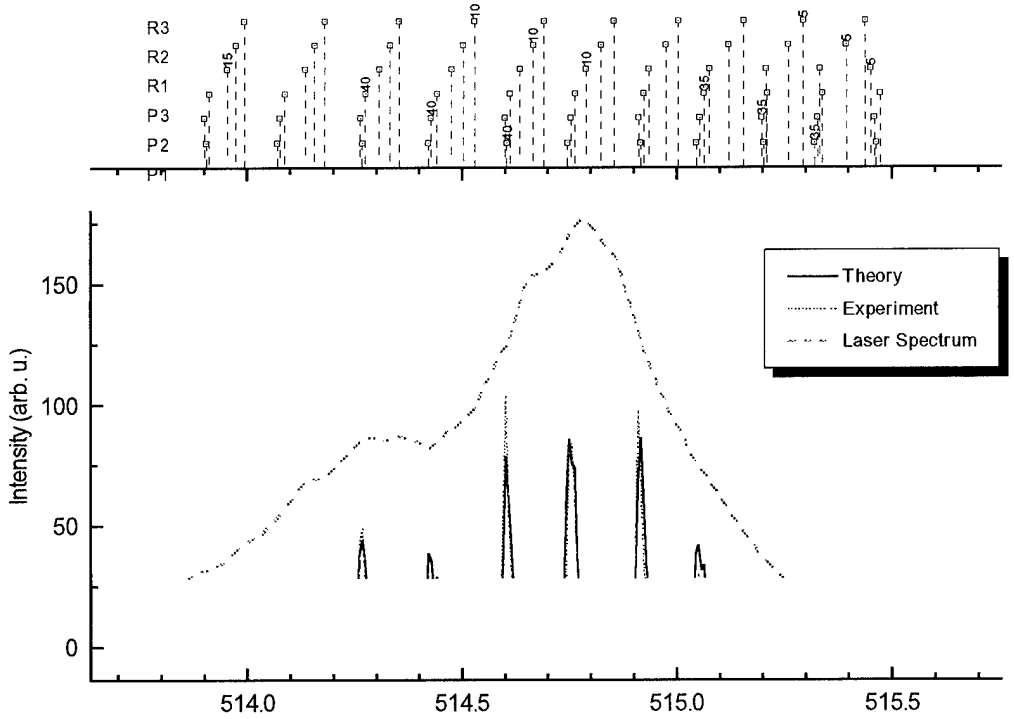

Figure Multiplex DFWM spectrum of C_2 and least squares best fit. The upper graph is included for spectral identification. The spectrum shown encompasses more than 60 lines in the R and P branches.

Multiplex spectra were obtained containing more than 100 rotational transitions of the $d^3\Pi_g \leftarrow a^3\Pi_u$ (0,0) Swan band system of C_2. For sensitive temperature measurements to be made, spectra containing both low ground state energy R branch transitions ($J \sim 7$ -11) and higher ground state energy P branch lines ($J \sim 32$ -42) were recorded. The modeless laser frequency spectrum was also recorded concurrently with the DFWM spectrum on a different part of the CCD chip, enabling referencing to the relative laser intensity to be made. Measurements of the variation of the signal level with the input intensity, yielded a dependence of the signal level on input intensity of approximately $I_{signal} \propto I_{laser}$. This indicates that the input intensity was of the order of I_{sat}. It has been shown experimentally that for a wide range of intensities around I_{sat} the variation of signal with dipole moment follows a μ^4 dependence. Synthetic C_2 spectra were therefore calculated assuming a linear dependence of signal on laser power at the relevant frequency, with a variation with dipole moment of μ^4. Such synthetic spectra were then fitted to the recorded experimental spectra using temperature as a variable parameter to improve the quality of the fit. An example of one such multiplex spectrum and theoretical fit along with the laser spectral profile is shown in the accompanying figure. The best fit for this spectrum corresponds to a temperature of 2990 K. A typical set of 100 such spectra (each spectrum the product of two laser shots) yielded a temperature of approximately 2990 K with a single temperature standard deviation of 320 K (~10%). This mean temperature is consistent with that expected for a flame of this type[9].

This work has indicated the viability of single shot multiplex thermometry using DFWM of the C_2 radical as an accurate and consistent measure of temperature. The use of the dye laser fundamental output to obtain frequencies resonant with the C_2 transitions means a large number of rotational transitions can be covered in a single shot. The relatively high intensities obtainable at the wavelength also make the technique especially suitable for temperature measurement in 1 or more dimensions. Further work is being conducted on DFWM thermometry using the OH and C_2 radicals. The latest experimental results will be presented at the meeting.

References:

[1] P. Ewart, S.V. O'Leary, *Opt. Lett.*, **11**, 279 (1986).
[2] K. Nyholm, M. Kaivola, C.G. Aminoff, *Opt. Comm.*, **107**, 406 (1994).
[3] T. Dreier, D.J. Rakestraw. *Opt. Lett.*, **15**, 71 (1990).
[4] I.P. Jefferies, A.J. Yates, P. Ewart., in *Coherent Raman Spectroscopy.* World Scientific. Ed. E. Castelucci and R.Righini and P. Foggi, p 129, (1993).
[5] B. Yip, P.M. Danehy, R. K. Hanson. *Opt. Lett.*, **107**, 751 (1992).
[6] R.L. Abrams, R.C. Lind, *Opt. Lett.*, **2**, 34 (1978).
[7] J. Cooper, A. Charlton, D.R. Meacher, P. Ewart, G. Alber, *Phys. Rev. A*, **40**, 5705 (1989).
[8] P. Ewart, *Opt. Comm.*, **55**, 124 (1985).
[9] A.G. Gaydon, *Flames, their structure, radiation and temperature.* Wiley, NY, (1990).

DEGENERATE FOUR-WAVE MIXING SPECTROSCOPY USING PICOSECOND LASERS: THEORETICAL ANALYSIS

Thomas A. Reichardt and Robert P. Lucht, Laser Diagnostics Laboratory, Dept. of Mech. and Ind. Engineering, University of Illinois, 1206 W. Green Street, Urbana, IL 61801 (Phone: 217-333-5056, Fax: 217-244-6534)

1. Introduction

Degenerate four-wave mixing (DFWM) has emerged in recent years as a potentially powerful technique for quantitative measurement of minor species in gas-phase media.[1,2] However, a complicated collision-rate dependence of the DFWM signal is observed when lasers with pulse lengths of several nanoseconds are used.[3-5] On the other hand, picosecond lasers possess pulse widths shorter than the typical collisional time in atmospheric gas-phase media, and use of such lasers for DFWM measurements[6] could reduce the sensitivity of the technique to the collision rate.[2,7] While pulsed lasers are usually utilized to perform gas-phase DFWM measurements, DFWM analytical models are generally limited to the assumption of continuous wave (cw) laser inputs. These cw models have been applied successfully to modeling gas-phase DFWM with nanosecond-pulse lasers, where the pulse length (~10 nsec) is much longer than the typical collisional time (~100 psec) in atmospheric-pressure flames. In this paper, we use direct numerical integration (DNI) of the density matrix equations to investigate theoretically the use of lasers with pulse lengths (τ_L) much shorter than characteristic collision times (τ_C) for quantitative DFWM spectroscopy in gas-phase media. Both purely homogeneously broadened resonances and resonances that are both collision- and Doppler-broadened are considered.

2. Calculation of the DFWM Signal using Direct Numerical Integration

The time-dependent density matrix equations for a nondegenerate two-level system irradiated by two pump beams and a probe beam are given by[8]

$$\frac{\partial \rho_{11}(z,t)}{\partial t} = -\frac{i}{\hbar}(V_{12}\rho_{21} - \rho_{12}V_{21}) + \Gamma_{21}\rho_{22}\ , \quad (1)$$

$$\frac{\partial \rho_{21}(z,t)}{\partial t} = -\rho_{21}\left(i\omega_{21} + \gamma_{21}\right) - \frac{i}{\hbar}V_{21}\left(\rho_{11} - \rho_{22}\right), \quad (2)$$

where the diagonal matrix elements ρ_{11} and ρ_{22} are proportional to the populations of level 1 and 2 and the off-diagonal matrix element ρ_{21} describes the coherence between levels 1 and 2. In Eqns. (1) and (2) $\hbar$ is Planck's constant (J-sec), Γ_{21} is the population transfer rate from level 2 to level 1 (sec^{-1}), ω_{21} is the angular frequency of the two-level resonance (sec^{-1}), and γ_{21} is the coherence dephasing rate (sec^{-1}). The interaction term $V_{21} = -\vec{\mu}_{21} \bullet \vec{E}(z,t)$, where $\vec{\mu}_{21}$ is the electric dipole matrix element (C-m) and $\vec{E}(z,t)$ designates the combined electric fields from the probe and two pump beams (V/m). The collisional width (FWHM) of the resonance is given by $\Delta\omega_C = 2\gamma_{21}$. The manipulation of these equations for solution by direct numerical integration has been described in detail by Lucht et al.[5] and Reichardt and Lucht.[9] We assume equal intensities for the forward and backward pumps, and set the peak probe intensity (I_{pr}) equal to one-fourth the value of the peak pump intensity (I_{pump}). We assume a 3° angle between the forward pump and probe beams. The three pulses arrive in the medium so that the peaks of the pulses temporally coincide in the exact center of the interaction length at time $t = 0$ sec.

3. Temporal Development of the Short-Laser-Pulse DFWM Signal

The temporal dependence of the DFWM signal generated for 100-picosecond laser pulses (τ_L = 100 ps) interacting with a homogeneously broadened resonance is shown in Fig. 1(a). We define the laser pulse width, τ_L, as the FWHM of the Gaussian envelope for the single-mode electric field intensity of the pump and probe pulses. If $\tau_L << \tau_C$, the pumping rate is faster than the medium can relax through collisions. It has been suggested that if the laser pulses interact before a significant number of collisions can occur, the DFWM signal intensity may be essentially independent of the collisional environment. However, Fig. 1(a) demonstrates that as the collisional rate decreases, the signal decays at a slower rate. The laser pulses may interact before collisions can occur, but Fig. 1(a) shows that the polarization established by the laser pulses in a homogeneous system continues to radiate until it is destroyed by collisions. For such conditions, contrary to expectations, the signal intensity will indeed be still dependent on the collision rate.

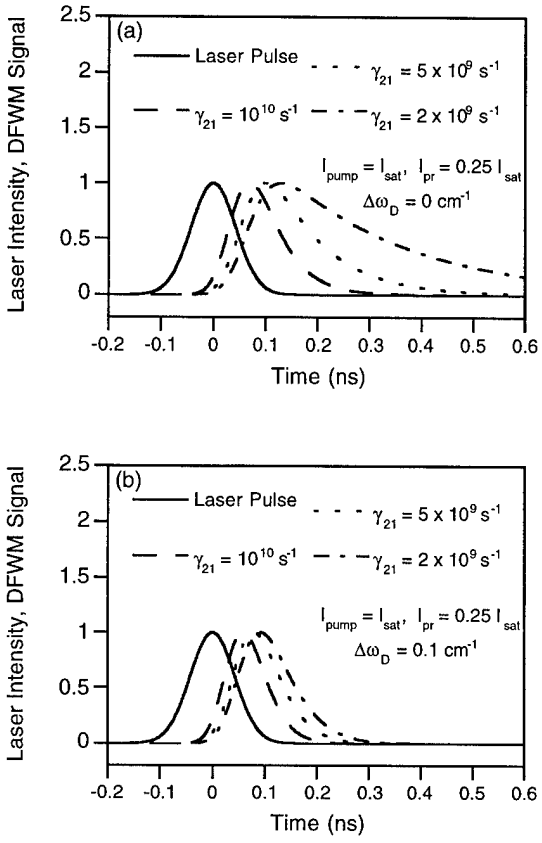

Fig. 1. Temporal development of the DFWM signal for a homogeneously (a) and inhomogeneously (b) broadened resonance. For each collision rate, the laser intensity has been set equal to the saturation intensity. The laser pulse intensity envelope is shown for reference. All waveforms have been normalized to a maximum value of unity.

The purely homogeneous case is not of great interest for combustion diagnostics in the ultraviolet or visible regions of the spectrum because for gases at atmospheric pressure the Doppler width of the resonance line is comparable to or greater than the homogeneous width. Doppler broadening is included in our DNI calculations by the solution of the density matrix equations for numerous closely spaced velocity groups. The different velocity groups will have different resonance frequencies in the laboratory frame. As the laser pulses pass through the interaction region, a polarization is established in each of the velocity groups; the magnitude of this polarization depends on how effectively the laser can couple with each velocity group. Figure 1(b) includes Doppler broadening for the same conditions as shown in Fig. 1(a). We set the Doppler width of the resonance ($\Delta\omega_D / 2\pi c$) equal to 0.1 cm^{-1} (FWHM). Inclusion of Doppler broadening temporally shortens the DFWM signal; the signal intensity profile follows the input pulse envelope much more closely. Now that we have included molecular motion, the molecular dipoles oscillate with a spread of resonance frequencies and the signals in Fig. 1(b) consequently exhibit faster decays.

4. Variation of DFWM Reflectivity with Collisional Rate

DFWM can be used as a diagnostic because the magnitude of the polarization established by the lasers is proportional to the number density of the probed species. The signal strength in DFWM measurements is usually reported in terms of the reflectivity (R), which is defined in the steady-state regime as the ratio of the signal intensity to the probe intensity. For the transient regime, we define the reflectivity as the ratio of the integrated signal energy to the probe pulse energy. With either definition, the reflectivity is dependent on the electric field intensity, and will therefore be proportional to the square of the number density.

Figure 2 displays the DFWM reflectivity for a homogeneously broadened resonance as a function of τ_L / τ_C for several laser pulse intensities. For each curve the pump laser intensity, defined in terms of the Rabi frequency $\Omega_{pump} = \mu_{21} A_{pump} / 2\hbar$,[5] remains constant while the collision rate is varied. As we approach the region for which $\tau_L >> \tau_C$, the value of $R \propto (\gamma_{21})^{-6}$. As we approach the region for which $\tau_L << \tau_C$, we see that the reflectivity continues to increase with decreasing collision rate. The temporal extent of the signal, and thus the integrated intensity, is inversely proportional to the collisional rate.

Figure 3 displays the reflectivity curves for the conditions discussed for Fig. 2, except we now include the effect of Doppler motion, setting $\Delta\omega_D$ = 0.1 cm^{-1}. For $\tau_L >> \tau_C$, the curves approach the same values for the reflectivity as found for the homogeneous case, because $\Delta\omega_D << \Delta\omega_C$. However, remarkably different results occur for the fully transient regime where $\tau_L << \tau_C$. The fall-time of the DFWM pulse is nearly the same as the fall-time of the laser pulse, which is faster than the collision rate. Doppler motion decreases the signal intensity for two reasons: (1) the laser pulses interact less efficiently with the molecules, and (2) the polarization established by the DFWM interaction is dephased by the molecular motion. Therefore, although

the DFWM signal is independent of collision rate for $\tau_L << \tau_C$, the signal level is dependent on the Doppler width.

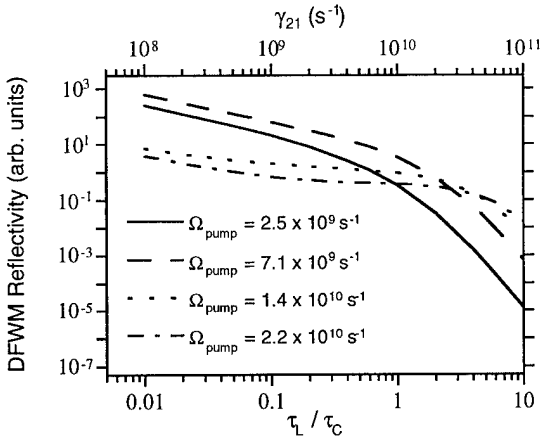

Fig. 2. DFWM reflectivity for a homogeneously broadened resonance as a function of τ_L / τ_C for several laser pulse intensities. For each curve, the laser intensity remains constant while the collision rate is varied. The pulse length is constant at $\tau_L = 100\,\text{ps}$.

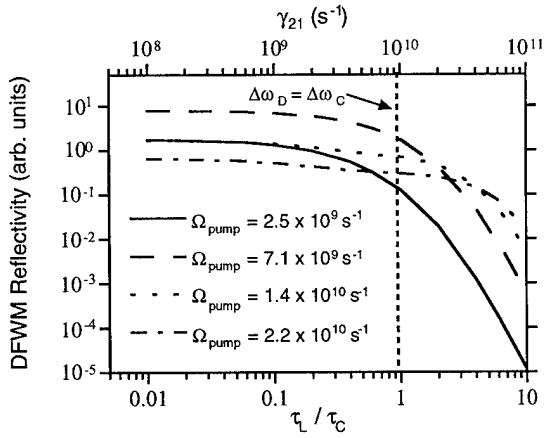

Fig. 3. DFWM reflectivity for a resonance with a Doppler width $\Delta\omega_D = 0.1\,\text{cm}^{-1}$ as a function of τ_L / τ_C for several laser pulse intensities. The laser intensities have been set equal to the same values used for Fig. 2, and the DFWM reflectivity axes for Figs. 2 and 3 can be directly compared.

5. Summary

We have investigated the use of short-pulse lasers ($\tau_L < \tau_C$) for quantitative DFWM spectroscopy in gas-phase media. For resonances that are both collision- and Doppler-broadened, a regime is reached for $\tau_L << \tau_C$ where the signal is independent of collision rate. For a purely collision-broadened resonance, this behavior is not observed: the signal strength always depends on τ_C because the polarization established by the laser pulses continues to radiate until it is destroyed by collisions. For a Doppler-broadened resonance, however, the dipoles in different velocity groups oscillate at different frequencies. Thus the macroscopic polarization decays quickly, with a time constant very similar to the laser pulse width. From the theoretical analysis presented in this paper, it is apparent that picosecond lasers could potentially provide a means for overcoming the complex collision-rate dependence of DFWM. However, to quantitatively measure number densities, one needs to account for variations in the Doppler width.

This work was supported by the United States Department of Energy, Office of Basic Energy Sciences, Division of Chemical Sciences, under Grant No. DE-FG02-94ER14469. TAR gratefully acknowledges the support of graduate fellowships from Du Pont and Exxon.

6. References

1. R. L. Farrow and D. J. Rakestraw, Science **257**, 1894-1900 (1992).
2. K. Kohse-Höinghaus, Prog. Energy Combust. Sci. **20**, 203-279 (1994).
3. R. L. Vander Wal, R. L. Farrow, and D. J. Rakestraw, *Twenty-Fourth Symposium (International) on Combustion*, (The Combustion Institute, Pittsburgh, Pennsylvania, 1993), pp. 1653-1659.
4. P. M. Danehy, E. J. Friedman-Hill, R. P. Lucht, and R. L. Farrow, Appl. Phys. B, **57**, 243-248 (1993).
5. R. P. Lucht, R. L. Farrow, and D. J. Rakestraw, J. Opt. Soc. Am. B **10**, 1508-1520 (1993).
6. Picosecond DFWM in an atmospheric flame was first demonstrated by M. A. Linne and G. J. Fiechtner, Opt. Lett. **19**, 667-669 (1994).
7. D. J. Rakestraw, L. R. Thorne, and T. Dreier, *Twenty-Third Symposium (International) on Combustion*, (The Combustion Institute, Pittsburgh, Pennsylvania, 1990), pp. 1901-1907.
8. R. W. Boyd, *Nonlinear Optics* (Academic, Boston, Mass., 1992) p. 191.
9. T. A. Reichardt and R. P. Lucht, "Effect of Doppler broadening on quantitative concentration measurements using degenerate four-wave mixing spectroscopy," J. Opt. Soc. Am. B, submitted for publication.

QUANTITATIVE DETECTION OF CH RADICALS BY LASER-INDUCED FLUORESCENCE IN ARCJETS AND FLAMES

Jorge Luque, Wolfgang Juchmann, Jay B. Jeffries and David R. Crosley
SRI International, Molecular Physics Lab, 333 Ravenswood Ave, California 94025

Flames and chemical vapour deposition (CVD) processes are examples of systems where the chemistry involved is very complex, and the outcome of final products is often strongly dependent on intermediate species present in very low concentrations. Optical methods are ideal for detection of these short-lived transient molecules, and laser-induced fluorescence offers the advantage of simultaneous measurements of concentrations and temperatures[1].

The CH radical appears in reactive systems with hydrocarbon reactants. Its role is now well established in flames, where it is a key intermediate in the formation of NO at temperatures below 1800 K by the so-called prompt NO mechanism[2]. A necessary step is the breakage of the strong N-N bond , which occurs through reaction of CH radicals: $CH + N_2 \rightarrow HCN + N$. The N atoms that are produced react inmediately with the air O_2 to form NO. In these conditions, the concentration of NO is directly related to the CH concentration. The situation is different in the deposition of diamond by CVD from CH_4/H_2 mixtures. The gas phase kinetics of the arcjet are dominated by a large atomic hydrogen mole fraction initially produced by dissociation of the molecular hydrogen in the arc. Succesive hydrogen abstractions from added methane by the atomic hydrogen produces CH, which reacts quickly with hydrogen and hydrogen atoms, although it is not well understood how the CH concentration is related to the quality of the deposited diamond.

Computer models are an important tool to describe flames and CVD processes[3,4], and the predictions can solve problems without performing experiments, but kinetics models require experimental data as input (mainly temperature profiles), and the output must be tested to ensure the reliability of the model. Concentrations are the most important quantity to be compared against model predictions. The CH radical is very reactive, and its steady state concentrations are very low, around parts per million. Low concentrations are a challenge for accurate measurements, and the reason why there are very few absolute data of this radical in either combustion[5] or CVD[6] systems. In this work we use linear LIF to measure CH concentrations and we show that errors less than 35% are attainable.

The flame experiments in this work have been carried out in a propane/air flame at a constant pressure of 40 Torr on a 6 cm diameter porous plug burner in a low pressure chamber. The dc-arcjet reactor is operated with a mixture of hydrogen and argon at a pressure of 25 Torr; methane is added at the exit of the diverging nozzle. The distance between the nozzle and the cooled substrate where the diamond grows is 42 mm. Both experimental setups are designed to gain easy optical access. The laser pulse from a dye laser is constrained to a waist of 1 mm or less at the window entrance. The burner and the arcjet nozzle and substrate assembly can be translated to acquire LIF spatial profiles. The signal is detected at a right angle to the laser beam, and is either integrated with a boxcar or digitized when temporally resolved data are needed.

LIF is a sensitive and selective technique. Linear unsaturated LIF avoids problems related to saturation, in particular the definition of the probed volume, but in exchange requires the knowledge of collisional quenching. Also the signal/noise ratio is lower than in saturated LIF. The relationship between the detected signal S_F and the molecular concentration N is given by:

$$S_F = N \cdot f_B \cdot B \cdot E_L \cdot \Gamma \cdot \frac{\tau_{eff}}{\tau_o} \cdot \frac{\Omega}{4\pi} \cdot \xi \cdot \eta \cdot l$$

This equation is valid so long as the laser intensity is low and the feedback by amplified spontaneous emission is neglegible, and the flourescence signal is fully integrated in time. Note that the signal is not dependent on the laser temporal length or laser beam cross-section. In the expression f_B is the Boltzmann factor, B is the absorption coefficient for the rotational transition excited, E_L is the laser energy, Γ is the lineshape overlap integral, the ratio τ_{eff}/τ_0 is the fluorescence quantum yield with τ_{eff} as the effective lifetime including collisional quenching and τ_o is the radiative lifetime. Ω is the solid angle, ε is the transmission efficiency of the optics, η is the photoelectric efficiency of the photomultiplier, and l is the effective optical path length.

There are three different electronic transitions of the radical CH in the UV-visible region, the A-X (430 nm) and B-X (390 nm) are well known. Recently, we have measured experimental vibrational transition probabilities for these band systems[7]. These data together with calculated wavefunctions, Honl-London factors and experimental radiative lifetimes furnish very accurate absorption and emission coefficients for the transitions picked out in the absolute measurements.

The Boltzmann factor is calculated from the temperature measured through LIF excitation scans. We have made comparisons using in CH A-X (0,0) Q branch, CH B-X(0,0) R branch and OH A-X (0,0) R branch in the propane flame. The corresponding temperatures are 1600 ± 60 K, 1570 ± 50, and 1620 ± 60 K, at the same point in the flame. This excellent agreement is possible only with the newly calculated absorption coefficients. In the arcjet we use two-line LIF excitation scans in the R branch to determine a temperature of 2000 ± 150 K at the half-distance between the nozzle and the substrate, which compares well with multiline LIF temperature determination with seeded NO[8].

Fluorescence quantum yields are obtained from temporally resolved measurements. We find different effective lifetimes in the flame and in the arcjet. For example, CH B v'=0 has a lifetime of 54 ± 3 ns in a flame and 36 ± 4 ns in the arcjet. This behavior is a consequence of different pressure, temperature and chemical composition of these systems.

The lineshape function Γ is a normalized convolution of the laser lineshape with the CH absorption lineshape. The laser lineshape was measured to 0.22 cm^{-1} with the use of an etalon, the absorption profile is dominated by the Doppler effect at this low pressures and high temperatures. This term is often overlooked, but we find a correction of 30% due to this factor.

The remaining terms are related to the collection of the signal. There are not easy to measure directly and it is more convinient to calibrate them with another optical technique. Raman and Rayleigh scattering are well suited for this task. During the calibration we keep the same laser, geometry and detection system employed for the LIF signals. The calibration signal for either Raman or Rayleigh signal is[1]:

$$S_R = N \cdot \frac{1}{hcv} \cdot \left(\frac{\partial \sigma}{\partial \Omega}\right) \cdot \Omega \cdot \varepsilon \cdot \eta \cdot l$$

N is the number density of the gas, v is the frequency of the scattered photon and $(d\sigma/d\Omega)$ is the averaged cross section. From the plot of scattering signal versus the product of laser energy and pressure (we use N_2 for Rayleigh and H_2 for Raman measurements) we determine the experimental factor $\Omega\varepsilon\eta l$, since the other quantities are known.

The following table is a summary of the LIF absolute concentration measurements, in ppm, of CH radical in a 40 Torr propane/air flame, stoichiometry 1.15, using the different electronic transitions and calibration methods. The measurements were performed at the peak of the CH distribution.

Calibration Method	Electronic Transition A-X	B-X	
Rayleigh	5.3± 2.1	4.8 ± 2.0	5.1 ± 1.6
Raman	6.5 ± 3.2	6.7 ± 3.2	6.6 ± 2.3
	5.9 ± 2.2	5.7 ± 1.9	5.8 ± 1.5

Four independent values are available: two different electronic bands with two separate calibrations for each. A comparison between calibration methods shows a difference of 30% in the final concentrations, with an average of 5.1 ± 1.6 ppm for the Rayleigh method and 6.6 ± 2.4 ppm for Raman. This shows that, despite the systematic discrepancy, both values agree to within the error bars. More remarkable is the agreement between the B-X and A-X systems in each case, within 10%, which is notably less than the estimated error. The error propagates easily in this kind of measurements that requires independent knowledge of many quantities, we present a table with all the error sources and their estimated contribution to the total error:

Factor in the concentration	Relative error
Rayleigh calibration	10-15%
Raman calibration	20-25%
Overlap integral/Laser bandwidth	5%
Boltzmann factor (temperature)	2%
Absorption or emission coefficient	3-5%
LIF signal	< 10%
Effective lifetime	5%

The CH LIF concentration profile in figure 1 has been normalized with the absolute value obtained at the peak of the concentration in the flame. A chemical kinetic model has been developed based on the GRI mechanism, the comparison reveals that the model is able to reproduce the position and width of the CH distribution , but overpredicts in 20-30% the amount of CH in the flame. The concentration profile is radically different in the arcjet in figure 2, and it is uniform between the nozzle and the substrate. However, the number density are in the same order of magnitude in these very different chemical enviroments. Both absolute concentration profiles are good examples of the possibilities of quantitative LIF.

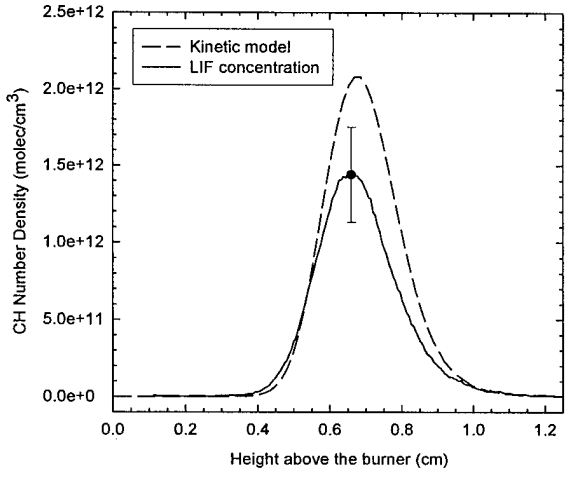

Figure 1 . LIF CH number densitiy measured in a 40 Torr propane/air flame compared to a kinetic model applied to the same flame.

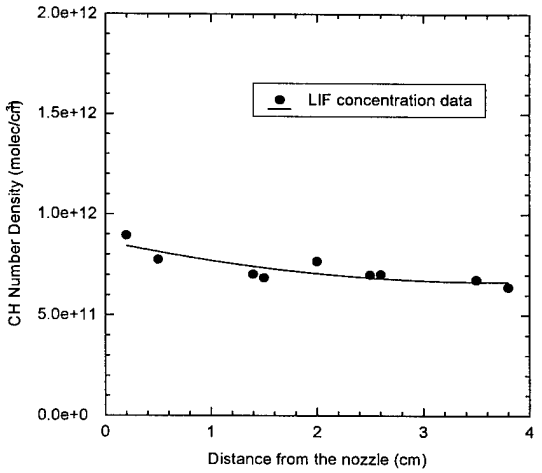

Figure 2. LIF CH number density profile in dc-arcjet $H_2/Ar/CH_4$ at 25 Torr.

This work was supported by the basic research group of the Gas Research Institute, the Air Force Office of Scientific Research, and the Office of Naval Research.

REFERENCES:

1. A.C. Eckbert. *Laser Diagnostics for Combustion Temperature and Species,* vol 7 of Energy and Engineering Science Series. Abacus Press, Tunbridge Wells, Kent, (1988).
2. J.A. Miller and C.T. Bowman, Prog. Energy Combust. Sci. **15**, 287 (1989).
3. D. E. Heard, J. B. Jeffries, G.P. Smith, and D.R. Crosley, Comb. and flame, **88**, 137 (1992).
4. M. E. Coltrim, D.S. Dandy, J. Appl. Phys., **74**, 5803 (1993).
5. K. Kohse-Hoinghaus, R. Heidenreich and TH. Just, Twentieth International Symposium on Combustion, The Combustion Instute, 1177 (1984).
6. W. Jacob, M. Engelhard, W. Moller and A. Koch, Appl. Phys. Letts, **64**, 971 (1994)
7. J. Luque and D.R. Crolsey, J. Chem. Phys, accepted.
8. E. A. Brinkman and J. B. Jeffries, AIAA, 95-19555, 95-1955, 26th Plasmadynamics and Lasers Conference, San Diego (1995).

A new approach to laser-induced fluorescence detection of nitric oxide in high pressure flames

Christof Schulz, Volker Sick*

Physikalisch-Chemisches Institut

Universität Heidelberg

Im Neuenheimer Feld 253

69120 Heidelberg

Germany

Phone: +49 6221 56 2503, Fax: +49 6221 56 2503, e-mail: sick@sun0.urz.uni-heidelberg.de

Johannes Heinze, Winfried Stricker

DLR, Institut für Physikalische Chemie der Verbrennung

Pfaffenwaldring 38-40

70546 Stuttgart

Germany

Phone: +49 6221 6862 381, Fax: +49 62216862 578, email: Johannes.Heinze@dlr.de

Laser induced fluorescence of nitric oxide is commonly used for detection of this major pollutant in combustion processes. Mostly, excitation within the A-X (0,0) band is used next to excitation of the D-X (0,1) band. However, for real engine applications strong absorption of the laser beam prevents the application of these schemes. Exciting in the A-X(0,2) band circumvents these problems and allows the sensitive two-dimensional detection of nitric oxide in engines fueled with iso-octane or Diesel fuel.

Understanding the spectroscopy of the (0,2) band is important for a quantitative analysis of the fluorescence signals. We therefore measured excitation/emission spectra in lean laminar, premixed methane/air flames (ϕ=0.9) at pressures between 1 and 40 bar.

Since the transition starts from a higher vibrational level, the ground state population is small even at combustion temperatures and fluorescence signals will be weak despite the large B coefficients for the (0,2) band. An amplified dye laser system at 248 nm or a tunable KrF excimer laser can be used to excite the NO (0,2) band [1]. These laser systems are capable to deliver pulse energies in excess of 100 mJ. Planar imaging experiments are thus possible using this transition.

The broadband absorption caused by many intermediates, especially under high pressure combustion conditions, is much reduced at 248 nm. Additionally the high nitric oxide concentrations, as observed in engines can lead to significant absorption of the laser beam at 226 nm as well. The small Boltzmann fraction for v"=2 results in very small absorption cross sections and thus neglectible absorption.

For the temperature range where nitric oxide is formed in flames, mainly at temperatures higher than 1700 K, the change of the Boltzmann fraction is aceceptably small to be neglected for semi-quantitative nitric oxide concentration measurements.

The optimal detection range for the fluorescence was chosen at shorter wavelengths relative to the excitation wavelength. This avoids problems with interference due to Raman signals which become an increasing problem with increasing pressure. The interference due to oxygen fluorescence compared to detection strategies involving excitation of the (0,0) band is currently under investigation but first results indicate a somewhat lower interference. Figure 1 shows an emission spectrum recorded in a laminar, premixed methane/air flame at 40 bar, ϕ = 0.9. The KrF excimer laser was tuned to the O-branch of the NO A-X (0,2) band. While the Raman Stokes lines are a significant portion of the emissions at longer wavelengths, their influence on the anti-Stokes side is much smaller.

Figure 2 presents the change of the excitation spectrum as a function of pressure. Shown are measured spectra in comparison to calculations. Whereas at 1 bar many lines are rotationally resolved, the lines blend at higher pressure, resulting in a continuum absorption at pressures of 40 bar.

The influence of fluorescence quenching can be taken into account, since there is a variety of data available for the v'=0 state, which show that for combustion conditions, the total quenching rates are more or less constant for many engine conditions [2].

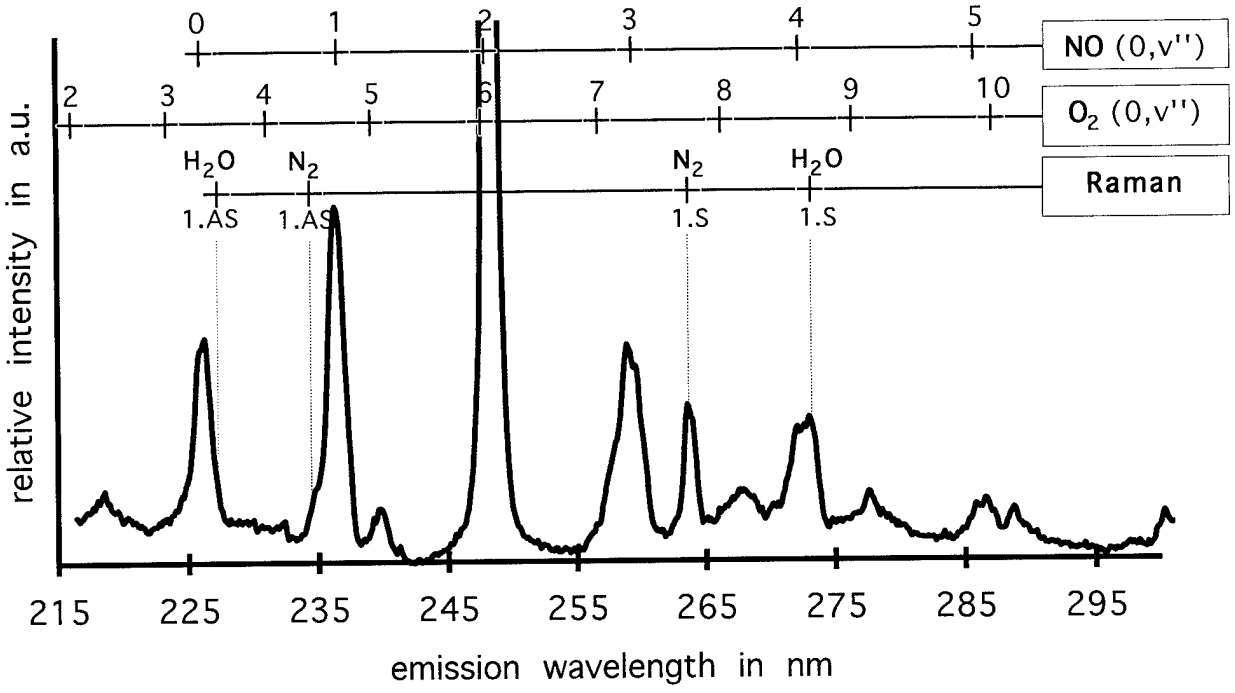

Figure 1: Emission spectrum measured in a lean 40 bar methane/air flame (doped with 370 ppm NO) after exciting at 247.95 nm

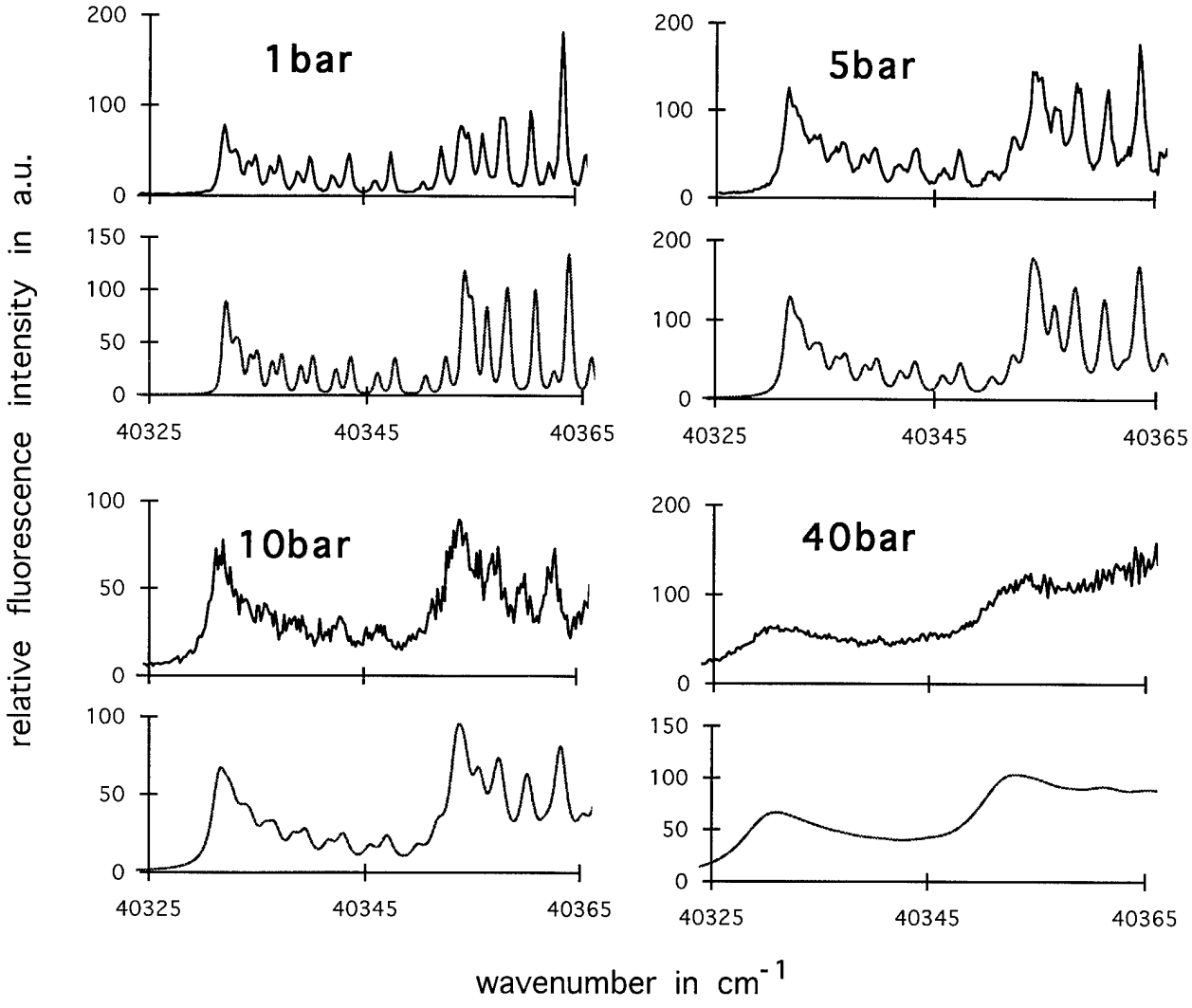

Figure 2: Measured and calculated NO A-X (0,2) spectra for various pressures

With the approach as presented here, the LIF detection scheme with excitation at 248 nm can be used to measure NO concentration distributions even at higher pressures, e. g. engine conditions.

REFERENCES

[1] C. Schulz, B. Yip, V. Sick, J. Wolfrum, 'A Laser-Induced Fluorescence Scheme for measuring Nitric Oxide in Engines' Chem. Phys. Letters 242, 259-264 (1995)

[2] A. Bräumer, V. Sick, J. Wolfrum, V. Drewes, R. R. Maly, M. Zahn, 'Quantitative two-dimensional measurements of Nitric Oxide and Temperature Distributions in a Transparent SI Engine', SAE Paper No. 952462 Toronto (1995) and references 14-16 therein.

IN-FLIGHT LASER INDUCED FLUORESCENCE FROM MICROGRAVITY DROPLET COMBUSTION

Michael Winter
United Technologies Research Center
411 Silver Lane, MS/90
East Hartford, Connecticut 06108
phone: 203-727-7805
fax: 203-727-7911

Introduction

Most propulsion and energy utilization devices rely on the spraying of liquid-phase propellants, in the form of fuel or oxidizer, into an energy conversion chamber. The behavior of individual droplets in a spray combustor is a critical part of the combustion process. Basic understanding is best advanced by well-controlled experiments and simplified calculations. A great deal of attention has been paid to studying the combustion of individual droplets,[1,2] which is the simplest example of non-premixed combustion. These single-droplet flames provide an idealized geometry for investigating the interaction of the physical and chemical processes involved. A significant means of simplifying droplet combustion is to approach the phenomena in a microgravity environment.

Optical diagnostics offer several advantages over physical probes because they permit nonintrusive multi-point measurements. Nonintrusive measurements are of particular importance for droplet combustion and transport in microgravity environments, where physical contact would introduce an unacceptable level of perturbations. The resolution available with these diagnostics can also isolate transport to length scales much smaller than the droplet diameter. These diagnostics, however, can be particularly difficult to implement in a microgravity environment.

Approach

A better understanding of the combustion process can be achieved by identification of the position of the flame front for detailing quasi-steady combustion behavior. This can be accomplished using Planar Laser-Induced Fluorescence (PLIF) of OH[3] or another flame front marker which is typically performed by tuning a laser to the molecular absorption and recording the emitted radiation with a two-dimensional detector. Laser sources and detection systems capable of operating under the power and shock environments typical of parabolic flight conditions for microgravity are now available.

Experimental Methods and Design

UTRC has designed and built an apparatus for performing measurements aboard the NASA Learjet, DC-9 and KC-135 aircraft facilities. A new Nd:YAG laser and frequency doubled dye laser or nitrogen pumped dye laser are currently part of the system for OH or sodium PLIF respectively. The system remains operational and flight ready; low gravity testing has been performed.

Package

An overview photograph of the apparatus is shown in Fig 1. The system as seen contains a nitrogen pump laser, tunable dye laser, two camera systems-one intensified, two time code generators, two VCRs, a Macintosh IIci computer with image digitization hardware and experiment control software, timing electronics, and power distribution. The package also contains a windowed combustion vessel capable of a wide range of pressures.

Controls

Droplet combustion occurs within the combustion vessel that houses the remote control systems on an internal multi-level platform consisting of triangular sections and threaded rod. In the center resides a fiber droplet holder surrounded by the droplet deployment and ignition hardware. The multi-level platform is complete with servo-actuators capable of deployment of a droplet onto a fiber, removing

the deployment needle, introducing and energizing the igniter, igniting the droplet, and retracting the ignitor, all through remote operation via the control system joysticks and switches on the control box. A second multi-level combustion platform is available that includes a levitator. A CCD video camera is used to monitor the procedure, and the images are displayed on a 2 in. LCD monitor attached to the control box. A second 2 in. LCD monitor is attached to the control box to display the images from the intensified CCD camera recording the PLIF data. The controls box joysticks and actuators are modified radio controlled airplane equipment. The control system box can be seen in the top of Fig. 1.

Laser/Camera

Advanced laser diagnostics involving imaging of fluorescence fields, typically rely on high-power lasers, and sophisticated and extremely sensitive camera systems. The apparatus uses a pulsed nitrogen laser that produces 0.3 mJ at 337 nm in a 3 ns pulse. A Nd:YAG pumped dye laser system that provides 2 mj at 283 nm will also be discussed.

Two camera systems are currently housed in the flight apparatus. One is an intensified, cooled CCD capable of external triggering. A second CCD camera is used for observing droplet loading and ignition, and recording the flame luminosity during a burn. Both cameras are provided with microscope optics to resolve both the droplet and surrounding flow field. The images from both cameras are passed through synchronized time code generators which superimpose a time code signal on each one. This allows later comparison between the luminosity and the PLIF signals on a frame by frame basis. The time coded images are then recorded on 8 mm videocassettes for later analysis. The PLIF signals are also recorded through a frame grabber resident in the Macintosh IIci included in the flight rig.

Results and Discussions

PLIF from burning droplets under microgravity conditions was extremely successful. The nitrogen-pumped dye laser was formed into a sheet <250 μm wide and directed across the top of the droplet. The dye laser was tuned to 589 nm to pump sodium as described above. The laser-induced fluorescence was recorded in two-dimensions. Figure 2 shows a comparison of the laser-induced fluorescence image along with the luminosity image from the exact same instant in time. The luminosity image displays the full spherical envelope flame around the droplet while the PLIF image only provides flame position information over the droplet. The PLIF image, however, only corresponds to a 3 ns instant in time corresponding to the laser pulse duration while the luminosity image is temporally integrated over the video frame time.

Successful radical chemiluminescence, PLIF and visible flame luminosity images were obtained. Initial analysis indicates that the broadband visible flame luminosity and radical chemiluminescence agree well in mapping the flame front position. The resulting data were processed to provide information on droplet regression rate and flame diameter as a function of time. These data are shown in Fig. 3 where the results are shown in terms of flame stand off ratio as a function of time for luminosity, radical emission at 308 nm, and sodium PLIF. Similar behavior is seen for each. However, the luminosity consistently over-predicts the flame diameter relative to the radical emissions and PLIF data. The flame position as determined from the PLIF is consistent with the radical emissions. Future efforts will be directed at recording PLIF from OH radicals directly.

Conclusions

An instrument has been designed, built, and tested for performing laser diagnostic measurements of droplet combustion in low gravity flight aircraft. The results show successful application of PLIF relative to luminosity and radical emission near 308 nm.

Acknowledgement

I would like to thank Jason S. Wegge for his expert technical assistance. His contributions to the design and assembly of the experimental apparatus were extremely valuable. I would also like to thank Dr. Alan Eckbreth, Dr. Howard Ross, Professor Fred Dryer and Professor Forman Williams for their encouragement and useful discussions. We appreciate the efforts and assistance of Dr. Randy Vander Wal and the staff at the NASA LeRC Flight Research Laboratory.

References

1. Law, C. K., *Recent Advances in Droplet Vaporization and Combustion*, Prog. Energy Combust. Sci. 8, 171-201 (1982).
2. Sanders, B. R. and Bergen, N. E., *Workshop on Mass, Momentum, and Energy Exchange in Combusting Sprays: Droplet Studies*, Report SAND89-8442, Sandia National Laboratories, Livermore, CA (28-29 March 1988).
3. Hanson, R. K.; 1986: Twenty-First Symposium (International) on Combustion, p. 1677.

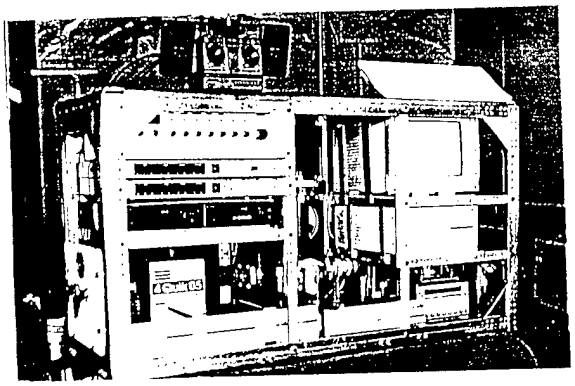

Figure 1. Photograph of the UTRC/NASA laser diagnostics for microgravity droplet combustion apparatus.

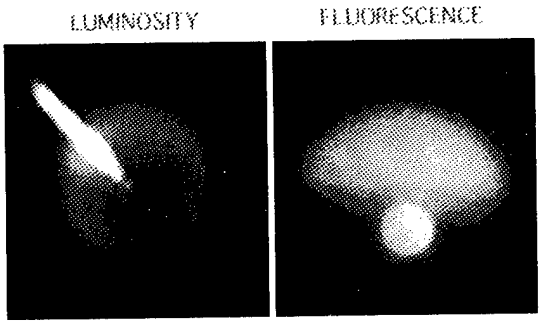

Figure 2. Comparison of PLIF of sodium and flame luminosity.

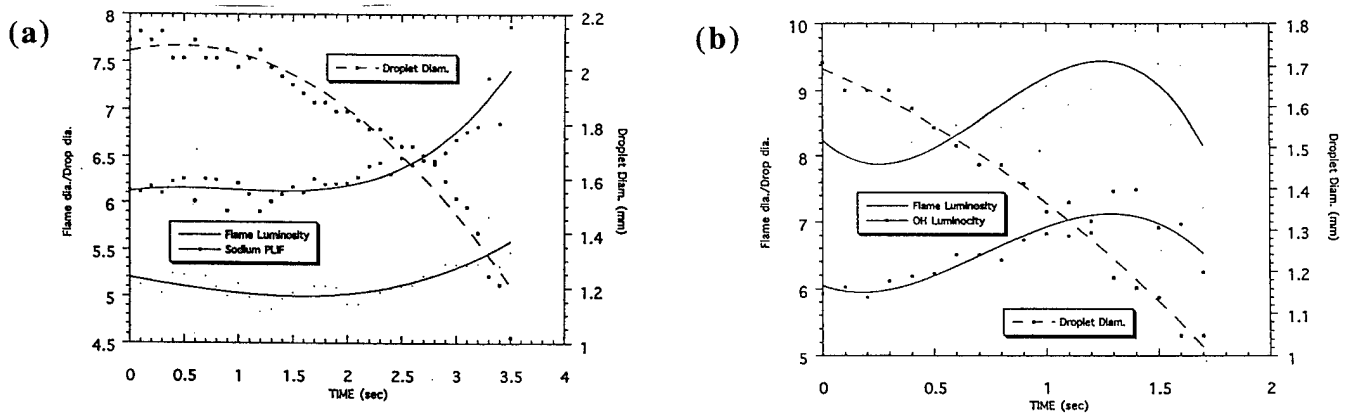

Figure 3. Results are shown for flame standoff and droplet diameter as a function of time for (a) luminosity and sodium PLIF and (b) luminosity and radical emission at 308 nm.

OH, NO, and Soot Measurement in Diesel Spray Flames Using Laser Induced Fluorescence and Laser Induced Incandescence

Hiroshi NAKAGAWA , Hiroyuki ENDO,
MITSUBISHI HEAVY INDUSTRIES, LTD., Nagasaki R & D Center, Internal Combustion Engine & Hydraulic Equipment Lab., 5-717-1, Fukahori-Machi Nagasaki 851-03, Japan, tel: 0598-34-2430, fax: 0958-34-2435

Yoshihiro DEGUCHI ,
MITSUBISHI HEAVY INDUSTRIES, LTD., Nagasaki R & D Center, Applied Physics Lab., 5-717-1, Fukahori-Machi Nagasaki 851-03, Japan, tel: 0598-34-2321, fax: 0958-34-2345

Matsuhei NODA ,
MITSUBISHI HEAVY INDUSTRIES, LTD., Advanced Technology Research Center, Base Technology Research Lab., 8-1, Sachiura, 1-chome, Kanazawa-ku, Yokohma, 236, Japan, tel: 045-771-1282, fax: 045-771-3879

Hiroshi OIKAWA , and Taizo SHIMADA
MITSUBISHI MOTORS CORPORATION., Advanced Engine R & D Group, Engine Research Dept. Office of Truck & Bus 21-1, Shimomaruko, 4-Chome, Ohta-Ku, Tokyo 146, Japan , tel: 03-3757-735, fax: 03-37574-7368

1. Introduction

Although the time-space mechanism of NOx formation in diesel injection combustion in high temperature and pressure has conventionally been pursued by the sampling method and so forth[1], the cause-effect relationship on its formation factors still remains to be more accurately clarified. In our present research, NO, OH and soot in diesel fuel flames from a single injection in high temperature and pressure were measured using a motoring compressed injection test system by applying laser induced fluorescence (LIF) [2][3][4][5][6] and laser induced incandescence (LII) [6][7], both of which can provide unperturbed measurements necessary for clarifying formation characteristics of harmful exhaust substances from diesel fuel flames in high pressure.

2. Measurement

2.1 LIF In LIF measurement, excited molecules are transferred to other energy states through processes of emission, collision, predissociation and so on, after absorption of incident light. Problems in LIF measurement in high temperature and pressure are associated with the background fluorescence from molecules like aromatic hydrocarbons, absorption of laser rays by soot, liquid fuels, and so on, besides the change of the quenching rate and temperature dependence of the excited energy level. In the present study the background fluorescence interference could be monitored by measuring two wavelength regions ("wavelength region in which fluorescence from the measured molecule emerges" and "wavelength region in which the background fluorescence only emerges"), and using off-resonance laser beam of the measured molecule.

For the OH measurement, excitation line was selected among (1,0) band in $A^2\Sigma^+ - X^2\Pi$ transition and (1,1) and (0,0) fluorescence signals were detected. For the NO measurement, (0 ,0) band in $A^2\Sigma^+ - X^2\Pi$ transition was used. As numerous absorption lines of O2 exist near NO (0 ,0) band (226nm), the absorption line was selected based on the excitation spectrum simulation of NO and O2 in high pressure. Only the (0,2) band NO fluorescence appearing at 248nm was measured to minimize the effects of fluorescence from other molecules and flame luminescence.

2 .2 LII In LII, the high-energy laser beam is irradiated at solids like soot to raise the solid temperature to 4,000K - 5,000K. Because the luminescence intensity of the uv wavelength jumps with increasing temperature, the laser excited soot can be observed. The second harmonic (532nm) of YAG laser was used as the incident beam and luminescence intensity at 300nm - 350nm was measured as a LII signal.

3. Test Apparatus

3.1 Combustion test system Configuration of the test system is outlined in Fig. 1. The Combustion test system was provided with windows for the laser sheet incidence at the side of the combustion chamber and with an observation window at the top of the piston to measure signal light in a single cylinder motoring engine. The fuel used was a mixed fuel (50:50 in volume ratio) of n-tetradecane and i-octane to minimize production of exhaust particles[7] . Injection of the fuels into the combustion chamber was made by an in-line fuel pump for diesel engines. The suction air was made oxygen-rich in order to minimize formation of particles obstructive to the laser

measurement and to maximize formation of NO, and pressurization by a blower and heating by a heater were used to raise temperature and pressure during compression. The geometrical relationship between the flame and the laser sheet was set as shown in Fig. 2.

3.2 Optical system The optical system used in this study is shown in Fig.1. The prototype of the combustion and plasma analysis system made by Mitsubishi Heavy Industries, Ltd. was used for the LIF measurement. YAG laser was used as the light source to excite the dye laser. The dye laser is converted to the uv region through the wavelength converter, which was irradiated to the engine as a laser sheet through cylindrical lenses. After removing visible light by specially coated uv mirrors and filters, the fluorescence signal was collected through a uv lens and detected through two ICCD cameras.

Synchronization of the system was based on the motoring rotation and measurement at any crank angle was available by sending a signal in an adequately time delay relative to the motoring rotation to the laser and the ICCD cameras.

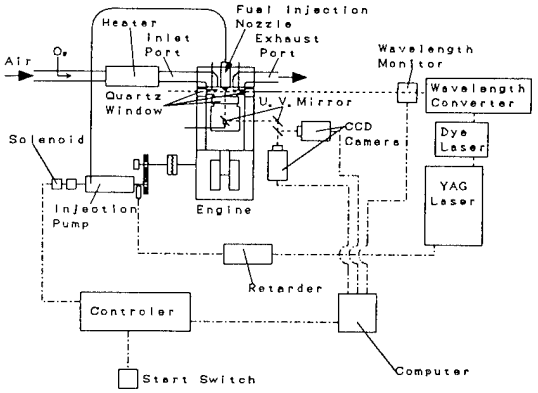

Fig.1 Configuration of Test Section

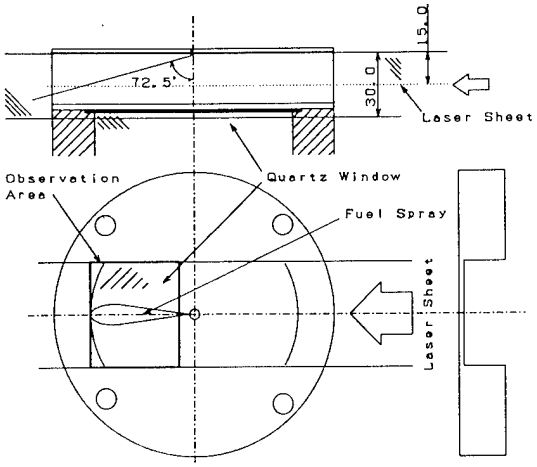

Fig.2 Arrangement of Laser Sheet and Flame in Combustion Camber

4. Results

Test condition is listed in Table 1. Pressure change in the combustion vessel and the heat release rate calculated on this pressure change are shown in Fig. 3, and measured results of OH, NO and soot in Fig.4. These results were corrected by the laser intensity at the measurement region. From the upper block, Fig.4 shows, respectively, the direct flame images taken by a high-speed camera, flame luminescent intensity detected through the ICCD camera, laser-induced OH fluorescence intensity, laser-induced NO fluorescence intensity and laser-induced soot luminescence intensity. Here, Signals were integrated by five cycles of the combustion process.

Table 1 Test Conditions

Compression Ratio	8.157
Fuel Injection Nozzle	ϕ 0.30×1×145°
Engine Speed	1200min^{-1}
Fuel Quantity	60mm^3/st
Fuel Injection Timing	5BTDC
Swirl Ratio	0.0
Fuel	i-Octane(50%)+n-Tetradecane(50%)
Inlet Air Temperature	393±5K
Inlet Air Pressure	2.97±5×10^{5}Pa
Inlet O_2 Concentration	34±2%

The observed results show that combustion is initiated nearly at the timing of the top dead center and luminous flame is no longer observed at 30 degrees after the top dead center. The observed results show that OH is present outside the region where the flame luminescence is observed and it is recognized that reaction process is still taking place at timing of 40 degrees after the top dead center where the flame luminescence is no longer observed. The NO distribution is located slightly outside the flame luminescence, as almost the same region as that of OH, and its presence region tends to increase in the latter period of combustion process as compared with the heat release pattern of Fig.3. This factcorresponds to the formation process of NO estimated from an extended Zeldovich mechanism that formation of NO can slightly delay relative to the heat release. The soot formation occurs in the fuel-rich region in the flame center and shows a trend nearly similar to the flame luminescence.

For forthure research, problems as shown below remain.

(1) Quantitatively of the measured results・・・Quantitativeness of measurements must be improved by correcting fluorescence intensities by the factors like temperature, pressure and co-existing chemical species.

(2) Conditions of the combustion · · · Because flames measured were different from the actual injection flames in diesel engines in terms of the oxygen concentration, the fuel properties and so on, measurement in closer conditions of the practical diesel engine is necessary.

5. Conclusions

Combustion products, such as NO, OH and soot, in combustion of diesel spray flame using a single injection in high temperature and pressure were measured based on LIF and LII and the following conclusions were drawn.

(1) OH is present in a band-like zone outside the region where the flame luminescence is observed and present after the completion of flame luminescence.

(2) NO is present slightly outside the flame luminescence zone and its region is almost the same as that of OH and tends to increase in the latter period of the combustion process.

(3) Formation of soot takes place in the center zone of the flame and shows an approximate agreement to the flame luminescence zone.

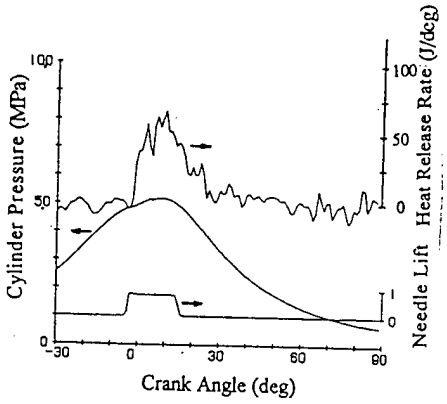

Fig.3 Pressure Change and Heat Release Rate in Combustion Process

References

(1) Y.Aoyagi, T.Kamimoto, Y.Matsui, and S.Matsuoka, SAE Paper 800254, (1980)
(2) M.Noda and Y.Deguchi, M.H.I. Technical Review, Vol.30, NO.3, p.196, (1993)
(3) Y.Deguchi, M.Murata, M.Noda, M.Sota, and M.Inada, M.H.I. Technical Review, Vol.32, NO.3, p.137, (1995)
(4) Y.Deguchi, et.al., Proceedings of 1995 Yokohama Gas Turbine Congress, II-321, 1995.
(5) P.,Andresen, et.al., Applied Optics, Vol.29 No.16, p.2392, 1990.
(6) B.Alatas, J.A.Pinson, T.A.Litzinger, and D.A.Santavicca, SAE Paper 930973, (1993)
(7) C.Espey and J.E.Dec, SAE Paper 930971, (1993)

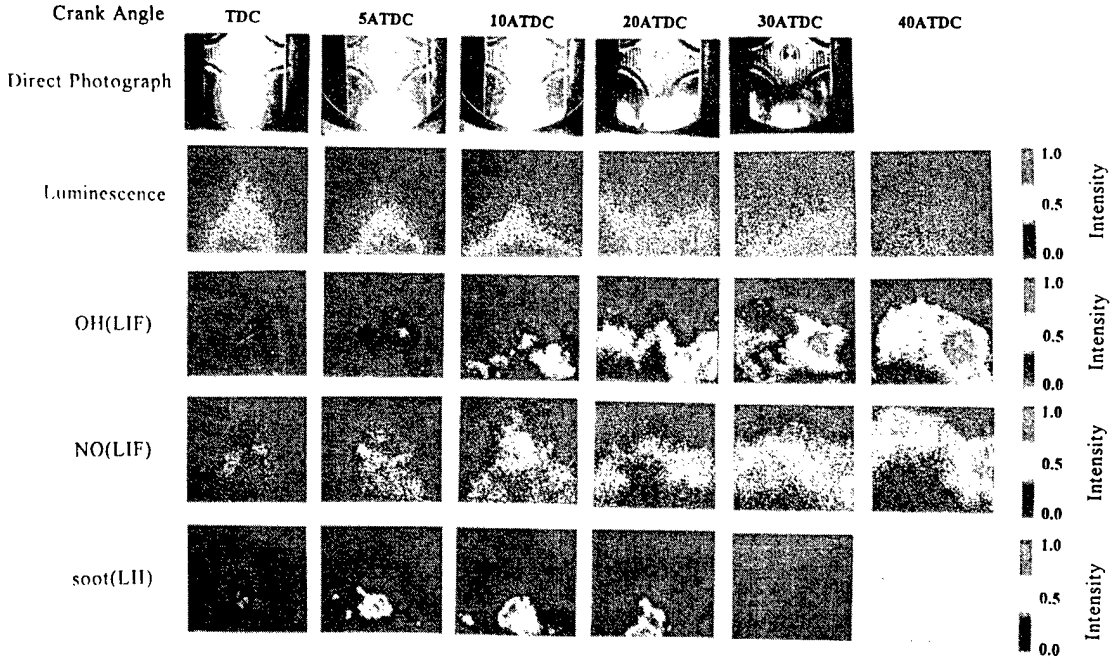

Fig.4 LIF and LII Results

Application of Laser Induced Fluorescence and Spontaneous Raman Scattering to Technically Applied Combustion Systems: Four Cylinder Spark Ignition Engine and Oil Burning Furnace

V. Beushausen[1], M. Knapp[1], A. Luczak, S. Eisenberg[1]
and Peter Andresen[2]

[1]Laser Laboratorium Göttingen e.V., Hans-Adolf-Krebs-Weg 1, 37077 Göttingen, Germany
[2]University of Bielefeld, Universitätsstrasse 25, D-33615 Bielefeld, Germany

In this paper the successful application of spontaneous vibrational Raman scattering (VRS) and laser induced (predissociative) fluorescence (LIPF) to technical applied combustion systems like a mass production internal combustion engine and a commercial oil burning furnace - both are modified for optical access - is described. It will be shown that these techniques can be used as a tool for design and optimization purposes as well as for fundamental research.

The VRS signal has the unique advantage of being species specific and linearly proportional to species number density (1). In this work we present one dimensional spatially resolved measurements of the air/fuel ratio and the residual gas content in single working cycles of a four cylinder internal combustion enginge (ICE). We also report first measurements of the temperature development during the compression stroke of the ICE via VRS and LIPF excited by 193 nm excimer laser light. In addition three dimensional spatially resolved distributions of fuel-, O_2- and H_2O-concentrations as well as temperature inside the turbulent spray flame of a 30KW oil burning furnace will be presented.

With LI(P)F it was possible to visualize 2-D and 3-D distributions of the combustion intermediate OH (2-7). and the pollutant NO directly inside the combustion of the enginge and the oil spray-flame burner. It turned out that the relative density of the OH-radical at a given time is a very good measure of the intensity of the combustion. In addition, the structure of the flame front and its propagation through the combustion chamber could be visualized by 2-D OH imaging.

A significant portion of air pollution that originates from ICEs and furnaces is caused by NO_x emissions. Directly emitted NO_x is a primary component for photochemical reactions producing secondary products like ozone and nitric acid (summer smog). In order to optimize combustion processes regarding to these emissions knowledge about the NO_x-formation process and the location of NO_x-formation areas inside the flame are very important. For the engine application this paper shows the first NO LIF images excited by a tunable KrF excimer laser at 248nm during combustion and exhaust stroke.

The application of the laser diagnostic techniques to the oil burning furnace revealed averaged, relative 3-D density distributions of NO (LIPF-measurements) and also 3-D-temperature distributions (SRS-measurements). In order to visualize the the flow pattern and the local turbulence level inside the flame NO was seeded to the combustion air and was subsequently detected inside the flame using LIPF. The seeding position inside the mixing head was strongly localized by use of a thin spatially fixed seeding tube (∅ 3mm). 3-D detection of the seeded NO inside the flame visualizes the flow and turbulence pattern of the reactive flow. Moving the NO-seeding position then offers the possibility to localize those

positions inside the mixing device from which the flow enters the hot NO-producing areas of the flame. The measurements showed that this knowledge can be used to cool the flame selectively just in the hot areas by recirculating inert exhaust gas at these positions inside the mixing head. It is shown that already 3 % well aimed exhaust gas recirculation at special positions inside the mixing device leads to 50% NO-reduction.

Figure Caption:

Fig.1: Section of the ICE cylinder. Optical access is achieved by windows in cylinder head and piston

Fig.2: Single shot raw image taken at crank angle 690° (just before ignition) with a spectrograph in front of the camera.

Fig.3: A series of single laser shot images of vibrationally excited NO taken in subsequent engine cycles. The numbers mark the crank angles of the images.

Fig.4: 3-D distributions of a) the relative density of the OH-radical, b) the concentration of unburned fuel, c) the temperature (measured by SRS), d) the relative concentration of NO in the flame of the oil burning furnace.

REFERENCES

(1) ECKBRETH, A.C. Laser diagnostics for combustion temperature and species, 1988 (Abacus Press, Cambridge, USA).

(2) GRÜNEFELD, G., KNAPP, M., BEUSHAUSEN, V., ANDRESEN, P., HENTSCHEL, W., MANZ, P., In-cylinder measurements and analysis on fundamental cold start and warm-up phenomena of SI engines, SAE paper, Fuels & Lubricants Oct. 1995, in press.

(3) GRÜNEFELD, G., BEUSHAUSEN, V., ANDRESEN, P., HENTSCHEL, W., A major origin of cyclic energy conversion variations in SI-engines: cycle-by-cycle variations of the equivalence ratio and residual gas of the initial charge, SAE paper No. 941880, 1994.

(4) ANDRESEN, P., MEIJER, G., SCHLÜTER, H., VOGES, H., KOCH, A., HENTSCHEL, W., OPPERMANN, W., ROTHE, E., Fluorescence imaging inside an internal combustion engine using tunable excimer lasers, Appl. Opt. 29, pp. 2392-2404, 1990.

(5) SERPENGÜZEL, A., HAHN R.T., ACKER W.P., Single pulse planar laser induced fluorescence imaging of hydroxyl radicals in a spark ignition engine, SAE paper No. 932701, 1993.

(6) ROTHE, E. W., HAN, A., HITCHCOCK, L.M., GU, Y., RECK, G.P., Rayleigh and predissociative fluorescence imaging of densities from an internal combustion engine using a tunable KrF laser, SPIE Proc. 2122, pp. 79-82, 1994.

(7) HEYWOOD, J.B., Internal combustion engine fundamentals, 1988 (McGraw Hill).

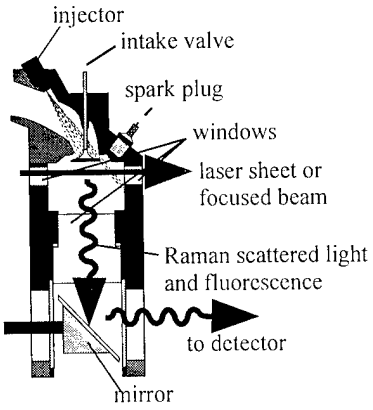

Fig.1

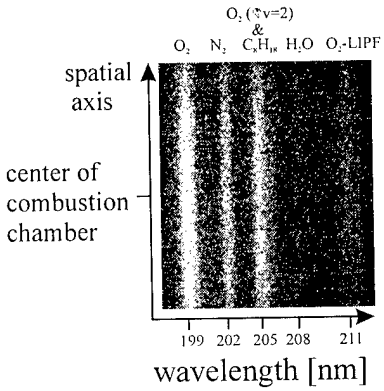

Fig. 2

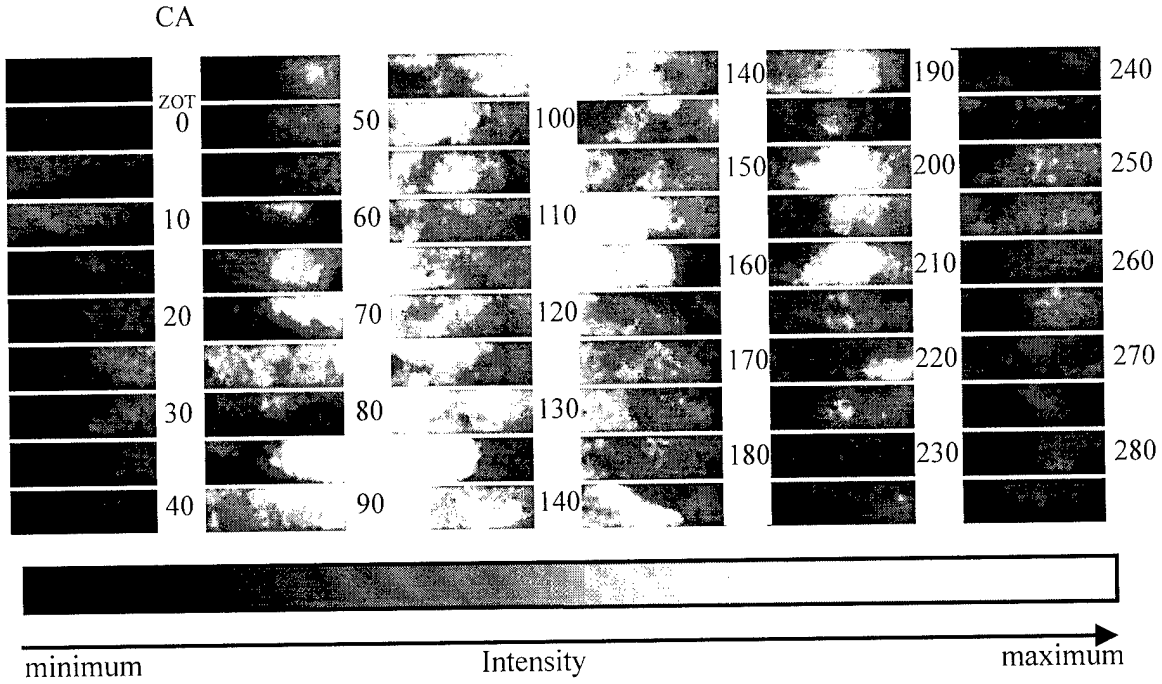

Fig. 3

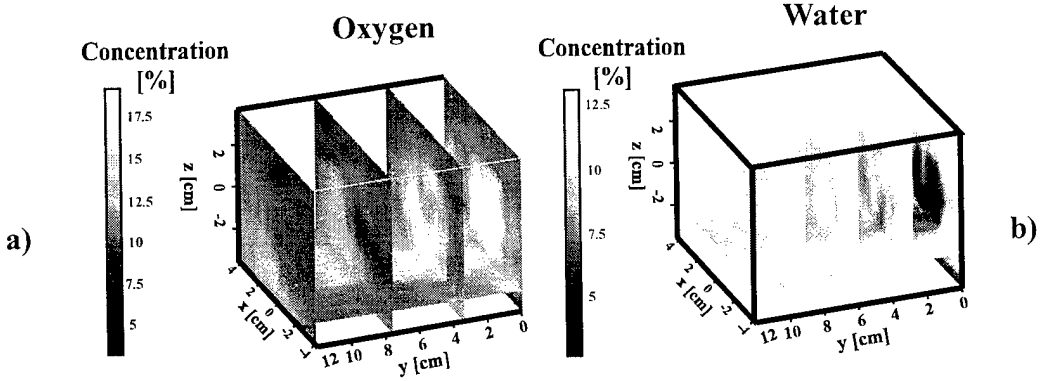

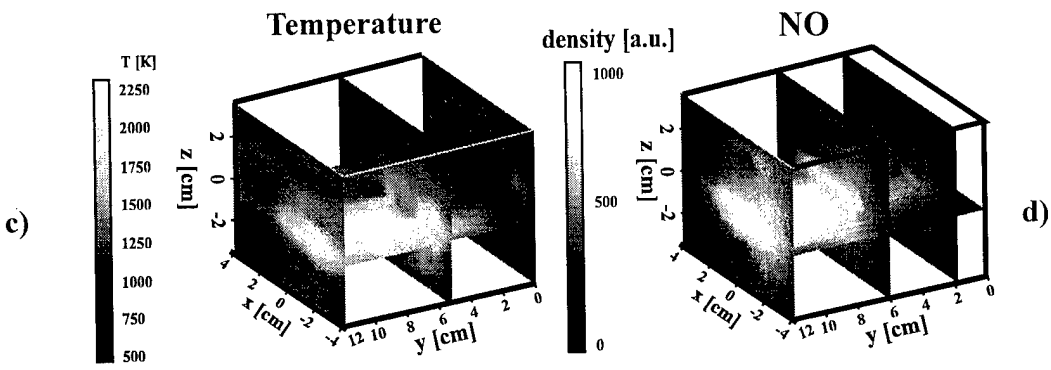

Fig. 4

Multiplex polarization spectroscopy of OH for flame thermometry

M.J. New and P. Ewart

Clarendon Laboratory, Oxford University,
Parks Road, Oxford, OX1 3PU, UK.
Fax: +44 1865 272400; Phone: +44 1865 272220
Email: P.Ewart@physics.oxford.ac.uk

A. Dreizler and T. Dreier

Universitat Heidelberg, Physikalisch-Chemisches Institut,
Im Neuenheimer Feld 253, D-69120 Heidelberg, Germany.

Laser-based techniques for combustion diagnostics are becoming increasingly important as they allow remote and non-intrusive measurements of flame parameters with high spatial and temporal resolution. Linear light scattering methods such as Laser Induced Fluorescence, Rayleigh and Raman scattering have been successfully applied [1]. In some situations non-linear processes such as coherent anti-Raman scattering (CARS) offer certain advantages over linear techniques. CARS is a four-wave mixing process and generates a signal in the form of a coherent beam of radiation but is suitable only for the detection of majority species [1]. Degenerate four-wave mixing (DFWM) is an important resonant technique which has been used to detect [2] and image [3] minority species in flames and also has the advantages inherent to a coherent process.

A possible additional non-linear technique is polarization spectroscopy (PS) which has received attention recently for application to combustion diagnostics. PS allows combustion species at trace levels to be detected with high signal to noise ratios for relatively low beam energies. PS has the advantages of simplicity, only two beams need aligning and no phase matching requirements must be met, high spatial resolution and a coherent signal beam for efficient signal capture and noise discrimination. PS has been successfully applied to the detection, imaging and temperature determination of OH in a flame [4] and to the detection of C_2 in an oxy-acetylene flame [5].

Traditional methods of recording a spectrum by tuning the wavelength of a narrow bandwidth dye laser have the disadvantage that they allow only a time average of the temperature to be derived. For turbulent environments it is essential to record instantaneous spectra (or single laser pulse spectra). Multiplex CARS [1] and DFWM [6] spectra have been produced using broad bandwidth dye lasers allowing single-shot measurement of temperature. We report here the first observation of multiplex Polarization Spectroscopy. Several transitions in the $A^2\Sigma$–$X^2\Pi(0,0)$ band of OH around 306nm in a flame have been recorded yielding single shot and averaged spectra from which flame temperatures have been derived.

In PS an intense circularly polarized pump beam optically pumps a transition on resonance producing a selective depopulation of the degenerate M_J levels of the lower rotational level with angular momentum J. The resulting anisotropy in the spatial distribution of angular momenta

causes the medium to become birefringent to the incoming probe beam. If the probe beam is passed through two linear polarizers the rotation of the plane of polarization in the medium on resonance can be detected as an emerging beam from the second polarizer. A rigorous theoretical treatment of PS is not available but a simple semi-classical approach demonstrates that an unsaturated PS signal is proportional to laser power to the third power, to the lower level population and Einstein B coefficient squared, and to certain J dependent factors. We assume an equilibrium Boltzmann distribution for the rotational level populations and the flame temperature may be derived from the gradient of a Boltzmann plot.

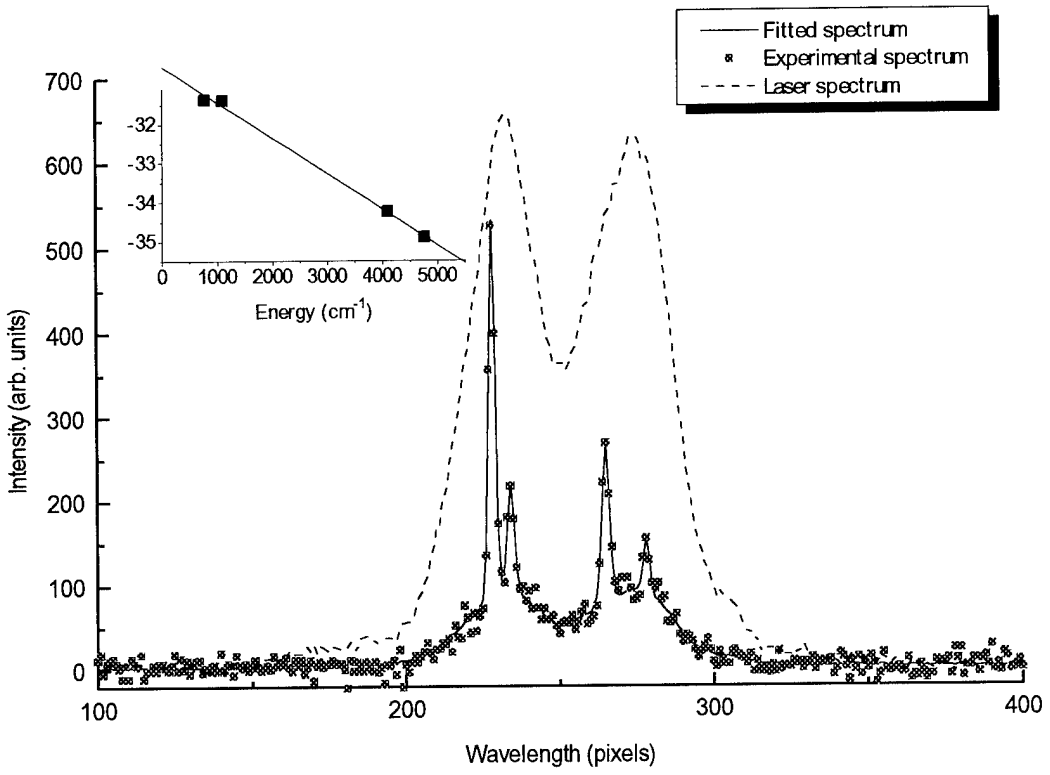

Figure Multiplex PS spectrum of R_1 lines 6,12,5 and 13 (left to right) of OH in a flame. The fitted spectrum is shown together with the laser profile. The Boltzmann plot and least squares fit for this spectrum is inset.

Our source of broad bandwidth radiation is a *modeless* laser (ML) [7] which minimizes spectral noise arising from fluctuations of cavity modes inherent in conventional lasers. The output of the ML was frequency doubled using two KDP crystals to provide a wider spectral coverage in order to obtain signals from four or five transitions simultaneously. A pulse energy of 0.5mJ of ultraviolet was sufficient for the experiment as PS saturation levels may be reached at relatively low beam intensities. The signal to noise levels of the PS spectra also depend on the extinction ratios of the crossed polarizers and ours had a ratio of 10^6. The signal beam was analyzed with a 1m spectrograph with a 2400lmm^{-1} grating in second order and spectra were collected on an unintensified CCD camera. The flame used was a premixed methane/air flame.

Multiplex spectra of OH were obtained showing up to five transitions in the region of the R_1 bandhead. The laser spectrum was recorded simultaneously with the PS signal on a different region of the CCD chip allowing the PS spectrum to be referenced to the laser intensity. Measurements of the variation of PS signal with pump beam intensity yielded a saturation curve with I^2 dependence at low intensities (the probe beam intensity being held constant). All spectra were recorded in the unsaturated regime. Single-shot spectra and spectra averaged by summing ten laser shots were used to derive temperatures. The figure shows a typical ten shot PS spectrum showing four lines with a fitted theoretical spectrum. The signal strengths measured from the areas of the fitted Gaussian line shapes were referenced with the laser spectrum and a Boltzmann plot was produced and a temperature calculated. The spectrum shown yielded a temperature of 2179 ± 96K and a set of one hundred spectra gave a normal distribution with mean temperature 2187K and standard deviation 92K. The measured temperature is slightly higher than expected for a flame of this type (CARS measurements gave a mean temperature of 2130K) and this is attributed to absorption of the beams. Measurements of the amount of absorption in the flame have been made and work continues to provide a correction for its effect.

In conclusion, we have demonstrated the principle of multiplex Polarization Spectroscopy and its application to thermometry by recording broadband spectra of OH in a flame.

References

[1] A.C. Eckbreth, *Laser Diagnostics of Combustion Temperature and Species,* (Abacus, Cambridge, Mass., 1988)
[2] P. Ewart and S.V. O'Leary, Opt. Lett., **11**, 279, (1986)
[3] D.J. Rakestraw, R.L. Farrow and T. Dreier, Opt. Lett., **15**, 709, (1990)
[4] K. Nyholm, Opt. Comm., **111**, 66, (1994)
[5] K. Nyholm, M. Kaivola and C.G. Aminoff, Appl. Phys. B, **60**, 5, (1995)
[6] I.P. Jefferies, A.J. Yates and P. Ewart, in *Coherent Raman Spectroscopy* p.129 (World Scientific, Ed. E. Castelluci, 1993)
[7] P. Ewart, Opt. Comm., **55**, 124, (1985)

Thursday, March 21, 1996

Poster Session II

LThD 4:00 pm-6:00 pm
Windsor Ballroom

Laser-Induced Gratings in the Red System of Molecular Oxygen

W. Hubschmid, R. Bombach, and B. Hemmerling

Paul Scherrer Institut, CH-5232 Villigen PSI, Switzerland
Phone: +41 56 310 2938, FAX: +41 56 310 2199, Email: Hubschmid@psi.ch

Energy transfer processes involving singlet states of O_2 are of great and continuous interest in atmospheric and biological research. Due to the low excitation energies the states $^1\Delta_g$, and $^1\Sigma_g^+$ are studied most extensively. The forbidden nature of optical transitions to the ground state makes the singlet molecules metastable. Thus, quite slow nonradiative processes can be studied. The singlet states of oxygen offer therefore a good possibility to analyse different contributions to laser-induced gratings. On the other hand, the analysis of the temporal evolution of the laser-induced gratings may prove to be a powerful method to study energy transfer processes.

Laser-induced gratings are formed in a medium by the spatially sinusoidal intensity pattern from the interference of two intersecting laser beams. Electrostriction and fast release of excitation energy generate, at any point, two sound waves propagating in opposite directions, see e.g. Ref.1. Their wavelength and direction match the interference geometry, and they build up a spatially periodic time dependent density grating. Additionally, a stationary grating is formed by the spatially modulated population difference between excited and ground state caused by the absorption process. Likewise, a stationary grating is caused by the isobaric density wave accompanying electrostriction and liberation of thermal energy. In order to use laser-induced gratings for diagnostic purposes, it is necessary to address all of the above mentioned grating contributions.

For the experiments described in this paper, the two grating excitation beams were provided by a single-longitudinal-mode optical parametric oscillator (Continuum HRL-100Z). The pulse length was about 5 ns and the bandwidth is specified to be smaller than 500 MHz. Focused by a lens (f = 1000 mm), the two excitation beams overlapped each other in a sample cell with an angle θ of about 1° at the focus. The total intensity at this point was about 10 GW/cm^2. A second lens of the same type was used to recollimate the two excitation beams, and to focus the counter propagating beam of a cw Ar^+ laser (Innova 70-4) reading out the laser induced grating in a planar backward phase matching geometry. The power of the Ar^+ laser was 1.7 W running in single line mode at λ = 514.5 nm. The read-out beam was aligned to satisfy the Bragg condition and to overlap the focus of the excitation beams. Oxygen with a purity of 99.5% was used throughout the measurements, and no special care was taken to remove residual water form the gas or the sample cell. Synchronously to the recording of the laser-induced grating spectrum, the laser power was monitored and an absorption spectrum with a path length of 10 m in a cell containing pure oxygen at 1 bar was taken. In order to allow for time resolved acquisition of single pulse signals, a digitizer (Tektronix TDS 544A) with a bandwidth of 500 MHz and a sampling rate of 10^9 s^{-1} was employed.

Figure 1 shows the temporal behaviour of the reflectivity of a laser-induced grating formed by a single pulse of the excitation laser in a mixture of 1 bar oxygen and 0.05 bar carbon dioxide. The laser is tuned to the $^PP(9)$ line in the 0-0 band of the $^1\Sigma_g^+ \leftarrow {}^3\Sigma_g^-$ system of O_2 at 763.6328 nm. The light intensity of the read-out laser reflected by the grating is plotted versus time. The overall appearance of the temporal evolution of the signal is similar to the one of an electrostrictive and thermal grating [2]. The most striking difference is the appearance of a broad unstructured hump following at later times the first, oscillating part of the observed signal. This part of the signal can be explained by assuming a long living population grating together with a fast energy release

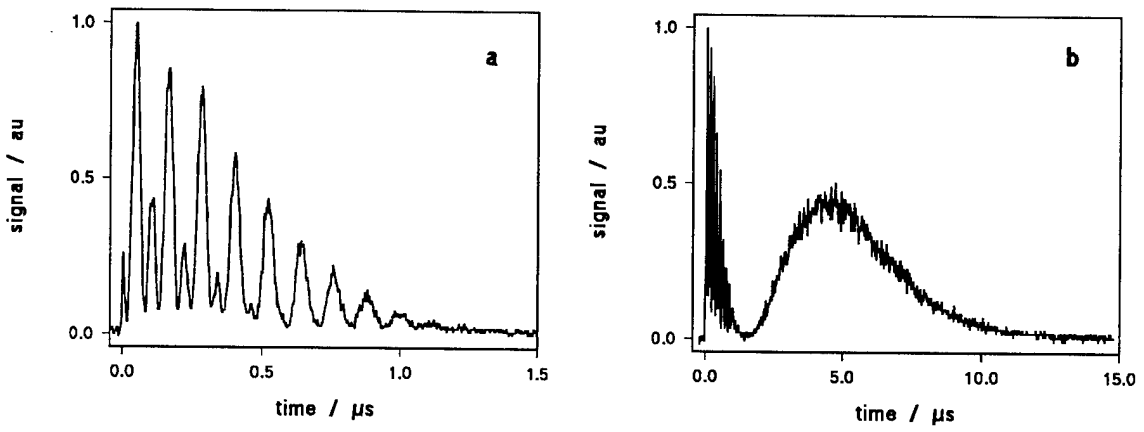

Fig.1 Laser-induced grating signal obtained in a mixture of 1 bar O_2 and 0.05 bar CO_2. (a) depicts the first part of the signal with higher temporal resolution.

resulting in a thermal grating. Due to a slow further energy liberation process, an additional thermal grating is generated. It consists mainly of a stationary part, which decays by thermal conductivity, leading to the broad unstructured hump. Sytematic measurements have been carried out concerning the dependence of the temporal evolution of the laser-induced grating signal on laser intensity, pressure, and quenching partner.

Wavelength scans of the excitation laser have been carried out in pure oxygen at a pressure of 1 bar covering the spectral range of the ^{R}R and the ^{R}Q branch in the 0-0 band of the $^1\Sigma_g^+ \leftarrow {}^3\Sigma_g^-$ system. Figure 2a shows the spectral behaviour of the oscillating part of the signal in the wavelength range 759.95 nm to 761.50 nm together with the simultaneously recorded absorption spectrum. The spectrum resulting from the broad unstructured part of the signal is depicted in Fig.2b. The oscillating part of the signal is strongly enhanced in case of molecular resonance. E.g., the signal obtained at the $^{R}Q(11)$ line is 40 times stronger than the nonresonant electrostrictive signal which appears as constant background in Fig.2a. The unstructured part of the signal is free of any background. However, due to the low self-quenching efficiency of oxygen in the $b\,^1\Sigma_g^+$ state the signal is by a factor of about 30 smaller than the electrostrictive signal.

All the line positions in the absorption spectrum, and in the oscillating and the unstructured part of the laser induced grating spectrum agree with each other within the measurement accuracy of $\pm 0.01 cm^{-1}$. For the absorption lines a linewidth of $0.1 cm^{-1}$ (FWHM) is measured which agrees well with literature values and is mainly attributed to pressure broadening. The laser-induced grating signals have a linewidth of about $0.07 cm^{-1}$ (FWHM).

The addition of an efficient quencher to the oxygen sample leads to a strong enhancement of the thermal signal. In order to demonstrate the sensitivity of the laser-induced grating technique, we looked for lines of the isotopic molecule $^{16}O^{18}O$ occuring in natural O_2 with an abundance of 0.4%. For that purpose, water with a pressure of 0.018 bar corresponding to the vapour pressure at room temperature was added to oxygen at a pressure of 1 bar. In $^{16}O^{18}O$ the transition frequencies are shifted to higher frequencies compared to the frequencies in $^{16}O_2$. In the spectral range 765.6 nm to 763.8 nm, it was possible to resolve the transitions $^{P}P(17)$, $^{P}P(15)$, $^{P}P(13)$, and $^{P}P(11)$ of the 0-0 band in the $^1\Sigma_g^+ \leftarrow {}^3\Sigma_g^-$ system of $^{16}O^{18}O$. Most of the other isotopic lines are blended by the wings of the strong transitions belonging to the homonuclear molecule.

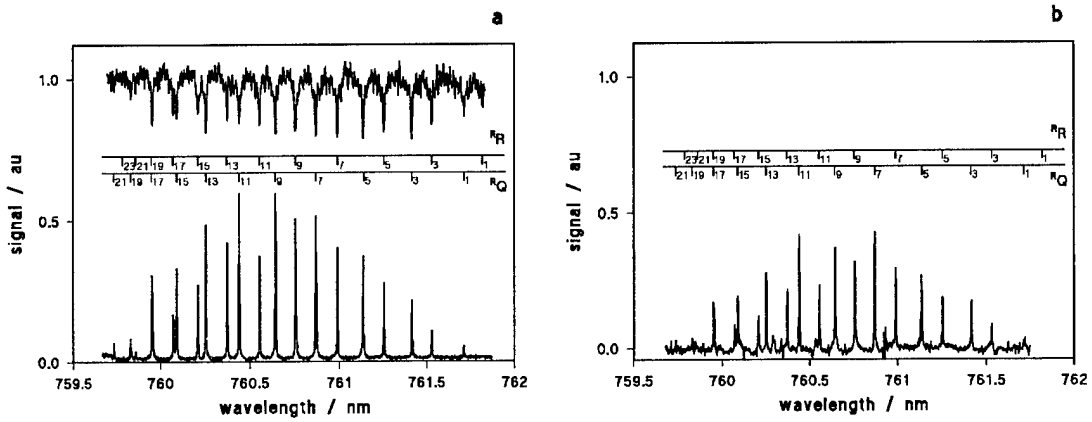

Fig2. (a) Absorption spectrum (upper trace) and spectrum derived from the oscillating part of the laser-induced grating signal (lower trace), (b) spectrum derived from the unstructured part of the laser-induced grating signal.

References

[1] A. Stampanoni-Panariello, B. Hemmerling, and W. Hubschmid, Phys.Rev. A 51 (1995) 655.

[2] W. Hubschmid, B. Hemmerling, and A. Stampanoni-Panariello, J. Opt. Soc. Am. B 12 (1995) 1850.

Nitrocompound Analysis by 226 nm Laser Photofragmentation/Fragment Detection

R.L. Pastel[1] and R.C. Sausa

U.S. Army Research Laboratory
AMSRL-WT-PC
Aberdeen Proving Grounds, MD 21005-5066

The development of fast and sensitive detectors for NO_x ($NO+NO_2$) and nitrocompounds is important in many military and civilian applications.[2,3] Some applications include environmental compliance to state and federal regulations, clean up of ammunition sites, aviation security, and atmospheric monitoring.

We report the analysis of trace nitrocompounds by laser photofragmentation/fragmentation detection (PF/FD). The technique uses a 226 nm laser both to photolyze the analyte and to detect the characteristic NO fragment. NO is detected by laser-induced fluorescence (LIF) or resonance enhanced multiphoton ionization (REMPI) via the NO $A^2\Sigma^+$-$X^2\Pi$ (0,0) transitions near 226 nm.[2-4] The LIF and REMPI techniques are compared and various nitrocompound limit of detections (LODs) are reported.

A schematic of the experimental apparatus is depicted in Figure 1. The apparatus consists of miniature electrodes for ion detection and a photomultiplier tube with a 225 - 400 nm bandpass filter for fluorescence detection. A single excimer pumped dye laser equipped with a second harmonic doubler generates 20 μJ 225 nm pulses for nitrocompound photo-fragmentation and NO excitation.

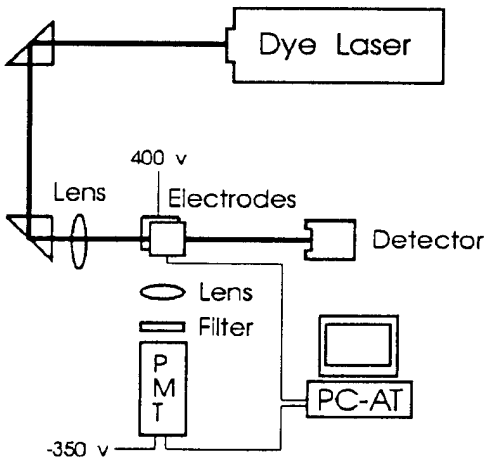

Figure 1: Experimental apparatus

Figure 2 shows the sensitivity plots of NO LIF and REMPI from photofragmentation of CH_3NO_2 at 226.5 nm for photofragmentation and fragment excitation. The analyte concentration is measurable below the limit of detection (LOD), 0.2 ppm and 12 ppm for REMPI and LIF, respectively. LODs of NO, NO_2, CH_3NO_2, $C_6H_5NO_2$, diethyleneglycol dinitrate (DEGDGN), and trinitrotoluene (TNT), are also measured.

The LODs of CH_3NO_2 and $C_6H_5NO_2$ are greater than the NO_2 LODs which is greater than NO LODs. This trend suggests that one UV photon fragments CH_3NO_2 and $C_6H_5NO_2$ into NO_2,[5] and a second photon fragments NO_2 into NO.[6] DEGDN and TNT have LODs between the CH_3NO_2 LOD and NO_2 LOD.

The REMPI LODs are 50 times greater than the LIF LODs. This difference may be due to the difference in collection efficiencies of our apparatus. REMPI collection is nearly 100% efficient, while the fluorescence collection is 2% efficient.

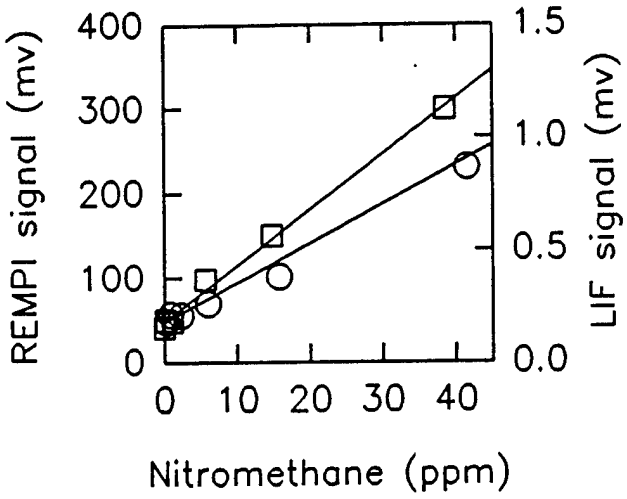

Figure 2: CH_3NO_2 REMPI (□) and LIF (o) sensitivities

In short, the PF/FD enables a simple device to analyze trace nitrocompounds by REMPI and LIF NO fragment detection. The technique is sensitive, selective, and offers real-time and *in-situ* monitoring capabilities.

References

1. Presenter, ARL-SCEEE Postdoctoral Fellow.

2. G. W. Lemire, J. B. Simeonsson, and R. C. Sausa, *Anal. Chem.*, **65**, 529 (1993).

3. J. B. Simeonsson, G. W. Lemire, and R. C. Sausa, *Appl. Spectrosc.*, **47**, 1907 (1993).

4. D. C. Jacobs, R. J. Madix, and R. N. Zare, *J. Chem. Phys.*, **85**, 5469 (1986).

5. L. Bigio, R. S. Tapper, and E. R. Grant, *J. Phys. Chem.*, **88**, 1271 (1984).

6. L. J. Butler, L. Krajnovich, and Y. T. Lee, *J. Chem. Phys.*, **79**, 1708 (1983).

CARS Temperature Measurements in a Driven Jet Diffusion Flame

R. D. Hancock*, F. R. Schauer*, and R. P. Lucht
Department of Mechanical and Industrial Engineering, University of Illinois, 1206 W. Green St., Urbana, IL 61801
(Phone: 217-333-5056, Fax: 217-244-6534)
*Also with Wright Laboratory, Wright-Patterson AFB, OH 45433
V. R. Katta, K. Y. Hsu
Innovative Scientific Solutions, Inc., 3845 Woodhurst Ct., Dayton, OH 45433 (Phone: 513-255-8781)

INTRODUCTION

This paper discusses the use of a broadband coherent anti-Stokes Raman scattering (CARS) system to investigate local gas temperatures during a vortex/flame interaction. The CARS system is first used to obtain flame temperature measurements in a series of near adiabatic hydrogen/air flames produced with a Hencken burner (Hencken, 1994; Hancock, et al., 1996). These temperatures are compared to adiabatic flame temperatures found using the NASA-Lewis equilibrium code (Gordon and McBride, 1976) and a computational fluid dynamics code developed by Katta, et al. (1994). These results help to validate the CARS system. Next, the CARS system is used to obtain local gas temperature measurements in an undriven hydrogen/nitrogen jet diffusion flame and during a vortex-flame interaction in the same flame, but under driven conditions. Experimental results (Hsu, et al., 1993; Carter, et al., 1995) and direct numerical simulations (Katta and Roquemore, 1995) indicate that preferential diffusion (manifest as Lewis number), acting together with flame curvature, influence the local flame temperature along the flame surface. Under certain conditions the local temperature will rise even though the flame is positively stretched–a condition which is typically thought to cause a reduction in local flame temperature. In this paper such a condition is investigated for a hydrogen/nitrogen diffusion flame using CARS and direct numerical simulations.

EXPERIMENTAL

The three main components of this experiment are the Hencken burner, the diffusion flame burner, and the CARS instrument.

The accuracy and precision of the CARS system were investigated using a Hencken burner. The Hencken burner has an array of fuel tubes that are placed in a stainless steel honeycomb structure. Air flows through the honeycomb structure, and the resulting flames are flat, uniform, steady, and nearly adiabatic for sufficiently high flow rates. There is a large volume above the 36.5 mm square honeycomb surface where the flame temperature is radially and axially uniform. Temperature measurements in hydrogen/air flames were collected at the 3.81 cm axial location directly above the center of the burner. The air flow was constant at ~60 SLPM (0°C) and the hydrogen was varied to produce equivalence ratios ranging from 0.5-2.5.

The driven jet diffusion flame apparatus consists of a 2.54 cm diameter axisymmetric fuel tube that contracts to a 1 cm diameter sharp-edged nozzle. The fuel tube is surrounded by a 15.24 cm diameter coflow of air at 0.48 m/s that helps to remove room air disturbances. The fuel jet consists of 15.0 SLPM (0°C) of hydrogen and 6.25 SLPM (0°C) of nitrogen, resulting in an average peak centerline axial velocity of 4.9 m/s at room temperature. A periodically repeating vortex is formed inside the diffusion flame by passing the fuel over a pulsating loud speaker located in a chamber directly below the fuel tube. The loud speaker is pulsed at 20 Hz causing the fuel jet to experience periodic accelerations in velocity which produce mushroom-shaped vortices that grow radially outward when faster moving fluid runs into slower moving fluid in front of it. The driving pulse and laser are phase-locked in order to permit the vortex-flame interaction to be investigated at a fixed phase of its development. The vortex and flame structures have been found to be reproducible to within ~100 μm from cycle to cycle.

A broadband CARS instrument is used in this experiment. A detailed treatment of CARS is found in other sources (Eckbreth, 1988; Greenhalgh, 1994). An example of a broadband CARS spectra obtained with this CARS system is shown in Fig. 1. It has a spectral resolution of ~0.59 cm^{-1}. The 532-nm frequency-doubled output of a Continuum injection-seeded Nd:YAG laser was used for the two pump beams and to pump a modeless dye laser (Ewart, 1993). The three laser beams were crossed and focused in the flame producing a diagnostic volume in which over 95% of the CARS beam was generated in a region less than 2.0 mm long and ~50 μm in diameter. The resulting CARS signal was focused into a 1-meter spectrometer where it was spectrally dispersed and detected using a 512 x 512, back-illuminated unintensified CCD array. All of the nitrogen CARS spectra collected are the average of 100 laser shots. Averaging is acceptable in the driven jet diffusion flame because the vortex-flame interaction event and laser pulse are phase-locked and repeatable. The nitrogen CARS spectra were fit using the CARSFT code developed at Sandia National Laboratories (Palmer, 1989). Based on the quality and high spectral resolution of the CARS spectra obtained, it is conservatively estimated that the accuracy and precision of the nitrogen CARS temperature measurements are better than 2% (±40 K at 2000 K) and 0.5% (±10 K at 2000 K), respectively.

NUMERICAL MODEL

The direct numerical simulations of the diffusion flames are performed using a code developed by Katta (Katta, et al., 1994). Time-dependent, axisymmetric Navier-Stokes equations are solved along with species and energy conservation equations in the cylindrical coordinate system. The hydrogen/air chemical kinetics model includes 14 species and 54 reactions. Temperature and species-dependent properties are incorporated.

RESULTS AND DISCUSSION

This section includes experimental and computational results for both the Hencken burner and the driven jet diffusion flame. The Hencken burner results are used to validate the CARS system as an accurate and precise instrument for flame temperature measurements. The diffusion flame results illustrate the application of the CARS system to measuring local flame temperatures that are observed during vortex-flame interactions.

Peak flame temperatures were obtained in the Hencken burner with broadband CARS and adiabatic flame temperatures were calculated with the NASA-Lewis equilibrium code and the CFD code by Katta, et al. (1994) for equivalence ratios ranging from 0.5 to 2.5 for the hydrogen/air flame. As illustrated in Fig. 2, the nitrogen CARS temperatures are very close to the predicted adiabatic flame temperatures and are on average ~10 K lower. These results shown in Fig. 2 indicate that for sufficiently high flow rates the Hencken burner flames are nearly adiabatic, that the CARS system is providing accurate temperature measurements, and that the chemical mechanism in the CFD model is in excellent agreement with the equilibrium code predictions.

CARS measurements and numerical calculations are shown for both the undriven and driven hydrogen/nitrogen flames. Shown in Fig. 3 is a split experimental and computational image of the driven flame. The left half of the image shows the flame zone as indicated by OH laser-induced fluorescence and the shear layer is marked by TiO_2 particles formed using reactive Mie scattering (RMS) (Chen and Roquemore, 1986). The right side is an image of the computational model. The vortex is marked using particle traces, and the peak flame temperature locations are marked by dots. Figure 4 is a comparison between the temperature profiles obtained using CARS and the numerical model at the 15.24 mm axial location for the undriven flame. Figure 5 is a plot of the peak flame temperatures versus axial location for the undriven and driven flames using CARS and the numerical model. While absolute agreement between CARS and the numerical model is not perfect, similar temperature profile trends are observed. Better temperature agreement should result as the numerically modeled vortex is made to more closely resemble the experimental vortex. Additional flames and driving conditions are currently under investigation. The results presented herein and additional results to be presented orally indicate that the temperature in the driven flame can vary significantly from the steady-state undriven flame temperature.

SUMMARY AND CONCLUSIONS

Nitrogen CARS temperature measurements were obtained in a hydrogen/air flame produced with a Hencken burner. The nitrogen CARS temperature measurements were on average ~10 K lower than the equilibrium code predictions for the hydrogen/air flames. These results support the use of the Hencken burner as a validation device for the CARS system used to obtain detailed temperature measurements in the driven jet diffusion flames. It was found that the temperature in the stretched region of a driven hydrogen/nitrogen diffusion flame can vary significantly from the local undriven flame temperature due to non-unity Lewis number effects and flame curvature.

ACKNOWLEDGMENTS

Financial support was provided by Systems Research Laboratories, Inc., and the Aero Propulsion and Power Directorate of Wright Laboratory (USAF).

REFERENCES

Carter, C. D., et al. (1995). CS/WS/MN Sections of the Combustion Institute.

Chen, L.-D. and W. M. Roquemore (1986). Combust. Flame **66**(1): 81-86.

Eckbreth, A. C. (1988). Laser Diagnostics for Combustion Temperature and Species. Cambridge, Abacus Press.

Ewart, P. (1994). X Laser Systems, 55 Benmead Road, Kidlington, Oxon. OX5 2DB, U.K.

Gordon, S. and B. J. McBride (1976). NASA SP-273.

Greenhalgh, D. A. (1994). Inelastic Scattering Laser Diagnostics; CARS, Planar LIF and Planar LII. Optical Diagnostics for Flow Processes. L. Lading, G. Wigley and P. Buchhave. New York, Plenum Press: 357-389.

Hancock, R. D., et al. (1996). Manuscript in preparation for submission to Combust. Flame.

Hencken, K. (1995). Research Technologies, Inc.

Hsu, K. Y., et al. (1993). AIAA 93-0455.

Katta, V. R. and W. M. Roquemore (1995). Combust. Flame **100**: 61-70.

Katta, V. R., et al. (1994). Combust. Flame **96**: 60-74.

Palmer, R. E. (1989). The CARSFT Computer Code for Calculating Coherent Anti-Stokes Raman Spectra: User and Programmer Information, Sandia National Laboratories.

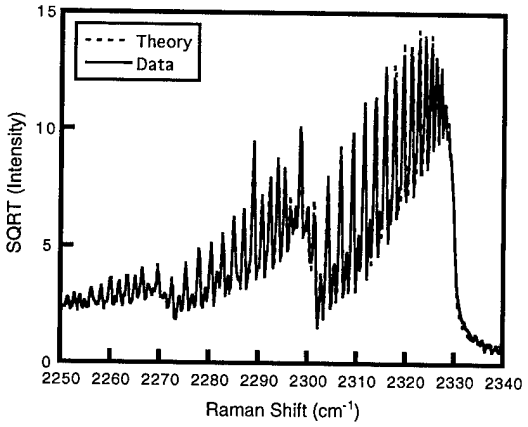

Figure 1. Typical CARS Sprectrum

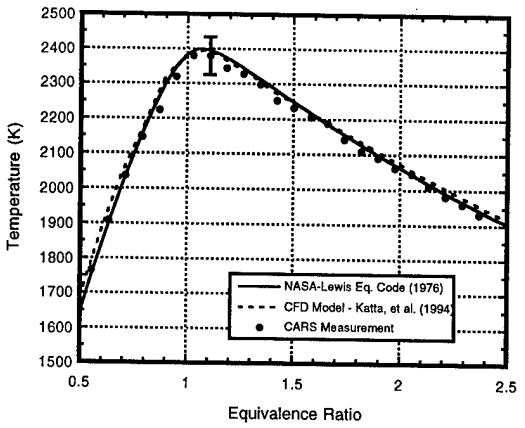

Figure 2. Hencken Burner Temperatures

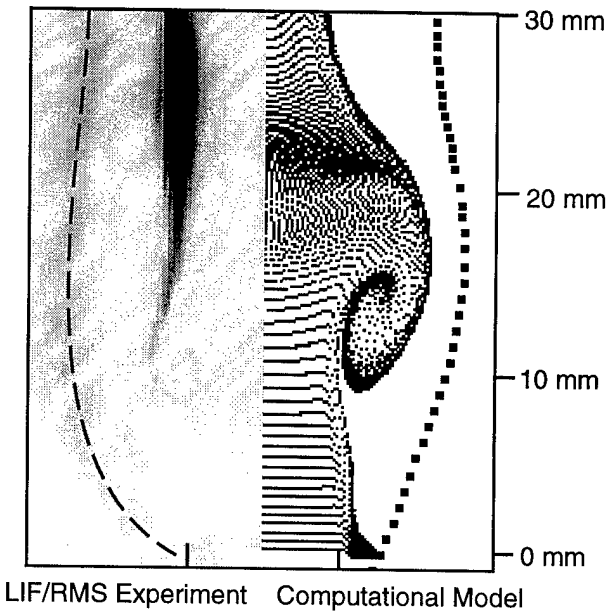

Figure 3. Comparison of Experimental and Computational Images of the Driven H_2/N_2 Flame

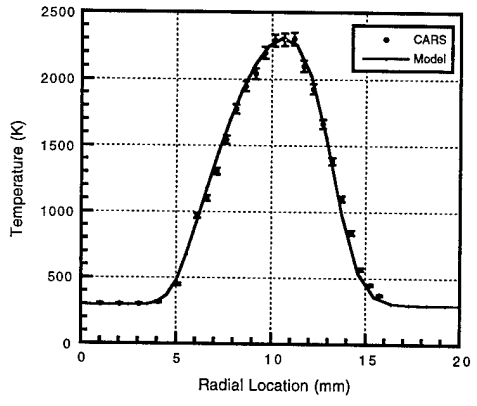

Figure 4. Undriven Radial FlameTemperature Profiles at the 15.24 mm Axial Location

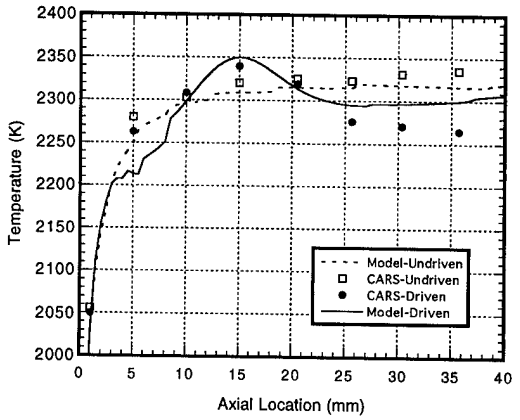

Figure 5. Comparison of Axial Temperature Profiles for Undriven and Driven Flames

Two Photon Resonant Detection of N_2 Using Polarization Spectroscopy and Laser Induced Fluorescence

C. Kaminski, B. Löfstedt, R. Fritzon, and M. Aldén
Department of Combustion Physics, Lund Institute of Technology,
PO Box 118, 22100 Lund, Sweden.
Tel: +46 (0)46/2229728; Fax: +46 (0)46/2224542
E-Mail: clemens.kaminski@forbrf.lth.se

Introduction

Molecular nitrogen, N_2, is one of the most important molecules in combustion and environmental diagnostics since it constitutes the major species of our atmosphere. For temperature and concentration measurements N_2 CARS has been developed into a highly robust and accurate tool. There are environments where N_2 concentrations are too low for CARS to be applicable. In this case excitation schemes can be used which have been developed to allow direct access to electronic resonances of N_2 via multi-photon transitions [1]. Almost all detection schemes of these techniques employ further resonant multi-photon steps to create N_2^+ ions and the resulting signal electrons are collected by electrodes (resonance enhanced multi-photon ionisation - REMPI) [2,3].

A different approach was developed by the present group involving 2 photon excitation in the $a\ ^1\Pi_g$ $(v'=1) \leftarrow X\ ^1\Sigma_g^+$ $(v''=0)$ system of neutral N_2 and subsequent 3 photon ionisation to the $B\ ^2\Sigma_u^+$ state of N_2^+ (2+3 LIF) [4]. The advantage here is that subsequent $B \rightarrow X$ fluorescence of N_2^+ can be detected directly without need to insert potentially disturbing electrodes required for electron counting. Since the molecular ground state of N_2 is scanned the technique has potential as a thermometry probe. A problem with LIF, however, is its severe sensitivity to molecular quenching which reduces signal strengths and complicates the interpretation of resulting spectra.

Recently it has been suggested that two photon resonant polarization spectroscopy (TIPS) does not suffer from molecular collisions [5]. The present work reports on the first observation of two photon resonant polarization spectroscopy (TIPS) in neutral N_2. (2+3) LIF scans were performed simultaneously to allow a direct comparison between the two techniques. The advantages and potential of N_2 TIPS from these preliminary results are discussed and effects of collider species on both processes are discussed.

Experimental

The experimental details for TIPS and (2+3) photon LIF can be found in [6] and [4], respectively. Tuneable radiation around 283 nm was generated by use of a frequency doubled dye laser system pumped by a Nd:YAG laser. Around 10 mJ and 100 μJ of pulse energies were available for the TIPS pump and probe beams, respectively. Polarizations were linear with the probe polarization at 45 degrees to the pump beam polarization. The beams were focused to cross in the interaction region by a single 300 mm lens. Fluorescence was collected simultaneously by imaging the interaction volume at right angles to the beam propagation direction.

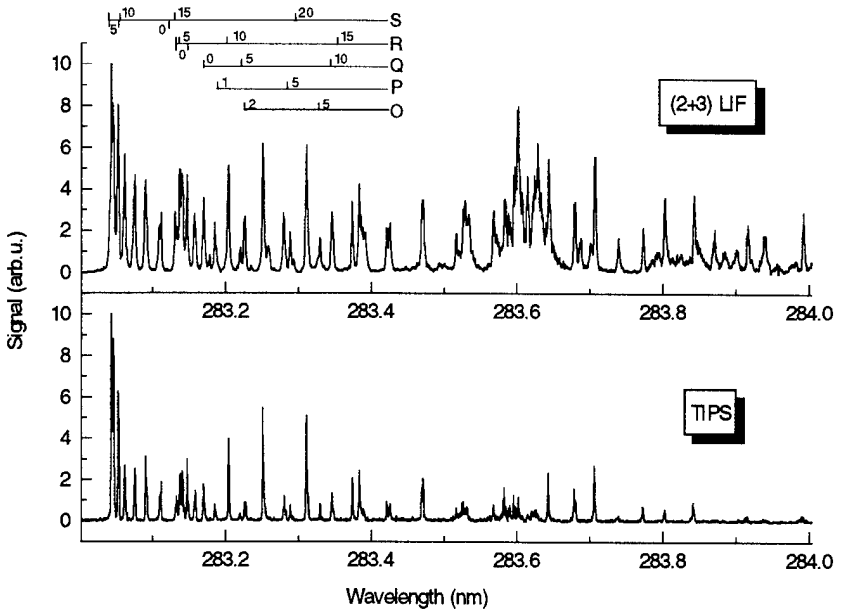

Figure 1: Simultaneous (2+3)LIF and TIPS spectra of the $a\ ^1\Pi_g\ (v'=1) \leftarrow X\ ^1\Sigma_g^+\ (v''=0)$ system of N_2

Results and Discussion

Fig.1 shows the first reported TIPS spectrum of N_2. The upper trace shows a simultaneously recorded (2+3) LIF spectrum. The spectra correspond to a flow of pure room temperature N_2 at atmospheric pressure. The much larger linewidth of the LIF spectrum is evident and may be due to saturation broadening. The three photon ionisation process to the *B* state of N_2^+ has a low cross section [7] and thus the 2 photon resonant $a \leftarrow X$ transition in neutral N_2 may saturate before detectable N_2^+ fluorescence results.

The spectra are assigned to the known transitions of N_2 in the $a \leftarrow X$ band. It is not clear presently what the complicated structure appearing around 283.6 nm is due to. This band has not been observed in connection with REMPI experiments reported in the literature (see for example [3]). The corresponding TIPS signal is much weaker in this region. It is possible that the structure arises from a resonant 3 photon process in the $b\ ^1\Pi_u \leftarrow X\ ^1\Sigma_g^+$ transition with subsequent 2 photon ionisation to the *B* state of N_2^+. The higher order resonance could then also explain the large drop in the corresponding polarization spectroscopy signal.

The TIPS signals corresponding to this scan were extremely large and had to be attenuated by a 10^{-4} neutral density filter to avoid saturation of the PMT. This large signal strength shows that the technique is promising as a potential sensitive probe for N_2 detection. Experiments using a specially designed gas cell are currently under way aimed at establishing ultimate detection sensitivities of the two techniques. Experiments in air-fed flames are also being performed to test the applicability of the technique for combustion diagnostics.

Fig.2 shows LIF and TIPS signals near the S-branch bandhead as a function of laser power on logarithmic scales. Linear fits to the data revealed a cubic intensity dependence of the (2+3) photon LIF signal suggesting that the 3-photon ionising step is the rate limiting process in the interaction. The TIPS signal, on the other hand, follows a 5th order dependence and corresponding shot to shot fluctuations are much larger compared to the fluorescence signals. We have currently no explanation for this high order power dependence of the TIPS signal which is in contrast to previous observations in other species [5,6].

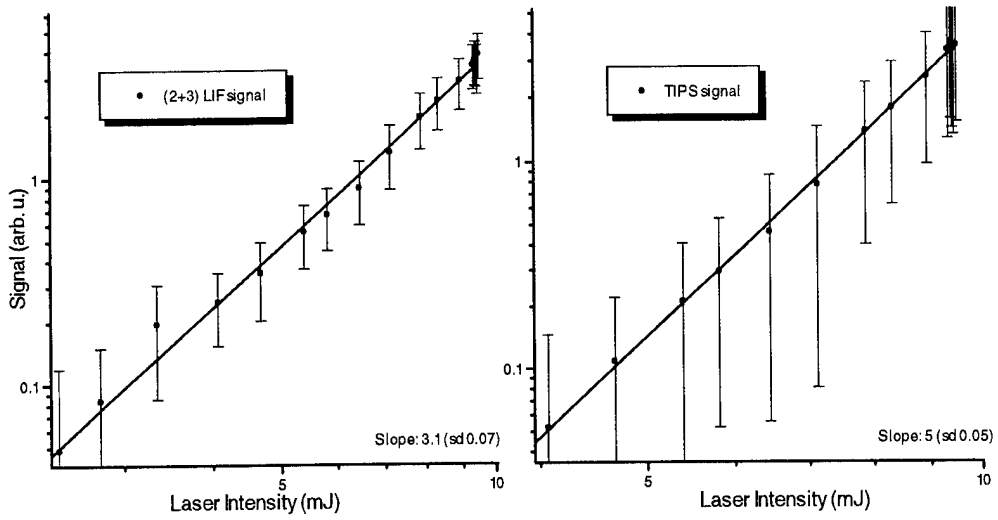

Figure 2: Power dependencies of (2+3) LIF and TIPS signals

Measurements conducted in room temperature laboratory air revealed that the (2+3) photon LIF signal is severely quenched by O_2. The LIF signal decreased by a factor of ~7 in air compared to pure N_2. The corresponding TIPS signal is much less affected by the presence of O_2 and dropped only by a factor of about ~1.5 which is in accordance with a quadratic scaling of the TIPS signal with species density. A quantitative comparison of quenching effects by different collider species is currently being conducted.
In air a strong background signal was observed which was found to be due to O_2. The O_2 signals were true polarization spectroscopy signals which disappeared if either the pump or probe beams were blocked. TIPS scans in pure O_2 flows revealed no discernible structure and only increased baseline noise levels in N_2 scans. In contrast, no fluorescence was evident in pure O_2 flows.

Conclusion

We have performed the first reported two photon polarization spectroscopy (TIPS) experiments in molecular N_2. Preliminary results suggest that the technique has potential as a sensitive probe for N_2 detection. Furthermore, the technique seems much less prone to molecular quenching collisions than multi-photon LIF. Current efforts are aimed at the synthesis of theoretical N_2 TIPS and (2+3) LIF spectra to evaluate the potential of the techniques for thermometry applications. Flame and cell experiments are being performed to evaluate the techniques for their applicability in practical combustion and environmental diagnostics.

Bibliography

[1] N van Veen and P Brewer and P Das and R Bersohn. *J. Chem. Phys.*, 77:4326, 1982.
[2] S T Pratt and P M Dehmer and J L Dehmer, *J. Chem. Phys.*, 81:3444, 1981.
[3] K L Carlton and K H Welge and S R Leone, *Chem. Phys. Lett.*, 115:492, 1985.
[4] M Aldén and W Wendt, *Opt. Comm.*, 69:31, 1988.
[5] K Danzmann and K Grützmacher and B Wende, *Phys. Rev. Lett.*, 57:2151, 1986.
[6] K Nyholm and R Fritzon and N Georgiev and M Aldén, *Opt. Comm.*, 114:76, 1995.
[7] H Helvajian and B M Dekoven and A P Baronavski, *Chem Phys.*, 90:175, 1984.

NO Laser-Induced Fluorescence as a Flame Thermometer

Jorge Luque, Masayuki Tamura, Joel E. Harrington,
Gregory P. Smith, David R. Crosley, and Jay B. Jeffries
Molecular Physics Laboratory
SRI International
Menlo Park, California 94025

Measurement of the temperature field is crucial to understanding combustion in practical devices. Imaging of laser-induced fluorescence (LIF) from NO molecules seeded into the flow is an attractive method to determine the temperature field.[1] If the seeded NO does not react or become diluted in the flow, accurate temperature measurements can be made from single line excitation with careful consideration of energy transfer and quenching collisions, overlap of laser and transition bandwidth, and detector bandwidth.[2] However, NO reacts in the flame front of hydrocarbon flames via reburning phenomena. We investigate the accuracy of LIF measurements of gas temperature using NO seeded into a premixed, laminar, low-pressure methane/air flame. The NO LIF temperature measurements are compared with temperatures determined from rotational distributions measured with LIF using OH as a function of height above the burner. Using the OH temperature profile, the chemical composition of the flame is predicted from a model of the combustion chemistry. This model predicts the amount of NO as a function of reaction time (height above the burner) including reburning in the flame front, the dilution from the combustion products, and the axial transport. The predicted major species concentrations are used to calculate the rate for NO(A) collisional quenching which are compared to measured quenching rates. In the flame front CH temperature measurements using LIF from A-X and B-X electronic transitions are compared to the OH results.

Low-pressure, premixed, laminar flames have been used in our laboratory for quantitative LIF studies of temperature[3 & 4] and OH concentration,[5] to study the chemistry of prompt NO in 30 Torr methane/air flames,[6] and to understand fuel additive effects in 40 Torr propane/air flames.[7] For the current study, it is important to time resolve the NO LIF decay, and to use a stable flame with a significant (0.5 cm) lift of the flame front above the burner surface. We have chosen a slightly rich (Φ=1.07) flame of methane, oxygen, and nitrogen at 25 Torr. To obtain a stable flame at this low pressure on our 6 cm McKenna burner with a 1 cm wide shroud flow of argon, we increased the oxygen/nitrogen ratio from 20/79 found naturally in air to 30/70.

Gas temperatures derived from rotational excitation scans of OH LIF are used for a temperature standard in our low pressure flames.[3-7] The excitation laser wavelength is scanned across a series of R branch lines in the 0-0 band of the A-X transition of OH. The detector bandwidth is tailored to provide uniform response over 15 nm centered at 310 nm to avoid any bias in the detection efficiency as different rotational transitions are excited. To mitigate the rotational dependence of the OH quenching, the OH LIF is collected with a time gate short compared to the fluorescence lifetime is used.[3] Because the transition moment for the OH A-X transition varies with internuclear separation, which leads to a rotational dependence of the electronic transition moment;[8 & 9] appropriate rotational linestrengths are crucial for accurate temperatures in diatomic hydrides. The gas temperature measurements as a function of distance above the burner determined from OH LIF rotational level scans are presented in Fig. 1. The error bars indicate the 2-σ statistical uncertainty and the accuracy is estimated to be $\pm$50K.

Figure 1 also shows temperatures determined from CH LIF near the peak of the CH concentration using rotational scans from A-X (solid triangle) and B-X (open circle) transitions. Appropriate rotational linestrengths for CH transitions are also crucial,[9] especially for the B-X transition where the transition moment varies significantly with rotational level. Like OH LIF, a wide detector bandwidth is needed for CH to avoid a varying detector efficiency with different rotational transitions. The time gate for the detection of

CH B-X is quite important. If the signal is time integrated for the fluorescence lifetime, rotational energy transfer can move some of the excited molecules into levels which predissociate. This predissociating RET is more likely for transitions with high rotational level near the predissociation threshold, producing a rotational dependent signal which must be accounted for to avoid an error the derived gas temperature. A time gate short compared to the RET will avoid this potential source of error. In reference 3 we found a difference between rotational temperatures derived from CH A-X and B-X transitions; this difference was produced by a combination of RET induced predissociation and a poor choice of rotational linestrengths. Using correct rotational linestrengths and short time gates, we find extraordinary agreement among CH and OH LIF temperatures as shown in Fig. 1.

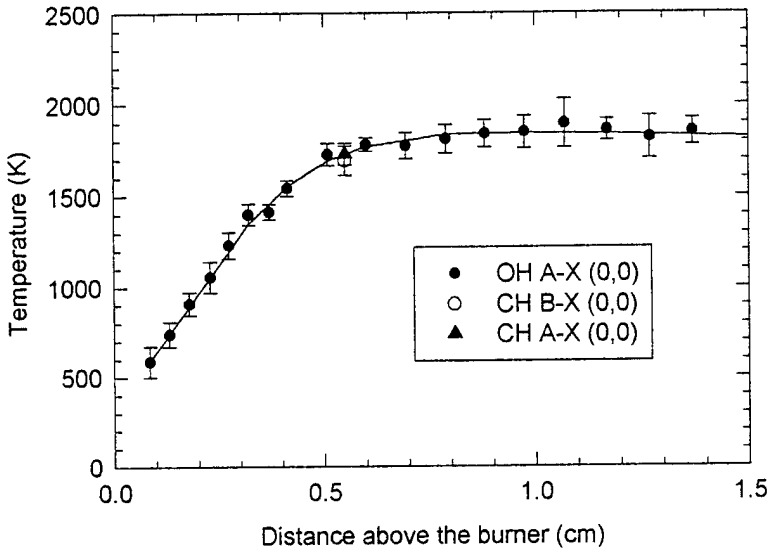

Figure 1. OH LIF temperature profile in the flame with CH A-X and B-X LIF temperatures in the flame front.

The gas temperature profile is used to constrain a model of the gas chemistry with 1000 ppm of NO added to the total flow. The influence of dilution and reburning are evident in the prediction of NO molefraction shown in Fig. 2. Complete combustion of methane and oxygen to carbon dioxide and water do not produce a change in the total number of moles of gas. However, in our low-pressure flame there are more moles of flame products than feedstock gas. First, in the low-pressure flame the combustion is not complete within the flow time at a height 3 cm above the burner; second, the gas temperature is still high at this burner height producing an equilibrium concentration of radicals, H_2, and CO; third, the fuel/oxidizer ratio is slightly rich. All of these conditions combine to dilute the added NO by 8% at 2 cm above the burner. In the flame front, the reburning reactions reduce the NO nearly another 16%. Axial diffusion of flame product water and radicals back toward the burner surface and the depressed NO molefraction in the flame front reduce the NO at the burner surface. The variation of NO with height above burner must be known to use the NO LIF signal intensity to determine gas temperature from a single transition.

The measured quenching rate of NO as a function of height above the burner is compared to calculated quenching rates using the gas composition of predicted by the model and selected quenching cross sections. We find the quenching rate nearly constant in this flame; there is a drop of approximately 20% from the feedstock to the flame front and a 10% rise of the quenching rate into the burnt gases. The

calculation predicts the quenching value quite well including the minimum in the flame front creating an optimistic outlook for predictions of NO quenching rates in practical combustors.

The intensity of NO(A-X) LIF from the isolated $Q_1(16.5)$ line as corrected for variation of the molefraction of the added NO is shown in Fig. 2. A quenching correction is avoided in this low-pressure flame using a 6 ns time gate on the signal which is short compared to the fluorescence lifetime. The importance of the overlap of the lineshape of the NO transition and the bandwidth of the excitation laser has been discussed[2] previously. In this work, the Doppler width of the NO transition is comparable to the laser bandwidth and the overlap integral must be explicitly evaluated. For our conditions, the overlap integral varies from 0.85 at 300K to 0.55 at 2500 K. We find that the LIF signal strength from NO A-X $Q_1(16.5)$ varies by a factor of 15 over the temperature range 300-2000K providing a good thermometer. With the flame extinguished we calibrate the NO one-line signal intensity from a 300 K cold gas flow. We find the temperatures determined from one-line LIF measurements agree well with the OH LIF rotational scans except quite near the burner surface.

Two-line LIF measurements on the seeded NO can be used to determine the temperature from a ratio of the fluorescence intensity from two different transitions, avoiding many of the accuracy and calibration difficulties of absolute intensity measurement methods. Fig. 3 shows two-line excitation scans at several heights above the burner on the $O_{12}(1.5)$ and $O_{12}(19.5)$ transitions, as well as the variation of the signal intensity for these transitions as a function of temperature. We find these two lines provide a quite sensitive thermometer between 300 and 1000 K and an adequate thermometer between 1000 and 3000 K. These two transitions are only 0.005 nm apart and thus the excitation scan time is quite short. Fig. 3 shows the good agreement between two-line NO temperatures and the OH rotational scan temperatures in this low-pressure flame.

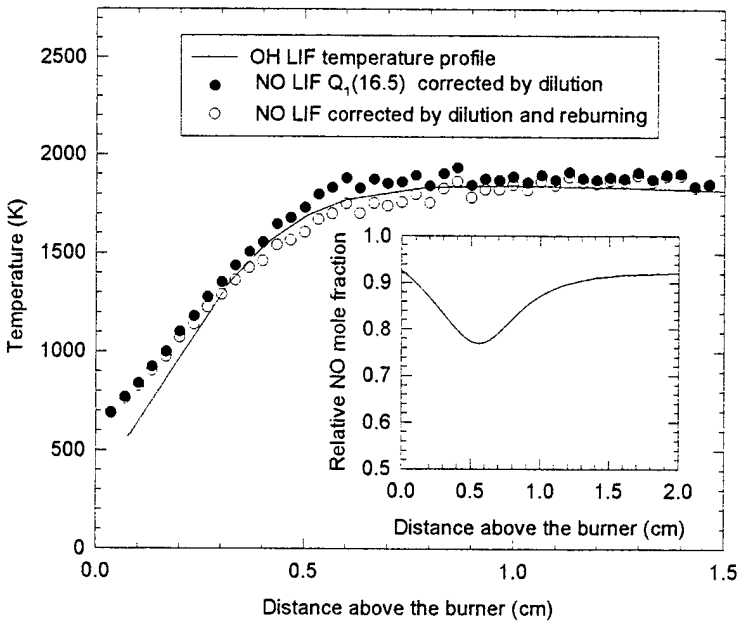

Figure 2. One-line NO A-X $Q_1(16.5)$ LIF flame termperature profile. Enclosed window: NO mole fraction in the flame predicted by the model calculation.

We find good agreement between LIF temperature measurements in OH (A-X), CH (A-X), CH (B-X), and seeded NO one and two-line measurements. One line temperatures measurements require modeling the NO reburning.

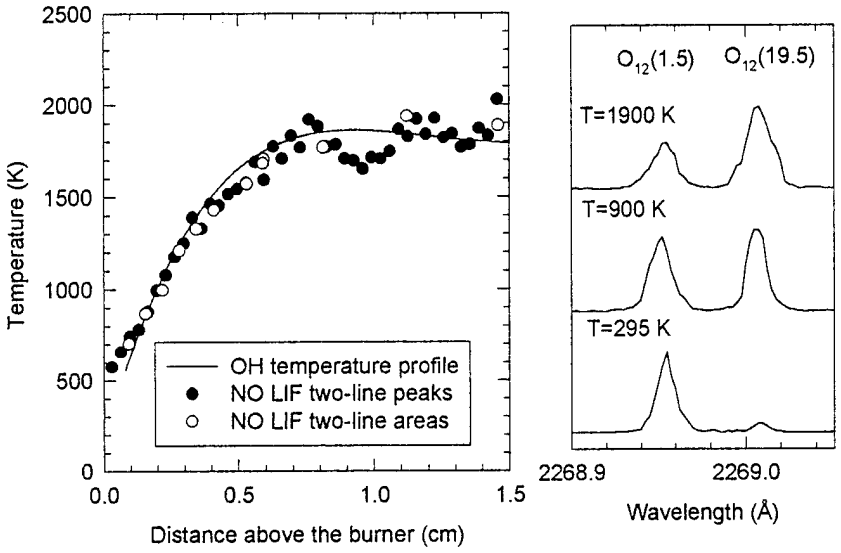

Figure 3. Left: Comparison of OH LIF temperature profile in 25 Torr flame with two-line NO LIF temperatures determined from either areas or peaks. Right: Two-line NO excitation spectra in 25 Torr flame for three different temperatures.

This work was sponsored by the New Energy and Industrial Technology Development Organization (NEDO) by the New Industrial Furnaces of Higher Thermal Efficiency project, through the Tokyo Gas Co., Ltd.

References:

1. J. M. Seitzmann, G. Kychahoff, and R. K. Hanson, Opt. Lett. **10**, 439 (1985).
2. M. P. Lee, B. K. McMillin, and R. K. Hanson, Appl. Opt. **32**, 5379 (1993).
3. K. J. Rensberger, J. B. Jeffries, R. A. Copeland, K. Kohse-Hoinghaus, M. L. Wise, and D. R. Crosley, Appl. Opt. **28**, 3556 (1989).
4. D. R. Crosley and J. B. Jeffries, "Temperature Measurements by Laser-Induced Fluorescence of the Hydroxyl Radical," in **Temperature: Its Measurement and Control in Science and Industry,** Vol. 6, J. F. Schooley, Ed., American Institute of Physics, NY (1992), p. 701.
5. K. Kohse-Hoinghaus, J. B. Jeffries, R. A. Copeland, G. P. Smith, and D. R. Crosley, 22d Symposium (Int) of Combustion, The Combustion Institute, Pittsburgh, PA, 1988, p. 1857.
6. D. E. Heard, J. B. Jeffries, G. P. Smith, and D. R. Crosley, Comb. and Flame, **88**, 137 (1992).
7. U. Westblom, F. Fernandez-Alonso, C. R. Mahon, G. P. Smith, J. B. Jeffries, and D. R. Crosley, Comb. and Flame, **99**, 261 (1994).
8. I. L. Chidsey and D. R. Crosley, J. Quant. Spectrosc. and Radiat. Trans. **23**, 187 (1980).
9. J. Luque and D. R. Crosley, to be published.

High Resolution Visible Laser Spectroscopy of Molecular Ions

Q. Tu, V. I. Harvey, R. W. Marawar and John W. Farley
Department of Physics, University of Nevada, Las Vegas
4505 S. Maryland Parkway
Las Vegas, NV 89154- 4002
Phone : (702) 895 - 3084
Fax : (702) 895 - 0804

Molecular ions have posed a formidable challenge to spectroscopists due to the difficulty in generating sufficient concentrations of ions to produce a detectable signal. The high chemical reactivity of molecular ions and the mutual Coulomb repulsion of like charges result in small densities of ions, whose signal can be masked by larger densities of neutrals. For a long time spectroscopic information was limited to observations in optical emission. In the last two decades, spectroscopists have developed new techniques to study molecular ions[1,2].

Many of the previous spectroscopic measurements of molecular ions have been Doppler-limited in resolution. Oka[1], Saykally[1], and others have performed infrared spectroscopy of ions in a velocity-modulated discharge. The laser-induced fluorescence (LIF) technique has been used for those ions having an allowed electronic transition.

In the present work, we demonstrate a sub-Doppler technique on the heavily studied molecular ion N_2^+, which has been chosen as a benchmark. Our experimental technique uses an ion beam and a single mode cw dye laser in a coaxial geometry. A kinematic velocity-bunching effect[3] results in sub-Doppler resolution. This is one of the very few single-photon sub-Doppler spectroscopic techniques.

The ion beam arrangement also has many advantages over the commonly used discharge tube. Besides the narrow (sub-Doppler) linewidth, the ion beam apparatus can also distinguish the spectrum of different ions using the Doppler shift between the lab frame and the ion rest frame. Since the speed of the ions in the interaction region depends on the ion mass and charge, the Doppler shift of the resonant frequencies also depends on the ion mass and charge. Measuring the spectrum at different in beam energies allows determination of the mass of the spectral carrier. This difference is important because in a discharge tube there is no direct way to distinguish between masses and hence the assignment of the mass of the spectral carrier can be complicated and sometimes nearly impossible.

The schematic of the apparatus is shown in Figure 1. A 6-inch diffusion pump produces a background pressure of 2 x 10^{-6} Torr in the chamber. A hot cathode, high pressure discharge source is used to generate N_2^+ ions. An electrostatic lens system coupled with electrostatic quadrupole beam benders is employed to extract the ions from the discharge source and transport them through the interaction region. The interaction region is a 7 cm long equipotential tube with 1 mm apertures at each end. The kinetic energy of the ions in the tube is determined by the potential difference between the tube and the anode of the ion source. The ions are collected in a Faraday cup and the ion current is measured with an electrometer. A typical ion current is 200 nA to 400 nA.

An actively stabilized Coherent CR-699-21 ring dye laser with Kiton Red dye is used. Typical laser output power was 300 mW. About 80% of the laser power entering the apparatus interacts with the ions. The wavelength of the laser is measured using a Burleigh wavemeter. The resonances are detected by allowing the ion beam to collide with the buffer gas and detecting the surviving ion beam current. Because the collisional cross-section depends on the internal state of the ion, the surviving ion beam current changes when the laser frequency is resonant with the ions. The laser beam is chopped at 1 kHz and a lock-in amplifier referenced to the chopper is used to demodulate the signal from the electrometer.

There resonances can be obtained either by varying the laser frequency or by fixing the laser frequency and varying the voltage on the equipotential tube. Typical data is shown in Figure 2. With a calculated differential Doppler shift of about 54 MHz/V, the linewidth can be deduced to be 150 MHz. The best previous measurement of the A←X system of N_2^+, performed by Miller et al.[4] using LIF, had a linewidth of 2 GHz. In the present work, we have improved the resolution by an order of magnitude, obtaining a typical linewidth of 100 - 150 MHz. We have thus resolved many A←X transitions that were previously unresolved or partially resolved[5].

In conclusion, we have demonstrated a flexible technique that has been used to perform high resolution spectroscopy. The technique is broadly applicable to a range of problems in chemical and environmental analysis. The frequency resolution of 0.2 ppm is 10-20 times better than that obtained by conventional Doppler-limited spectroscopic techniques. The collisional detection technique is generally applicable to molecular ions. Our first experiments were performed on the benchmark ion N_2^+, but the technique may be easily extended

to a variety of species by simply choosing an appropriate dye and performing modifications to the discharge source.

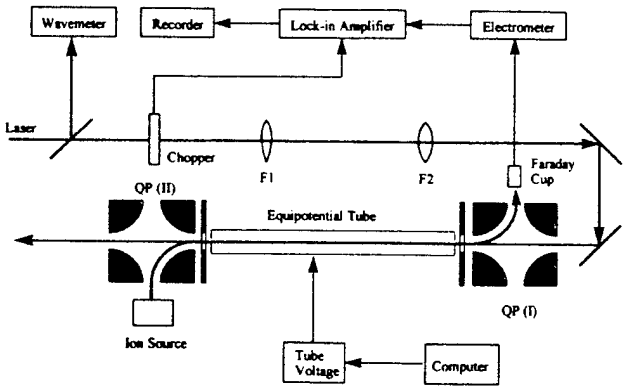

Figure 1: Schematic of the apparatus

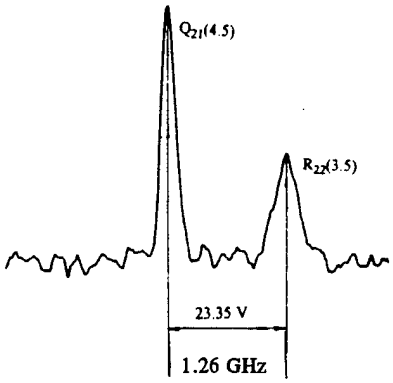

ν_{lab}= 16365.06 cm^{-1}

Figure 2: Resonant Signals

References:

1. Molecular Ions: Spectroscopy, Structure and Chemistry, edited by T. A. Miller and V. E. Bondybey (North-Holland, Amsterdam, 1983)

2. R. J. Saykally and R. C. Woods, Annu. Rev. Phys. Chem. **32**,403 (1981)

3. M. Al-Za'al, H. C. Miller, and John W. Farley, Phys. Rev. A 35, 1099 (1987)

4. T. A. Miller, Tetsuo Suzuki and Eizi Hirota, J. Chem. Phys. 80(10), 4671 (1984)

5. Qiang Tu, A dissertation submitted in partial fulfillment of the requirements for the degree of Doctor of Philosophy (Physics), University of Nevada, Las Vegas (1995)

Effects of Valence Electron Shell Structure on Ion Beam Sputtered Neutrals

Chun He

Molecular Physics Laboratory, SRI International, Menlo Park, CA 94025,

Phone: (415)859-4686; Fax: (415)859-6196

Z. Postawa

Institute of Physics, Jagellonian University, 30-059 Krakow, ul. Reymonta 4, Poland,

S. Rosencrance, R. Chatterjee, D. E. Reiderer, B. J. Garrison and N. Winograd

Department of Chemistry, The Pennsylvania State University, University Park, PA 16802

Energetic ion impact on a solid initiates a complex dynamical chain of events which include atomic motion, electronic excitation, ionization, and desorption of atomic and molecular species. Measurements on the desorbed particles during the ion-solid interaction process provide a valuable opportunity to understand the ion-solid interactions.[1-2] For more than three decade, research has been focused on understanding the formation of electronic excited states subsequent to ion bombardment in order to establish the role of inelastic energy transfer on ionization and sputtering yield[2]. The widely accepted conclusion is that the rate of relaxation is determined by the energy gap between the excited and ground state, i.e., the larger the magnitude of the excitation energy the more rapid relaxation of the electronic excitation.

We report experiments on Ni atoms ejected from a Ni{001} single crystal due to 5 keV Ar ion bombardment. The measurements are electronic state-selected, kinetic energy and angle-resolved. The ejected Ni atoms are selectively ionized from fine structure states a^3F_J (J = 4,3,2) and a^3D_J (J = 3,2,1) which have valence electron configuration of $3d^84s^2$ and $3d^94s^1$, respectively. Nickel atoms ionized from the closed s-shell states a^3F_4, and a^3F_3 show a general profile predicted by an analytical model[3], indicating the interactions between nuclei and the solid crystal are mainly responsible for the observed angular anisotropy. Nickel atoms ionized from the open s-shell states a^3D_3 and a^3D_2 also show a distinctly different distribution. However there is a clear evidence that valence electron shell structure is an important factor in determine the angle-integrated kinetic energy distribution while the magnitude of the excitation energy seems to be less significant.

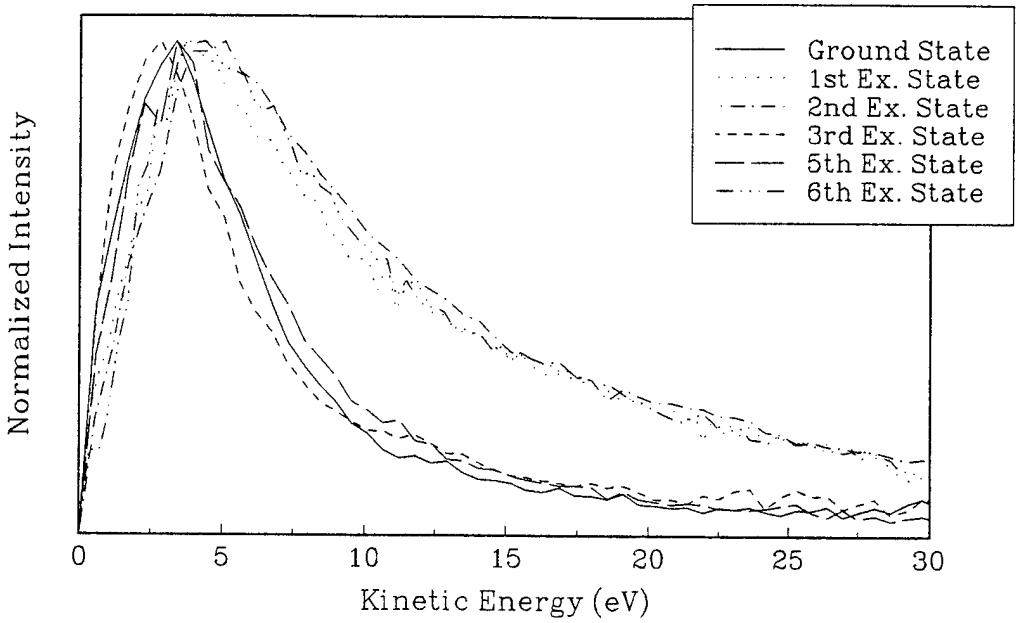

Fig. 1 Angle-integrated energy distributions of the measured Ni atoms in the six metastable states which belong to the closed *s*-shell structure, a^3F_4 (ground state), a^3F_3 (third-excited state, 0.165 eV) a^3F_1 (fifth-excited state, 0.275 eV), and to the open *d*-shell structure, a^3D_3 (first-excited state, 0.025 eV), a^3D_2,(second-excited state, 0.109 eV) and a^1D_2 (sixth-excited state, 0.422 eV), for the <100> azimuthal direction.

The kinetic energy distributions of the measured Ni atoms in the metastable, open *s*-shell states a^3D_3, and a^3D_2, and closed *s*-shell states a^3F_4, and a^3F_3, are presented in Fig. 1 for the <100> azimuthal direction. From these plots it is immediately evident that the velocity distributions of Ni atoms from different electronic states with different excitation energies but the same electronic shell structure, look similar. Velocity distributions of Ni atoms with different electron-shell structures are remarkably different, even when they have almost similar excitation energies. The kinetic energy distributions along the <110> azimuth show the same character as those along the <100> direction.

There are two important, and quite different features between these two groups of states. First, the velocity distributions from a closed *s*-shell are all peaked at the same value of 3.2 eV, which is about 1 eV smaller than whose from the open *s*-shell structure, all of which are peaked at

4.4 eV. In the language of Thompson,[3]the open *s*-shell states have a larger effective "surface binding energy". The result is consistent with the electron shell structure model proposed earlier[4]. These atoms are effectively shielded by the filled *s*-orbital and do not interact as strongly with the metal electrons while departing from the surface. That is, the effective surface binding energy is smaller for atoms having a closed outer shell orbital and is larger for atoms having an open outer shell orbital. Secondly, the atoms ejected from states of open *s*-shell configuration have broader kinetic energy distributions than those from states of closed *s*-shell configuration. As these plots are all normalized to their peak intensities, and the ejected particles of high kinetic energy are less likely to be influenced from the interaction with the surface, this observation implies excited Ni atoms with an open *s*-shell electron configuration are more likely to de-excite than atoms with a closed *s*-shell configuration.

In summary, we have performed quantum-state specific, angle- and energy-resolved study of Ni atoms sputtered from 5 keV Ar ion bombarded Ni{001}. Angular distributions of excited state Ni atoms show basically the same angular anisotropy regardless of their excitation energy and electron configuration, indicating the interactions between nuclei and the solid crystal are mainly responsible for the observed angular anisotropy. However there is a clear evidence that valence electron shell structure is the dominant factor in determine the angle-integrated kinetic energy distribution while the potential energy effect is of secondary importance.

References

[1]. W. O. Hofer, Topics in Appl. Phys. 64, 15 (1991).

[2]. M. L. Yu, Topics in Appl. Phys. 64, 91 (1991).

[3]. M. W. Thompson, Philos. Mag., 18, 377 (1968).

[4]. B. I. Craig, J. P. Baxter, J. Singh, G. A. Schick, P. H. Kobrin, B. J. Garrison, and N. Winograd, Phys. Rev. Lett., 57, 1351 (1986).

Factors Affecting Detection Sensitivities of Sputtered Neutrals Using Ultra-High Intensity Laser Post-Ionization

Michael L. Wise and Stephen W. Downey
AT&T Bell Laboratories
600 Mountain Ave.
Murray Hill, NJ 07974
(908)582-3727 FAX (908)582-3609

Ultra high intensity post ionization mass spectrometry combines many positive features of secondary ionization mass spectrometry (SIMS) and sputtered neutral mass spectrometry (SNMS). All of these techniques use ion beam sputtering to sample the material or structure in question, affording both depth profiling and surface analysis with excellent depth resolution. Post-ionization is one form of SNMS, using a laser to photoionize sputtered atoms and is relatively free from SIMS-type matrix effects. The main question of ultra high intensity post ionization is can most or all elements be detected with nearly equal efficiency? If so, then no standards are required for quantitative analysis. The ratio of signals would be equal to the ratio of elemental concentrations. By contrast, SIMS requires a standard for each analyte determined in each matrix present in the sample because ionization yields vary by many orders of magnitude. Ideally, ultra high intensity post-ionization(1) detects all species similarly with one set of laser conditions, including electronically excited atoms or molecules. Other forms of SNMS detect neutrals with varying efficiency (electron impact) or require different laser parameters (like resonant post-ionization) for multi element detection. This paper will address the sputtering of the sample, which determines the species to be ionized. The partitioning into atoms, molecules or ions strongly affects the uniformity of detection efficiency.

The post-ionization laser system is capable of delivering focused intensities of greater than 10^{14} W/cm^2 to the ionization source of a magnetic sector mass spectrometer. The laser is a regeneratively amplified Ti:sapphire system based on an argon-ion pumped, self mode-locked oscillator and a frequency doubled YAG pumped amplifier. The output pulses contain up to 1 mJ of energy in a pulse width of 100 - 150 fs and are focused to a diameter of about 50 μm. The pulse width is measured by a scanning Michelson interferometer type autocorrelator with 10 fs resolution. The laser pulses entering the chamber are synchronized with a pulsed, Xe^+ primary ion beam for sample sputtering. An ion pulse precedes a laser pulse by about 2 μs and is about 0.5 μs in duration. All the timing delays are set to maximize the laser beam/sample atom cloud overlap in space and time for greatest detected signal while minimizing sample erosion during data acquisition. Depth profiles consist of alternating cycles of continuous, sputtering for material removal and pulsed sputtering for static analysis of the crater bottom.

The samples analyzed are ion implanted standards so that the relative sensitivity of the implanted species to the matrix can be determined. Zn is

implanted (1 x 10^{15} /cm^2, 360 keV) into InP and $In_{0.4}Ga_{0.1}As_{0.3}P_{0.2}$ grown by organic metal vapor phase epitaxy (OMVPE) on InP. Si is implanted with a triple implant of Mg (1.5 x 10^{14} /cm^2, 140 keV), Cu (4.2 x 10^{13} /cm^2, 200 keV) and Al (1.25 x 10^{14} /cm^2, 170 keV). By comparing post-ionization signal ratios to the implant/matrix atomic concentration ratios, deviation from ideal uniform relative sensitivity factors, RSFs, will be highlighted.

Under the conditions used here, I >10^{14} W/cm^2, ionization proceeds by a prompt, tunneling mechanism(2) that is very dependent upon ionization potential. Zn is studied because it is an important p-type dopant in optical materials and it may be problematic to detect because it has a rather high ionization potential, 9.4 eV. Figure 1 shows a depth profile of ^{64}Zn and its relation to the bulk concentration of ^{113}In. The Zn concentration is determined from the known implant dose and the crater depth. The information about the RSF's for Zn and In are evident in the comparison between the known In and Zn concentration and their corresponding signals. In this case, excellent agreement between the atomic signals and atomic density is seen. Both species are detected with the same overall efficiency. Added confidence is given to these results because Rutherford backscattering verified that the In concentration in the sample is 40%. Another profile also confirms that the In/Ga UHIPI ratio is equivalent to their concentration ratio. Phosphorous was not detected with the same efficiency because of its high ionization potential (11 eV), requiring even higher intensity for completing the ionization. Also, more P is sputtered in molecular form.

Three factors affecting post-ionization atomic RSF's are molecular partitioning, velocity differences and element dependent volumes of ionization. Detecting the molecular fraction (or mutiply charged ions) requires mutiple mass monitoring. Velocity differences can be corrected for based on an assumption that if all species are sputtered with equal energies (E), then their velocities (V) scale as $m^{1/2}$ because E = 1/2 mV^2, where m is the mass. The velocity is important because detection of sputtered species by pulsed lasers constitutes a density detector if the atoms do not move significantly through the laser beam volume on the time scale of the laser pulse. Slight variations in the detection volume may exist between species due to differences in ionization potential or if any accidental resonances exist which bring the wings of the laser beam into play, increasing the effective beam size.

Figure 2 shows the depth profile of the triple implant (Al, Cu, and Mg) in Si. Cu and Mg exhibit the same RSF without any corrections. The Si and Al signals differ slightly than their predicted by the determined concentrations. No molecules were monitored, and recently we have determined that dopant-Si species are more abundant than previously thought.

In summary, post-ionization, has been used to depth profile dopant implants in Si and InP related materials. RSF's are very nearly equal for very different ionization potential elements sputtered from different matrices. This will be of crucial importance when post-ionization is applied to the characterization of sub micron devices and their defects where the ability to detect all elements with high and nearly equal efficiency will be key to their successful characterization.

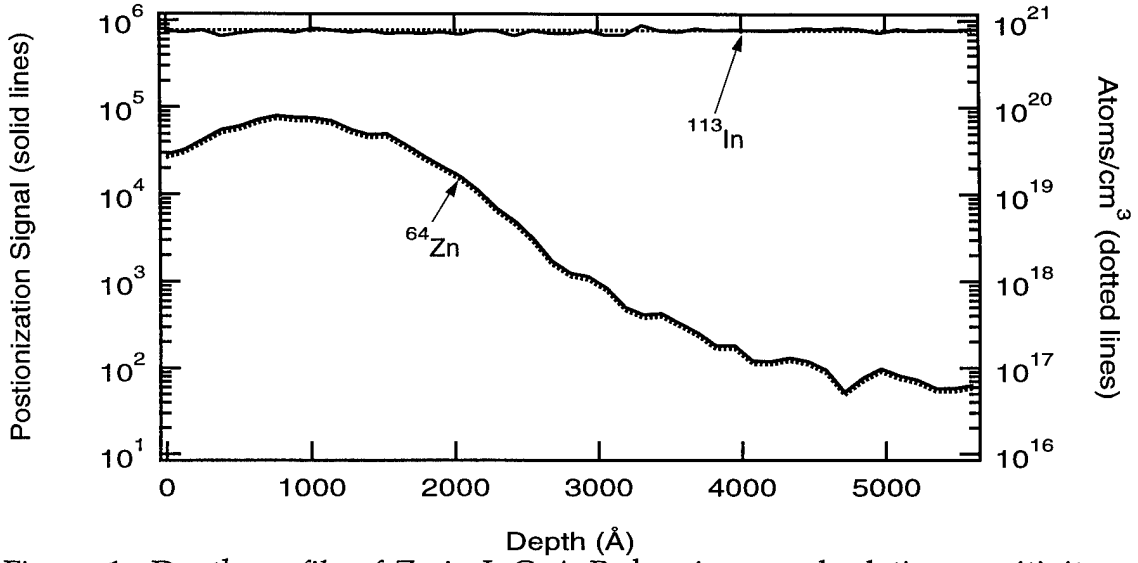

Figure 1. Depth profile of Zn in InGaAsP showing equal relative sensitivity for Zn and In.

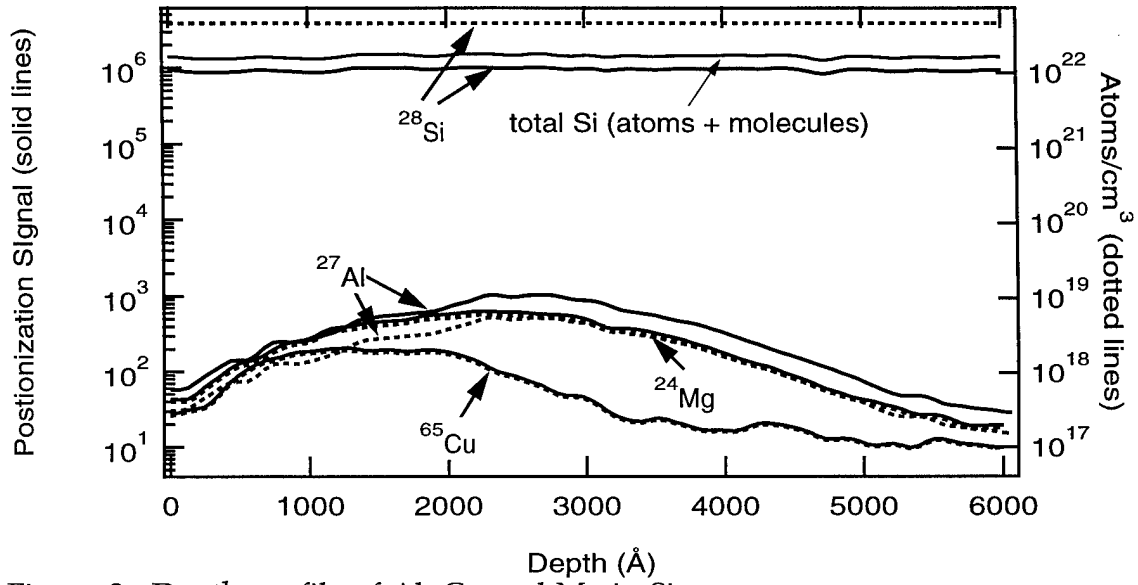

Figure 2. Depth profile of Al, Cu and Mg in Si.

1. M. J. Dyer, L. E. Jusinski, H. Helm and C. H. Becker, Appl. Surf. Sci, 52, 151 (1991).
2. P. Dietrich and P. B. Corkum, J. Chem. Phys., 97, 3187 (1992).

Resonant Laser Ablation Ion Trap Mass Spectrometry - Recent Applications for Chemical Analysis

Chris G. Gill, A. W. Garrett, P. H. Hemberger and N. S. Nogar
(505)665-4896 FAX(505)665-6023
Chemical Science and Technology Division, MS J565
Los Alamos National Laboratory
Los Alamos, NM 87545

Introduction

Resonant Laser Ablation (RLA) is a useful ionization process for selectively producing gas phase ions from a solid sample. Recent use of RLA for mass spectrometry by this group [1] and by others [2] has produced a wealth of knowledge and useful analytical techniques. The method relies upon the focusing of modest intensity laser pulses ($\leq 10^7$ W·cm^{-2}) upon a sample surface. A small quantity of material is vaporized, and atoms of desired analyte are subsequently ionized by (n+m) photon processes in the gas phase (where n = # of photons to a resonant transition and m = # of photons to exceed the ionization limit). We have been using (2+1) resonant ionization schemes for this work; a comprehensive list of (2+1) transitions used by this and other research groups has been published elsewhere [3].

Quadrupole ion trap mass spectrometry is realizing a very prominent role in current mass spectrometric research. Ion traps are versatile, powerful and extremely sensitive mass spectrometers, capable of a variety of ionization modes, MS^n type experiments, high mass ranges and high resolution, all for a fraction of the cost of other instrumentation with similar capabilities. Quadrupole ion traps are ideally suited to pulsed ionization sources such as laser ionization methods, since their normal operational method (Mass Selective Instability [4]) relies upon the storage of ions from a finite ionization period followed by ejection and detection of these ions based upon their mass to charge ratios.

2. Selective Ionization for Trace Atomic Analysis

As with all ion storage mass spectrometric methods, the effects of space charge are experienced when too many ions are created and subsequently stored by the mass analyzer. The effects of space charge upon ion traps include severely degraded resolution and even a total loss of meaningful analytical signal. For trace analysis, it is desirable to either store selected analytes, or to use a selective ionization scheme (i.e. RLA) for the desired analyte. Application of either or both of these methods allows elimination of unwanted matrix species ions from the ion storage volume, eliminating the effects of space charge. The selective nature of RLA is presented: no signal is observed for modest laser plulse energies(~20 μJ/pulse) unless the laser is tuned to a resonant transition for a component in the sample. The etch rate for RLA was determined (using 100 Å Copper films on Silicon wafers) to be 0.33 pg/shot. The RLA Pb(2+1) mass spectra for lead (26.5 ppm) in NIST sample # 494 (unalloyed copper) was readily obtained with significant ion signal for all naturally ocurring lead isotopes. Assuming that the etch rate is similar for thin film copper and bulk copper, this results in an absolute detection limit of ~9 attograms. This is a conservative value, since the signals observed for lead were much larger than the standard 3σ from the background typically used to calculate detection limits.

3. Selective Reagent Ion Source for Ion Chemistry Investigations

Mass spectrometric investigations of the gas phase chemistry of metal ions have been conducted as early as the 1970's. These early studies involved metal ion affinity investigations for simple compounds. This early work used thermionic emitters for metal ion production and FT-ICR mass spectrometers for reaction and product analysis. A recent review of gas phase metal ion chemistry [5] is given to which readers can refer for additional information.

The use of quadrupole ion trap mass spectrometers for metal ion chemistry can be traced back to Cooks and co-workers [6] who examined the chemistry of gold ions with benzene. Recent

quadrupole ion trap research by Brodbelt et.al. [7] used laser desorption to generate a variety of metal ions for gas phase ligand complexation investigations.

A variety of metal ion sources have been used for gas phase ion chemistry studies. Alkali metals are readily generated via thermionic emission sources, and various metal carbonyls can be reduced by electron impact to yield naked metal ions. An alternate mode for creating gas phase metal ions is through laser ablation of pure metal and mixed metal samples within the mass spectrometer. A potential deficiency of any of these methods arises when the researcher wants to compare reactivities of different metal ions with the same chemical system(s). Previous work with pure metal ion sources required that the metal source be changed; this often involving in the temporary corruption of the high vacuum environment, and leading to altered though similar conditions after the change. Alternately, if a mixed metal source was used, the reactions due to the various reactants had to be sorted out simultaneously, potentially leading to very complex chemistry.

Research in this laboratory has been directed at using Resonant Laser Ablation (RLA) as a means of selectively creating different types of ions from a multicomponent sample. This work demonstrates an alternative strategy for the investigation of the gas phase ion chemistry of a variety of metal ions under identical chemical conditions, since all ions investigated can be created selectively from the same sample by simply tuning the ablation (dye) laser to the appropriate "2+1" transition for the desired metal ion. This method is not only simple to implement, but allows rapid changes between different types of metal ions without disruption of the vacuum environment or altering sample geometry.

For a test system, we chose the reaction of several first-row transition elements (Cr^+, Fe^+, Ni^+ and Cu^+) with acetone. This reaction system, and similar reactions with other aldehydes and ketones, has been studied previously,[8] and serves as a convenient test to benchmark this technique. Figure 2 shows the observed trends for the various metal ions reactivity with acetone.

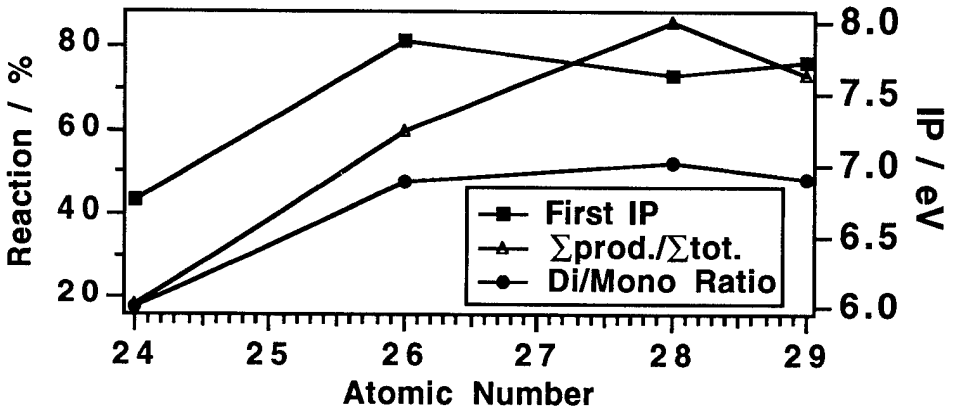

Figure 2: Reactivity trends for first row transition metals with acetone.

The results of this study show an increase in reactivity (ΣProducts / ΣTotal) as the ionization potential of the specific metal reagent ion increases, for both mono- and bi-adduct formation. This observation is consistent with the findings of other researchers [9], who conclude that the IP of gas phase metal ions is directly related to their observed gas phase reactivity.

4. Transition Metal CI for "difficult" Environmental Contaminants

The structure of certain chemical compounds makes "fingerprint" analysis difficult. The tri-butyl ester of phosphoric acid (TBP), is used as both a plasticizing agent and as a metal complexation agent for actinide chemistry. Environmental contamination by TBP is difficult to diagnose: TBP has low volatility, is thermally unstable, does not absorb in the visible spectrum, and gives predominately low mass fragments by electron impact ionization. In efforts to alleviate the difficulties associated with TBP analysis, it's gas phase ion chemistry with first row transition metal ions (Cr^+, Fe^+, Ni^+, Cu^+) was examined. Both iron and nickel ions yield TBP adducts that

lose 2 hydrogens, whereas chromium and copper form direct condensation products. Similar results have been reported for metal ion reactions with ketones, the differing reaction products explained by d electron configurations. The metal ion CI mass spectra are relatively simple, with large ion signals observed for the parent adduct species. The characteristic isotopic patterns for the metal ions in question confirm that the observed adduct species are indeed metal containing products.

Further investigations involving trace quantities of TBP upon a sample insertion probe for RLA/LD type experiments proved difficult: the TBP adduct signals rapidly decay upon probe insertion into the mass spectrometer. It is assumed that the TBP simply evaporates from the probe, with no direct laser desorption observed. To solve the volatility problem, a modified zeolite sample (containing silver) was prepared. This material was head space equilibrated with a small amount of TBP (gas phase interaction); subsequent analysis of the zeolite by using Ag(2+1) RLA @ 469.84 nm resulted in a mass spectrum (Figure 2), which shows ion signals for $Ag(TBP)^+$, as well as the loss of one, two and three butyl groups.

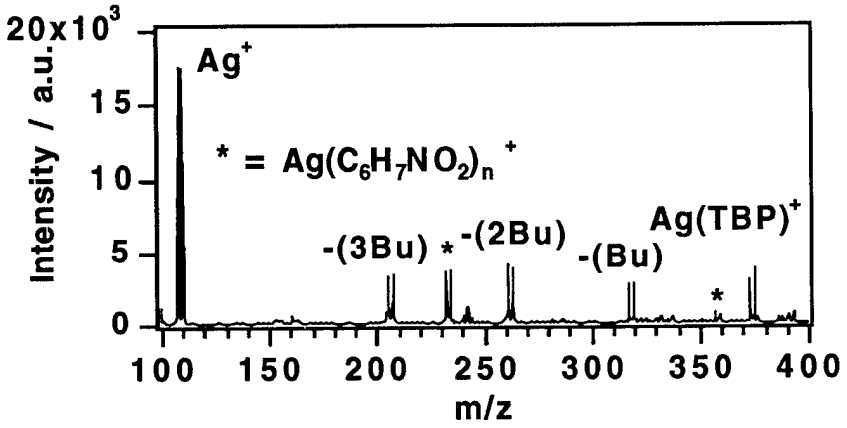

Figure 2: The Ag(2+1) RLA mass spectrum for a silver modified zeolite equilibrated with TBP headspace vapors. The zeolite was mounted on a type 304L Stainless steel probe with Ethyl-Cyanoacrylate Glue.

The characteristic doublet isotopic distribution for silver ($^{107}Ag = 0.5184$, $^{109}Ag = 0.4816$) is observed for all the TBP condensation products, as well as for adducts that originate from the ethyl-cyanoacrylate (super glue) used to mount the zeolites to the probe. The origins of the fragmentation of the TBP are under investigation, as they may be from catalytic cracking by the zeolite or from decomposition during the RLA process. Current research includes the use of these modified zeolite sorbents for environmental measurements, as well as direct approaches to the analysis of TBP in environmental samples.

5. References

1. Eiden, G.C., Anderson, J.E. & Nogar, N.S. *Microchem. J.* **50**, 289-300 (1994).
2. Borthwick, I.S., Ledingham, K.W.D. & Singhal, R.P. *Spectrochim. Acta* **47B**, 1259-65 (1992).
3. Gill, C.G., Allen, T.M., Anderson, J.E., Taylor, T.N., Kelley, P.B., Nogar, N.S. *Appl. Opt.* **submitted** (1995).
4. Stafford, G.C., Jr. , P.E.K., Syka, J.E.P., Reynolds, W.E. & Todd, J.F.J. *Int. J. Mass Spectrom. Ion Processes* **60**, 85-98 (1984).
5. Teesch, L.M. & Adams, J. *Org. Mass Spectrom.* **27**, 931-43 (1992).
6. Louris, J.N., Brodbelt-Lustig, J.S., Kaiser, R.E. & Cooks, R.G. in *36th ASMS Conference on Mass Spectrometry and Allied Topics* 968 (San Francisco, CA, 1988).
7. Wu, H.F. & Brodbelt, J.S. *J. Am. Chem. Soc.* **116**, 6418 (1994).
8. Burnier, R.C., Byrd, G.D. & Freiser, B.S. *J. Am. Chem. Soc.* **103**, 4360-7 (1981).
9. Allison, J. & Ridge, D.P. *J. Am. Chem. Soc.* **101**, 4998-5009 (1979).

Particle Sizing From Multi-Wavelength Frequency Domain Measurements of Photon Migration

Joseph E. Pierce and Eva M. Sevick-Muraca
Purdue University, School of Chemical Engineering
West Lafayette, IN 47907-1283
Phone: (317) 496-2739 Fax: (317) 494-0805

Introduction

Particle density and size distribution are critical process parameters in many of today's industrial processes that involve dispersed phase process streams. For example, granulation, crystallization, emulsion polymerization, and liquid-liquid extraction lack the appropriate monitoring techniques to facilitate process control and optimization. Optical sensors involving dynamic light scattering, turbidity, and backscatter have been proposed in the past. Yet these optical sensors are restricted to process streams that are either relatively non-scattering by industry standards, or require calibration to the process streams which they are intended to monitor. The latter is especially detrimental for successful implementation of optical sensors in the chemical based industries. When process disturbances occur, the optical sensor is intended to provide important and accurate information to the controller for corrective action. If the calibration of the sensor is invalidated due to changing process stream composition (as might happen during process disturbances), then the accuracy of the feedback signal may cause catastrophic results if actuation is based upon it. Thus, a robust, self-calibrating optical sensor is required for optimization of many processes in the chemical-based industries.

To date, there is no dependable, self calibrating method for on-line measurement of particle or dispersed phase size distribution. Most size determining techniques require time consuming off-line analysis, which does not allow for direct monitoring of process conditions and timely feedback for process control and optimization. Thus, it is desirable to develop a technique to measure these parameters in *real-time* and *on-line* in order to provide improved process and quality control. Frequency domain measurements of photon migration provide the necessary information to determine particle size distribution on-line. Such techniques are non-invasive, and are self-calibrating and can be made in real time. In this work,we demonstrate frequency-domain measurements in polystyrene and lipid emulsion concentrated suspensions.

Method of Approach: Frequency-domain measurements

Instead of monitoring the *amount* of light backscattered or transmitted through a process stream, we monitor the *time-dependent* light propagation characteristics. Light whose intensity is sinusoidally modulated at megahertz frequencies is launched into the process stream or sample via fiber optics. The re-emitted light is phase-shifted and amplitude-demodulated with respect to the incident light due to its propagation through the dense, highly scattering medium. From measurements of this phase shift and amplitude demodulation, the optical properties of the medium (i.e. scattering and absorbtion coefficients) can be determined.

Gratton *et al.*[1] have shown that the relative phase-shift (i.e. phase-shift at source detector separation, r, minus the phase-shift at source detector separation, r_o) in an infinite medium is given by

$$\theta_{rel} = \theta(r) - \theta(r_o) = (r - r_o)\left(\frac{c^2\mu_a^2+\omega^2}{c^2D^2}\right)\sin\left[\frac{1}{2}\tan^{-1}\left(\frac{\omega}{c\mu_a}\right)\right] \qquad (1)$$

where D is the optical diffusion coefficient given by

$$D = \frac{1}{3(\mu_a + \mu_s')}$$

Here, $\theta(r)$ is the measured phase shift (radians) ; c is the speed of light in the medium (cm/s); μ_s' is the isotropic scattering coefficient (cm^{-1}); and μ_a is an absorption coefficient (cm^{-1}) due to light absorping chromophores.

For our studies of polystyrene and intralipid solutions, the absorption coefficient is small and equation (1) can be simplified to:

$$\theta_{rel} = (r - r_o)\left(\frac{1}{\sqrt{2}}\right)\left(\frac{3\omega\mu_s'}{v}\right)^{1/2} \qquad (2)$$

Inspection of equation (2) shows a linear relationship between relative phase-shift, θ_{rel}, and modulation frequency to the one half power, $\omega^{1/2}$. Thus, by taking measurements of phase-shift at multiple source-detector separations and multiple modulation frequencies, the effective scattering coefficient, μ_s', can be determined from the linear slope of θ_{rel} vs. $\omega^{1/2}$.

Experimental measurements of phase-shift in optically dense media

Experimental measurements of phase-shift and amplitude demodulation were conducted using the system illustrated in Figure 1. The source consists of a Ti:Sapphire laser (Spectra Physics, CA) operating at a repetition

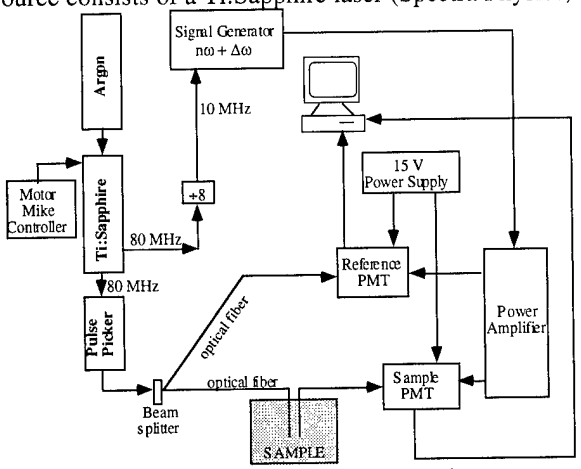

Figure 1. Ti:Saphire frequency domain system

rate of 4 Mhz. The solid state laser provides wavelength ranges from 750 - 1000 nm and 325 - 500 nm when a frequency doubling crystal is employed. The average power is approximately 20 mW. A glass slide beam splitter reflects <1% of the pulse train which is collected by an optical fiber and detected at the reference PMT. The unreflected pulse train is directed into the sample by a 1000 mm optical fiber which was held in place vertically in a cylindrical tank (9 in. o.d.). The re-emitted light was collected using another fiber and was detected at the sample PMT. The PMTs are gain modulated at a harmonic frequency of the laser repitition rate plus an offset cross correlation frequency of 100 Hz. A commercial electronics package and data acquisition modules (ISS, Champaign, IL) were used to report the phase-shift of the re-emitted light relative to the incident light as a function of modulation frequency.

Optically dense samples monitored with measurement of phase-shift

Lipid emulsions: Lipid emulsions (Intralipid, Kabi Pharmacia, Inc.) of 0.5, 1.0, and 1.5% by volume were evaluated at a wavelength of 780 nm. Figure 2a shows that measurements of phase-shift versus $\omega^{1/2}$ for a 1.5% Intralipid solution results in a linear relationship as described by equation (2). Upon evaluating the slope, we obtain a scattering coefficient μ_s'=16.9 cm^{-1} which agrees with the value of μ_s'=15.9 cm^{-1} obtained from an independent experiment using integrating sphere measurements.

Polydisperse polystyrene suspensions Suspensions (1% by volume) were obtained from Dow Chemical[2] and studied at multiple wavelengths. Dynamic light scattering analysis provided estimations of the particle size distributions which were used to compute an isotropic scattering coefficient from Mie theory[3]. Figure 2(b) shows that for a 1% solution at at 782 nm, measurements of phase-shift vary linearly with $\omega^{1/2}$ as described by equation (2). Upon evaluating the slope, we obtain a scattering coefficient of μ_s'=36.1 cm^{-1}.

Table I illustrates the values of isotropic scattering coefficients as a function of wavelength determined from Mie theory with dynamic light scattering data and those computed from phase-shift measurements.

Table 1.Polydisperse polystyrene microspheres (1% by volume), mean particle diameter, D_p=0.553mm

Wavelength nm	Mie Theory μ_s' (cm^{-1})	Frequency Domain μ_s' (cm^{-1})
390	53.6	70.6
400	52.8	76.8
405	52.5	63.5
734	35.2	42.4
782	33.4	36.1
800	32.3	38.0

As illustrated in the table, the discrepancy between Mie theory and frequency-domain measurements is significant, especially at blue wavelengths where the assumption of negligible absorption may be questionable. In addition, the hydrodynamic particle size measurements from dynamic light scattering do not provide the same particle size for comparison. Nonetheless, the value of isotropic scattering coefficient obtained independently from time-domain measurements[4], (μ_s'=37.3 cm^{-1}); Mie theory and dynamic light scattering measurements[5] (μ_s'=33.7 cm^{-1}), and frequency-domain measurements (μ_s'=36.1 cm^{-1}) match well at 780 nm.

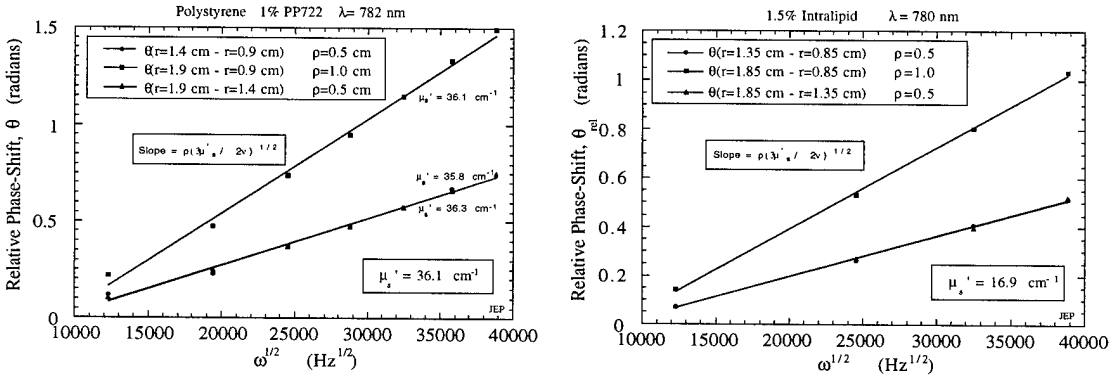

Fig. 2 a) 1.5% Intralipid emulsion b) 1.0% Dow latex polystyrene microspheres.

Determination of Particle Size Distribution:

Once phase-shift measurements have been analyzed to determine the experimental scattering coefficients at multiple wavelengths for a particular sample, the values can be used in an inverse algorithm developed by Jeff Kao. This inverse algorithm however, is ill-conditioned and requires regularization techniques, similar to that posed for turbidity measurements[6]. Preliminary computational work has shown that a given particle size distribution with added noise can be recovered through the inverse algorithm[7].

Acknowledgments:

This work is supported in part by the National Science Foundation Young Investigator award and the National Science Foundation Industrial/University Cooperative Research Center for Industrial Pharmacy.

References:

1. J.B. Fishkin, Peter T.C. So, A.E. Cerussi, S. Fantini, M. A. Franceschini, E.Gratton, Applied Optics, 34, n7, March 1995, 1143-1155.
2. Chuck McDonald, Dow Chemical Company, Midland Michigan.
3. Craig F. Bohren,Donald R. Huffman,Absorption and Scattering of Light by Small Particles,Wiley &Sons,1983
4. Jeff Y. Kao, School of Chemical Engineering, Purdue University, unpublished data
5. Steve Nail, School of Industrial Pharmacy, Purdue University
6. J.B. Rawlings, S. Miller, and W.R. Witkowski, Ind. Eng. Chem. Res., 1993, 32, 1275-1296.
7. Jeff Y. Kao, Eva M. Sevick, Particle Sizing Using Time-Domain Photon Migration Techniques, 1996 OSA presentation

Particle Sizing Using Time-Domain Techniques of Photon Migration

Jeffrey Kao and Eva Sevick-Muraca, Ph.D.
Department of Chemical Engineering
1283 Chemical Engineering Building
Purdue University
West Lafayette, IN 47907-1283
(317) 496-2739
Fax: (317) 494-0805

The objective of this research is to develop non-invasive, uncalibrated methods for measuring the particle size distributions within optically dense polydisperse media. Our work is subdivided into addressing two goals. First, we must measure isotropic scattering coefficients of polydisperse media and successfully compare them with values predicted by theory. Secondly, from multi-wavelength measurements of scattering coefficients, we must recover the particle size distribution. We describe these two steps as forward and inverse problems.

Background

When photons travel through a highly scattering medium, their movement becomes random. By approximating these photons as random walkers, their propagation can be described with a diffusion equation[1]:

$$\frac{1}{c}\frac{\partial}{\partial t}\phi(r,t) - D\nabla^2\phi(r,t) + \mu_a\phi(r,t) = 0 \qquad (1)$$

where c is the speed of light [length/time], ϕ is the fluence [photons/area/time], μ_a is the absorption coefficient [length^{-1}], μ_s is the scattering coefficient [length^{-1}], g is the anisotropy coefficient, and D is the optical diffusion coefficient [$1/D = 3(\mu_a + (1\text{-}g)\mu_s)$]. Assuming the zero fluence boundary condition, this differential equation can be solved for an impulse entering a transmittance geometry[1]:

$$\begin{aligned} I(t) = -D\nabla = (4\pi Dc)^{-3/2} t^{-5/2} \exp(-\mu_a ct - \frac{\rho^2}{4Dct}) \\ \times\{(d-z_0)\exp[-\frac{(d-z_0)^2}{4Dct}] - (d+z_0)\exp[-\frac{(d+z_0)^2}{4Dct}] \\ + (3d-z_0)\exp[-\frac{(3d-z_0)^2}{4Dct}] - (3d+z_0)\exp[-\frac{(3d+z_0)^2}{4Dct}]\} \end{aligned} \qquad (2)$$

where d is the sample width, and z_0 is mean scattering length [$1/z_0 = (1\text{-}g)\mu_s$]. The solution predicts that if an impulse is launched into a highly scattering medium, the light transmitted will be a broadened distribution depending on the optical properties of the medium.

Single Photon Counting Measurement of I(t)

In this work, single photon counting measurements were conducted to measure the broadened, re-emitted pulse of light. A Ti:Sapphire laser (Spectra Physics, CA) was used as the light source in this experiment. The solid state laser provides wavelength ranges from 750 - 1000 nm and 325 - 500 nm when a frequency doubling crystal is employed. Average powers were approximately 10 mW. Single photon events were detected via a R1894 Hamamatsu photomultiplier tube operated in photon counting mode. The instrument function of this system was approximately 0.7 ns and was convolved with the model described in Eqn (2) for the accurate regression of absorpton and isotropic scattering coefficients.

Figure 1a illustrates a typical re-emitted broadened pulse at 390 nm for a monodisperse

suspension of 0.780 micron polystyrene beads at a 0.5 vol. %. From Mie theory, the expected isotropic scattering coefficient should be 24 cm^{-1}. Regression to Eqn (2) convolved with the instrument function yields an isotropic scattering coefficient of 25 cm^{-1}. The solid line denotes the regression result.

Figure 1b shows the experimental broadened pulse at 780 nm for a bimodal ditribution containing 0.17 vol. % of 1.053 micron diameter polystyrene beads and 0.33 vol % of 0.202 micron diameter polystyrene beads. From Mie theory and the relationship:

$$(1-g)\mu_s = \frac{3Q_{scat}^{bead\#1}(\lambda,n,r_1)}{4r_1}\phi_1 + \frac{3Q_{scat}^{bead\#2}(\lambda,n,r_2)}{4r_2}\phi_2 \qquad (3)$$

where ϕ_i is the volume fraction of bead with radius r_i, $(1\text{-}g)\mu_s$ is the isotropic scattering coefficient for the mixture, andQ_{scat} is the Mie scattering efficiency the isotropic scattering coefficient was predicted to be 13 cm^{-1}. The regressed value which predicts the solid line was found to be 16 cm^{-1}. The discrepancy may be due to the assumption in Eqn (3) of independent scattering between the two particle sizes.

Figure 1a.

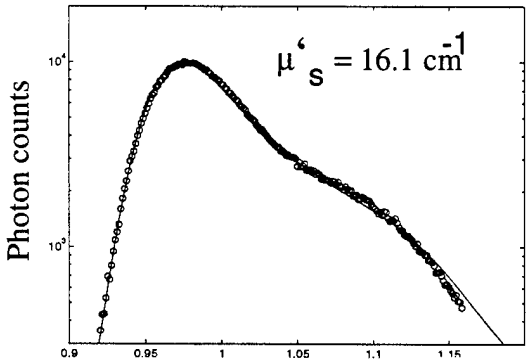

Figure 1b.

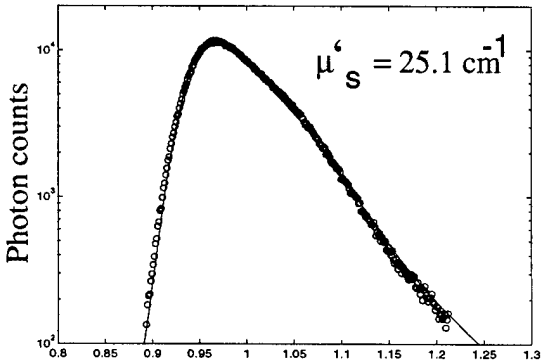

Inverse Problem of determining size distribution from isotropic scattering

Once measurements of isotropic scattering coeffficients are made at several wavelenghts, they must be used as inputs to an inverse solution. For a system of independent spherical scatterers with a distribution of sizes, the isotropic scattering coefficient can be discretized and given by:

$$\mu_s'(\lambda_i) = \sum_{j=1}^{N} \frac{3}{2}\Phi \frac{Q_{scat}(\lambda_i,x_j,n_i)}{x_j}[1-g(\lambda_i,x_j,n_i)]f(x_j)\Delta x \qquad (4)$$

where λ_i is the i^{th} wavelength, x_j is the j^{th} particle size, Φ is the total volume fraction of solids, Q_{scat} is the scattering efficiency (Mie theory), and f(x) is the differential volume fraction such that f(x)dx is the volume fraction of particles with diameter between x and x+dx. For multi-wavelength measurements, this summation can be recast into the matrix form

$$\underline{\mu} = \underline{\underline{B}}\underline{w} \qquad (5)$$

where the matrix μ represents the matrix of measurements made at several wavelengths, λ_i:

$$\mu_i = \mu_s'(\lambda_i)$$

and **B** is the scattering matrix computed for the given refractive index difference, a set of average

sizes, and experimental wavelength:

$$B_{ij} = \frac{3}{2}\frac{Q_{scat}(\lambda_i, x_j, n_i)}{x_j}[1 - g(\lambda_i, x_j, n_i)]\Delta x$$

The matrix **w** is the desired unknown and is the product of the total volume fraction of solids times the volumetric size fraction:

$$w_j = \Phi f(x_j)$$

To re-iterate, the vector μ contains experimentally measured quantities, the matrix **B** contains quantities which can be computed, and the vector **w** contains the desired unknowns. The recovery of the desired unknowns thus becomes a problem of inverting this matrix equation. Unfortunately, matrix **B** is usually, ill-conditioned, requiring optimization methods for this inversion.

Figure 2a shows a sample computation of the isotropic scattering coefficients for a 2.5 vol % polystyrene suspension. With Gaussian noise of 2 cm^{-1} added, the reconstruction using second-order Tikhanov regularization is shown in Figure 2b. The recovered volume fraction of solids is 0.027, matching the volume used in the forward solution. While Garcia-Rubio and coworkers[2] have similarly demonstrated reconstruction of particle size distribution from turbidity measurements, we demonstrate reconstruction from isotropic scattering coefficients made from self-calibrating measurements of photon migration.

Figure 2a.

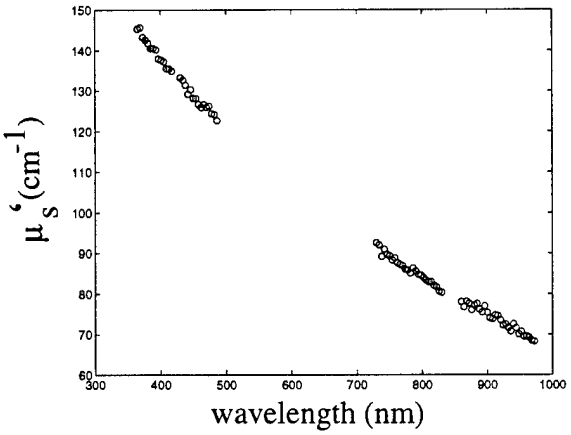

Figure 2b.

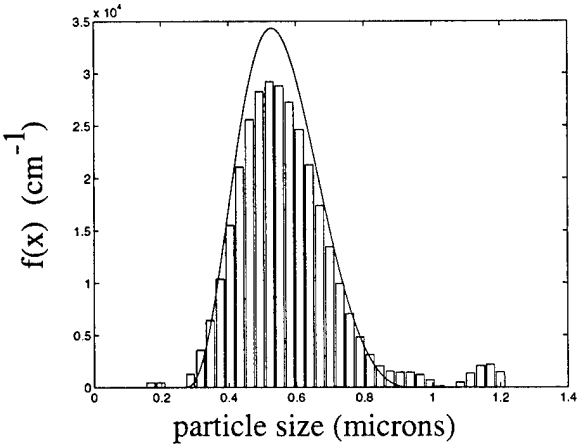

Acknowledgment:

This work was supported in part by the National Science Foundation Young Investigator Award and the University of Tennessee Measurements and Control Engineering Center.

References

1. Patterson, Michael S., B. Chance and B.C. Wilson. "Time resolved reflectance and transmittance for the non-invasive measurement of tissue optical properties." Applied Optics, v.28, n.12, p. 2331-2336 (June 15, 1989).

2. Eliçabe, Guillermo E. and Luis H. Garciá-Rubio. "Latex Particle Size Distribution from Turbidimetric Measurements." Adv. Chem. Series, vol. 227, ch. 6 (1990).

Mean Orientation Measurements of Fibrous Aerosols in Atmospheric Boundary Layer Turbulence

R. K. Newsom, C. W. Bruce, A. J. Jelinek, M. Thurston
New Mexico State University
Physics Department (3D)
Las Cruces, New Mexico 88003-0001
Email: mewsom@nmsu.edu
Fax: (505)646-1934
and
Army Research Laboratory
White Sands Missile Range, New Mexico 88002-5501

It is well known that thin axisymmetric particles such as fibers sedimenting in a quiescent medium with a Reynolds number of order unity ($R_e \approx 1$) will align their symmetry axes perpendicular to their fall direction. It is not clear to what extent this behavior remains in effect when the particle is subject to the randomizing forces imposed by turbulence. The goal of this research is to establish a firm connection between the degree of horizontal orientation of a large ensemble of fibers in the atmospheric boundary layer and the mean kinetic energy density associated with the turbulent motion of the air.
For the current experiment the mean orientation of the suspension is obtained from measurements of the extinction coefficients for two orthogonally polarized fields using a simple millimeter-wave transmissometer. Simultaneously, a sensitive hot wire anemometer measures fluctuations in the air velocity at a fixed point near the transmissometer measurement region. Turbulent energy spectra are computed from the hot wire data. The mean orientation of the suspension is then compared to the energy contained within a band limited region of the turbulent energy spectrum.

Fibers used in this experiment are composed of graphite and have lengths of about 3mm and diameters of about 10μm. The microwave source used in this experiment produces a 35GHz field, corresponding to a wavelength of about 8.7mm. For fiber lengths less than the half wavelength of the incident electric field, **E**, the extinction cross section varies approximately as the cosine squared of the angle between **E** and the fiber symmetry axis.[1] Since the fibers are moderately conducting much of the extinction is due to absorption. Multiple scattering effects are completely negligible.

Roughly speaking the Reynolds number, R_e, is a characteristic ratio of inertial to drag forces acting on a fluid particle in the vicinity of the fiber. As R_e increases from zero the time scale associated with the fiber's relaxation to a stable horizontal position decreases. For fibers considered in this study R_e is of order unity based on the fiber length as the characteristic dimension and a terminal fall speed of approximately 3cm/second as the characteristic flow speed. At these intermediate Reynolds numbers orientational effects may become significant under ordinary atmospheric flow conditions. Measurements of the mean orientation performed under quiescent laboratory conditions have confirmed that these same fibers display a high degree of horizontal orientation.[2]

Field measurements were performed at a test site located on the floor of a large, flat desert basin. The transmissometer was positioned 5 meters above the ground with a separation between transmitter and receiver of about 3 meters. Fibers were dispersed into the atmosphere approximately 20 to 50 meters upwind of the transmissometer. As the aerosol cloud drifts into the measurement region of the transmissometer a drop in the power output of two polarization sensitive receivers is registered. Figure 1 shows the result of one fairly typical field trial. This figure shows the variation in the extinction coefficients for horizontal and vertical polarizations as a function of time as the cloud drifts through the transmissometer.

For a given trial the average orientation is obtained from the microwave data by computing a point by point ratio between the extinction coefficients for horizontal and vertical polarizations. This ratio (referred to as the H/V ratio) is then averaged over that trial. If the azimuthal orientations of the fibers are assumed to be uniformly random then this ratio gives

$$\frac{\langle \cos^2 \theta \rangle}{\langle \sin^2 \theta \rangle},$$

where θ is the angle from the vertical direction.

One dimensional spatial frequency spectra were computed from the hot wire data by assuming Taylor's frozen field hypothesis. Under this assumption the time variation in the

velocity signal measured by the hot wire is related to the spatial variation of the velocity field by

$$k = \frac{\omega}{u_o}.$$

In this expression ω is the angular frequency of the fluctuating (temporal) velocity signal, u_o is the mean wind speed and k is the spatial frequency or wave number. The time variation of the velocity signal, $u(t)$, is transformed to a spatial variation by subtracting out the mean value, u_o, and using $x = u_o t$. The energy spectrum was computed using

$$E(k) = \frac{1}{2\pi u_o T}\left|\int_0^{u_o T} u(x)e^{ikx}dx\right|^2,$$

where T is the total time of the trial. Figure 2 shows a typical one dimensional spatial frequency energy spectrum. This spectrum corresponds to the same field trial as the transmissometer data shown in figure 1.

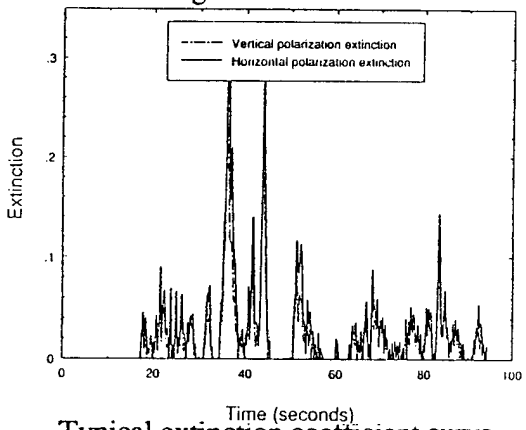

Figure 1 Typical extinction coefficient curve.

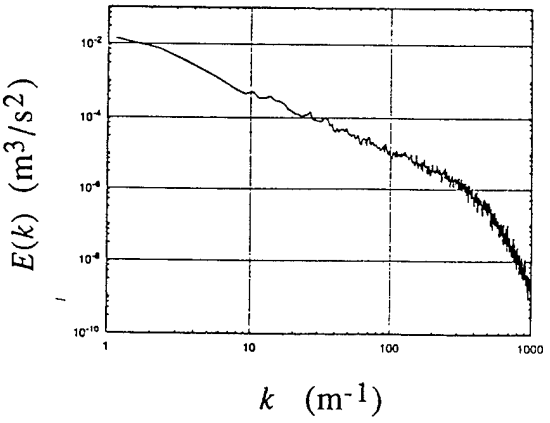

Figure 2 Typical turbulent energy spectra computed from the hot wire anemometer.

The turbulence spectra are integrated over a wave number band to give a quantity proportional to the mean fluctuational kinetic energy density contained within that wave

number band. The relevant wave number region is not well defined because the spectral response of the fibers' rotational motion is extremely broad. However, it appears that spatial frequencies significantly below $10m^{-1}$ play a small roll in the rotational motion of the fibers. Figure 3 shows the result of plotting the H/V ratio versus the energy spectrum integrated from $k=10m^{-1}$ to $k=500m^{-1}$ for a given trial.

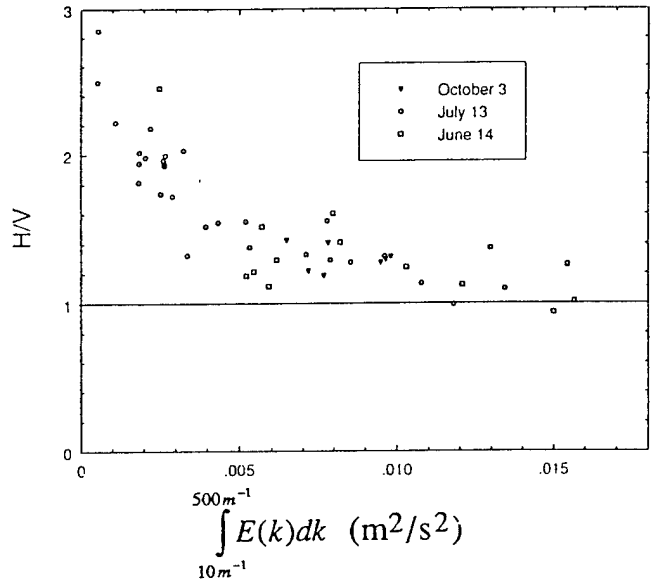

Figure 3 Experimental results showing degree of orientation versus "band-limited" mean fluctuational kinetic energy density.

Efforts are also under way to develop a model of the fiber dynamics that can be used to predict the optical properties of fibrous aerosols in turbulence. At this time the results of the modeling work are still in a preliminary stage. In addition, data reduction of field data using fibers of different lengths and diameters is currently under way. Thus it will be possible to compare tendency to orient under similar turbulence conditions to various fiber geometries.

References

1 K. P. Gurton and C. W. Bruce, "Parametric study of the absorption cross section for a moderately conducting thin cylinder", Appl. Optics **34** (15), 20 May 1995.

2 R. K. Newsom and C. W. Bruce, "Dynamics of fibrous aerosols in a quiescent atmosphere," Phys. Fluids **6** (2), February 1994.

Four Wave Mixing Diagnostics of Atmospheric Regions with an Excess of Charged Aerosol Concentration.

K.A.Boyarchuk, G.A.Lyakhov and Yu.P.Svirko

General Physics Institute, 38 Vavilova Street, Moscow 117942, Russia

Fax: +7 095 135 32 84. Tel: +7 095 143 26 60. E-mail: kirill@boy.gpi.ru

In this paper we address the phenomena of four-wave mixing and stimulated Brillouin scattering (SBS) in a medium containing free electric charges. Under SBS the hypersonic wave at the frequency of the Stokes shift Ω [1] gives rise to oscillation of the all particles of the medium near their equilibrium positions. In an electrically neutral medium equilibrium quantities of the positive and negative charged particles per unit volume are the same. However their mobilities are slightly different. Therefore, the magnitudes and phases of their oscillations near equilibrium positions are not equal to one another. This results in transient electric charge separation in acoustic field [2]. That is, under SBS the excitation of hypersonic wave in the medium with free electric charges leads to the generation of the electric charge density wave of the same frequency in the medium [3].

The presence of charge density oscillations in the medium with free electric charges allows us to influence the light scattering with *ac* electric field. In particular, the microwave field at the frequency of $F = \Omega/\pi$ gives rise to parametric coupling between counter-propagating hypersonic waves of the frequency Ω [3,4]. This results in the parametric excitation of the anti-Stokes light wave at the frequency $\omega_a = \omega + 2ku$ propagating in the same direction as the Stokes wave.

In the four-wave mixing geometry when the hypersonic wave of the frequency Ω is generated by two counter-propagated light waves at the frequencies ω and $\omega - \Omega$, the above mechanism permits the parametric excitation of the counter-propagated wave at the anti-Stokes frequency. This is the phenomenon of the microwave driven four-wave mixing. In this paper we discuss main features of this phenomenon. We suggest that the microwave driven four-wave mixing could be employed for remote sensing of atmospheric regions with an excess of charged aerosol concentration.

The interaction of the electric field $\boldsymbol{E}$ with isotropic medium may be described on the basis of the following equations [2,4]:

$$\frac{\partial \rho}{\partial t} + \nabla(\rho v) = 0 \qquad (1)$$

$$\rho\frac{\partial \boldsymbol{v}}{\partial t} + \rho(\boldsymbol{v}\nabla)\boldsymbol{v} = -\nabla p + \eta\nabla^2\boldsymbol{v} + \rho\frac{\partial \epsilon}{\partial \rho}\nabla\frac{\boldsymbol{E}^2}{8\pi} + q(N_+ - N_-)\boldsymbol{E} \tag{2}$$

$$\frac{\partial(N_+ - N_-)}{\partial t} + \nabla(\boldsymbol{V}_+N_+ - \boldsymbol{V}_-N_-) = 0 \tag{3}$$

$$m_\pm\frac{\partial \boldsymbol{V}_\pm}{\partial t} + a_\pm\boldsymbol{V}_\pm = -m_\pm\frac{\partial \boldsymbol{v}}{\partial t} \tag{4}$$

Here ϵ, ρ, η, p and $\boldsymbol{v}$ are the dielectric constant, the density, the viscosity, the pressure and the particles velocity in the medium respectively; $\boldsymbol{V}_\pm$, $N_\pm$, $m_\pm$ and $a_\pm$ are the velocities relatively to the neutral molecules of the medium, the concentrations, the masses and the friction coefficients of particles with electric charge $\pm q$ respectively.

Let us consider the light wave propagating along the x axis of the laboratory Cartesian coordinate frame. In the presence of microwave wave at the frequency of the twice Brillouin shift the electric field in the medium may be presented in the following form: $E_x = E_m exp\{2i\Omega t\} + c.c.$, $E_z = E_i exp\{i\omega t - ikx\} + E_s exp\{i(\omega-\Omega)t - ikx\} + E_a exp\{i(\omega+\Omega)t + ikx\} + c.c.$ where E_m is the electric field strength of the microwave field, E_i, E_s and E_a are the magnitudes of the interacting light wave respectively, $\Omega = 2ku$, $k = \omega n/c$, n is the refractive index of the medium. The interaction of the microwave and light waves results in generation of the counter propagated hypersonic waves at the frequency Ω: $\rho' = \rho - \rho_0 = \rho_s exp\{i(\omega-\Omega)t - ikx\} + \rho_a exp\{i(\omega+\Omega)t + ikx\} + c.c.$ In the linear approximation with respect to E_m we get from (1-4)

$$\rho_s = -i\frac{\rho_0^2\frac{\partial \epsilon}{\partial \rho}}{2k\gamma u}\frac{E_i E_s^*}{8\pi}, \quad \rho_a = -i\frac{\rho_0^2\frac{\partial \epsilon}{\partial \rho}}{2k\gamma u}\frac{E_i^* E_a}{8\pi} - \psi\rho_s \tag{5}$$

Here $\psi = (qN_0E_m^*/2k\eta)[(\Omega + i\nu_-)^{-1} - (\Omega + i\nu_+)^{-1}]$ is the parameter of coupling of the counter propagated hypersonic waves, $\nu_\pm = a_\pm/m_\pm$ determine the mobility of the positive and negative ions.

Substituting $\epsilon = n^2 + (\partial\epsilon/\partial\rho)\rho'$ into wave equation yields :

$$E_a = \frac{1}{2}\psi g I_i L E_s \tag{6}$$

where $g = (\rho_0\partial\epsilon/\partial\rho)^2/2\eta\epsilon uc$ is the increment of the SBS [1], $I_i = c|E_i|^2/8\pi$ is the incident wave intensity, L is the length of the medium. That is, the microwave induced four-wave mixing in results in generation of the coherent light wave at the frequency $\omega_a = \omega + \Omega$. The magnitude of this wave is proportional to the concentration of the charged particles in the medium.

Having in view employment of this phenomena in remote sensing of the charged particle concentration, let us estimate the sensitivity of this method. If we combine mutually coherent Stokes and anti-Stokes waves on the detector we obtain the electric current at the microwave frequency $2F$. If the detector bandwidth is $\Delta\nu = 1/\tau_s$ where τ_s is the pulse duration of the Stokes wave, the signal-to-noise ratio is [5]

$$\frac{S}{N} = \frac{1}{2}|\psi| GL\frac{W_s}{\hbar\omega_a} \tag{7}$$

where $G = gI_i$, W_s is the energy of the wave at the frequency ω - Ω.

The coupling parameter ψ is dramatically dependent on the origin of the charged particles, specifically, on the ratio $\nu_{\pm}/\Omega$. This may be estimated as $6\pi\eta r_{\pm}/m_{\pm}\Omega$, where $r_{\pm}$ are the radii of the charged particles. In the lower atmosphere when positive charges mainly adsorbed to water aerosol the correspondent friction coefficient may be estimated as $\nu_+ = 9\eta/2\rho_+ r_+$ where $\rho_+ = 1$ g cm^{-3}. By substituting $\eta \simeq 10^{-4}$ g s^{-1} cm^{-1}, $u \simeq 3\ 10^4$ cm/s and $\lambda = 10^{-4}$ cm one may obtain that $\nu_+ = \Omega$ if the radius of aerosol drop is roughly 10^{-6} cm. The maximum of the size distribution function of the atmospheric aerosol corresponds to $(2 \div 3)\times 10^{-6}$ cm [6]. Therefore the inequality $\nu_+ < \Omega < \nu_-$ is valid and the coupling parameter may be estimated as $\psi = qN_0E_m^*/4k^2\eta u$.

From (7) one may find that when $GL \simeq 10$, $W_s \simeq 1$ mJ, $E_m \simeq 1$ mV/cm, the signal-to-noise ratio for microwave driven four wave mixing in lower atmosphere is tends to 1 at the concentration of the elementary electric charges $N_0 \simeq 10^7$ cm^{-3}. Under normal conditions $N_0 = 10^2 \div 10^4$ cm^{-3}, however the concentration of the electric charges in lower atmosphere is dramatically increased by nuclear pollution [7]. This could be detected by using the phenomenon of the microwave driven four wave mixing.

References

1. V.S.Starunov and I.I.Fabelinskii, Sov. Phys. Usp. **12**, 463 (1970).
2. J. Stuer and E.Yeager, in: W.P.Mason, ed., *Physical Acoustics*, (New York: Academic Press, 1963), v. 2, pt A, 351.
3. K.A.Boyarchuk, Yu.P.Kuleshov, G.A.Lyakhov and Yu.P.Svirko Sov. Tech. Phys. Lett. **17**, 277 (1991).
4. K.A.Boyarchuk, G.A.Lyakhov and Yu.P.Svirko, J. Phys. D: Appl. Phys. **26**, 1561. (1993).
5. C.G.Bachman, *Laser radar system and techniques* (Dedham, Mass: Artech Hause, 1979).
6. R.G.Fleagle and J.A.Businger, *An introduction to the atmospheric physics*, (New York: Academic Press, 1979).
7. Junge, C., E., 1963, *Air chemistry and radioactivity*, (New York: Academic Press).

Extinction, Absorption, and Backscatter Cross Sections for Homogenous and Coated Fibrous Aerosols at Millimeter Wavelengths

K.P. Gurton, C.W. Bruce, A.V. Jelinek
U.S. Army Research Laboratory / Battlefield Environment Directorate
White Sands Missile Range, New Mexico 88002-5501
tel. (505) 678 1585 fax. (505) 678 2432

Introduction

Analytic techniques describing the electromagnet behavior, even of simple straight fibers of finite conductivity, have been developed only recently.[1] The electromagnetic modeling of fiber-like particles formed (for example) in the process of burning hydrocarbons, i.e. soot, is very difficult.[3-4] Although several analytic and numeric techniques are available, good experimental analogs have been lacking and the few that do exist are restricted to scattering only.

Three separate studies are presented, each designed to measure a specific component of the extinction. Two of the three techniques involve measurements of a single fiber while the third utilized a two dimensional array. Studies were conducted at various millimeter wavelengths. This proved to be an ideal portion of the spectrum in which to compare with the theory. Particles of interest are characterized as having moderate to good electrical conductance. All calculation conducted were based on the modified propagator approach of Waterman and Pedersen.

This report is intended to be summary of results only. A brief description outlining the basic principles for each measurement is presented. The reader is urged to consult the following references for a more complete development of techniques presented here.[5,6]

Method

The first system was developed to measure the absorption cross section for a single carbon fiber at 35 GHz as a function of length, diameter, and orientation with respect to the electric field. Typical lengths of fibers considered ranged from 1 to 20 mm and diameters from 2 to 15 um.

The first method involved measuring the total absorption cross section for a moderately conducting particle. The approach taken was based on the simple premise that a particle absorbing electromagnetic radiation experiences an increase in temperature. After the temperature of the particle has reached a steady state any heat generated within the particle will be conducted to the surrounding gas. If the particle is enclosed in a fixed volume a change in pressure will result. This time dependent change in pressure is directly related to the absorption process. The results of the absorption study are presented in figures 1 and 2. As seen in fig. 1 the change in slope near $kh \approx 1$ (where k is the propagation vector and h is the fiber half-length) marks the onset of modal effects as predicted. The lack of any resonate behavior is typical for moderately conducting particles in

which induced currents are highly damped. For $kh > 4$ the computed absorption per unit volume remains flat out to $kh \approx 200$ (not shown here).

For the diameter dependence study two different conductivities were considered. As expected the higher conductivity fibers exhibited slightly less absorption as the amount of total scattered energy increased. As seen in both figures good agreement with theory was found.

Graphs involving orientational effects for rotations in either the E or H planes were quite featureless and both obeyed an approximate cosine squared dependence for all lengths considered (not shown here).

One apparent weakness of the above technique was that the particle had to be a relatively good absorber, i.e., moderately conductive. To investigate fibers with larger electrical conductivities a transmissometer arrangement was constructed to measure the extinction for a two dimensional array of fibers. Straight, well

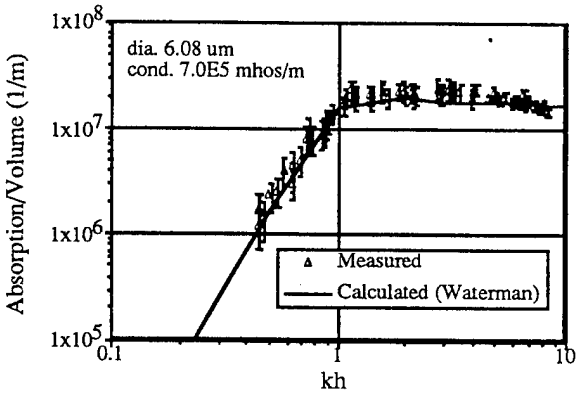

Fig. 1

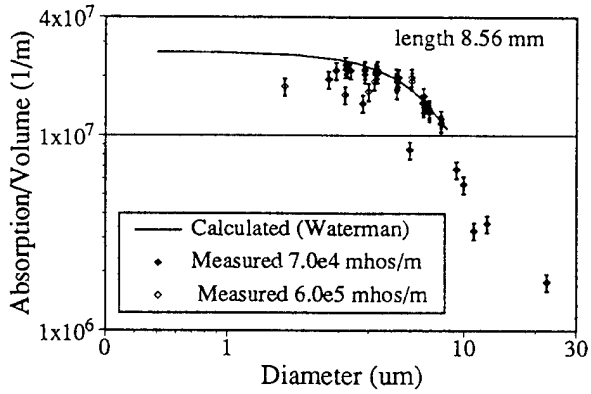

Fig. 2

separated fibers were arrayed in planes normal to the propagation vector k for measurements over a frequency range of 20 to 160 GHz. The fiber half-length h was chosen so that the key parameter kh varies from about 0.9 to about 7. All fibers were oriented parallel with the incident E-field. Fiber composition was graphite coated with nickel to a thickness that should appear to the incident waves as solid nickel. The resulting spectra exhibit the expected strong scattering resonances and agreed in form and magnitude with theory in the vicinities of the anti-resonances. The latter provided a strong test for the assumed form of the current function induced in the fiber (until very recently the exact form of this function was rather uncertain). Graphical comparisons of the computed and measured spectra show good agreement, see fig. 3.

The third experiment presented represents preliminary results of an ongoing study and was developed to measure the effects on extinction that various thin metallic coatings would have when applied to a dielectric fiber. One of the most sensitive parameters to changes in thin conducting films is backscatter. A backscatter arrangement consisted of a non-conducting circular mounting bracket to which a single fiber was attached. This mounting bracket was rotated at a given frequency ω_r. The rotating fiber was then irradiated in the reaction field at 35 GHz. The resulting

modulated backscattered signal was fed into a lock-in amplifier tuned to ω_r. Although the measurement was conducted in the reaction field of the radiator, the resulting signal was assumed proportional to the absolute backscatter.

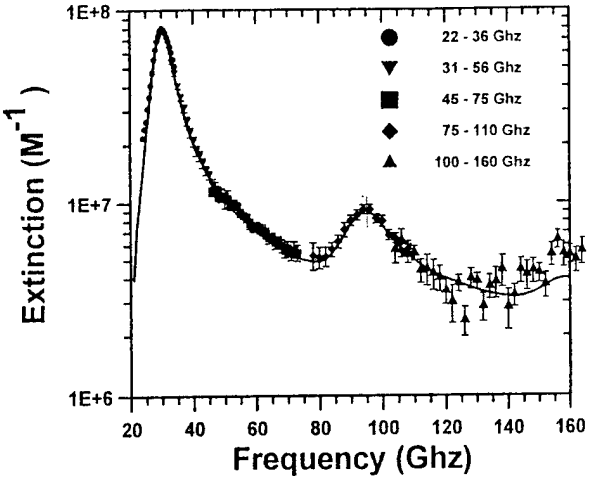

Fig. 3

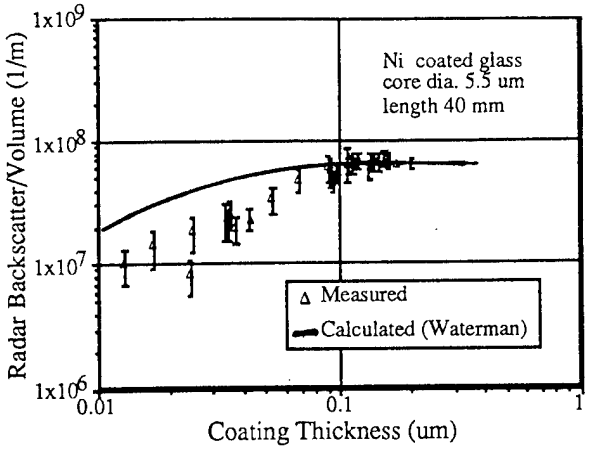

Fig. 4

At the time of writing only results for Ni coated glass fibers were available, see fig. 4. Although the agreement with theory seems rather poor, this was attributed to improper use of the bulk value for electrical conductivity of Ni. Calculations are currently being conducted using the "actual" measured functional dependence for the conductivity. For reasons not stated here, the conductivity is often a function of film thickness (especially as thicknesses approach the mean free path of the conduction electrons). The author believes that when this function is properly incorporated into the theory that agreement will be more reasonable. Nevertheless both curves compare well with a classical skin depth for Ni of 0.7um. Figure 4 shows that a metallic coated fiber reaches a solid equivalence at approximately half the skin depth.

In conclusion three techniques have been developed to investigate some key features of the electromagnetic interaction for certain fibrous aerosols. Although thin fibers were considered here there exists no fundamental reason why these techniques can't be applied to other geometries. Scaling these techniques with respect to wavelength are possible so long as the indices of refraction remain constant with scaling. Good agreement with theory was found throughout and gave further evidence to the validity of the form of the induced current function used by Waterman.

This work was performed while the author held a National Research Council-ARL/BED Research Associateship.

References

1 P.C. Waterman, J.C. Pedersen, J. Appl. Phys. **78**, No.2, 656-667 (1992).
2. C.W.Bruce, T.F. Stromberg, K.P. Gurton, J.B. Mozer, Apl. Opt. **30**, No.12, 1537, (1991).
3. M.F. Iskander, H.Y. Chen, J. E. Penner, Appl. Opt. **28**, No.15, 3083, (1989).
4. B.L. Drolen, C.L. Tien, J. Quant. Spectrosc. Radiat. Transfer **37**, No.5, 433 (1987).
5. K.P. Gurton, C.W. Bruce, Appl. Opt. **34**, No. 15, 2822-2828 (1995).
6. A.V. Jelinek, C.W. Bruce, J. Appl. Phy., **78**, No. 4, 2675-2678 (1995).

Prognosis for a mid-infrared magnetic rotation spectrometer for the *in situ* detection of atmospheric free radicals

C. Chackerian, Jr., T. A. Blake, C. R. Mahon and J. R. Podolske.

We investigate magnetic rotation spectroscopy as a technique for the ultrasensitive detection of free radical molecular species in the Earth's atmosphere. In order to design field instruments which have parts per trillion by volume per second sensitivity we obtain a quantitative description of experiments we have done at higher concentration levels.

For convenience we performed experiments on the nitric oxide (NO) molecule using a tunable laser diode radiation source. The verified theory is used to specify an instrument which can make *in situ* measurements on NO and NO_2 in the earth's atmosphere at a sensitivity level of a few pptv/sec. The theoretical calculations are based on non-adjustable molecular parameters such as a particular molecular transition's frequency, intensity, broadening coefficient and magnetic tuning rate.

Figure 1 shows a spectrum of the Q-branch region of the fundamental rovibrational band of NO. The 2f method of detection used is commonly also used in experiments to detect trace atmospheric species. Figure 2 shows the magnetic rotation spectrum on the same sample used for Fig. 1 with the exceptions that (1) the gas sample is placed in the bore of a solenoid magnet with an oscillating magnetic field of 141 Gauss and (2) a polarizer is placed before the solenoid and a nearly crossed analyzer is placed after the solenoid. Figure 3 shows an overlay of a calculated and experimental spectrum of NO. The calculation of the spectrum contains no adjustable parameters.

We found that the S/N in our experiments were limited by detector noise and optical path length thru the sample as well as laser power. Toward increasing the optical path thru the sample we have designed a Herriott multiple-pass cell contained in the flat-field of a solenoid.

C. Chackerian, Jr. and J. R. Podolske are with the NASA-Ames Research Center, Moffett Field, CA 94035-1000. T. A. Blake is with Battelle/PNL, P.O. Box 999, MS K3-58, Richland, WA 99352. C. R. Mahon is with the Space Physics Research Institute, 572 Hyannis Drive, Sunnyvale, CA 94087-1315.

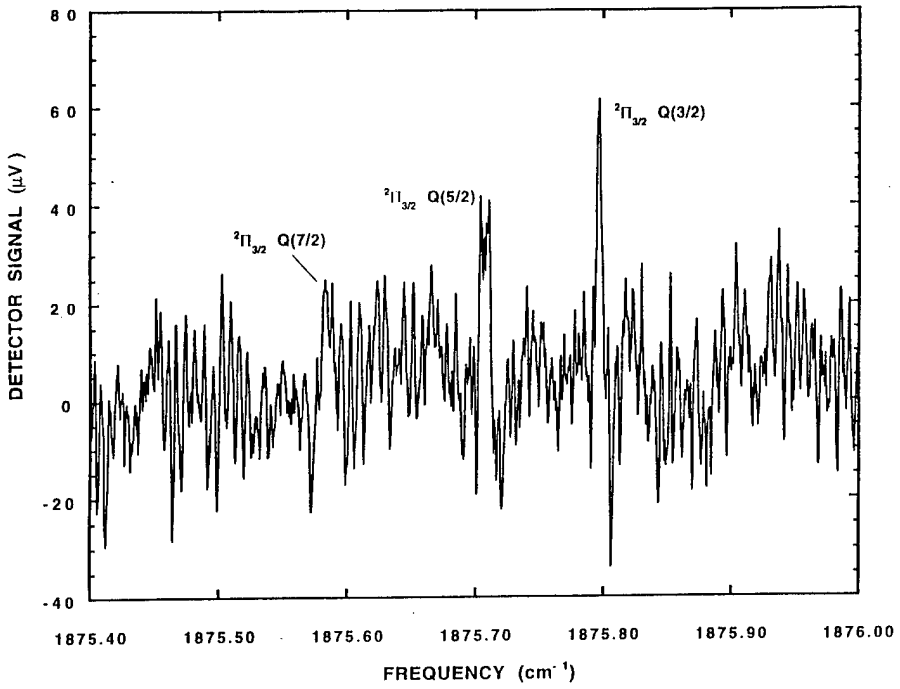

Fig.1.Wavelength modulated spectrum of the Q-branch region of nitric oxide. Gas sample: 67 mbar of 4 ppm NO in N_2 with a 12 cm pathlength. The lock-in detection was 2f at 1.8 kHz and 100 msec time constant.

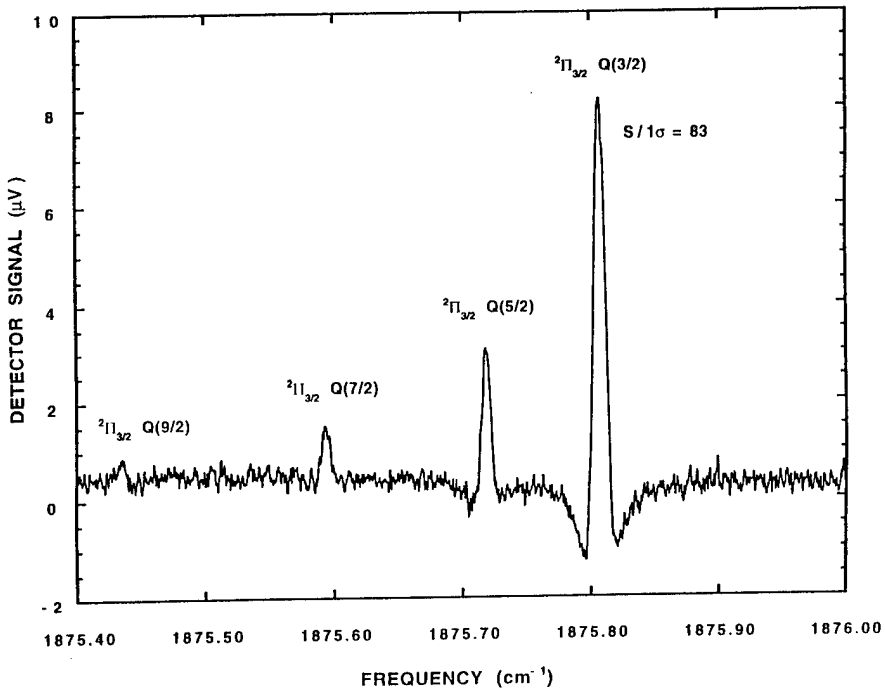

Fig.2. Magnetic rotation spectrum of the Q-branch region of nitric oxide. Gas sample was 67 mbar of 4 ppm NO in N_2 with a 12 cm pathlength. Peak magnetic field strength was 141 Gauss and the analyzer angle was 85°. The lock-in detection was 1f at 922 Hz and 100 msec time constant.

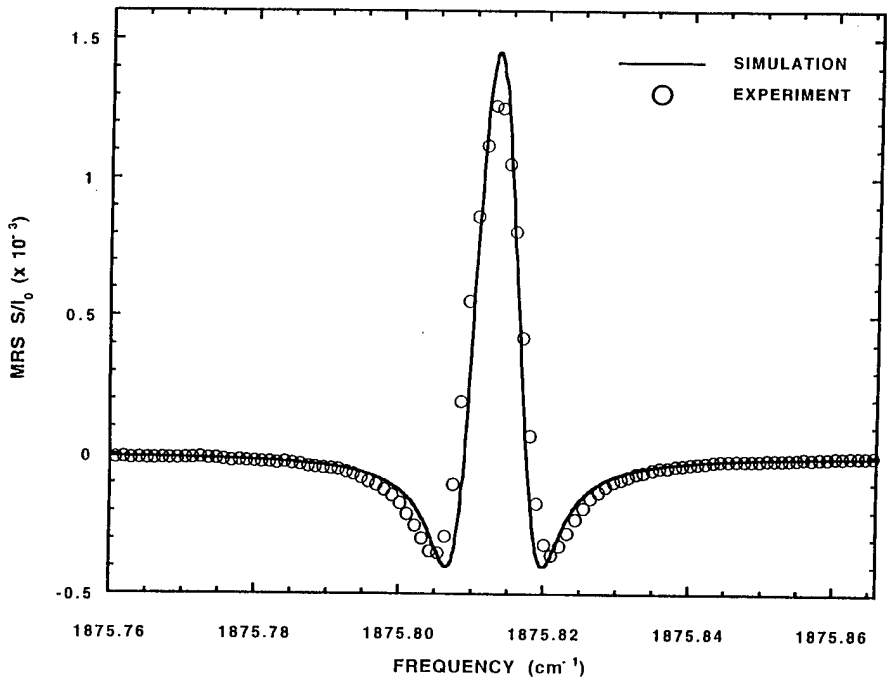

Fig.3. Overlay of simulated (solid line) and experimental (open circles) lineshapes for the nitric oxide $^2\Pi_{3/2}$ Q(3/2), v = 1 ← 0 transition. The gas sample was of 20 mbar of 0.39% NO in N_2 at 296 K over a 12 cm pathlength. The peak field strength was 339 Gauss. The analyzer angle was 85° with respect to the incident polarization. Lock-in detection was 1f at the field modulation frequency of 922 Hz with a 100 msec time constant.

On the Use of Line Strengths in Applied Diatomic Spectroscopy

James O. Hornkohl, C. Parigger, and J. W. L. Lewis
The University of Tennessee Space Institute
Center for Laser Applications
Tullahoma, Tennessee 37388-8897
Phone: 615-393-7338, Fax: 615-454-2271

1. Introduction

According to a postulate of quantum mechanics, the probability of a transition from state $|n'J'M'\rangle$ to state $|n''J''M''\rangle$ is controlled by the absolute square of the matrix element $\langle n'J'M'|\mathbf{O}|n''J''M''\rangle$ in which $\mathbf{O}$ is the operator responsible for the transition, J is the total angular momentum quantum number, M is the quantum number for the z-component of the total angular momentum, and n denotes all other required quantum numbers. By definition, the sum of all such squared matrix elements which contribute to the same observation is called the *line strength*.[1–4] Thorne's table 9.1[3] gives the equations for the Einstein coefficients and the oscillator strength in terms of the electric dipole line strength.

Although the molecular line-strength is the fundamental and general quantity for the computation of theoretical quantum transitions, its use in applied spectroscopy is less common. The following gives examples of the utilty of the line strength in applied diatomic spectroscopy.

2. Diatomic Line Strength

The Wigner-Eckart theorem splits each transition matrix element into two parts, one part which is specific to the particular transition in question and a second more general part which is controlled only by the angular momentum of the initial and final states. The diatomic electric dipole line strength separates into

$$S(n'v'J', n''v''J'') = S_{\mathrm{ev}}(n'v', n''v'')\ S(J', J'') \tag{1}$$

where v is the vibrational quantum number and $S_{\mathrm{ev}}(n'v', n''v'')$, the electronic-vibrational strength, is given by

$$S_{\mathrm{ev}}(n'v', n''v'') = \left|\langle v'|\mathcal{R}_{n'n''}(r)|v''\rangle\right|^2 \tag{2}$$

in which $\mathcal{R}_{n'n''}(r)$ is the electronic transition moment and r is the internuclear distance and the unitless factor $S(J', J'')$ is the Hönl-London or rotational line strength factor.

There are two basic algorithms for computation of diatomic spectra, the term-value method and the Hamiltonian diagonalization method. In the first, semi-empirical term value equations for the upper and lower states, and experimentally determined molecular parameters are used to compute the line positions. Completely separate equations for the line strengths are used to compute the intensities. The association of each line wavenumber with the corresponding line strength is not automatic. In the second algorithm, Hamiltonian matrices for the upper and lower states are numerically diagonalized. If the Hamiltonian matrices are computed in, for example, the Hund's case (a) basis, then the matrix elements from which the line strength is computed are expressed in terms of the case (a) matrix elements and the eigenvectors of the orthogonal matrices which diagonalized the upper and lower Hamiltonians. Thus, in the Hamiltonian diagonalization algorithm the natural correspondence of line strength with line position is enforced. Displaced lines, extra lines, and missing lines can be accounted for in the Hamiltonian diagonalization method but not the term value method. In principle, the angular momentum selection rules and the parity selection rules perfectly parallel each other in diatomic spectroscopy. Implementation of the angular momentum selection rules is particularly simple in the Hamiltonian diagonalization algorithm: The Hönl-London factor is vanishing for forbidden transitions, non-vanishing for allowed transitions.

The principal advantages of numerical diagonalization of the Hamiltonian matrices are high accuracy and generality. In practical terms, it is much simpler to write a FORTRAN subroutine that handles essentially

all types of diatomic Hamiltonians than to write a subroutine that covers all term value equations, and accurate Hönl-London factors are obtained with little additional effort.

The practical realization of the line strength concept in diatomic spectroscopy is a line strength file, a line-by-line electronic table of the line positions (vacuum wavenumber), upper and lower term values, the electronic-vibrational strength, the Hönl-London factor, and the upper and lower J and v quantum numbers. A line strength file provides a very convenient separation of the applied quantum mechanics required for creation of the line strength file from applications of diatomic spectroscopy such as temperature measurement. The user of the line strength must understand the physical significance of this quantity but need not understand every detail required for its computation.

3. Examples

Line strength files for individual transitions of selected diatomic molecules have been applied in spectroscopic studies.[5–9] The efforts include the molecules CN, C_2, N_2^+, NH, OH, NO, N2, CO, H_2, N_2. Figures 1-2 show example comparisons between experimental and synthetic C_2 diatomic spectra, and Fig. 3 shows a synthetic high-resolution spectrum.[10] A single, simple FORTRAN routine was used for the computation of all of the synthetic spectra. Analogous comparison graphs can be generated for other diatomic molecules - only the line-strength files are different for the synthetic spectra.

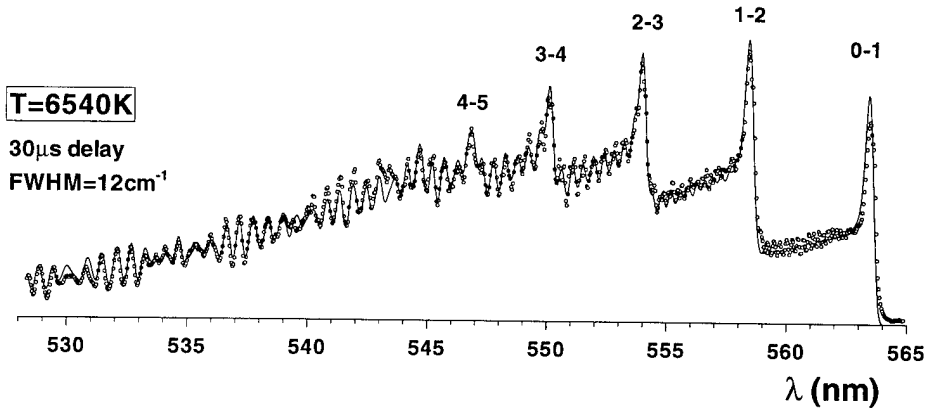

Fig. 1. $C_2 d^3\Pi_g \leftrightarrow a^3\Pi_u$ Swan band: high temperature plasma emission spectrum and fit.

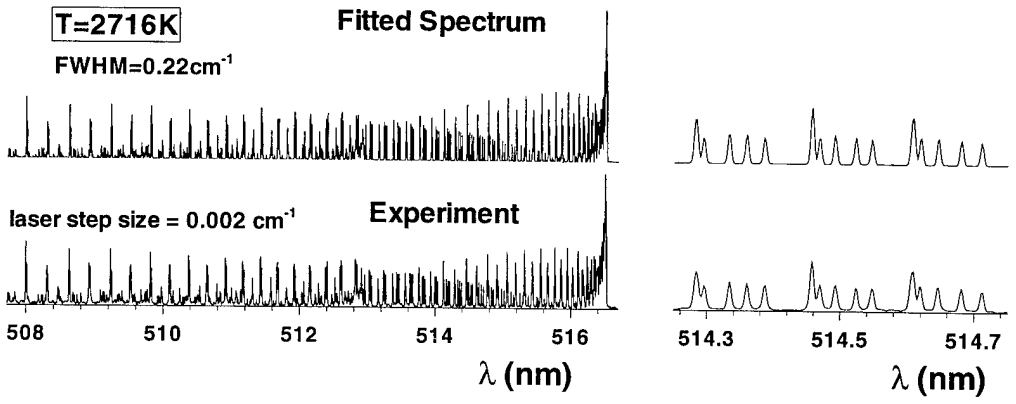

Fig. 2. C_2 Swan bands: laser induced fluorescence spectrum and fit, and expanded view on right.

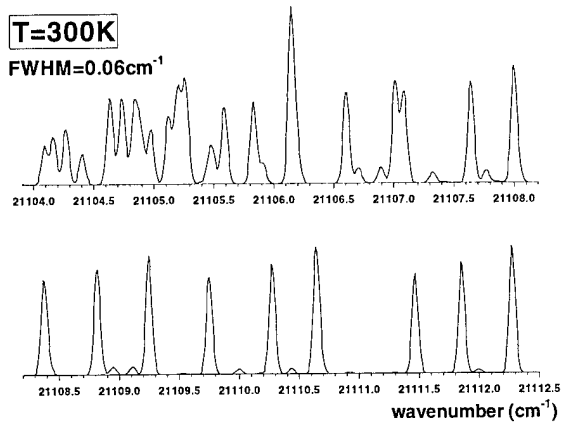

Fig. 3. Synthetic spectrum of C_2 Swan 1-0 band corresponding to Fig. 2 of Suzuki et al.[10]

1. E. U. Condon and G. H. Shortly, *Theory of Atomic Spectra*, Cambridge Univ. Press, London (1964).
2. H. R. Griem, *Plasma Spectroscopy*, McGraw-Hill, New York (1964).
3. A. P. Thorne, *Spectrophysics*, Chapman and Hall, London (1974).
4. I. I. Sobelman, *Atomic Spectra and Radiative Transitions*, Springer-Verlag, Berlin (1979).
5. J. O. Hornkohl, C. Parigger, and J. W. L. Lewis, "Temperature measurements from CN spectra in a laser-induced plasma," J. Quant. Spectrosc. Radiat. Trans. 46, 405 (1991).
6. C. Parigger, D. H. Plemmons, J. O. Hornkohl, and J. W. L. Lewis, "Spectroscopic temperature measurements in a decaying laser-induced plasma using the C_2 Swan system," J. Quant. Spectrosc. Radiat. Trans. 52, 707 (1994).
7. C. Parigger, D. H. Plemmons, J. O. Hornkohl, and J. W. L. Lewis, "Temperature measurements from first-negative N_2^+ spectra produced by laser-induced multiphoton ionization and optical breakdown of nitrogen," Appl. Opt. 34, 3331 (1995).
8. D. H. Plemmons, C. Parigger, J. O. Hornkohl, and J. W. L. Lewis, "Laser induced plasma temperature determination using time-resolved NH molecular spectroscopy," in Modern Spectroscopy of Solids, Liquids, and Gases, 1995 Technical Digest Series (Optical Society of America, Washington, DC, 1995), pp. 86-88.
9. J. O. Hornkohl and C. Parigger, "Angular Momentum States of the Diatomic Molecule," accepted for publication in Am. J. Phys. (1996).
10. T. Suzuki, S. Saito, and E. Hirota, "Doppler-limited dye laser excitation spectrum of the C_2 Swan band ($v' - v'' = 1 - 0$)," J. Molec. Spectrosc. 113, 399 (1985).

Diagnostics of Boundary Layer Chemistry in an Atmospheric Pressure Plasma

Thomas G. Owano, Edward H. Wahl, Charles H. Kruger
High Temperature Gasdynamics Laboratory, Department of Mechanical Engineering
Stanford University, Stanford, California 94305-3032
Ph. (415)723-1295, Fax (415) 723-1748

Richard N. Zare
Department of Chemistry, Stanford University, Stanford, California 94305-5080
Ph. (415) 723-3062, Fax (415) 723-9262

Introduction

It can be quite difficult to probe the harsh and potentially nonequilibrium environment of atmospheric pressure Plasma-Assisted Chemical Vapor Deposition (PACVD) reactors [1]. Sensitive measurement of temperature and trace radical concentrations within the reacting substrate boundary layer is a challenging problem in atmospheric pressure reactors due to the highly luminous environment, small spatial scales, and steep thermal and concentration gradients. It is in this environment where the application of sensitive, nonlinear, laser based diagnostic techniques can complement the abilities of more conventional diagnostic techniques such as optical emission spectroscopy (OES) and laser-induced fluorescence (LIF), and allow the detailed measurement of temperature and trace radical concentrations to be made, and compared to models of the deposition environment. The application of a powerful non-linear laser spectroscopy, degenerate four wave mixing (DFWM), as a gas-phase optical diagnostic has opened the door for significant advancement in the area of atmospheric pressure plasma chemistry, since it can provide high sensitivity and spatial resolution with a coherent, phase conjugate signal which can be readily discriminated against the plasma luminosity [2].

DFWM has been employed as a spectroscopic probe of a thermal plasma, diamond CVD environment. It is found to be an extremely useful nonintrusive probe of the plasma, capable of providing high spectral and spatial resolution, and permitting measurements of temperature and relative species concentrations of trace radicals under conditions in which other spectroscopic techniques fail. In-situ measurements of CH and C_2 radicals have been performed to determine spatially resolved profiles of vibrational temperature, rotational temperature, and species concentration in the thin boundary layer of a diamond-growth substrate immersed in a flowing atmospheric pressure plasma. Results of these measurements are compared with the predictions of a detailed numerical simulation, and found to be in agreement.

Results

The applicability of in-situ DFWM to the atmospheric pressure diamond synthesis environment has been investigated using an atmospheric pressure ICP reactor. It was desired to make in-situ measurements during normal operation of the atmospheric pressure RF-ICP diamond synthesis reactor - with a substrate in place, and growing diamond. The conditions chosen for these studies were indeed diamond growth conditions (although they were not optimized for best possible growth) and all measurements reported here were taken with the growing substrate in place. The reactor gas feed mixture was comprised of 106.5 l/min Ar, 12.0 l/min H_2, and 0.8% to 10% CH_4 (in H_2) premixed before introduction to the plasma torch.

Calorimetric energy balance of the reactor indicates a net plasma enthalpy of 6 kW leaving the nozzle exit. The molybdenum substrate had a measured surface temperature of 1035°C.

The CH radical was probed with in-situ DFWM measurements of the CH $A^2\Delta \leftarrow X^2\Pi$ (0,0) system near 431 nm. Figure 1 shows a DFWM spectrum of one R branch group taken with approximately 10 μJ laser beam energies.. The v″=0 and v″=1 sets of the individual R(5) branch lines are closely grouped and permit determination of vibrational temperatures. The Q branch region allows fairly rapid measurements of several v=0 lines, thus permitting measurements of rotational temperature. The C_2 radical was probed with in situ DFWM measurements of the C_2 $d^3\Pi_g \leftarrow a^3\Pi_u$ (3,1) system near 437 nm.

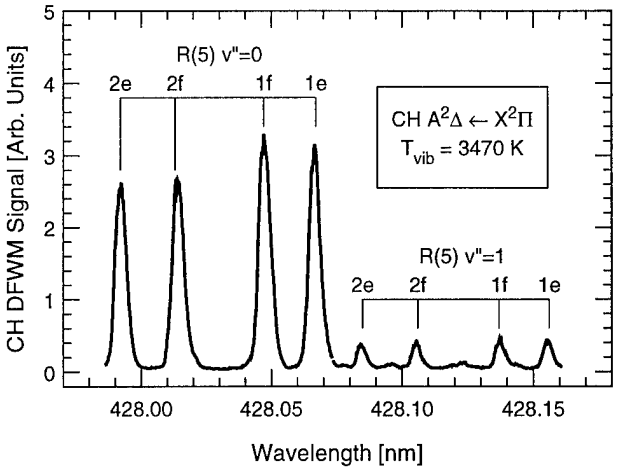

Figure 1. CH R(5) v"=0 and v"=1 components.

Temperature and concentration profiles within the reacting boundary layer were probed using DFWM. A comparison of measured CH vibrational and rotational temperatures along the stagnation line of the substrate with values from a computational simulation [3] is shown in Figure 2. Boundary conditions for the simulation are the measured freestream temperature of 3900 K, an estimated freestream velocity of 8 m/s, and the measured substrate temperature of 1035°C. We can see the predicted thermal boundary layer (≈6mm thick) with a steep fall off in temperature very close to the substrate. The measured CH vibrational temperatures are in close agreement with the predictions, although the loss in signal of the v=1 transitions in the cooler region very near the substrate prevents accurate vibrational temperature measurement for distances < 2mm. Rotational temperatures measurements from the CH v=0 lines, which remain strong enough for accurate measurement closer to the substrate, are in good agreement with both the measured vibrational temperatures and the computational simulation. It is possible to make measurements even closer to the substrate, but for these experimental conditions the CH concentration in that region has dropped below approximately 2 ppm, which is our current detection limit.

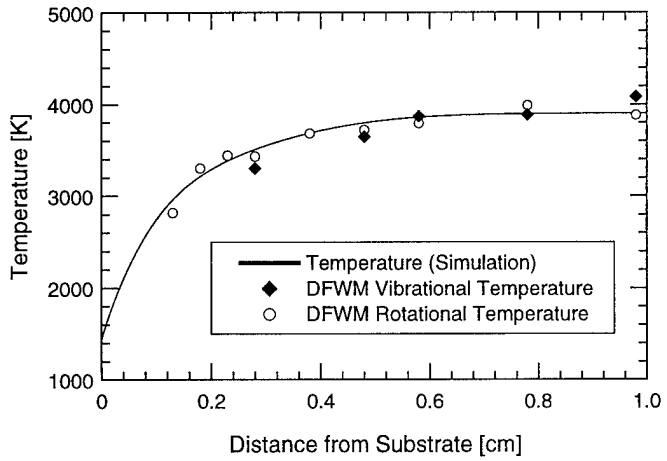

Figure 2. Boundary layer temperature profiles.

Measurements of the relative CH and C_2 mole fractions within the substrate boundary layer are compared to results of the computational simulation in Figures 3 and 4. In Figure 3, the CH mole fraction is approximately 20 ppm in the freestream (4100 K) and is predicted to first rise within the approximately 6 mm thick boundary layer (due to production) as the plasma cools toward approximately 3700 K, reaching a peak of approximately 55 ppm at 2 mm from the

substrate surface, then to be destroyed as the plasma cools further on its approach to the substrate surface. In Figure 4, we see a similar behavior for the C_2 concentration profile with a much higher peak concentration (~300 ppm). We can see that the DFWM measurements of relative CH and C_2 mole fraction (which have been scaled to the peak of the predicted curve) correspond closely to the predicted concentration in both trend and magnitude, accurately reflecting the production and destruction of the radicals within the boundary layer and demonstrating the ability of DFWM to probe this small, harsh reaction zone.

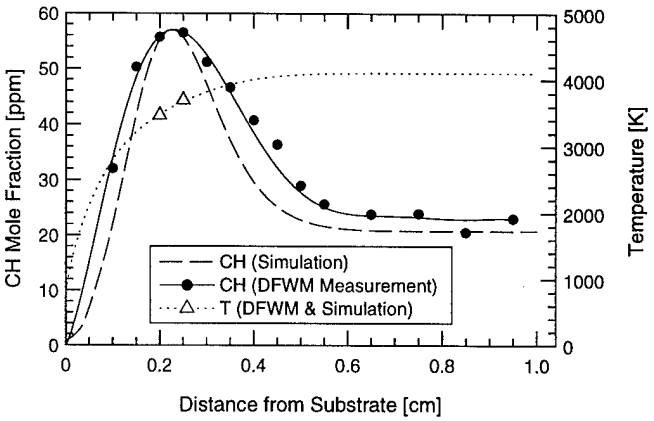

Figure 4. CH concentration profile.

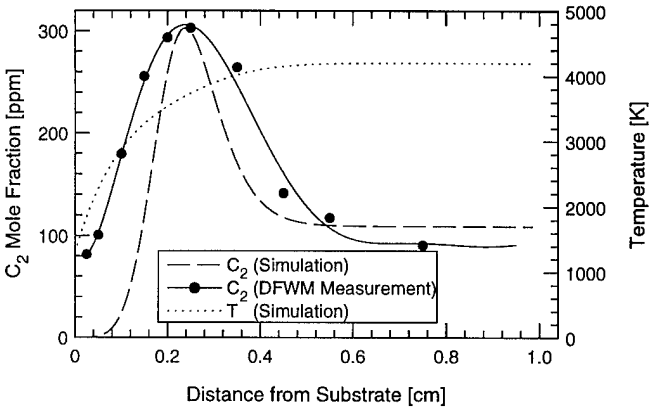

Figure 5. C_2 concentration profile.

Conclusions

Degenerate four-wave mixing has been demonstrated as a sensitive, spatially resolved diagnostic of boundary layer chemistry in thermal plasma CVD of diamond. The coherent, phase-conjugate signal produced in this technique enables the rejection of intense plasma luminosity, and allows the accurate interrogation of temperature and trace (ppm level) radical concentrations within the reacting plasma. In-situ measurements of vibrational and rotational temperatures, as well as relative CH and C_2 radical concentrations in the reacting boundary layer of a diamond growth substrate are found to be in good agreement with model predictions.

References

1. S.K. Baldwin, T.G. Owano, and C.H. Kruger, *P. Chem. and P. Proc.* **14**, 383 (1994).
2. D.S. Green, T.G. Owano, S. Williams, D.G. Goodwin, R.N. Zare, and C.H. Kruger, *Science* **259**, 1726 (1993).
3. D.G. Goodwin, and G.G. Gavillet, *J. Appl. Phys.* **68**, 6393 (1990).

Spatial maps of analyte and Ar buffer gas atoms and ions by LIF in ICP-MS

B.Duersch*, Y.B.Chen*, A.C.Ciocan** and P.B.Farnsworth*+

*- Brigham Young University, Chem. Dept., Provo-Utah, 84602, USA

**- Institute of Atomic Physics, Magurele-Bucharest, POBox MG-07, Romania

+-To whom correspondence should be sent

Laser induced fluorescence as a selective and sensitive diagnostic tool is used for ion beam analysis downstream from the skimmer in an ICP-MS. Using selected spectral lines, analyte atoms and ions and Ar metastable atoms are measured for a range of ICP operating conditions, vacuum pressures and over a wide range of element's masses. To our knowledge, optical measurements of ions extracted from an ICP, either by emission [1-2] or by laser induced fluorescence [3-4], were limited to the first stage of ion extraction and only few probe elements were chosen.

The experiments are performed by optical probes (excitation and collection optics) to which both the laser excitation radiation and fluorescence signal are transmitted through optical fibers. Inside the vacuum chamber the optical probes are mounted on a computer-controlled xyz stage which allows spatial mapping of atoms and ions. The spatial resolution is limited to the diameter of the laser beam. Two tunable laser beams, from dye lasers for analytes, and from a

diode laser for Ar, are used for excitation of selected transitions.

The results are expected to lead to the development and better understanding of the ion extraction and transport mechanisms in mass spectrometers using inductively coupled plasmas as ion sources. Specific goals are a better understanding of "non-spectroscopic" interelement interferences generally attributed to mass-dependent space-charge effect in the ion beam sampled from the ICP, and optimization of the ion beam shape from the ICP, for use with the time-of-flight mass spectrometer.

Bibliography:

1. R.S.Houk and H.B.Lim, Anal.Chem **58**, 3244 (1986).

2. A.L.Gray, J.Anal.Atom.Spectrom. **4**, 371 (1989).

3. H.B.Lim, R.S.Houk, M.C. Edelson and K.P.Carney, J.Anal.Atom.Spectrom. **4**, 365 (1989).

4. A.A.Verbeek, paper #SL6.3, XXVIII CSI Meeting, York, England

Friday, March 22, 1996

Diagnostics of CVD Processes

LFA 8:00 am-9:45 am
Windsor Ballroom

Jay Jeffries, *Presider*
SRI International

Optical Diagnostics of VUV Laser CVD of Semiconductors

M. Barth, J. Knobloch and P. Hess

Institute of Physical Chemistry, University of Heidelberg,
Im Neuenheimer Feld 253, D-69120 Heidelberg, Germany

Amorphous hydrogenated germanium (a-Ge:H) was deposited using an ArF excimer laser (193 nm) and Ge_2H_6 as source gas in parallel configuration. The dependence of the film properties on the deposition parameters such as substrate temperature, laser power, digermane partial pressure and total pressure was fully characterized. The results obtained for the Urbach energy, hydrogen content, Tauc gap, density, E-modulus as well as dark and photoconductivity show that high quality material can be deposited by ArF laser CVD.

Nucleation and growth of the germanium films was studied for hydrogen terminated Si(111) substrates, prepared by chemical processing, and for Si(111) wafers with the native oxide layer. Spectroscopic ellipsometry (1.2 eV - 4.7 eV) reveals striking differences in the growth process. In the case of the H-terminated surface the experimental data could only be fitted by assuming a $Si_{1-x}Ge_x$ alloy with x=0.12. The presence of a native oxide layer seems to prevent the formation of an alloy by separating the silicon substrate from the active germanium precursors forming the film. A comparison of the growth rates for the two surfaces yields a much higher initial deposition rate on the native oxide surface. The evolution of the relative volume void fractions with film thickness shows that the transition from cluster growth to uniform bulk growth of high quality material starts at 1.6 nm on H-terminated silicon and at 3.5 nm on the native oxide covered Si surface.

Amorphous hydrogenated silicon (a-Si:H) was deposited using a F_2 laser (157 nm) and Si_2H_6 as source gas in parallel configuration. The dependence of the film properties on the deposition parameters such as substrate temperature, laser power, disilane partial pressure and total pressure was fully characterized. The results obtained for the Urbach energy, hydrogen content, Tauc gap, density, E-modulus as well as dark and photoconductivity show that high quality material can be deposited by F_2 laser CVD.

Nucleation and growth of the amorphous silicon film was monitored in situ by transmission FTIR spectroscopy on a silicon substrate covered with the native oxide layer. Monolayer sensitivity was achieved in the detection of SiH_x stretching modes. A band observed at 2100 cm^{-1} during the initial stage of growth is attributed to cluster formation involving higher hydrides. Coalescence occurs at a thickness of about 20 Å and is characterized by the occurrence of the SiH band at 2000 cm^{-1}, which increases proportional to the thickness of the film. This is in good agreement with results obtained by Collins et al. using spectroscopic ellipsometry to monitor a-Si:H film growth initiated by plasma CVD. In the FTIR experiments the film thickness was determined in situ using a quartz crystal microbalance reaching monolayer sensitivity.

REMPI/TOF-MS Diagnostics for Monitoring CVD Reactive Intermediates

R. W. Shaw
Chemical and Analytical Sciences Division,
Oak Ridge National Laboratory
Oak Ridge, TN 37831-6142
PHN: 423/574-4920
FAX: 423/574-8363

L. L. Jones, and C. S. Feigerle
Department of Chemistry
University of Tennessee
Knoxville, TN 37996-1600
PHN: 423/974-2129
FAX: 423/974-3454

We have examined the correlation of gas phase species concentrations in a chemical vapor deposition (CVD) reactor with diamond film growth process parameters and film characteristics. The experiments were performed in a hot filament CVD reactor fitted for orifice sampling and resonantly enhanced multiphoton ionization (REMPI) time-of-flight mass spectrometry for gas analysis. The mass spectrometer was used to monitor the chemical species present immediately above the diamond growth surface. Stable products were monitored using electron impact ionization. REMPI was employed for the detection of radicals, including atomic hydrogen and methyl radical, since species such as CH_3+ can be artificially produced by dissociative electron impact ionization of stable molecules. Measurements were made of the filament and substrate temperature dependence of the H, CH_3, CH_4, and C_2H_2 relative concentrations. Scanning electron microscopy and Raman spectroscopy were utilized to analyze diamond film morphology and quality.

The chamber was divided into three regions: the growth region, the expansion region, and the mass spectrometer. A sampling orifice (200 μm diameter) separated the growth and expansion regions, while a skimmer (0.5 mm diameter) separated the expansion region and the mass spectrometer. A 76 mm diameter quartz tube enclosed the growth region. The substrates were abraded 2 cm^2 Si wafers, either (111) or (100). A substrate heater was designed to provide independent substrate

temperature control as well as a uniform lateral temperature. Noble gases were included in the feed gases to provide an internal standard for signal normalization by which systematic effects could be eliminated. The UV beam employed for REMPI was produced by frequency doubling the output of a Nd:YAG-pumped pulsed dye laser using ß-BaB_2O_4 crystals. The laser beam was focused in the extraction region of the mass spectrometer using a 200 mm focal length quartz lens. Results were obtained for an initial gas composition of 0.5% CH_4 and 1% each of He, Ne, and Ar in H_2 with a total flow of 100 sccm.

Atomic hydrogen was detected using the (2+1) REMPI line at 243.13 nm through the 2s intermediate level. The observed spectral linewidth was 0.01 nm fwhm. The H REMPI signal strength dependence on filament temperature was measured, with the substrate temperature held constant at 730 °C. The production of hydrogen atoms follows an exponential growth and does not saturate over the normal range of filament temperatures used for diamond film growth. The relative H atom concentration decreased with increasing substrate temperature, for a fixed filament temperature (1890 °C). Such a trend is interpreted as due to an activated surface recombination, resulting in the consumption of atomic hydrogen. McMaster et al[1] have proposed a model that predicts the gas composition as a function of surface temperature. The H atom destruction probability on the surface was assigned an activation energy of 7.3 kcal/mol. The model predicts that as the substrate temperature decreases, the atomic hydrogen mole fraction will increase, in agreement with our results.

The CH_3 (3+1) REMPI signal exhibited a slowly increasing growth as a function of increasing filament temperature (at constant substrate temperature) with an onset at approximately 1300 °C. The CH_3 REMPI signal was relatively independent of substrate temperature, at fixed filament temperature. The CH_3 concentration in the near surface gases appears to be determined predominately by the filament temperature, i.e., the production rate. These measurements represent the first REMPI detection of CH_3 using orifice sampling. Celii and Butler[2] and Corat and Goodwin[3] sampled the near surface gases by passing an excitation beam through the reactor gases, but in close proximity to the substrate surface. Hsu[1] employed orifice sampling, but used low energy electron impact ionization.

The chemistry occurring in a hot filament CVD reactor during diamond deposition is complex, including both gas phase and surface reactions. Through the use of orifice sampling to probe the near surfaces gases, insight has been gained on the reactions of the dominant stable and radical species.

Acknowledgements:

Research sponsored by the National Science Foundation (grant CTS-9202575) and by the U.S. Department of Energy, Office of Basic Energy Sciences, under contract DE-AC05-84OR21400 with Lockheed Martin Energy Systems.

References:

1. McMaster, M. C.; Hsu, W. L.; Coltrin, M. E.; Dandy, D. S.; *J. Appl. Phys.* **1994**, *76*, 7567.

2. Celii, F. G.; Butler, J. E.; *J. Appl. Phys.* **1992**, *71*, 2877.

3. Corat, E. J.; Goodwin, D. G.; *J. Appl. Phys.* **1993**, *74*, 2021.

Investigation of Stagnation-Flow Diamond-Forming Flames Using Advanced Laser Diagnostics

KENNETH E. BERTAGNOLLI and ROBERT P. LUCHT
Laser Diagnostics Laboratory, Department of Mechanical and Industrial Engineering
University of Illinois at Urbana-Champaign, 1206 West Green Street, Urbana, IL 61801
Phone: (217) 333-5056 Fax: (217) 244-6534

INTRODUCTION

The deposition of polycrystalline diamond films has been demonstrated for a wide variety of flames and plasmas. Uniform diamond deposition was demonstrated recently in a rich $H_2/C_2H_2/O_2$ flat flame stabilized in the stagnation region of the deposition substrate [1,2]. Continued development of this technology depends strongly on increased understanding of the diamond growth process through experimental and theoretical studies [3].

Stagnation-flow diamond-forming flames have been modeled recently by Meeks et al. at Sandia National Laboratories [4]. The results predict super-adiabatic flame temperatures and peak atomic hydrogen concentrations near 7%. Atomic hydrogen is believed to play a crucial role in the deposition of high quality diamond film [5]. Little experimental data is available to verify these computations, however.

This paper describes the preliminary results of our study to provide accurate temperature and hydrogen atom concentration measurements in stagnation-flow diamond-forming flames. We have constructed a combustion apparatus similar to the Murayama and Uchida burner [2]. Gas-phase temperature profiles are obtained using coherent anti-Stokes Raman scattering (CARS) spectroscopy of the hydrogen molecule [6]. Hydrogen atom concentration profiles are measured using three-photon excitation laser-induced fluorescence (LIF) [7]. Only laser-based diagnostic techniques are capable of providing the necessary spatial resolution and accuracy in this flame without perturbing the flow or chemistry.

EXPERIMENTAL APPARATUS

Fig. 1 is a schematic of the diamond-forming flame apparatus constructed in our laboratory. A rich mixture of C_2H_2, H_2, and O_2 is accelerated by a 3 mm-diameter nozzle to speeds between 40 and 50 m/s. The premixed jet then impinges on a water cooled, 15 mm-diameter molybdenum substrate located 4.5 mm above the nozzle exit. A flat flame is stabilized approximately 1 mm below the substrate in this geometry. The core gas flow is surrounded by a shield flow of hydrogen gas to prevent the formation of a room-air diffusion flame.

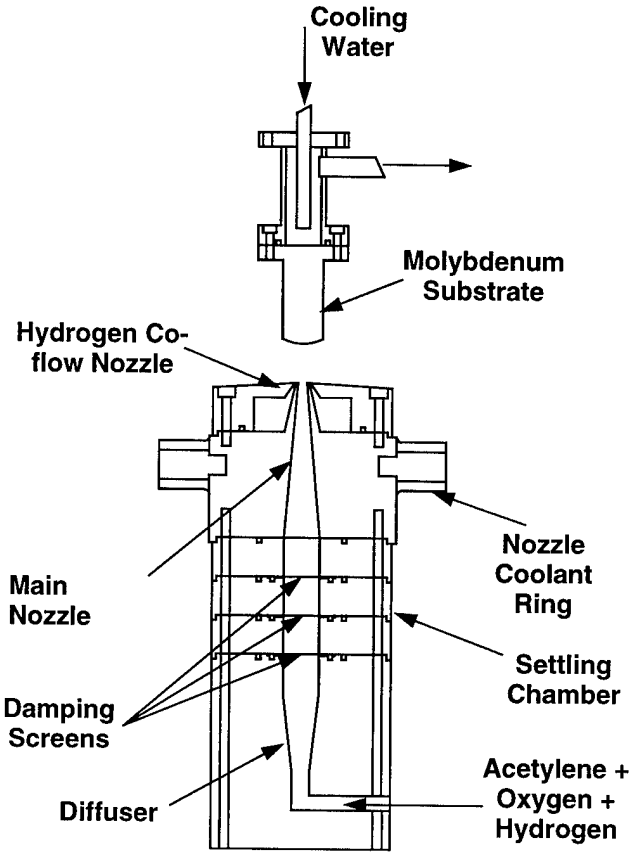

Fig. 1. Schematic of diamond-forming flame apparatus.

We have demonstrated diamond film formation under various run conditions. The films deposited during these runs were found

to consist of high quality diamond as analyzed with surface Raman spectroscopy.

RESULTS AND DISCUSSION

Hydrogen CARS

Hydrogen CARS temperature profiles were obtained in the diamond-forming flame under a variety of conditions. Fig. 2 shows the measured CARS temperature profile for one of the flames investigated. In this case, the mean nozzle exit velocity was 40 m/s and the overall flame equivalence ratio was 2.87. The substrate temperature—measured by two embedded thermocouples—was 1100 K. These conditions closely matched those reported by Meeks et al. in their model [4].

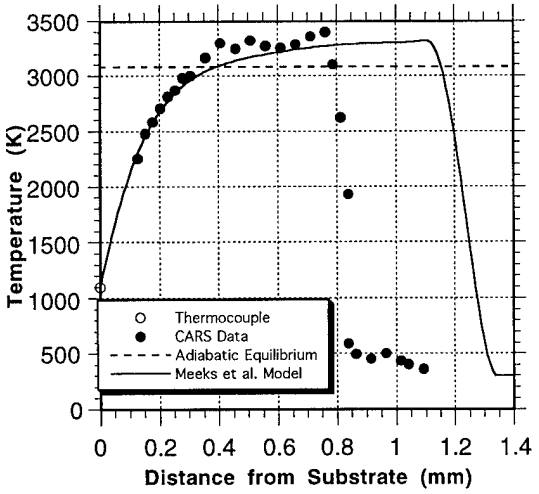

Fig. 2. Measured temperature profile in the diamond-forming flame, including Meeks et al. results [4].

The primary difference between the measurements and the calculation is the flame stand-off distance—the distance between the substrate and the steep temperature gradient indicating the start of the reaction zone. This variation was originally thought to be due to a non-uniform velocity profile at the nozzle exit. However, hot-wire anemometry measurements of jet velocity showed a nearly uniform profile. Another possible explanation could be the infinite stagnation plane assumption used in the model.

Overall, the measurements agree well with the calculations. Peak measured temperatures are above the adiabatic flame temperature, as predicted by the model. The CARS technique was also able to measure the temperature gradient to within 100 μm of the deposition surface.

Comparison to Nitrogen CARS

A comparison was made between H_2 CARS and N_2 CARS temperature measurements in a surface mixing, flat-flame burner (a so-called Hencken burner) to determine the accuracy of the H_2 CARS technique. Fig. 3 compares H_2 CARS temperatures to N_2 CARS temperatures obtained 3.8 cm above the burner surface in a hydrogen/air flame at various equivalence ratios. The maximum difference between the two techniques is on the order of 50 K. The CARS measurements are in good agreement with the calculated adiabatic equilibrium temperature for this flame.

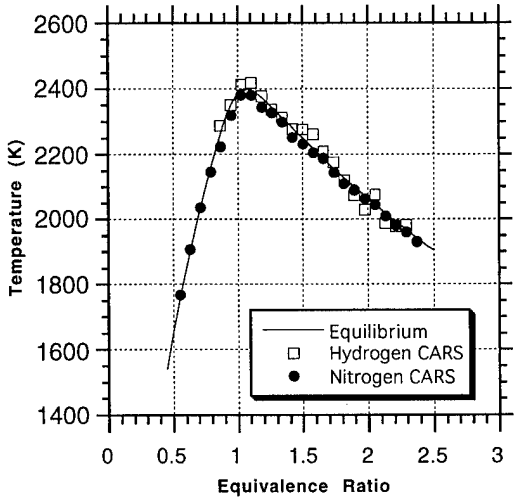

Fig. 11. Comparison of H_2 and N_2 CARS in a calibration flat-flame burner.

H-atom LIF

Atomic hydrogen was first detected in the Hencken burner to verify the three-photon excitation laser-induced fluorescence (LIF)

experimental technique. Detection of atomic hydrogen has proven to be quite challenging in the diamond-forming flame due to flame emission interference and the steep temperature gradients.

Fig. 4 shows a three-photon excitation fluorescence scan for atomic hydrogen in the diamond-forming flame under the same flow conditions as in Fig. 2. The two curves represent excitation both on and off the H-atom resonance averaged over 100 laser shots. The off-resonance signal could be due to PAH fluorescence or scattering of the excitation laser beam. Notice the large flame emission background even with a 100 shot average.

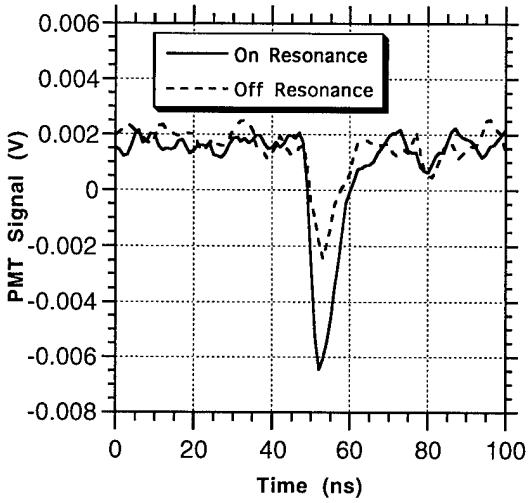

Fig. 4. H-atom LIF signal detected in the diamond-forming flame under flame A conditions.

Unfortunately, we are unable to show concentration profiles at this time, but we are encouraged by our initial success at detecting atomic hydrogen in the diamond-forming flame. We expect to improve the diagnostic over the next several months, enabling us to obtain quantitative concentration profiles.

CONCLUSIONS

In conclusion, we have successfully measured temperature profiles in the region near the deposition surface in a diamond-forming flame using H_2 CARS. These results are in excellent agreement with the numerical computations of Meeks et al. [4]. Our measurements confirm the super-adiabatic temperature predictions of the model. The measurements also capture the steep temperature gradient near the substrate surface. A comparison of H_2 and N_2 CARS temperature measurements in a calibration flat-flame burner showed excellent agreement, increasing our confidence in the accuracy of the results.

We were able to detect atomic hydrogen in the diamond-forming flame and the calibration burner using three-photon excitation LIF. Signal detection was complicated by the strong flame emission and steep temperature gradients. Future efforts will focus on making the measurements quantitative.

This work is supported by the National Science Foundation, Combustion and Thermal Plasma Program, Chemical and Transport Systems Division under Grant #CTS-9313829. The authors also gratefully acknowledge Dr. Roger Farrow at Sandia National Laboratories, Livermore, CA, for his helpful suggestions and insight.

REFERENCES

1. Murayama, M., Kojima, S., and Uchida, K., *Journal of Applied Physics* **69**: 7924-7926 (1991).
2. Murayama, M. and Uchida, K., *Combustion and Flame* **91**: 239-245 (1992).
3. Yarborough, W. A., and Messier, R., *Science* **247**: 688-696 (1990).
4. Meeks, E., Kee, R. J., Dandy, D. S., and Coltrin, M. E., *Combustion and Flame* **92**: 144-160 (1993).
5. Goodwin, D. G., *Journal of Applied Physics* **74**: 6888-6906 (1993).
6. Bergmann, V., and W. Stricker, *Applied Physics B* **61**: 49-57 (1995).
7. Alden, M., Schawlow, A. L., Svanberg, S., Wendt, W., and Zhang, P. -L., *Optics Letters* **9**: 211-213 (1984).

Laser-Induced Fluorescence Measurements of the Distribution of C_3 in the Plume of a dc-Arcjet During Diamond Deposition

George A. Raiche and Jay B. Jeffries
Molecular Physics Laboratory
SRI International
Menlo Park, California 94025

Thin films of diamond phase carbon can be grown by a wide variety of chemical vapor deposition techniques,[1] including hydrocarbon combustion and hydrogen rich hydrocarbon plasmas at atmospheric and sub-atmospheric pressures. The excellent thermal conductivity and high electrical resistance of diamond make it an attractive material for a wide variety of thermal management applications. Low cost, uniform deposition over large areas would make polycrystalline diamond an ideal substrate for high speed electronic circuit packaging in multi-chip modules. Thus, reactors which can rapidly deposit diamond and can be scaled to large area deposition are most attractive for these practical applications.

Polycrystalline diamond film grows beneath the stagnation point of the effluent plume from a dc-arcjet plasma. Large, free standing polycrystalline films 200-300 μm thick with thermal conductivity greater than 15 W/cm have been grown with dc-arcjet reactors. In an effort to provide effective, real-time process control for arcjet growth of diamond films, we have explored optical diagnostic measurements[2-6] on the gas-phase plasma plume. These measurements coupled with chemical models[7] will improve our understanding of the gas-phase chemistry precursor to diamond film CVD and aid the development of process control sensors.

We have constructed a dc-arcjet reactor optimized for optical measurements of the arcjet plume between the exit nozzle and the substrate. Hydrogen or a hydrogen and argon mixture is activated in the electrical discharge and expands through a converging/diverging nozzle. Methane is added to the activated hydrogen in the diverging nozzle. The gas plume exits the nozzle and has a well defined transit time to the boundary layer above the growing diamond surface. The diamond grows on a water cooled substrate below the stagnation point of the luminous plume of reactive arcjet effluent. Our reactor has optical access for laser-induced fluorescence (LIF) with an excitation laser crossing the arcjet plume and fluorescence collection f5 at right angles to the flow and laser beam. The laser and the optical collection is limited by apertures for a spatial resolution of 1 mm^3. The arcjet nozzle and substrate assembly can be translated in the excitation laser beam and LIF can be observed as a function of distance between the nozzle and substrate and at various radial distances in the plume. At our typical operating conditions, the nozzle to substrate distance is 42 mm and the plume is approximately 18 mm in diameter. The LIF is either dispersed in a 1/3 m monochromator or filtered with a bandpass of 10 nm centered at 420 nm and detected with a photomultiplier.

We identify the C_3 radical in the plume of our dc-arcjet reactor during diamond deposition using LIF. We find the C_3 concentration increases with reaction time downstream from the exit of the nozzle. In the freesteam flow of the reacting plume of arcjet effluent, we find the greatest concentrations of C_3 in a shell at the outer edges of the arcjet plume.

Figure 1 shows the LIF collected at 423 nm as a function of laser wavelength between 404.7 and 406 nm and a laser pulse energy of 5 μJ/pulse in the top panel. The lower two

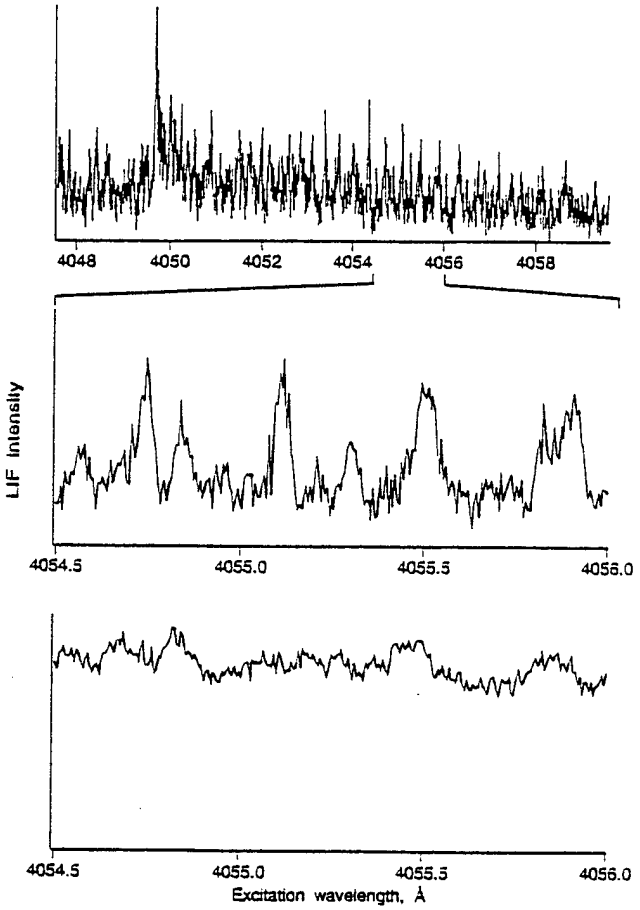

Figure 1

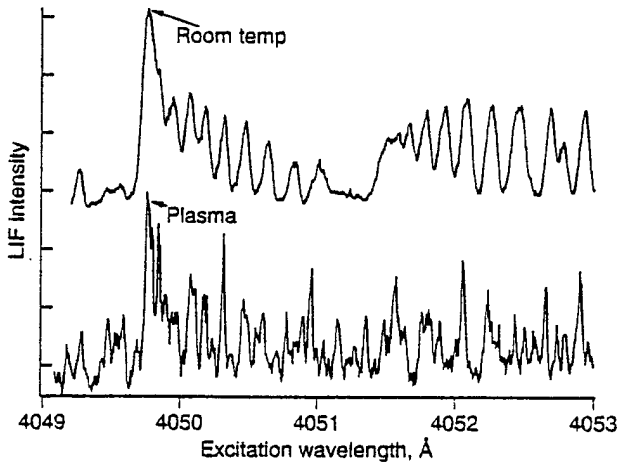

Figure 2

panels show the portion between 405.45 and 405.60 nm at 5 μJ/pulse in the middle panel and 500 μJ/pulse in the lower panel. In the bottom panel, the strong features evident in the low laser pulse energy are saturated and the weak features between them wash out any structure. This unstructured excitation spectrum initially lead us to believe we were observing LIF from polycyclic aromatic hydrocarbons in the arcjet plume.[4]

Subsequent observation of bandheads and regular rotational structure in excitation coupled with our earlier resolved fluorescence data, suggest C_3 as the origin of the LIF. Figure 2 shows the LIF from laser excitation between 404.9 and 405.3 nm in the 2000 K plume compared to a room temperature spectrum of C_3. The room temperature spectrum was taken with a significantly broader laser bandwidth; however, the figure unambiguously identifies the plume LIF near 405 nm to be from C_3.

In the middle of the plume on the centerline between the substrate and the nozzle, the C_3 LIF signal is weak with a significant non-zero background. The gas temperature peaks at the centerline of the plume near 2000 K and cools to 600 K at a radius of 12 mm. Figure 3 shows C_3 excitation scans 12 mm above the substrate at a radius of 0, 5 and 9 mm. The top panel on the centerline shows the hot C_3; the elevated baseline is the congested signal from the 80% of the molecules in thermally-populated excited vibrational states. The center panel at a radius of 5 mm shows the strong C_3 signal, and the bottom panel shows that beyond 8 mm radius there is very little C_3. Integration of the C_3 excitation spectrum from 404.95 to 405.15 nm integrates the signal from R branch from rotational levels from J=0 to J=52; which minimizes the variation in rotational partition function over the temperature range, 1000-2000 K where we observe C_3 in the plume. The vibrational partition function is calculated as a function of temperature by counting states using the spectroscopic data of Rohlfing et al.[11]

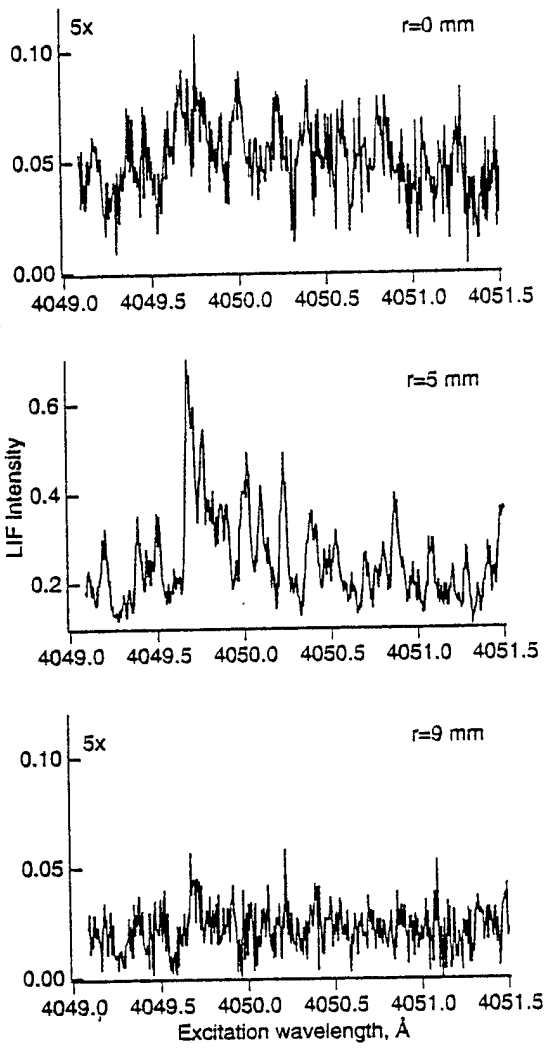

Figure 3

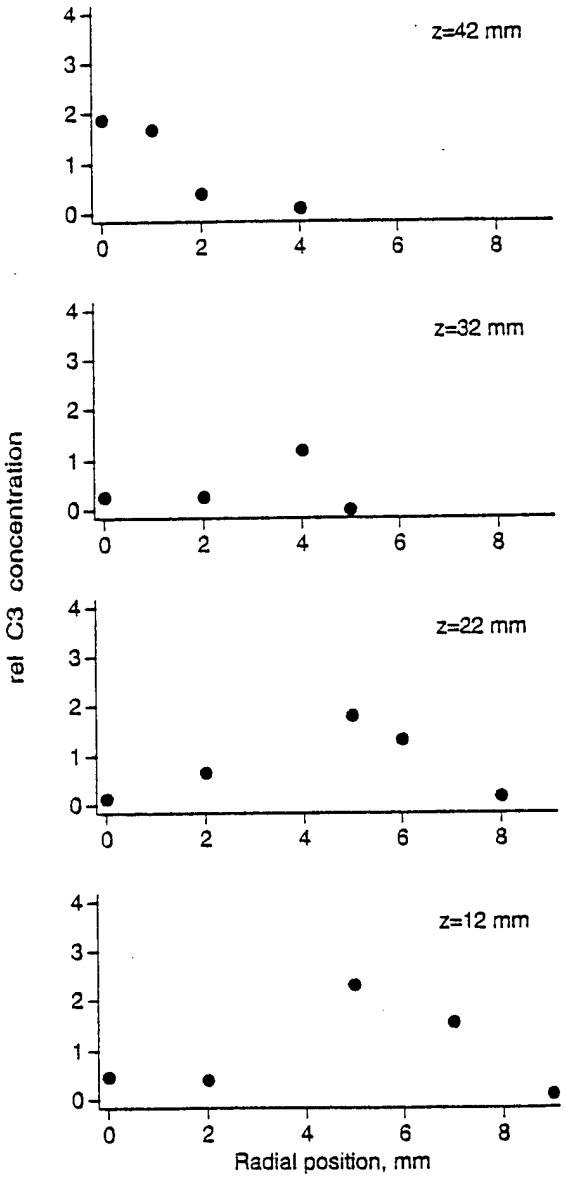

Figure 4

The LIF signal is corrected for the partition function variation with temperature and plotted in Figure 4 as a relative concentration as a function of plume radius for 42, 32, 22 and 12 mm above the substrate. Close to the nozzle, the plume is only 2 mm in diameter, only slightly larger than the spatial resolution of the measurement. 10 mm further downstream, in the second panel of Fig. 4, we observe the C_3 concentration to peak in a shell at a radius of 4 mm in the plume. The radius of the peak of the C_3 increases with increasing distance from the nozzle. The total amount of C_3 also increases with the reaction time in the plume. Closer to the substrate than shown in Figure 4, we find the C_3 in the boundary layer becomes much more uniform across the substrate.

These measurements show how spatially resolved LIF measurements of reactive intermediates can be used to characterize a practical deposition system. The chemical role of C_3 in the deposition of diamond is unexpected and unknown. Model calculations are currently underway to provide predictions to compare with the measured C_3.

This work is sponsored by ARPA via a subcontract with the Naval Research Laboratory.
The permanent address for G. A. Raiche is the Department of Chemistry, Hamilton College, NY.

References

1. F. G. Celii and J. E. Butler, Ann. Rev. Phys. Chem. **42**, (1991) 643-684.
2. G. A. Raiche and J. B. Jeffries, Appl. Opt. **32**, (1993) 4629.
3. G. A. Raiche and J. B. Jeffries, Appl. Phys. Lett. **63**, (1993) 3002.
4. J. B. Jeffries, G. A. Raiche, and M. S. Brown, SPIE **2124**, (1994) 270.
5. E. A. Brinkman and J. B. Jeffries, in *Diamond Materials IV*, ed. K. V. Ravi and J. P. Dismukes, Electrochemical Society Press, Pennington, NJ, 1995, p 461-466.
6. E. A. Brinkman and J. B. Jeffries, AIAA, 95-1955, 26th Plasmadynamics and Lasers Conference, San Diego, 1995.
7. G. P. Smith and J. B. Jeffries, in *Diamond Materials II*, ed. A. J. Purdes, J. C. Angus, R. F. Davis, B. M. Meyerson, K. E. Spear, and M. Yoder, Electrochemical Society Press, Pennington, NJ, 1991, p 194-201.
8. D. G. Goodwin, Appl. Phys. Lett. **59**, (1991) 277.
9. M. E. Coltrain and D. S. Dandy, J. Appl. Phys. **74**, (1993) 5803.
10. M. Frenklach and H. Wang, Phys. Rev. B **43**, (1991) 1520.
11. E. A. Rohlfing, J. Chem. Phys. **91**, (1989) 4531.

Trace NO_x Analysis by Laser Resonance-Enhanced Multiphoton Ionization Photoacoustic Spectroscopy near 454 nm

R.C. Sausa[1] and R.L. Pastel[2]
U.S. Army Research Laboratory
AMSRL-WT-PC
Aberdeen Proving Ground, MD 21005
Phone: (410) 278-7070 Fax: (410) 278-7070 Email: Sausa@arl.mil

There is a growing interest in laser-based analytical techniques for remote or *in situ* trace detection of NO_x ($NO+NO_2$) pollutants.[3] Much of this interest stems from concerns related to health and the environment. The detection of these species is also important in photofragmentation/fragment detection techniques being developed for the chemical analysis of energetic materials.[4,5]

In the present study, we employ a single 454 nm laser to detect trace NO and NO_2 concentrations at atmospheric pressure. NO is detected using miniature electrodes by (2+2) resonance-enhanced multiphoton (REMPI) processes via NO $A^2\Sigma^+$-$X^2\Pi$ (0,0) transitions, while NO_2 is detected using a miniature microphone by photoacoustic spectroscopy involving the NO_2 $\tilde{A}'\ ^2B_1(0,8,0)$ - $X\ ^2A_1(0,0,0)$ transitions. A potential energy diagram showing the physical processes in NO_2 PA and NO (2+2) REMPI detection is depicted in Figure 1. In PA detection, 454 nm radiation excites NO_2 into the $\tilde{A}'$ ($^2B_1$) or $\tilde{A}$($^2B_2$) states. Radiationless deactivation of excited NO_2 by inter- and intra-molecular interactions causes heat release inducing a pressure wave which generates the PA signal. PA detection is favored over ionization or dissociation at low laser intensities. In the visible and at low laser intensities,

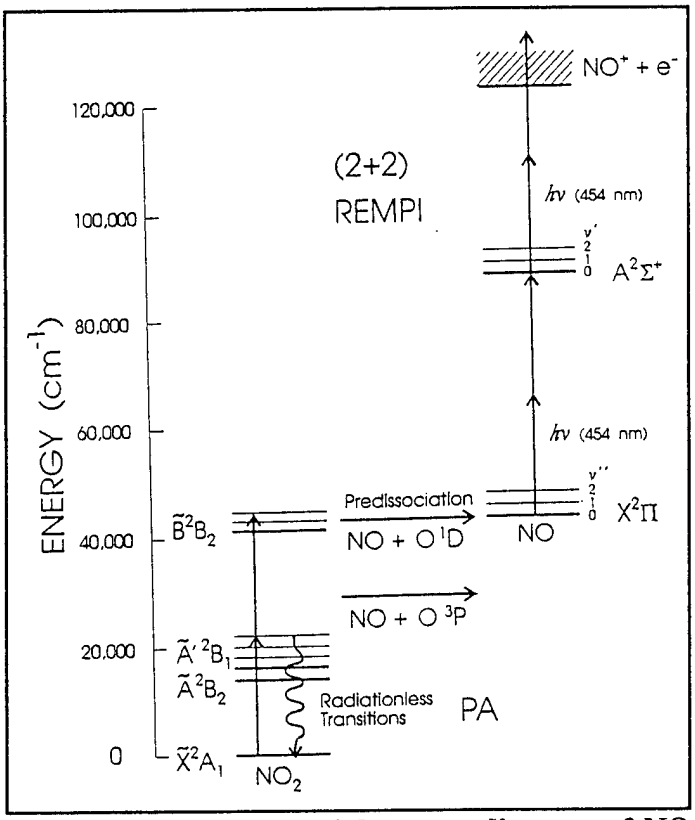

Figure 1: Partial potential energy diagram of NO and NO_2.

NO has a small absorption coefficient, hence no photoacoustic response. At high laser intensities, NO is ionized by 4 photon absorption, (2+2) REMPI. The ionization process is enhanced at 454 nm by two photon resonance with the $A^2\Sigma^+$ state. At high laser intensities, NO_2 photodissociates[6,7] and contributes to the "ambient" NO REMPI signal.

Rotationally resolved NO and NO_2 laser excitation spectra are recorded and characterized. To the best of our knowledge, this is the first time that a high resolution NO_2 visible PA spectrum is reported. The spectra recorded at 1 atm suggest that the technique is highly selective based on wavelength excitation. The sensitivity of the technique is also high, with NO and NO_2 concentrations measured as low as 20 and 100 ppb, respectively, at 1 atm. Limit of detections (LODs), defined as the concentration, C, equal to $3\sigma/S$, where S is sensitivity and σ is the standard deviation of the noise, are also determined. Presented in Figure 2 are the PA and REMPI sensitivity plots at 453.856 nm. Using the slope of the sensitivity plots and a noise determined from 20 independent 100 shot averages without analyte, LODs of 100 ppb for NO and 400 ppb for NO_2 are determined for 10 s integration time. Sensitivities in the low ppb are projected with an increase in laser energy and an improved system.

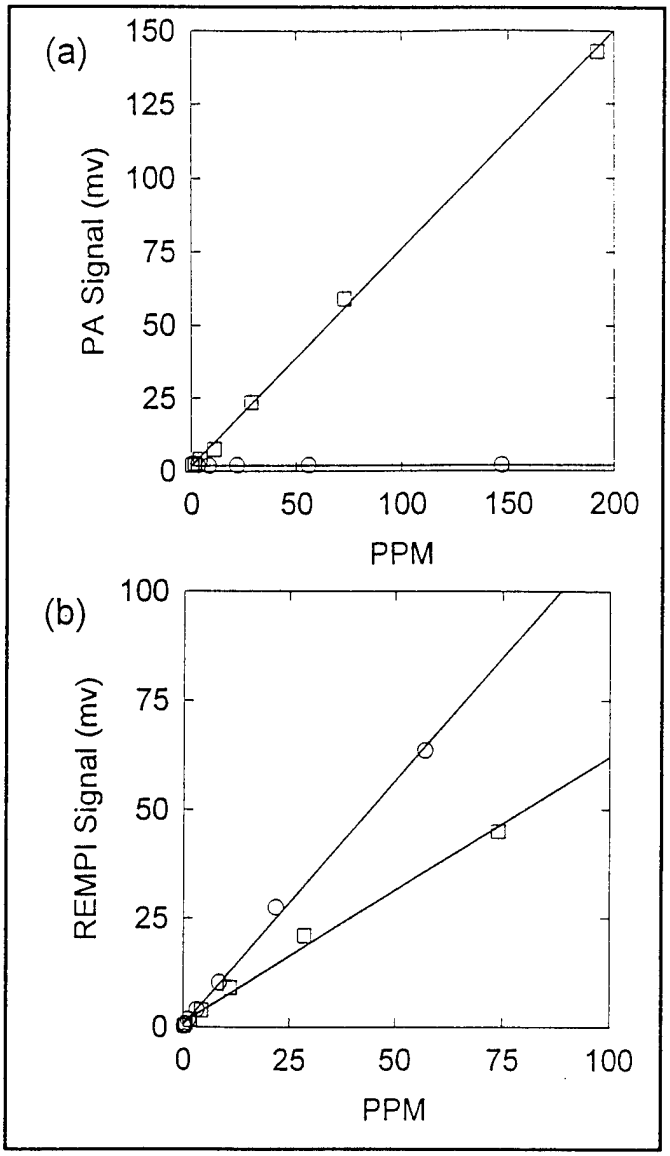

Figure 2: Plots of (a) NO PA (○) and NO_2 PA (□), and (b) NO REMPI (○) and NO_2 REMPI (□).

The absence of a NO PA signal in the visible enables NO-NO_2 mixture determination by combined PA-REMPI detection using single laser wavelength. Signal response and noise analyses determine the relative error due to computing the mixtures and the range that can be measured. These results will be presented and discussed at the meeting. The analytical implications of our technique for monitoring and quantifying NO_x

pollutants *in situ* and in real-time will also be discussed.

REFERENCES

1. Presenter and corresponding author.

2. ARL/SCEEE Postdoctoral Fellow.

3. J.B. Simeonsson and R. C. Sausa, *Appl. Specstrosc. Reviews*, to be published.

4. G.W. Lemire, J. B. Simeonsson, and R. C. Sausa, *Anal. Chem.* **65**, 529-533 (1993).

5. A. Marshall, A. Clark, K.W.D. Ledingham, J. Sander, R.P. Singhal, C. Kosmidis, and R.M. Deas, *Rapid Comm. Mass Spectro.* **8**, 521-526 (1994).

6. R.J.S. Morrison, B.H. Rockney, and E.R. Grant, *J. Chem. Phys.* **75**, 2643-2651 (1981).

7. L. Bigio, R. S. Tapper, and E. R. Grant, *J. Phys. Chem.* **88**, 1271-1273 (1984).

LASER-INDUCED CHEMISTRY WITHIN CLUSTERS

M. Z. Martin, S. R. Desai, C. S. Feigerle, and J. C. Miller

Chemical and Biological Physics Section,
Health Sciences Research, Oak Ridge National Laboratory,
P. O. Box 2008, Oak Ridge, Tennessee 37831-6125

and

Department of Chemistry, University of Tennessee,
Knoxville, Tennessee 37996

Tel: (423) 574-6239 Fax: (423) 576-4407 E-Mail: millerjc@ornl.gov

INTRODUCTION

Clusters comprise an interesting environment for the study of chemical reactions. Binary cluster complexes can be produced which combine a variety of potential reactant partners in various proportions in an intimate, yet controlled arrangement. Molecules or ions within such a cluster (i.e. solvated) have properties which are intermediate between those of isolated species and of species in solution or in bulk. Furthermore as the cluster size increases their properties may smoothly change until the condensed-phase regime is reached. But, since clusters are generated and interrogated in the gas phase, powerful techniques such as mass spectrometry may be used for characterization. Such clusters may then represent model environments which simulate real world situations such as aerosols or cells. Similarly, the chemistry of such clusters may also differ in significant ways from that of the isolated species.

In this presentation we will describe three examples where clustered molecules are photoexcited with a laser and the subsequent chemical reactions are followed by mass spectrometry. These include the cationic polymerization of carbon disulfide, the conversion of nitric oxide clusters to dinitrogen trioxide clusters and the generation and reactions of metal ions.

TECHNIQUE

Figure 1 is a schematic showing the present form of the laser ionization mass spectrometry apparatus. Briefly, the isentropic core of a pulsed supersonic expansion is selected by a skimmer and intersected at 90° with a focused laser beam. The mass-to-charge ratios of the ions which are formed by multiphoton ionization are analyzed using a linear time-of-flight mass spectrometer.

The pulsed valve is commercially available (R. M. Jordon Co.). A 0.5-mm diameter nozzle aperture and backing pressures of several atmospheres were typically used in these experiments. Gas

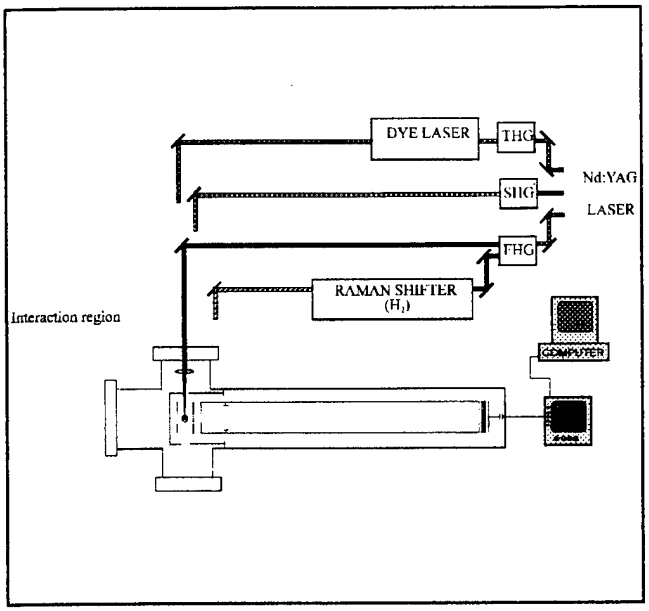

Figure 1 Schematic of the experimental apparatus.

pulse durations range from 70-100 μs depending on the carrier gas The laser beam is focused with a 75 mm focal length lens into the jet in the region between the extraction plates of a time-of-flight (TOF) mass spectrometer. The spectrometer is of the design introduced by Wiley and McLaren and has a mass resolution ($m/\Delta m$) of about 300 in the range of 1-2500 amu. A dual channel-plate electron multiplier is used to detect the photoions.

The laser system consists of an Nd:YAG laser (Quantel YG571C) which delivers 75 mJ in a 20 ps pulse (mode-locked operation) at the 1064 nm fundamental wavelength. The second, third, or fourth harmonic (532, 355, or 266 nm) of the 1064 nm output also is available. Raman shifting in hydrogen gas yields other useful wavelengths.

CARBON DISULFIDE POLYMERIZATION

Laser snow was the whimsical name given by Professor William Happer to his observation of precipitation of white particles following resonant laser excitation of a cesium/hydrogen mixture. Recently we have observed a modern analogue of laser snow. Although visible particles were not observed in this low pressure experiment, the mass spectrum following laser ionization of CS_2 clusters revealed the presence of polymers of sulphur and carbon sulfide ($S^+_{m=1-12}$ and $CS^+_{m=1-4}$, respectively). In addition, intermediate species such as $S^+_m(CS_2)_n$ provided clues to the polymerization mechanism.

Although the original laser snow involved collisions of excited atoms or molecules with other species, the cluster mechanism eliminates the need for collisions. When one member of a cluster of CS_2 molecules is excited it finds its next-door neighbor to be a suitable reaction partner and no collision is needed. Any extra energy due to the reaction can be used to eject weakly bound species from the cluster. The initially ionized molecule "eats" its way through the cluster like a molecular "Pac-man" creating bigger and bigger polymers with each bite. More details can be found in a recent publication [Desai et al., J. Phys. Chem. **99**, 1786 (1995)].

DINITROGEN TRIOXIDE CLUSTERS

The generation of $NO^+(N_2O_3)_n$ and $NO_2^+(N_2O_3)_n$ clusters from ionization of dilute NO/CH_4 expansions represents another example where photochemistry in a cluster is highly selective at producing certain types of cluster ions.

The TOF mass spectrum produced by two-photon ionization (266 nm) of a 5% CH_4 / 5% NO / 90% Ar/ trace H_2O mixture is shown in Figure 2. In contrast to what might be expected from such

a complex mixture, the spectrum is remarkably simple, consisting primarily of a single cluster ion series. Beginning at a mass of 106 amu, a series of peaks spaced by 76 amu with monotonically decreasing intensities is observed. Ten members of the series are seen in the figure but the series can be followed out to 1246 amu (16 members) in other spectra.

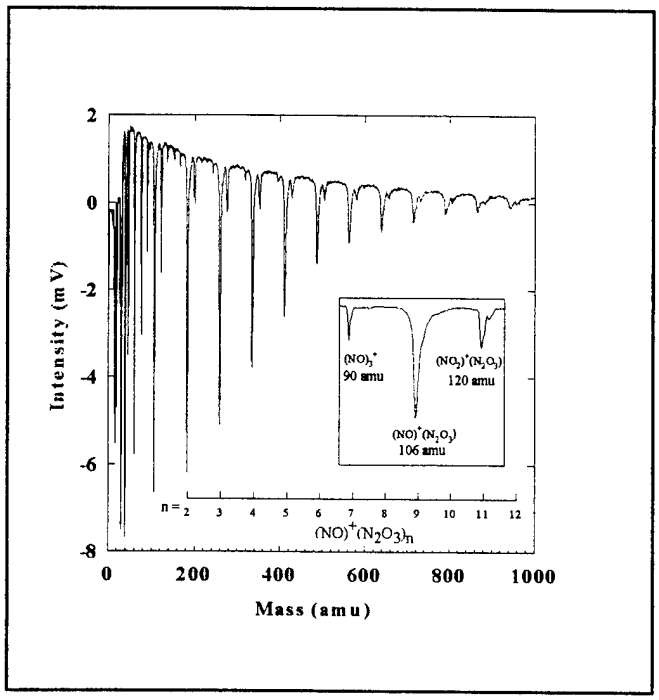

Figure 2 Photochemically produced $NO^+(N_2O_3)_n$ cluster ions.

Use of isotopically substituted nitric oxide confirms the assignment of the major peaks to the $NO^+(N_2O_3)_n$ clusters. Two additional cluster series, corresponding to inclusion of one less or one more oxygen atom in the cluster relative to $NO^+(N_2O_3)_n$, are observed in the spectrum shown in figure 2. The second major series of peaks is assigned to $(NO_2)^+(N_2O_3)_n$ clusters and the intensity of these peaks is about 25% of the corresponding $NO^+(N_2O_3)_n$ peak. A weaker third series corresponding to $(NO)_3^+(N_2O_3)_{n-1}$ is observed 16 amu to lower mass than each of the first five main peaks.

The conversion of nitric oxide clusters to clusters of dinitrogen trioxide appears to occur in a facile manner when excess energy during electron or photon impact is deposited in the cluster. In the present case, the role of the methane and water complicates the interpretation. More details may be found in an upcoming publication [Martin et al., submitted to J. Phys. Chem. (1995)]

METAL ION CHEMISTRY IN CLUSTERS

Very recently we have begun to investigate metal atom and/or ion chemistry in clusters by photolizing organo-metallic precursors combined in binary clusters with other reactant molecules. Results of such studies are important to such diverse fields as catalysis, chemical vapor deposition and corrosion.

In preliminary experiments, $Fe(CO)_5$ was expanded in argon and ionized with the 266nm YAG laser output. The resulting mass spectrum showed extensive stripping of the ligands and a large production of bare iron ions. This result was not unexpected as many previous experiments by others have shown similar results. What was unexpected, however, was the observation of large iron clusters, Fe_n^+. One previous study had reported this phenomenon but only at shorter wavelengths. The interpretation is somewhat complicated by the mass coincidence of iron and $(CO)_2$ of 56 amu. However, when nitric oxide was additionally present in the cluster, the evidence for chemical reaction was unambiguous. Ions such as FeO^+, $FeNO^+$, $FeNOCO^+$ and so on were clearly evident. Various ion-molecule reactions are assumed to be taking place within the cluster. Future work will focus on other common CVD precursors.

Friday, March 22, 1996

Environmental and Surface Analysis

LFB 10:15 am-12:15 pm
Windsor Ballroom

Timothy Harris, *Presider*
AT&T Bell Laboratories

Applications of acousto-optic tunable filters in environmental sensors

Xiaolu Wang
Brimrose Corp. of America
5020 Campbell Blvd. Ste E.
Baltimore, MD 21236

Acousto-optic tunable filters (AOTFs) are electronically addressable optical filters that provide rapid, random wavelength access, broad spectral coverage and moderately high spectral resolution. They are based on acousto-optic diffraction of light in an anisotropic medium. A piezoelectric transducer bonded to a birefringent crystal generates a traveling acoustic wave through the crystal, whenever it is excited by an applied RF signal. This acoustic wave establishes a periodic modulation of the index of refraction and generates a moving grating which allows diffraction of the incident light beam. For a given acousto-optic frequency, only a small wavelength band will satisfy the phase-matching condition and will be cumulatively diffracted. Varying the RF frequency has the resulting effect of changing the center of the optical bandpass. In addition, applying multiple RF frequencies simultaneously, result in multiple wavelength bandpasses.

The development of AOTF technology in the last two decades through many contributors, has resulted in a practical, general purpose spectroscopic device. There are AOTFs available which operate ranging from UV to IR wavelengths. While their applications in general spectroscopic systems are well established, developments in AOTF design and fabrication continue to enhance their appeal to developers of spectral imaging systems.

In this presentation, the AOTF's operation principles and different device configurations as well as the related spectroscopic systems will be reviewed with emphasis in environmental sensing applications.

Raman Applications with All-Silica Fiberoptic Probe

Yuan-Hsiang Lee[1], Sheng Dai[2], Jack P. Young*[1]

[1]Chemical & Analytical Sciences Division

[2]Chemical Technology Division

Oak Ridge National Laboratory

Oak Ridge, TN 37831-6142

Phone: 423-574-4922

Fax: 423-574-8363

e-mail: svl@ornl.gov

We have developed a unique all-silica fiberoptic probe that has the advantages of being simple and inexpensive to fabricate. The probe is useful for Raman, fluorescence, absorption, reflectance analysis over a wide temperature/pressure range and in corrosive chemical environments. The all-silica probe comprises one light exciting and six signal collecting optical fibers that are fused into a quartz tube under reduced pressure. No epoxy materials are required in the fabrication of the probe. Thus constructed, the probe is essentially a SiO_2 rod that maintains the optic characteristics of the individual fibers and has the thermal and chemical properties of SiO_2. We have evaluated the use of all-silica fiberoptic probe for normal Raman spectroscopy and investigated silver doped sol-gel films directly coated on the probe head for surface enhanced Raman scattering (SERS). The silver doped sol-gel films exhibit strong enhancement of Raman scattering from molecules adsorbed on the metal surface. We have applied the SERS-active films to both organic and inorganic analysis. In contrast to other silver surfaces, SERS response on our films develops rapidly and remains stable over long period of time (48

hours or more). We have also demonstrated analytical SERS enhancement for many inorganic ions, e.g. UO_2^{2+}, CO_3^{2-}, NO_3^-, NO_2^-, SO_4^{2-}, SO_3^{2-}. This presentation will describe and discuss our recent efforts toward the development of the all-silica fiberoptic probe, the fabrication of silver doped sol-gel films, and the analytical usefulness of both concepts.

Diode-Laser-Based Detection of BTXE-Aromatics in Oil Polluted Soil Samples

W. Schade and T. Blanke
Institut für Experimentalphysik, Universität Kiel, Olshausenstrasse 40,
D-24098 Kiel, Germany
Phone: +49-431-880-3839FAX: +49-431-880-3809
e-mail: PEX36@rz.uni-kiel.d400.de

The generation of tunable laser radiation in the spectral range between 4 and 10 μm is of general interest for the spectroscopy since most of the fundamental vibrational modes of molecules are within this spectral region [1]. There exist several conventional tunable cw-laser systems, like lead salt-diodes, color center-, optical parametric-, and CO or CO_2 side band lasers. However, they need cryogenic cooling, do not cover all spectral regions that are of general interest for the spectroscopy and in most cases they are very complicated and complex laser sources. This limits the possibilities for practical applications of mid-infrared absorption spectroscopy, e.g. in the trace analysis of environmental pollutants. Therefore there is still a lack in simple, compact, portable, and rugged mid-infrared laser sources. In this context diode-lasers and difference frequency generation (DFG) in new nonlinear media such as $AgGaS_2$ have drawn considerable interest in the construction of compact cw laser spectrometers [2,3].

In the present paper difference frequency generation of two single mode diode-lasers with powers of 30 and 50 mW in a 32 mm long $AgGaS_2$ crystal with a cut for type I noncritical phase matching at room temperature is applied to get a very compact tunable laser system for the mid-infrared spectral range. After optimization of the diode-laser beam profiles an infrared power of up to P_{DFG}=0.2 μW is obtained around λ_{DFG}=5 μm.

In Fig. 1 the schematic diagram of the diode-laser-DFG system is shown. The signal and pump waves are generated by single mode diode-lasers (Hitachi HL 7851G and Toshiba TOLD 9150) and the output wavelengths are centered at λ_s=785 nm and λ_p=682 nm, respectively. By changing the temperature of the two diode-lasers the tuning range is 780-790 nm and 681-684 nm. During single frequency operation the maximum output powers are measured to be P_s=50 mW and P_p=30 mW. Tunable DFG radiation is obtained in the spectral range 4.9-5.6 μm.

As typical for diode-lasers the output radiation is very divergent and non-isotropic in the horizontal (Θ_H) and in the vertical (Θ_v) direction of the emission. Therefore collimation optics (SK 9650, Schäfter&Kirchhoff) and anamorphic optics (SK 9650.AN2A, Schäfter&Kirchhoff) are applied to transform the non Gaussian beam profiles of the diode lasers into a nearly Gaussian beam. This is shown in Fig. 1b and c for the Toshiba laser-diode. Without anamorphic optics an eliptical beam profile with a ratio Θ_v/Θ_H=2.36 is obtained (Fig. 1b). The anamorphic optics consist of a system of cylindrical lenses. They expand the horizontal beam waist by a factor of two, which gives a nearly Gaussian beam profile with a diameter of about 3 mm (Fig. 1c).

The outputs of the diode-lasers have a polarization ratio of about 100:1. The appropriate polarization direction for 90° type I phase matching in the $AgGaS_2$ crystal is achieved by proper fixing of the diode-lasers in their housings. After beeing spatially overlapped by a polarization beamsplitter cube both beams are focussed into the nonlinear crystal by a convex lens (f=15 cm). The intensity distribution of the overlapping beams in

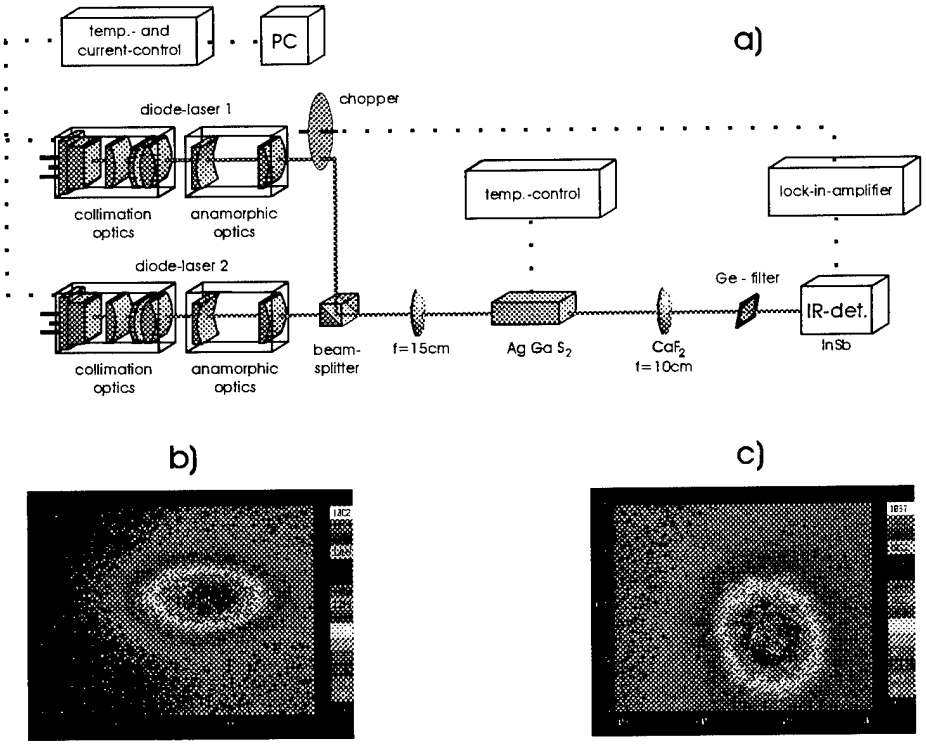

Fig. 1: (a) Experimental set-up of the diode-laser-DFG-system. Collimated beam profile of the Toshiba diode-laser without (b) and with (c) anamorphic optics.

the $AgGaS_2$ crystal is displayed in Fig. 2. A minimum beam waist of 38 μm is obtained. Because the diode-laser beam is approximated by a Gaussian beam, the waist is defined as the half of the width at $1/e^2$ intensity. The generated mid-infrared laser radiation is collimated by a CaF_2 lens (f=10 cm) and detected after a germanium filter with a liquid-nitrogen cooled InSb detector and a lock-in amplifier.

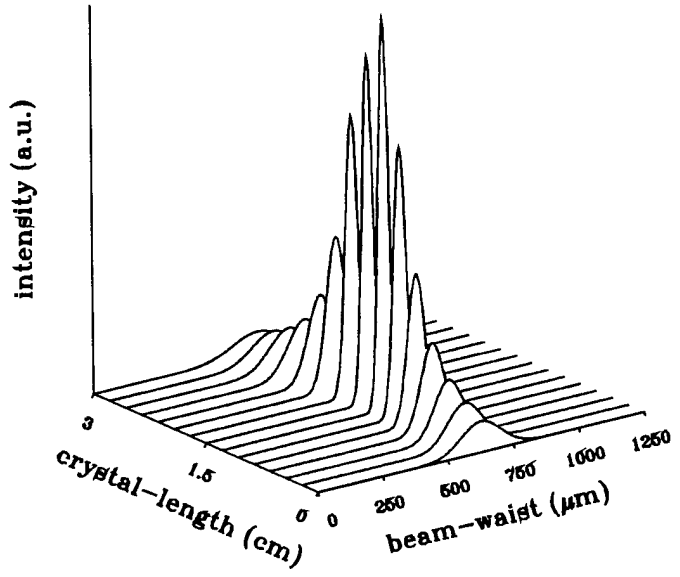

Fig.2: Spatially resolved intensity distribution of the focussed and overlapping diode-laser beams in the $AgGaS_2$ crystal.

In Fig. 3 the power of the generated DFG laser radiation is shown as a function of the input signal laser power. The power of the pump diode-laser is fixed at P_p=20 mW. Neutral density filters are applied to change the power of the signal diode-laser. As expected from the theory the DFG-power is increased linearly with the signal diode-laser power [4]. For P_p=20 mW and about 50 mW signal diode-laser power, a DFG-power of as much as 0.2 μW is obtained at λ_{DFG}=5.0 μm.

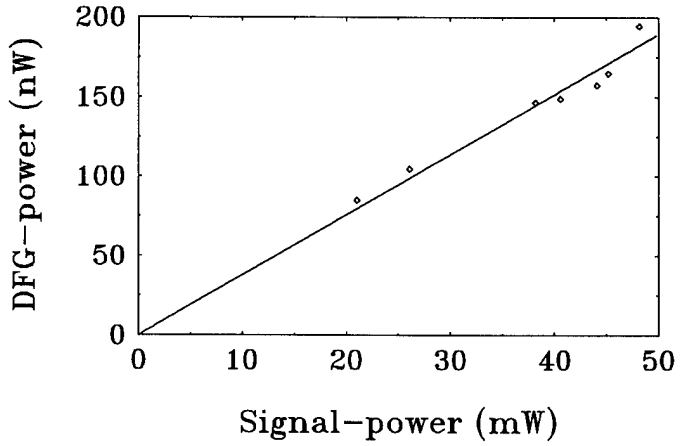

Fig. 3: Mid-infrared DFG-power as a function of the signal diode-laser power. The power of the pump diode-laser was fixed at P_p=20 mW during these measurements.

Such a diode-laser DFG spectrometer can now be applied for a quantitative analysis of BTXE-aromatics (benzene, toluene, xylene, and ethylbenzene) in oil or gas polluted soil samples. Contaminated samples are heated in a cell up to 200 °C. Depending on the boiling temperature the components with a low vapor-pressure (e.g. benzene: $T_{b.p.}$=80 °C) change first into the gas phase and can be detected by absorption spectroscopy [5]. In the mid-infrared spectral range between 5 and 10 μm there are several absorption lines that allow us to distinguish between benzene and toluene [6]. First spectroscopic results that are taken by this novel diode-laser DFG system will be reported.

This research is supported by the Technologiestiftung Schleswig-Holstein under contract 94-35i.

References

1. R. Grisar, G. Schmidtke, M. Tacke, and G. Restelli, eds., Monitoring Gaseous Pollutants by Tunable Diode Lasers (Kluwer, Dordrecht, The Netherlands, 1989).
2. P. Canarelli, Z. Benko, R. Curl, and F.K. Tittel; Opt. Soc. Am. B **9**, 197 (1992).
3. U. Simon, C.E. Miller, C.C. Bradley, R.G. Hulet, R.F. Curl, and F.K. Tittel; Opt. Lett. **18**, 1062 (1993).
4. T.-B. Chu and M. Broyer; J. Phys. **46**, 523 (1985).
5. J. Bublitz, A. Christophersen, and W. Schade; Fresenius J. Anal. Chem., submitted.
6. B. Schrader and W. Meier, eds., Raman/IR Atlas (Verlag Chemie GmbH, Weinheim, 1974).

RESONANT LASER ABLATION: APPLICATIONS AND MECHANISTIC ASPECTS

J. E. Anderson, A. W. Garrett, C. G. Gill, P. H. Hemberger and N. S. Nogar
(505) 665-7279, FAX (505)665-4631
Chemical Sciences and Technology, MS J565, LANL
Los Alamos, New Mexico 87545

T. M. Allen and P. B. Kelly
Department of Chemistry
University of California, Davis
Davis, California 95616

Introduction

Ever since the first report of laser action, it has been recognized that laser ablation (evaporation/volatilization) may provide a useful sampling mechanism for chemical analysis. In particular, laser ablation is rapidly gaining popularity as a method of sample introduction for mass spectrometry. Since its original description, numerous research papers and review articles have appeared on various aspects of laser mass spectrometry. While most laser ablation/mass spectrometry has been performed with fixed frequency lasers operating at relatively high intensities/fluences ($\geq 10^8$ W/cm^2, ≥ 1 J/cm^2), there has been some recent interest in the use of low-power tunable lasers to ablate and resonantly ionize selected components in the ablation plume. This process has been termed resonant laser ablation (RLA).[1] Potential advantages of RLA include: 1) simplification of the mass spectrum, by enhancement of signal from the analyte of interest; 2) improvement of the absolute detection limits by improving the ionization efficiency, and 3) improvement in relative sensitivity by reduction of spurious signal in the detection channel of interest (due to bleed through from adjascent mass channels or from isobaric interferences).

We report here on aspects of RLA behavior for a number of metals, alloys and thin films. The versatility of RLA is demonstrated, with results on a variety of samples and in several mass spectrometers. In addition, the application to depth profiling of thin films and multilayers is described; absolute removal rates and detection limits are also displayed. A discussion of possible mechanisms for low-power ablation is discussed.

Results and Discussion

Most experiments utilized an excimer-laser pumped dye laser for ablation/ionization, and either a linear time of flight (ToF) mass spectrometer, or an ion trap mass spectrometer (ITMS) for detection. The beam was typically passed through a variable attenuator to control the pulse energy, and a Soleil-Babinet compensator to control and rotate the plane of polarization.

a. General Considerations

RLA can be used to selectively address various elements in a multicomponent sample. Figure 1 shows typical mass spectra obtained with both the ToF and ITMS instruments. Each spectrum corresponds to irradiation of the surface at a different wavelength, corresponding to a "2+1" (photons to resonance + photons to ionize) ionization process for the labeled element. Several features are worth noting. First,

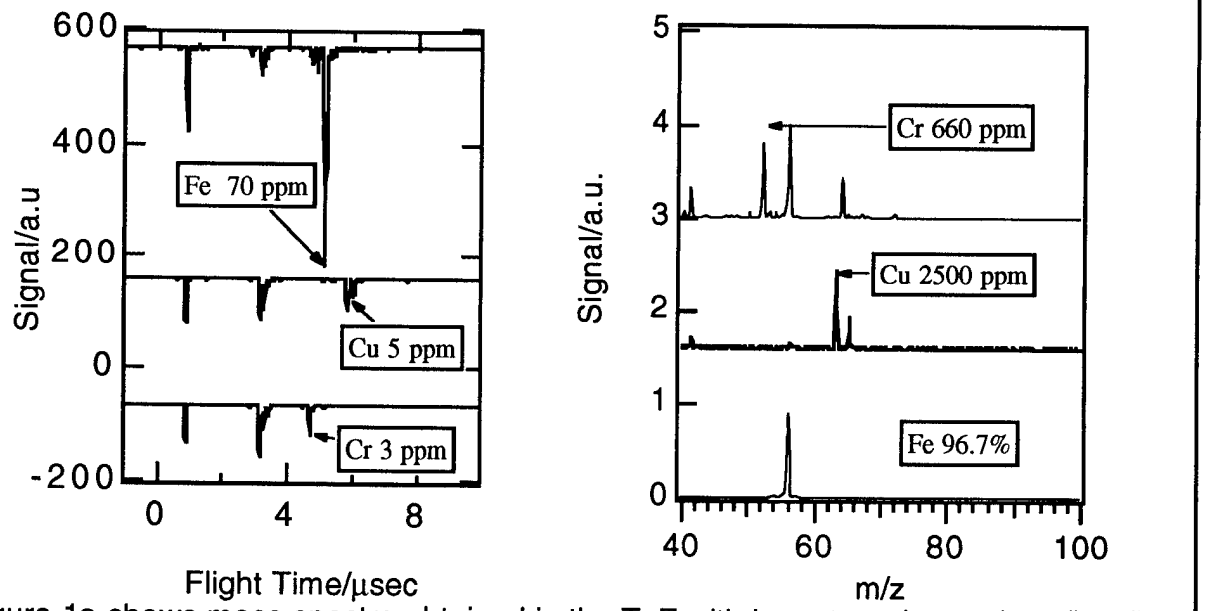

Figure 1a shows mass spectra obtained in the ToF with laser tuned to various "2+1" elemental resonances from a high-purity rhenium sample, while 1b shows similar results obtained with the ITMS from a high carbon steel sample.

signal was obtained with low pulse energies, typically 20 μJ (corresponding to a fluence ≈10 mJ/cm^2, or an intensity <10^7 W/cm^2). The observation of trace components at very low laser intensities is a significant virtue of this process; this sensitivity is due both to the resonant nature of the ionization process, and to the excellent overlap of the vaporized sample with the ionizing laser beam, as discussed below. Second, for very low concentration components, some interference may be seen: typically sodium and potassium, but in 1b (chromium) TiO is also observed. These components are presumably observed because of their high volatility and low ionization potential. They are thus easily vaporized, and ionized, by low-order non-resonant multiphoton processes. Last, using internal standards, we have been able to measure concentrations to an accuracy of ≈50%.

b. Thin film analysis and detection limits

A variety of metals have resonant transitions lying at similar energies, thus facilitating selective analyte ionization for a variety of components using the same laser dye. In addition, at the low fluences used, material removal rates are expected to be sub-monolayer per laser shot. With these characteristics, RLA has the potential for analysis of films and multilayer structures. We have demonstrated the use of RLA-mass spectrometry for the analysis of films using copper films of various thicknesses on Si(110) wafers, as a test case.[2] Figure 2a shows the copper RLA signal as a function of time for irradiation of a copper thin film (100 Å) on a silicon substrate. At a (rather high) pulse energy of 62 μJ, penetration of the film required 440 laser shots, resulting in a removal rate of ≈0.23 Å/shot. This removal occurs over a spot diameter ≈40μm, which allows us to calculate a total material removal per laser shot of 3.7 x 10^{-14} cm^3. If the copper film has the same density as bulk copper, this is a mass removal rate of 0.33 pg/shot.

To estimate the absolute sensitivity of RLA - ITMS, trace components of NIST standard reference materials (SRM's) were analyzed. The results for lead (26.5

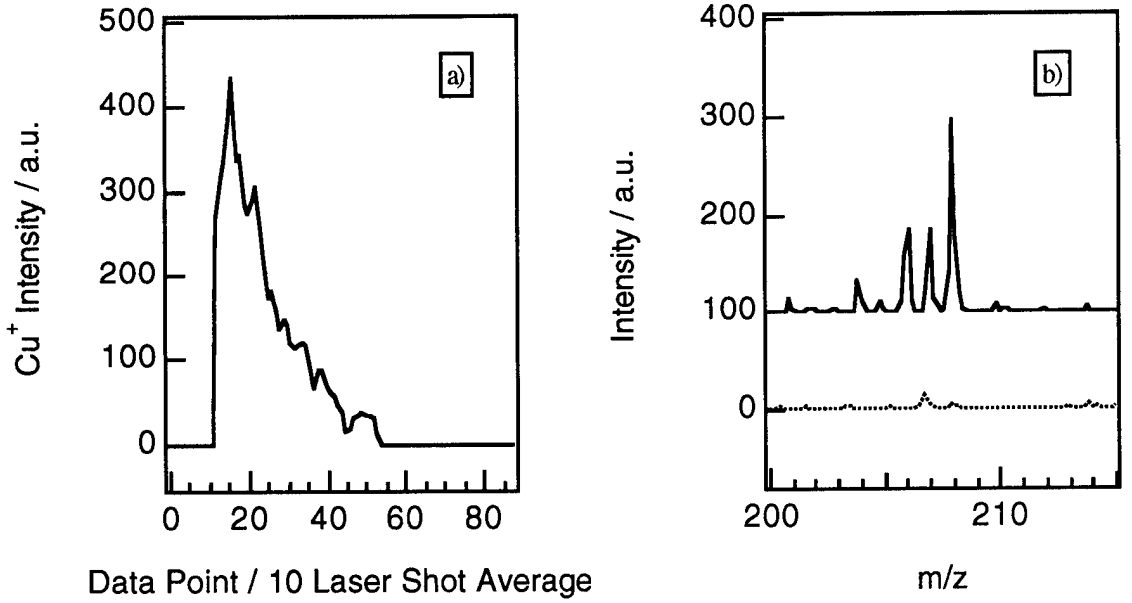

Figure 2a depicts removal rate for a 100 Å copper film from a silicon wafer; Figure 2b shows mass spectrum for lead on (upper) and off (lower) resonance.

ppm) in SRM 494 (unalloyed copper) are presented in Figure 2b. The high selectivity of RLA for the ionization of trace components in a complex matrix is observed, and when the mass removal rate determined above is factored in, the calculated absolute detection limit for RLA-ITMS is <9 attograms.

c. Mechanisms

Several observations suggest the observed ablation process may be nonthermal in nature.[3] The measured spot size of the laser and the ablation etch feature observed are significantly different, and may be seen as evidence of a nonlinear phenomena. In addition, microscopic examination of the laser ablated spots showed a series of lines in what appears to be an interference pattern, whose fringe spacing can be described by theoretical models based upon nonlinear growth processes. Laser polarization was observed to have a strong effect upon the RLA process, and was sample surface dependent. The variation in RLA intensity is consistent with the surface effects and polarization specificity of surface plasmon interactions. Based upon the experimental evidence and theoretical calculations presented, the desorption processes for RLA are non-thermal in nature, providing additional evidence for a nonlinear desorption mechanism based upon surface plasmon interactions.

References.

1. G. C. Eiden, J. E. Anderson, N. S. Nogar, Resonant laser ablation: semiquantitative aspects and threshold effects, Microchem. J., **50**, 289 (1994).
2. T. M. Allen, P. B. Kelly, J. E. Anderson, T. N. Taylor, N. S. Nogar, Depth profiling of copper thin films by resonant laser ablation, Appl. Phys. A: Mater. Sci. Process., **A61**, 221 (1995).
3. C. G. Gill, et al., Low-power Resonant Laser Ablation of Copper, Appl. Opt., **submitted**, (1995).

Quantitative Surface Analysis Using Photoionization of Sputtered Neutrals

Chun He and Christopher H. Becker
Molecular Physics Laboratory, SRI International
Menlo Park, CA 94025
Fax: (415)859-6196
Phones: (415)859-4686(CH), (415)859-5130(CHB)

I. Introduction

Surface quantitative elemental composition information is a fundamental measurement of critical importance to the design and evaluation of materials and components. Secondary ion mass spectrometry (SIMS) and spectroscopic techniques based on secondary electron energy measurements, such as electron spectroscopy for chemical analysis (ESCA) and Auger spectroscopy, are well-established analytical tools used to meet such a requirement in the industry. SIMS is a highly sensitive technique, capable of detecting trace element at ppm level. However, based on detection of ionized materials ejected during sputtering, SIMS has difficulties in quantification at surfaces and interfaces due to its well-known matrix effect. On the other hand, ESCA and Auger spectroscopy have good quantification capability, but low sensitivity. The detection limit of ESCA or Auger spectroscopy is $\leq$ 0.1% of the total sample composition[1].

Surface analysis by laser ionization (SALI) examines sputtered neutrals, taking advantage of the fact that neutral component typically constitutes the overwhelming majority of the sputtering yield. SALI employs nonresonant photoionization of sputtered neutrals followed by time-of-flight mass spectrometry. SALI can provide, in principle, a *universal* and *uniform* detection of all elements evolved from a surface. The detection sensitivity reaches ppm with submonolayer sampling. The large fluctuation of signal intensity associated with SIMS is not observed[1-2].

Here we present recent experimental results on nonresonant multiphoton ionization of species from several solid materials, NIST C1154 stainless steel, SiO_2, Ga As, and SiC single crystal using a well-characterized high intensity picosecond laser. These materials are of clear technological importance. They are also excellent samples in providing a stringent test for quantitative analysis because of the significant difference in ionization potentials of the elements involved. The experimental results demonstrate quantitative compositional analysis by driving relative sensitivity factors (RSFs) almost to unity.

II. Experimental

The details of the experiment have been described elsewhere[3-4]. Briefly, the experiments are performed on a newly constructed UHV analytical chamber which has an operating pressure of 1×10^{-9} torr. Mass spectra are recorded with a reflecting TOF system of 2-m effective path length. A 5 keV Ar^+ beam impinging at 60° from surface normal is used both for sample surface cleaning (30 $\mu A/cm^2$, 10 min), and sputtering (0.6 μA, 400 μm spot size) for SALI analysis. Photoionization of sputtered particles and gases is performed by using the second harmonic (532 nm) of a 35 ps Nd:YAG laser operated at 10 Hz. The laser beam is focused by a 10 cm focal-length, best-form lens situated at the end of a tube insert into the UHV chamber.

Photoion detection is by ion impact on dual microchannel plates at 2.4 keV impact energy followed by a variable amplification/attenuation electronics combination. The output analog signal is digitized by a 100 MHz transient digitizer controlled by a laboratory computer through a CAMAC interface. Mass spectra from sputtered surfaces are taken under steady-state conditions to avoid non-stoichiometric preferential sputtering.

Laser beam quality and spatial parameters at and near the focus are examined by a microscope objective and CCD camera assembly mounted on a precision xyz stage. The magnification of the microscope objective and CCD camera assembly is determined and verified by imaging a standard test target and pinholes with known diameters. The resulting laser-focus images are examined in real-time by a TV monitor via a video processing module.

III. Results and Discussion

The laser beam image at the focus presents a well-behaved Gaussian profile without hot-spots. The beam waist (radius) measured at $1/e^2$ of the peak intensity is 5.25 μm. With an energy of 44 mJ and pulse length of 35 ps the laser peak differential power density reaches 2.9×10^{15} W/cm^2 at the beam's center with an average power density over its beam waist 1.45×10^{15} W/cm^2. The term "power density" used in this paper is referred to the average power density over the beam waist. Knowing these beam parameters the saturation intensity and ion yield as a function of laser power density can be expressed in a quantitative way.

For a multiple-element sample containing a group of species *A*, *B* and *C*, the RSFs of the species *A* and *B*, with reference to species *C*, are defined as

$$RSF(A)=\frac{I_A/[A]}{I_C/[C]} \quad \text{and} \quad RSF(B)=\frac{I_B/[B]}{I_C/[C]}, \tag{1}$$

where I_A, I_B and I_C are signal intensities of species *A*, *B* and *C*, [*A*], [*B*] and [*C*] are concentrations of species *A*, *B* and *C* in the sample. A value of unity for RSFs for all species represents complete uniform detection sensitivity and thus reliable quantitation.

Mass spectra derived from ion beam sputtering of the C1154 stainless steel are presented in Fig. 1, at two laser power densities. The bulk composition of the C1154 is 64.5, 19.06, and 12.97 for Fe, Cr, and Ni, respectively. Obviously, at a laser power density of 3.3×10^{13} W/cm^2 the ionization is not uniform for *all* the species because the Cr^+ signal is stronger than that of Fe^+ although the abundance of Cr is smaller than Fe. The RSF ratio for Fe, Cr, and Ni, derived relative from peak area integration over various isotopes, is 1/5.8/2. A plausible explanation is that the first ionization potentials (IPs) for Fe, Cr and Ni are 7.87, 6.766 and 7.635 eV, respectively, and therefore four photons of the 532 nm laser, which has an energy equivalent to 2.33 eV, are needed to ionize Fe and Ni, but *three* photons are just barely enough to ionize Cr.

At a laser power density of 1.32×10^{15} W/cm^2, the intensity of $^{56}Fe^+$ increases substantially and surpasses the intensity of $^{52}Cr^+$. Moreover, at this power, double- and triple-charged species are observed for all three elements. The appearance of multiple-charged species is a solid evidence that ionization saturation has been achieved. The RSF ratio, derived from peak area integration over various single- and multiple-charged isotopes, is 1:1.09:0.84 for Fe, Cr and Ni, respectively. The signal intensities of these elements are true representations of their

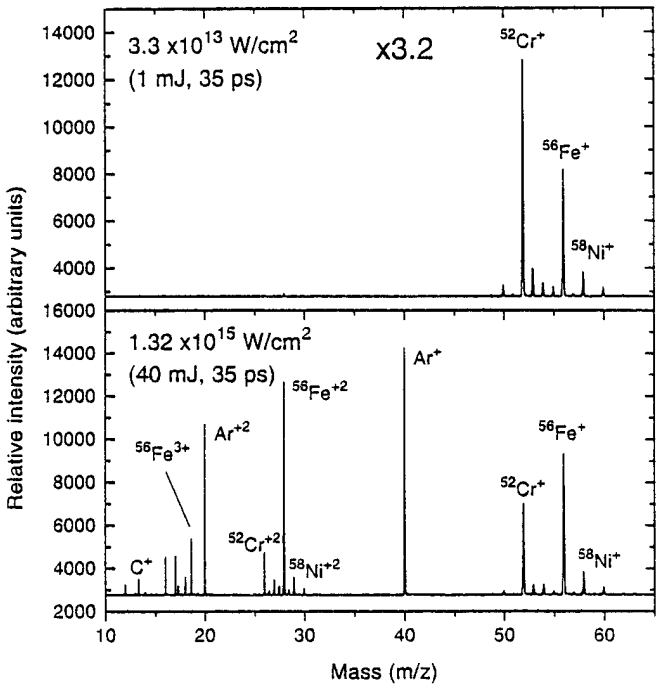

Fig. 1 Nonresonant MPI mass spectra of NIST C1154 stainless steel.

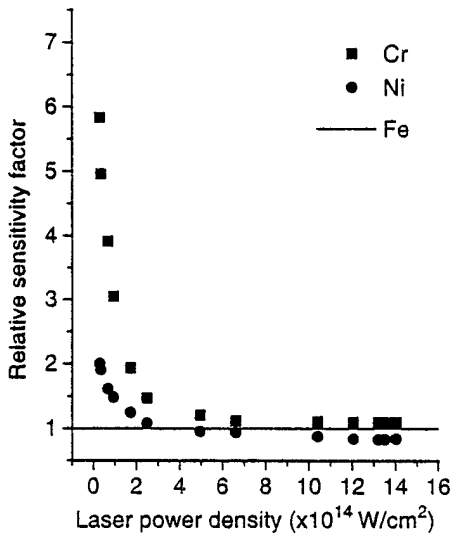

Fig. 2 RSF's of Fe, Cr and Ni as a function of laser power density.

concentration. The RSFs as a function of laser power density are plotted in Fig. 2 with Fe as the reference.

Experiments are also performed on SiO_2 thin film on Si substrate, GaAs single crystal and SiC single crystal. The common feature of these experimental results is that at lower laser power densities, complete quantitation is not achieved as ionization is not saturated for elements with high IPs. Elements which requires more photons for ionization show weaker signal intensities than whose requiring less photon for ionization. When the laser power density is boosted to 10^{14} - 10^{15} W/cm^2, ionization saturation is achieved for all elements.

IV. Conclusion

The four measurements presented here demonstrate the feasibility of performing quantitative surface and material analysis under high sensitivity conditions. The number of photons required for photoionization is of primary importance in reaching saturation. At high laser power densities, high-order nonresonant MPI not only can be saturated for elements and molecules with very high ionization potentials but also can lead to more uniformly-defined ionization volumes than for lower-order processes. Mass spectra truly representing surface composition can be obtained using high intensity laser of 10^{14} - 10^{15} W/cm^2 at 532 nm green light.

References

1. C. R. Brundle, C. A. Evans, Jr. and S. Wilson, *Encyclopedia of Materials Characterization*, Butterworth-Heinemann, Boston (1992).
2. C. H. Becker, *Ion Spectroscopies for Surface Analysis*, ed. by A. W. Czanderna and D. M. Hercules, p.273. Plenum, New York (1991) and references cited therein.
3. Chun He and C. H. Becker, Surf. and Interface Anal., in press
4. Chun He, J. Basler and C. H. Becker, J. Phys. Chem., submitted.

Characterization of Semiconductor Materials by the Photoionization of Sputtered Neutrals Using Ultra-High Laser Intensities

Michael L. Wise and Stephen W. Downey
AT&T Bell Laboratories
600 Mountain Ave.
Murray Hill, NJ 07974
(908)582-3727 FAX (908)582-3609

The depth profiling of dopant concentrations across ultrathin device structures is critical to microelectronic device design and fabrication. Secondary Ion Mass Spectrometry (SIMS) remains an extremely important technique for semiconductor characterization. However, secondary ion production during sputtering is extremely dependent on matrix composition, complicating the characterization of elemental concentrations at or near the interfaces of two materials . For this reason, complementary analytical techniques referred to as Sputtered Neutrals Mass Spectrometry (SNMS) have been developed. In SNMS, a laser beam is used to ionize the neutral species in the gas phase above the sample after ion beam sputtering. These "post-ionization" techniques can accomplish surface analysis and depth profiling with high sensitivity and relative freedom from matrix effects. The application of ultra-high intensity lasers ($>10^{14}$ W/cm^2) to the post-ionization technique creates the possibility that all the sputtered species, regardless of electronic structure, will be non-resonantly ionized with high efficiency[1]. Uniform ionization of all the sputtered species within the laser volume will greatly simplify the quantification of unknown materials.

The experimental apparatus used in these experiments is composed of a regeneratively-amplified Ti:sapphire laser (Clark CPA-1000) coupled with a magnetic sector SIMS instrument (VG). The laser produces 1 mJ pulses with pulse widths of 100-150 fs at 800 nm. Ion beam sputtering can be accomplished with a number of different elements. For surface analysis, the ion beam is pulsed at 1 kHz with 600 ns pulse widths in order to preserve the sample. To perform a depth profile, the ion beam is cycled between continuous, rasterred sputtering to create a crater and pulsed sputtering, during which the ion signals are measured.

The laser fires approximately 3 μs after the start of the sputter pulse and is focused ~100 μm in front of the sample. The focused beam diameter is calculated to be 40 μm. After losses, the laser pulse energy at the sample is ~800 μJ, creating laser intensities well in excess of 10^{14} W/cm^2. At these intensities, reference to the Keldysh Adiabaticity Parameter[2] and to studies on rare gas atoms[3] suggests that at least some of the ionization of the sputtered neutrals is occurring by a tunneling ionization (TI) mechanism. Non-resonant multi-photon ionization (MPI) also contributes, especially for those species with low lying electronic states. To determine if the ionization of a given species within the instrumental detection region was complete (saturation), ion yield versus laser intensity was measured for B, Ga, As, In, P, O, and Si as well as for their sputtered molecules. At saturation, only a slight increase in ion yield with laser intensity was measured reflecting only a slow increase in the ionization volume. Empirically, it was determined that

saturation occurs when Intensity(W/cm^2) > 4 x 10^{10} x IP(eV)^4, where IP is the ionization potential of the species of interest.

Figures 1-3 demonstrate the capabilities and limitations of the technique. Figure 1 shows a portion of the mass spectrum obtained from a GaAs matrix using Xe^+ sputtering. Singly, doubly, and triply charged ions of the primary matrix elements are resolved, demonstrating the ability to create ions even with high IP's. In addition, all singly charged dimers and trimers are detected, denoting that only moderate fragmentation is occurring during the ionization process. The relative sensitivity factors for Ga and As were determined by summing all the species measured in the GaAs mass spectra. When all the species containing Ga are summed and compared to all the species containing As, one finds that the total detected Ga:As ratio is 1: 1.3. The relative sensitivities for Ga- and As-containing species under these experimental conditions therefore appear similar. Equivalent studies of other matrices have also provided reasonably accurate quantitative representations of the actual matrix composition.

Figure 2 displays a depth profile of a sample composed of 1000 Å SiO_2 on a Si substrate. As expected oxygen-containing species decrease and exclusively Si-containing species increase in transitioning from the SiO_2 to the bulk Si. Importantly, the molecular species provide information about the actual bonding patterns in the respective matrices, indicating that the sputtering is not completely scrambling the bonding in the matrix. For instance, the Si_2^+ signal accounts for only 2% of the Si^+ signal in the SiO_2 while accounting for 22% in the Si bulk. Moreover, the post-ionization results predict the relative Si densities in the SiO_2 and bulk within a factor of two. If all the Si-containing species in the SiO_2 and Si are summed and compared, one finds that 4.6 times more Si is detected in the Si bulk than in the oxide. Most likely, incomplete detection (non-saturation) of the sputtered SiO_x species accounts for some of the error. Additionally, differences in the velocity and angular distributions of the different sputtered neutrals can affect detection efficiency.

Finally, Figure 3 shows a O_2^+ sputtered depth profile of a boron implanted sample composed of 1000 Å SiO_2 on Si (26 keV ^{11}B, 1x 10^{15} cm^{-2}). Three boron containing species are detected: B^+ (m/e = 11), BSi^+ (m/e = 39), and BO^+ (m/e = 27). Summing of these signals accurately depicts that half the boron dose is in the SiO_2 while the remaining half is in the Si bulk. This representation of the true boron profile is markedly better than measurements made by only detecting the secondary ions (SIMS). The boron SIMS signal unrealistically decreases by an order of magnitude when transitioning from the SiO_2 into the bulk Si using identical sputtering conditions to those used in the post-ionization experiments. This is the classic SIMS matrix effect. Nevertheless, it has been demonstrated with different sputtering conditions that the production of secondary ions can affect the post-ionization signals by detracting from the useful yield of sputtered neutrals. This effect has been shown for Xe^+ and Ar^+ sputtering on this sample.

A non-resonant, ultra-high intensity post-ionization technique utilizing intensities greater than 10^{14} W/cm^2 at 800 nm has been characterized. Multiply charged atoms as well as singly charged molecules are detected. The ionization process displays a strong dependence on ionization potential. Moreover, detection

sensitivity may depend on secondary-ion yields as well as variations in angular/velocity distributions during sputtering. Nonetheless, remarkably accurate representations of relative elemental concentrations can be obtained from a number of matrices without the use of standards.

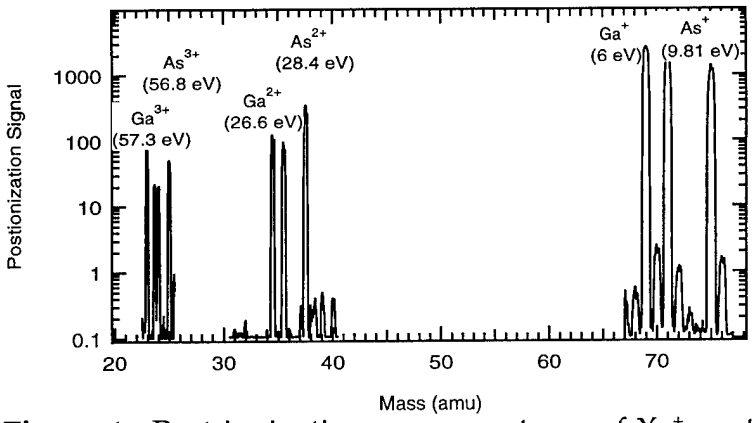

Figure 1. Post-ionization mass spectrum of Xe^+ sputtered GaAs. The total energy required for ionization is shown in parenthesis.

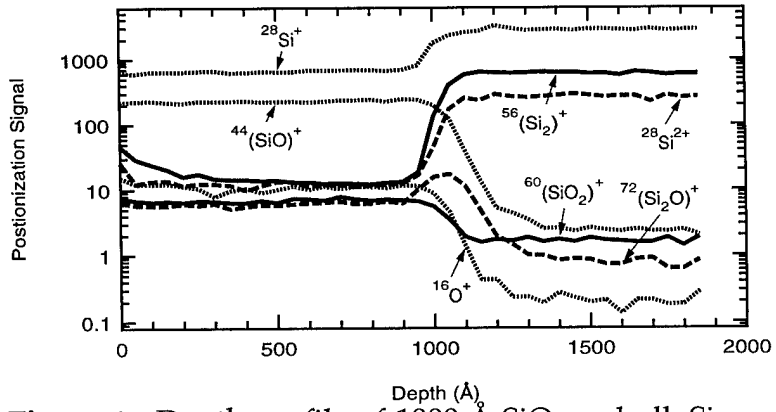

Figure 2. Depth profile of 1000 Å SiO_2 on bulk Si.

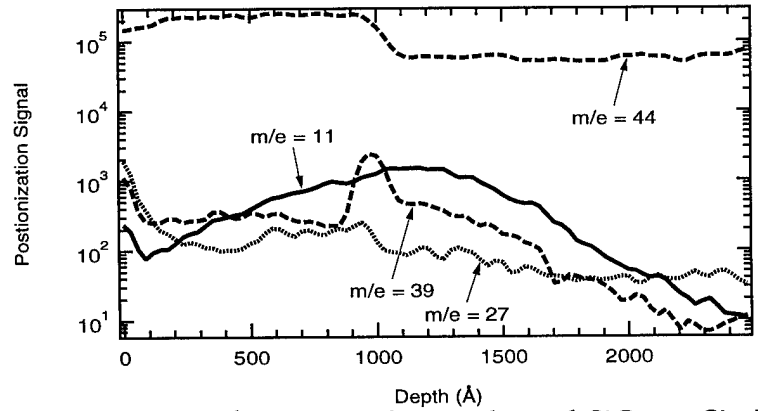

Figure 3. Depth profile of B implanted SiO_2 on Si. The peak in m/e = 39 at the interface is ^{39}K contamination.

1. C. H. Becker and J. S. Hovis *J. Vac. Sci. Technol. A* **12**, 2352 (1994).
2. L. V. Keldysh *Sov. Phys. JETP* **20**, 1307 (1965).
3. G. Gibson, T. S. Luk and C. K. Rhodes *Phys. Rev. A* **41**, 5049 (1990).

Ultratrace Analysis of Calcium with High Isotopic Selectivity by Resonance Ionization Mass Spectrometry

B.A. Bushaw[1], F. Juston, W. Nörtershäuser, N. Trautmann[2], P. Voss-de-Haan, K. Wendt

Institut für Physik, [2]Institut für Kernchemie, Universität Mainz, D-55099 Mainz, Germany
[1]Battelle Pacific Northwest Laboratories, P.O. Box 999, Richland, WA 99 352, USA
Tel: ++49-6131-39-2882, Fax: ++49-6131-39-2991, Email: WENDTαDIPMZA.PHYSIK.UNI-MAINZ.DE

Introduction:

Using resonance ionization mass spectrometric techniques (RIMS) for ultratrace analysis has a number of advantages over conventional techniques:

1. Extremely high sensitivity in the fg to ag range per sample is possible with the high cross sections for optical excitation.
2. Ultrahigh elemental and isotopic selectivity is achieved by the uniqueness of the optical resonance lines of individual elements and isotopes.
3. Background is strongly suppressed by subsequent mass spectrometry.

Unfortunately, the application of the technique is complicated by the complexity of the experimental set-up, particularly the laser system, and hence is limited to a small number of research institutes so far.

As part of the ongoing development work on RIMS trace determination techniques for radiotoxic isotopes at the university of Mainz, Germany, /Klu94, Wen95/, a method for ultratrace analysis of stable and long-lived calcium isotopes is presented. The experimental approach is based on multi step resonance ionization with narrow band continuous wave lasers on a thermal atomic beam which is combined with mass analysis in a commercial quadrupole mass spectrometer. This technique was first developed by one of the authors for low level radiotrace analysis of ^{210}Pb and ^{90}Sr /Bus92/. By introducing simple and inexpensive diode lasers for efficient optical excitation for replacement of the huge and expensive ion laser-dye laser combinations, a small and easy-to-handle trace determination instrument is under development, which will allow extremely high isotopic selectivities of more than 10^9 and overall efficiencies of up to 10^{-3}.

Experimental:

A simplified sketch of the ultratrace determination system under development is given in Fig. 1. The determination system is based on three components:
1. atomic beam oven and interaction region for resonance excitation and subsequent ionization,
2. quadrupole mass spectrometer with single ion detection, and
3. laser system for multi step resonant excitation and subsequent nonresonant ionization.

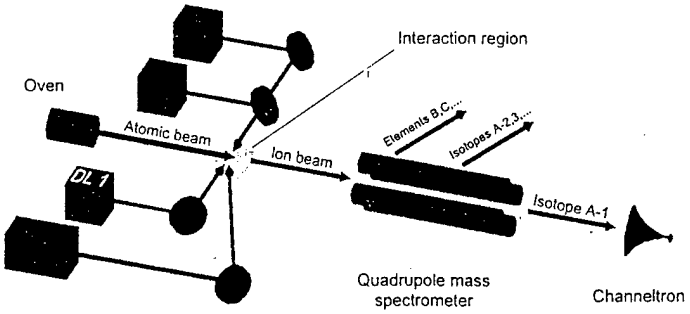

Fig. 1: *Simplified sketch of the system for isotope selective ultratrace determination of Ca by RIMS*

The construction of components 1 and 2 has already been given in detail elsewhere / Bus89/. The new component 3, the laser system, has been taylored to meet the requirements of narrow band multi step resonance excitation, as discussed e.g. in /Bus89/. Possible excitation schemes for resonance ionization in Ca I are given in Fig. 2. Three different excitation ladders have been tested subsequently representing the different stages of development for the one to three diode laser system. During these test experiments an existing Ar^+-laser has been used for efficient non-resonant ionization.

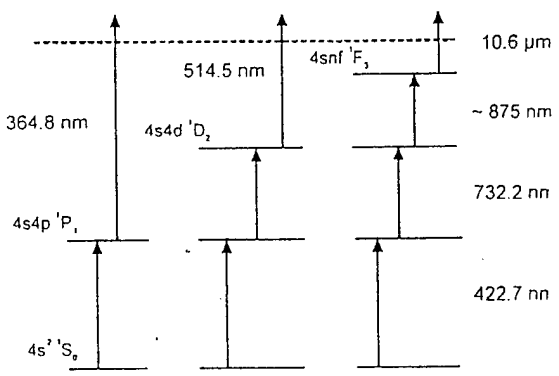

Fig. 2: *Possible excitation schemes for multi step resonance ionization in Ca I.*

The first excitation scheme (according to Fig. 2a), involves one resonant excitation at 422.7 nm, which is produced by external cavity frequency doubling of a diode laser, and non-resonant uv ionization. This scheme already gives high isotope selectivity of up to 10^8, stemming dominantly from the mass separation step, but only limited efficiency, due to the low efficiency of the non-resonant ionization process. Nevertheless, this simple scheme is well suited for precise measurements of isotope ratios. Both the selectivity and efficiency can be increased by using two resonant excitations according to Fig. 2b with visible non-resonant ionization and finally by three step resonant excitation and infrared ionization (Fig 2c). For both schemes external cavity diode lasers have been developed, which produce tunable narrow band laser light in the frequency range needed.

Results and Discussion :

The interest in isotope selective ultratrace determination in calcium is multifold, generally demanding high selectivity and sensitivity. For cosmochemical studies the determination of the isotope ratio of $^{46,48}Ca$ in small hypponite inclusions of meteorite material is of high interest. Here the suppression of isobaric interferences from ^{46}Ti, which limit conventional mass spectrometry, is mandatory. A typical result, demonstrating the high elemental and isotopic selectivity is given in Fig. 3, all trace isotopes $^{48,46,44,43,42}Ca$ are resolved, a strong titanium interference is completely suppressed. These sensitive isotopic ratio measurements of stable Ca trace isotopes are also used for isotope dilution techniques in medical studies on the kinetics of the calcium balance in-vivo, which governs diseases like osteoporosis. Here radioactive tracers might be replaced. Test measurements on the two and three step resonant excitation schemes have been carried out, but were limited due to frequency instabilities of the different diode lasers. A stabilization is under construction.

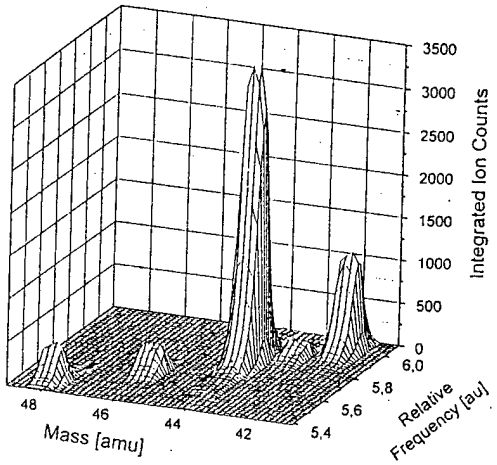

Fig. 3: *Typical two dimensional scan over the mass peaks of the trace isotopes $^{48,46,44,43,42}Ca$, showing the high resolution, low background and complete suppression of titanium isobaric interferences*

Conclusion and Outlook:

Isotope selective ultratrace determination in Ca has been demonstrated, using multi step diode laser RIMS. Experimental results on synthetical Ca samples demonstrate the versatility and the specifications of the technique concerning selectivity and sensitivity. First results on Ca-isotope ratio measurements in meteorite and medical samples are discussed. In a further stage of construction the technique shall be upgraded to reach isotopic selectivities of up to 10^{16} in the suppression of neighbouring isotopes, which enable isotope dating via ultratrace determination of the isotope ^{41}Ca ($t_{1/2}$= 1.03×10^5 a).

References:

/Bus89/ B.A. Bushaw, Prog. Anal. Spec. 12, 247 (1989)
/Bus92/ B.A. Bushaw, Inst. Phys. Conf. Series, 128, 31 (1992)
/Klu94/ H.J. KI ıge et al., Fres. J. Anal. Chem. 350, 323 (1994)
/Wen95/ K. Wendt et al, Physica Scripta T58, 104 (1995)

LASER APPLICATIONS TO CHEMICAL AND ENVIRONMENTAL ANALYSIS TECHNICAL PROGRAM COMMITTEE

J. Michael Ramsey, *Oak Ridge National Laboratory, General Chair*

Jay Jeffries, *SRI International, General Chair and OSA Technical Council Representative*

Kay Niemax, *University of Hohenheim, Germany, Program Chair*

Robert P. Lucht, *University of Illinois, Program Chair*

Ernesto Cespedes, *US Waterways Experiment Station*

Alan Fried, *National Center for Atmospheric Research*

Timothy Harris, *AT&T Bell Laboratories*

Ulrich Meier, *DLR EN-CV, Germany*

Andrzej Miziolek, *US Army Research Laboratory*

Reinhard Niessner, *Technical Universitat Munich, Germany*

Nick Omenetto, *European Commission, Joint Research Center, Ispra, Italy*

Jerry Seitzman, *Georgia Institute of Technology*

Volker Sick, *Universitat Heidelberg, Germany*

Michael Winter, *United Technologies Research Center*